BUCKLING STRENGTH OF STEEL THIN CYLINDRICAL SHELLS UNDER ELEVATED LOCAL AXIAL COMPRESSION

Thesis submitted in fulfilment of the requirements for the degree of

Doctor of Philosophy

by

Minjie Cai

Supervisors: Dr. J. Mark F.G. Holst

Professor J. Michael Rotter

Institute for Infrastructure & Environment, The School of Engineering & Electronics,
College of Science & Engineering, The University of Edinburgh
Crew Building, The King's Buildings, Edinburgh EH9 3JN, Scotland, UK

October 2003

DECLARATION

This thesis, entitled 'Buckling Strength of Steel Thin Cylindrical Shells under Elevated Local Axial Compression', is submitted to the Institute for Infrastructure & Environment, The School of Engineering & Electronics, The University of Edinburgh, Scotland, U.K., for the Degree of Doctor of Philosophy. The work described in this thesis was carried out by the candidate during the years 1999-2003 under the supervision of Dr. J. Mark F.G. Holst & Professor J. Michael Rotter.

The research was solely the work of the author except where otherwise acknowledged in the text and has not formed the basis of a submission for any other degree.

Three conference papers, which were based on the work described in this thesis, were presented in:

CONFERENCE PAPERS

Cai, M.J., Holst, J.M.F.G. and Rotter, J.M. (2002) "Buckling Strength of Thin Cylindrical Shells under Localized Axial Compression", the 15th ASCE Engineering Mechanics Division Conference, Columbia University, New York, June 2-5th, 2002, pp 99.

Cai, M.J., Holst, J.M.F.G. and Rotter, J.M. (2003a) "Parametric Study on the Buckling of Thin Steel Cylindrical Shells under Elevated Axial Compression Stresses", the 16th Engineering Mechanics Conference, University of Washington, Seattle, July 16-18th, 2003.

Cai, M.J., Holst, J.M.F.G. and Rotter, J.M. (2003b) "Buckling of Cylindrical Tank Shells under Local Axial Compression Stresses", Internal Conference on Design, Inspection, Maintenance and Operation of Cylindrical Steel Tanks and Pipelines, Under the auspices of ECCS, Prague-Kralupy and Vltavou, Czech Republic, October 8-11th, 2003, pp 70-76.

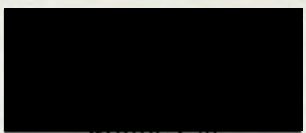

October, 2003

ABSTRACT

The thin cylindrical shell is important in many applications in civil engineering. Cylindrical shells are subject to vertical stresses in their walls as a consequence of silos friction between the stored solid and the wall. It is well known that shell buckling under axial compression is normally the controlling design consideration especially for steel silo and it is particularly sensitive to imperfections in the shell, and the changing patterns of behaviour with changing geometry, loading and boundary conditions.

Both experimental and theoretical observations show significant stress non-uniformity in the filling and discharging processes. However, the current design rules are principally based on an empirical interpretation of test data and hence a very simple load pattern is applied. Reliable quantification of this effect is still challengingly difficult.

This thesis explored a typical perfect/imperfect thin cylindrical shell under local axial compression. In order to address this issue in a rigorous and rational way, a full set of theoretical and numerical studies were examined, specifically the effect of geometric imperfections on shells subjected to axial non-uniform stress states. Emphasis was given to the non-linear behaviour caused by the large deflections but the influence of elastic-plastic material non-linearity was also taken into account. The ABAQUS finite element package was used to analyse the behaviour. Illustrated were stress redistribution, load-displacement path, local buckling, the effect of geometric imperfections due to fabrication process and the effect of classical steel material non-linearity. It is the objective of this thesis to provide design guidance of practical value for future silo design and construction.

The following steps were followed to achieve this aim:

First, the buckling analyses of perfect cylinder under various uniform/non-uniform axial compression were performed using the finite element method in order to obtain converged mesh for further study, to find the reference elastic critical load, and to explore the accuracy of the loading and boundary conditions applied.

Linear elastic analysis of perfect cylinder under local elevated axial compression was presented second. The meridional membrane stress distribution in the mid-plane, which was subjected to non-uniform axial compression on the cylinder wall, was examined in detail and a linear buckling analysis was performed limited in the small deflections, geometrically and materially linear range.

Two different buckling modes were identified, with corresponding and distinct buckling mode forms, by using the deflected shapes and axial membrane stress distribution of various geometry and loading configurations. The introduction of above distinguishing is a key feature of the whole study.

Third, a modified RIKS analysis was performed to get the load-displacement curve for some representative cases to deal with possible solution instabilities due to geometric non-linearity as well as material non-linearity with and without imperfections. A new defined approach was set up to obtain the critical buckling strength in the geometrically non-linear domain more efficiently.

Fourth, the stress pattern in the pre-buckling state before buckling under local elevated axial compression was studied to get the relationship between the high local axial stresses and the buckling strength.

Finally, the conclusions drawn from this research were summarised and recommendations for design and future research were made.

ACKNOWLEDGEMENTS

The author gratefully acknowledges the help and support from the following people and organisations during the course of this research:

First of all, the author would like to express his deep and sincere gratitude to his two supervisors, Dr. J. Mark F.G. Holst and Professor J. Michael Rotter for their continuous supervision, guidance and assistance during the four years of this study and producing this thesis as well as the initial motivation of this research from Professor J. Michael Rotter.

The financial supports from the British Government for an ORS award (ORS/C20-4, ORS/1999014046) and a Small Project Grant from the University of Edinburgh Development Trust (Ref. 77/2002) are gratefully acknowledged.

Thanks go to his friends at The School of Civil & Environmental Engineering (before), The Institute for Infrastructure & Environment, The School of Engineering & Electronics (later), University of Edinburgh, particularly Dr. Zhijun Zhong, Dr. Paul Hyton for their help in his study; Mr. Chris Burnside and Mr. Colin Higgs for their technical support and help as well as many happy memories from other friends at the school and wish them all the best in the future. Thanks also go to his friends in Shanghai and Edinburgh for their friendships and care.

Finally the author would like to express his special thanks to his wife Jie Sun, his other family members for their love, care and understanding during the last four years. Being with her is one of the most valuable experiences in his life!

Minjie Cai

CONTENTS

LISTS OF FIGURES

LISTS OF TABLES

Chapter 1

INTRODUCTION

1.1 Background

1.1.1 Silos

Containers for storage of bulk solids are called bins, silos or tanks and most are constructed using cylindrical shells. The term "cylindrical shells" is used here as it provides a generic description of the geometry for containers, which may be variously referred to above applications sharing the similar geometry shapes. Cylindrical shells or cylinders are widely used in many applications – space rockets, aircraft, motor vehicles, nuclear containment vessels, submarines, chimney pressure vessels, tanks and storage silos as well as domestic food and drink containers.

1.1.2 Silos in Civil Engineering

In civil engineering, silos, tanks, pipelines, chimneys, towers and masts are the primary applications of cylindrical shells and they are widely applied in the following industries: mining, chemical/agriculture/food processing, electrical power generation.

In terms of the material of construction, cylindrical shells can be separated into two different kinds – metal and concrete. Only metal cylindrical shells were studied here. Owing to their flexibility, lightness, fast construction speed and high mobility, metal cylindrical shells are widely used for short and long term storage and the number of metal silos has increased dramatically in recent years.

In terms of to their plan cross-section, silos can be divided into circular and rectangular silos (Figs. 1.1a & b). The advantage of the circular silo is that it is structurally efficient, while that of rectangular plan form has constructional convenience. Only shells of revolution were studied.

Metal silos may be ground-supported (Fig. 1.1a) and elevated (Fig. 1.1b) in terms of supporting system. Elevated silos have the advantage of discharging the solids by gravity. A typical form of such a metal silo structure is shown in Fig. 1.1c. It consists of a conical roof, cylindrical shell/barrel and a conical hopper for the main body; a column-supporting or on-ground supporting system; a loading-bearing skirt/ring and a transition system in between the vertical wall and the hopper.

1.2 Theory Development

The capacity of silos has also been increased sharply over the past few decades because higher demands from industry and modern technology make this possible. Since the metal cylindrical shell is a comparatively thin structure (with the radius-to-thickness ratio between 500 and 2000 in practice), its strength is very sensitive to local buckling and imperfections in the wall because of its dramatically weakening post-buckling strength. This is the key issue, which makes thin-walled cylindrical shells differ from other structural types (beams and columns) in civil engineering and it is since the interest of this study.

As one of the most important component of silos, the shell wall is a key issue for the design of the whole silo and this is the only part covered by this study. Shell wall design consists of two major parts: estimating the loads on the walls and assessing the strength of the walls.

1.2.1 Loads on Cylindrical Shell Walls

If the silo is filled with solids, the wall pressures can be closely predicted by the Janssen theory (Fig. 1.2; Janssen, 1895) on the condition that it is carefully symmetrically filled and appropriate material parameters are used to represent the solids. However, in the process of practical filling and discharging (especially during the discharging), the silo walls are subjected to much higher pressures or/and local lower pressures if either of above ideal conditions is met. Both of lower/higher local pressure can lead to serious conditions in the structure.

Since the loads on the walls are known to be closely related to the flow pattern, the study of flow patterns is essential to understanding the loading patterns on shell walls. There are two main flow patterns during the filling and discharging – symmetric and un-symmetric flow patterns (Figs. 1.3 & 1.4). Apart from the filling factors, a silo with a steep hopper and smooth wall surface is likely to develop mass flow, but a silo with a shallow hopper and a rough wall surface is likely to develop funnel flow.

As pointed above, the wall pressure can be exaggerated during the filling and discharging even in the extent of symmetrical loading (Fig. 1.5). In addition, more recent silo loading experiments (Pieper, 1969; Nielsen, 1983; Ooi et al., 1990) and theoretical studies show significant deviations from the classical Janssen theory (in axial direction (Nanninga, 1956; Jenike et al., 1973; Walker, 1966; Walters, 1973; Rotter, 1986b; Rotter, 1998) and in circumferential direction (Ooi and She, 1997)), which contribute further to the unsymmetrical loads on silo walls even under carefully symmetrical filling (Fig. 1.6).

Since it is still difficult to control the flow pattern during the filling and discharging, it is almost impossible to predict the flow pattern during the filling and discharging procedure as the designer's wish. Thus unsymmetrical pressure seems to be unavoidable in real structures and it can lead to a more serious design situation in silo structures (Fig. 1.7).

Because of the buckling susceptibility of the thin-walled cylinder, the vertical compressive stress in the silo wall, which accumulates from the wall friction, lead to the most failures in metal silos and this is naturally the controlling load case for the buckling analyses. Furthermore, the compressive stresses that lead to buckling failures also arise from unsymmetrical pressures during filling and discharging, from wind pressures when empty or accidental partial vacuum (Rotter, 2001). Unsymmetrical flow patterns contribute directly to the unsymmetrical loads (normal wall pressure and axial/circumferential compressive stresses) on silo walls, which cause compression that varies around the cylinder circumference and this leads to a local high axial compression on the shell wall (Rotter, 1986a; Rotter, 1998).

Because buckling is the predominant mode of failure of the shell, and internal pressure is beneficial when acting together with axial compression (Fig. 1.8), internal pressure is ignored in this first study of local loading. Unsymmetric loads need more attention than symmetric loads due to the possibility of local high axial compression occurring, which might lead to an instability in the structure (Rotter et al., 1986; Rotter, 1999b; Rotter, 2001a). This study examines the most critical state, that in which the shell is not subjected to any internal pressure, but with local unsymmetrical axial loads acting on the shell wall (Rotter, 2001b).

1.2.2 Buckling in Cylindrical Shell Walls

Structural members subjected to compression are susceptible to Euler buckling, and the Euler buckling stress of a given quantity of material is at its greatest when all the material is placed as far as possible from the rotation axis. According to this theory, shell structures are in a dilemma: on one hand, the thin-walled structures are the most efficient form for compression members; on the other hand, thin-walled structures under axial compression have to deal with the new problem of local instability due to its thin thickness. Usually the strength of a thin-walled structure is not controlled by the material strength but by elastic stability instead.

In thin-walled structures, the membrane stiffness is much greater than the bending stiffness. A thin cylindrical shell can store strain energy by membrane straining without deforming too much (still geometrically linear, which allows the adoption of the small deformation assumption), but it has to deform a lot in order to store the same stain energy in bending deformation. If there is an external disturbance, it will automatically convert part of the membrane energy into bending energy, which can result in large deformations (geometrically non-linear) and the whole process is called "buckling" (Bushnell, 1985). Different from concrete silos, metal silos generally have much thinner walls which make the buckling phenomenon to dominate the strength and cause most failures.

The "classical elastic critical stress" (Lorenz, 1908; Timoshenko, 1910; Southwell, 1914) is used as the reference value for buckling of an axially compressed perfect cylinder

under ideal conditions (of medium length, with pre-buckling stresses unaffected by the boundary conditions and boundaries that restrain circumferential displacements during buckling) for many decades. Although the complex buckling phenomena of a perfect cylinder make it a poor estimate for the experimental strengths of practical cylinders (Fig. 1.9), this critical stress continues to be treated as the reference buckling stress for problems under axial compression.

From the early 1960s, more analytical solutions (Timoshenko and Gere, 1961; Flügge, 1973; Brush and Almroth, 1976; Calladine, 1983; Yamaki, 1984) for a big variety of shell forms under various loading cases and boundary conditions were obtained. But they are still applicable in quite simple conditions (geometry and loading case) and far removed from the real world.

1.3 Experimental Observations

The buckling strength of an isotropic axially compressed thin cylindrical shell depends on its geometry (radius R, thickness t and length L), its elastic modulus E, the amplitudes and forms of minor imperfections in its geometry, the end boundary conditions and the pattern of loading. Since the 1930s, lots of observations from experiments induced a paradox: under both uniform and non-uniform axial loading, the buckling strengths of thin-walled cylindrical shells measured in laboratory tests are very scattered and lie far below the theoretical results – in a band between 0.2 and 0.5 of the theoretical results (Fig. 1.9).

A wider range of tests with different geometric parameters and materials (Harris et al., 1957; Fung & Sechler, 1957; Brush & Almroth, 1976) have been conducted investigating the buckling of uniform thin-walled cylindrical shells, but the puzzle remains. The reasons for both the scatter and the loss of strength are a major challenge to researchers, and continue to pose challenges to designers in determining how to ensure that practical shell constructions meet their requirements.

1.4 Relationship between Theory and Experiment

The strength of thin metal cylinders has long been known to be very sensitive to trivially small imperfections in the geometry (Koiter, 1945; Yamaki, 1984; Calladine, 1995), the boundary conditions, the joints and the material of the shell, the pre-buckling deformation, internal pressure, the residual stress and the uniformity of loading. The buckling strength of a thin cylindrical shell under axial compression is particularly sensitive to imperfections in the shell, and the changing pattern of behaviour with changing geometry, loading patterns and boundary conditions make the axially compressed cylinder a classical exemplar for behaviours that may be found in a less marked form in other structures or in shells under other loading conditions. For these reasons, the axially compressed cylinder has probably been the most extensively studied of all shell buckling conditions, giving a wealth of evidence from both experimental and theoretical work.

Geometric and boundary condition imperfections have been widely studied over the past half century, but till recently no appropriate way has been found to carry out the calculation of the rational arguments in theory and as a result, the big difference between the theoretical calculations of the buckling strength and the practical results (from experiments data to the existing silo or tank tests) remains a puzzle: the axially compressed cylinder may be one of the last classical problems in homogeneous isotropic structural mechanics for which it remains difficult to obtain close agreement between careful experiments and the best predictions from numerical modelling.

Due to the reasons above, the study of the buckling strength of a cylindrical shell is of direct relevance to the design of most metal silos. Of these, the geometric imperfections generally have the greatest influence (above 50% of total failure reduction) while the other individual ones are comparatively small (hold only 15% or less of total failure reduction). One of the most detrimental and well-defined imperfections is a local depression due to the rolling process of the steel plate and shrinkage of the weld or rivet influence (Fig. 1.10).

A considerable amount of work remains to be done to relate the design rules to computer predictions that account for geometric imperfections that can be used in appropriate tolerance measures to control and monitor construction. However, the most serious missing element in current research is an understanding of the effects of unsymmetrical axial stress distributions in the cylinder. Furthermore, the shell buckling strength under an axial compression that acts over only a part of the circumference (a typical unsymmetrical load on silo walls) may be significantly different, but the problem has been scarcely explored at all (Rotter, 1986a; Rotter, 1986b; Ansourian, 1992; Rotter, 1997). A circular silo is a shell structure and unsymmetrical pressures not only induce local bending, but also affect the whole silo with membrane stresses (Rotter, 1999). Thus, for very unsymmetrical stresses, additional research may be necessary to determine what is an appropriate criterion of failure and to discover the mechanism of this failure.

In summary, the load case combining the minimum internal pressure and unsymmetrical axial compression is critical to the strength analyses of cylindrical shells and the lack of method has been found to deal with it appropriately till recently. Reliable quantification of all above factors is still challengingly difficult, and the lack of knowledge often means that too much emphasis is placed on one of the two opposing goals of economy and safety, leading either to disasters or over-design.

1.5 Design Rules

Since the industrial use of metal thin cylindrical shells is vast, there is a rapid development in the design of silos recently. The internationally acknowledged current silo codes (Rotter, 2001b) are as follows:

1.5.1 Loading Codes

ACI standard on silo loads

ACI 313 (1991) "Standard Practice for Design and Construction of Concrete Silos and Stacking Tubes for Storing Granular Materials", ACI 313-91, with Commentary (ACI 313R-91) American Concrete Institute, Detroit, 27pp.

Australian standard on silo loads

AS 3774-1996 (1996) "Loads on Bulk Solids Containers", Australian Standard, Standards Association of Australia, Sydney, October.

DIN standard on silo loads

DIN 1055 (1987) "Design Loads for Buildings: Loads in Silo Bins", DIN 1055 Part 6, Deutsches Institut für Normung, Berlin, May.

Eurocode on silo loads

Eurocode 1: Basis of design and actions on structures: Part 4: Actions in silos and tanks, CEN ENV 1991-4: 1995.

1.5.2 Structural Design Codes

Eurocode on metal silo structures

Eurocode 3: Design of steel structures: Part 4.1: Steel silos, CEN ENV 1993-4-1: 1999.

Eurocode on shell strength and stability

Eurocode 3: Design of steel structures: General rules: Part 1.6: Supplementary rules for the strength and stability of shell structures: CEN ENV 1993-1-6: 1999.

Eurocode on metal tank structures

Eurocode 3: Design of steel structures: Part 4.2: Steel tanks, CEN ENV 1993-4-2: 1999.

Though there are many silo design codes, unfortunately the rate of failures in silo storage structures has been higher than for any other structural form for many decades, and continues to be high (Rotter, 1995). Metal cylindrical shells are significantly different from many other civil engineering structural forms in terms of the structural geometries, stress distribution and load conditions. All these factors cause much more complex failure modes. There are many reasons for the high failure rate and the lack of both loading and structure design standards are certainly important factors.

There are four key problems that regularly arise in the design and functioning of silos (Rotter, 2001):

A. the structural integrity of the silo may be jeopardised by pressures which are too high, too low or too unsymmetrical;
B. the stored solids may hang up in the container, or flow irregularly;
C. the filling or flow pattern may cause segregation of the solids;
D. the discharge may lead to unacceptable noises or motions (shaking, quaking and honking).

Among all four problems (Fig. 1.11), the wall properties, filling/discharging methods and solids properties contribute to the stress distribution in the stored solid, which influences the structural behaviour of the whole structure.

In terms of the design loading, the silo must sustain the internal pressure and frictional traction on the wall from the stored solids. These loads depend heavily on the silo geometry, the material properties, the flow pattern during the filling and discharging and the interaction between the solid and the wall. Prediction of these loads on the silo wall is still difficult.

In terms of the structural analyses, for both ground- and column-supported silos, the buckling of the cylindrical shell wall remains a most important part, which caused the majority of the failures in reality. Silo-buckling strength is usually very sensitive to fabrication imperfections, which often cannot be known with certainty at the design stage. The interaction between the solids and the wall also contributes to this uncertainty. Detailed descriptions of the different kinds of analyses that can be used are given in current Eurocode 3 Part 1.6 on the Strength and Stability of Shells (ENV 1993-1-6, 1999): A linear elastic stress analysis can provide the membrane stress and bending stress distribution and hence it is a useful tool to assess the structural strength. Large deflection is common in the thin-wall shell structures and stress-redistribution occurs in the elastic-

plastic domain. A geometrically non-linear, elastic-plastic analysis is needed to obtain the structural strength if all above considerations are included.

The current design rules are principally based on an empirical interpretation of test data but the test data unfortunately relate to laboratory models under very simple loading conditions, while the real structures are subjected to fairy complicated stress patterns as mentioned before. The size-effect and the different methods of fabricating the shells between lab and factory are certainly other very important factors. The extension of the design rules to cover more complicated stress states currently met has no good rational quantitative basis, neither in experiment nor in theory. Furthermore, many different design methods are in current use and the safety of a given structure as assessed by different rules may vary markedly.

Thus there is an urgent need to undertake rigorous studies to relate the current empirical design rules to theoretical predictions, and to extend the theoretical predictions to more complicated stress states close to those occurring in real situations. However, such studies are not straightforward, as they must take proper account of the weakening effect of the geometric imperfections, which can be in several different forms (modes), under different kinds of load patterns.

Most rules in silo loading standards are currently concerned predominantly with symmetrical pressure loadings and pay little attention to unsymmetrical pressure conditions. Furthermore, the best predictions from numerical modelling are not easily accessed by practising engineers. The study aiming for a set of simple empirically derived equations on the local buckling is since more urgent.

1.6 Research Philosophy

For the purpose of research, experimental studies and theoretical investigations are both very useful means of studying the structural behaviour. The concepts used in structural design are closely related to the behaviour of single structural members (e.g. beams and

columns) and to assemblages of these members into structural frameworks, for both of which there is wealth of experimental data.

Experiments are very expensive, especially for full-scale shell structures. Though there is rich evidence from lots of experiments on the buckling of shells, most of them do not have clearly defined and measured imperfections, and they were made using different fabrication methods, have simpler loading cases and boundary conditions, which makes it much difficult to achieve verification for the study (different from other structural types in civil engineering). In addition, the inevitable differences between test models and full-scale structures, the dispersed properties of solid inside, the cost of large-scale experiments are other obstacles of doing the experiments. In summary, thin shell structures exhibit rather more complex behaviour than other structural members, and many geometries and loading patterns have never been the subject of experimental studies. As a result, there are only very few tests that can be used as a verification of the calculation results. The special highly elevated load type of this study – localised axial compression is too difficult to define and implement in an experiment because of its complexity.

On the contrary, computer based methods employing numerical techniques like the finite element method are powerful tools for the structural analyses. The complex non-linear buckling and imperfection sensitivity can be accurately modelled numerically. Therefore, modern shell structural design must rely heavily on numerical analyses for cases for which no test data exist and understanding of shell structures (Rotter, 2002) though the drawback of this method is also obvious: all the conditions (definition of boundary conditions, initial deformation of the structure, imperfection profile, loading, material properties etc.) are too ideal to be implemented in practice even very complicated.

Because of all these difficulties, finite element investigations are used here and a comparison of some existing cases in the literature is used to verify the results of this study. The boundary conditions applied in the analyses have been carefully tested for the

resulting stress distributions and displacements. The corresponding part in the European Standard (ENV 1993-1-6, 1999) has also been used for this verification.

1.7 Aims

The aims of this study are to investigate numerically the buckling strength of cylinders with a locally axisymmetric imperfection under elevated local axial compression stresses. Emphasis is placed on the influence of local compression height and width. Furthermore it is the aim of this study to produce a rigorous and rationally based set of rules that can be adopted into current design standards.

Firstly, a review of current design guidelines, relevant theory, and several imperfection patterns was carried out to define the models, which were adopted for finite element analyses afterwards.

Secondly, a mesh convergence study was taken to ensure the accuracy of the analyses results and a converged mesh was produced as a result, which was adopted in the analyses after. A brief parametric study of uniform axial compression using finite element analysis was undertaken to explore two or three imperfection forms to identify the relationships between the empirical rules of the codes and imperfections appropriate to finite element analysis. This is also a very important step to verify the finite element analyses results by comparing with some existing cases in the literature for the same loading.

Thirdly, an investigation was conducted into the sources of non-uniform stresses in cylindrical shells with the aim of characterising all possible and realistic stress states. A simple model was designed to define the range of non-uniform stress states. Beginning with the imperfection forms previously calibrated against uniform compression and considering the effect of non-uniformity in the stresses, several imperfections patterns were explored for calculations of buckling resistance under non-uniform stress states. An example was constructed in accordance with the current design codes and then comparing with the results from FEA was conducted investigating various combinations of the non-

uniform stress state model and imperfection patterns. These resulted in a series of design charts and design formulae to identify safe working loads, failure criteria and failure mechanisms. A theoretical investigation examined the mechanics underlying failure in order to set up a model comparable with the results obtained previously and provided a better understanding of the phenomena.

Finally, the results were summarised in a series of simple design guidelines and their empirical equations in order to make the two contradictions - economy and safety reach a degree of balance and reduce the possibility of leading either to disasters or over-design of cylindrical shells in the future.

1.8 Research Procedure

Based on rigorous parametric linear and non-linear buckling analyses (some material non-linearity was also included), this study examined the elastic buckling strengths of thin cylindrical shells under uniform and non-uniform axial compression, with imperfections arising at circumferential welded joints. The effects of imperfection height, amplitude and the non-uniform stress distribution were thoroughly investigated.

Elastic shell buckling stability analyses may be performed using either geometrically linear or non-linear theory. A linear eigenvalue analysis (LEA) was used first on the geometrically perfect structure to obtain estimates of the elastic buckling load and the probable buckling mode, which are very useful for further study. Moreover, if the results of the present study are to be interpreted into the conceptual framework of the Euro-code for shell structures (ENV 1993-1-6, 1999), the critical stress of a linear eigenvalue analysis is needed as a key element of the description. It locates the structure correctly in the elastic-plastic interaction space by means of a slenderness parameter (Fig. 2.8). The critical load from a linear eigenvalue analysis depends only on the membrane stresses and is unaffected by bending stress (Rotter, 2002). There are two full parametric studies in this thesis: the first explored the height over which elevated axial compressive stresses occur. The second explored the effect of the width of this zone. The influence of

geometric imperfections was included throughout the whole study. Both of them contributed to the study of the elevated local compression.

Chapter 1 is concerned with the basic knowledge about the design of silos: loading and structural analyses. The development of the theory, different current design codes and their present status are presented here. The need for improvements and the aims of this study are also introduced. One of the key issues of this chapter is research philosophy, which will be applied throughout the whole study. The arrangement of the whole study is also set out in this chapter.

In Chapter 2, the theory of shell buckling is given in the context of uniform and non-uniform compression. Some classical buckling phenomena are described here. A historical review is presented in relation to the theory, experiment and computer aided analyses development within the buckling analyses of thin cylindrical shells.

Chapter 3 opens with a discussion of non-uniform compressive stresses. A full description is presented of the buckling analyses of a thin elastic cylindrical shell that is subjected to locally elevated axial compressive stress, which often occurs under realistic loading conditions applied to practical shell structures. The main purpose of the whole study is mentioned afterwards. The geometry of the model used in the computer analyses, and the imperfection characterisation are also specified.

In Chapter 4, a description of the computer modelling is presented. The mesh convergence study is detailed. The application of these into the finite element analysis package – ABAQUS, with different analyses types is stated and a special user-defined method is also described in detail. The master input file for the ABAQUS analyses and related FORTRAN files constructing the node, element and the load elements are used to perform the parametric study more efficiently.

Chapter 5 explores the buckling behaviour of a thin elastic cylindrical shell that is subject to locally elevated axial compressive stresses. Linear eigenvalue and geometrically non-

linear analyses have been conducted, and the effect of local geometrical imperfections on the non-linear buckling strength has been explored for a range of imperfection amplitudes. It is found that two different bucking modes can occur, depending on the local stress pattern in the neighbourhood of the peak stress. The relationship between the local stress pattern, the pre-buckling/buckling/post-buckling deformations and the buckling strengths is explored here for two examples, which set the scene for the extensive parametric study in the following chapters. A validation of the computer analyses results is also provided.

Chapters 6, 7 & 8 present the detailed parametric study results.

In Chapter 6, the locally elevated axial compressive stresses are studied and the emphasis is placed on the influence of compression width. Three different analyses types have been conducted according to the current Eurocode 3 Part 1.6 on the strength and stability of shells (ENV 1993-1-6, 1999). A set of design rules is given based on calculations. Local axisymmetric imperfections are explored and material non-linearity is also induced for some of the analyses on both perfect and imperfect cylinders. The influence of plasticity from those analyses is briefed as a conclusion for the rest of the elastic study.

Chapter 7 describes a similar parametric study, but the emphasis is put on the compression height. It keeps the same parameters as used in Chapter 6. This represents a continuum of the research in the elevated localised axial compression and the same three analyses are run for the purpose. Local axisymmetric imperfections are explored and a set of simple formulae is produced as a result.

Chapter 8 studies the relationship between very high local bending stresses and the buckling strength of a cylindrical shell under locally elevated axial compressive stresses. Some simple parameters are found to describe this and a comparison of different approaches is also provided. A method of distinguishing between the two discovered phenomena is presented.

Overall, these parametric studies are all naturally connected to the two distinct local buckling phenomena, which are discovered in Chapter 5. All corresponding rules and empirical equations are based on this discovery.

In Chapter 9, problem studied before, work had been done and discovery from the study as well as conclusions drawn from previous chapters are reviewed, and the areas in need of future research are highlighted.

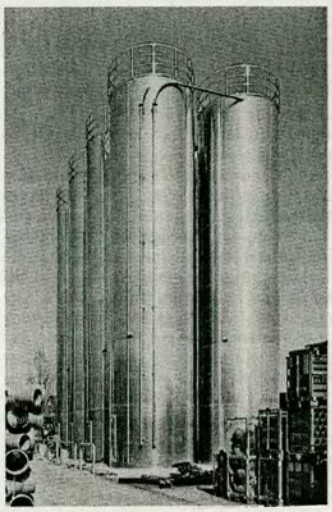

Bild 7.3-15
Zellenbatterie aus 8 Aluminium-Einzelzellen mit je 118 m³
für die Lagerung von PE-Granulat

a)

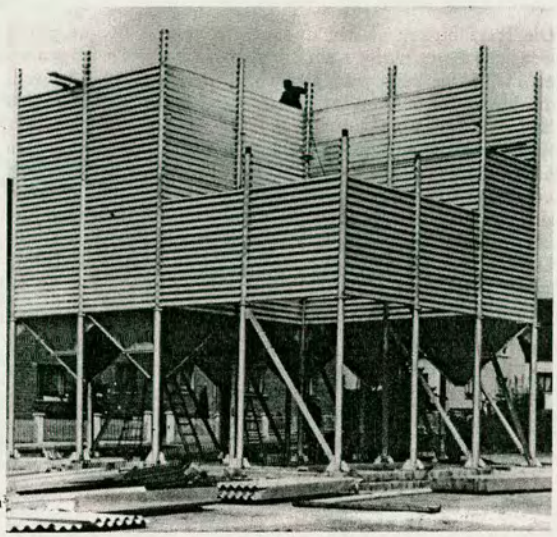

b)

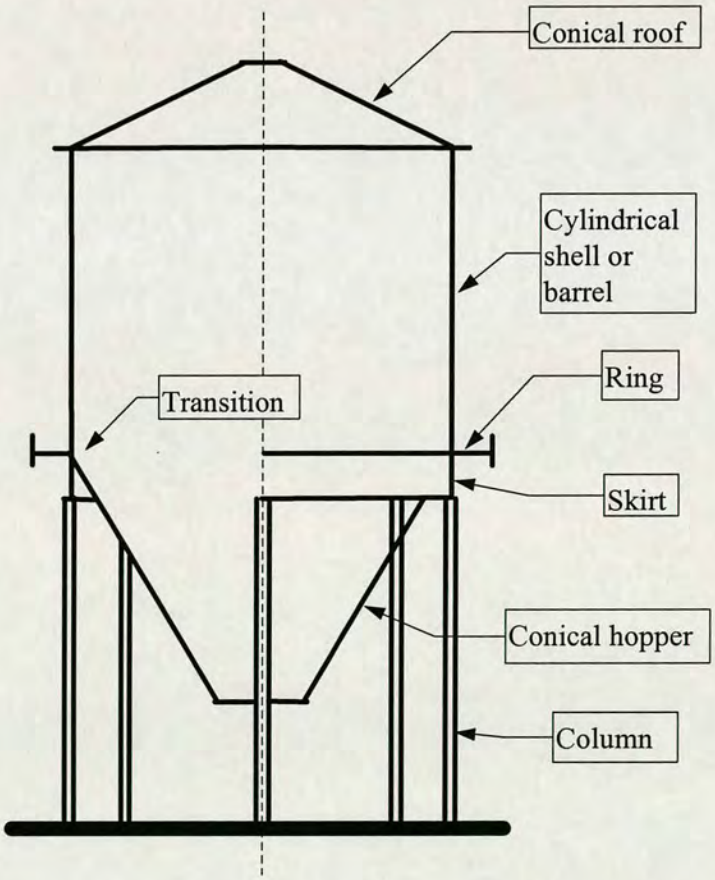

c)

Fig. 1.1 Silo and its terminology
(a & b after Martens, 1988; c after Rotter, 2001)

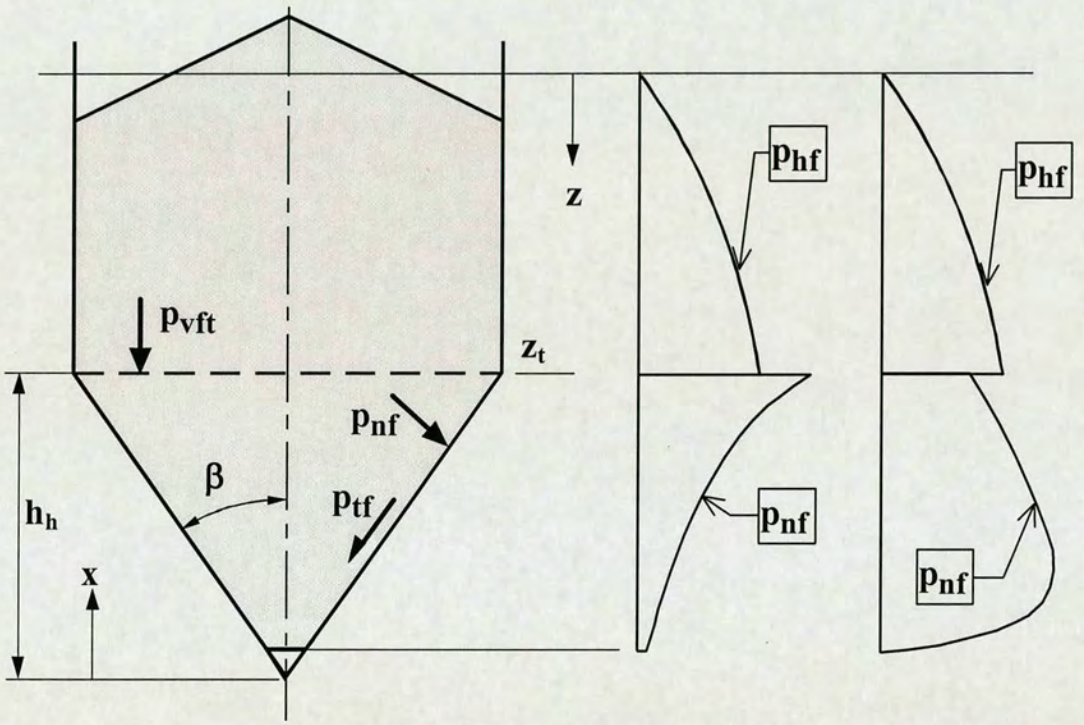

a) Hopper geometry b) Steep hopper pressures c) Shallow hopper pressures

Fig. 1.2 Filling pressures on steep and shallow conical hopper walls (after Rotter, 2001)

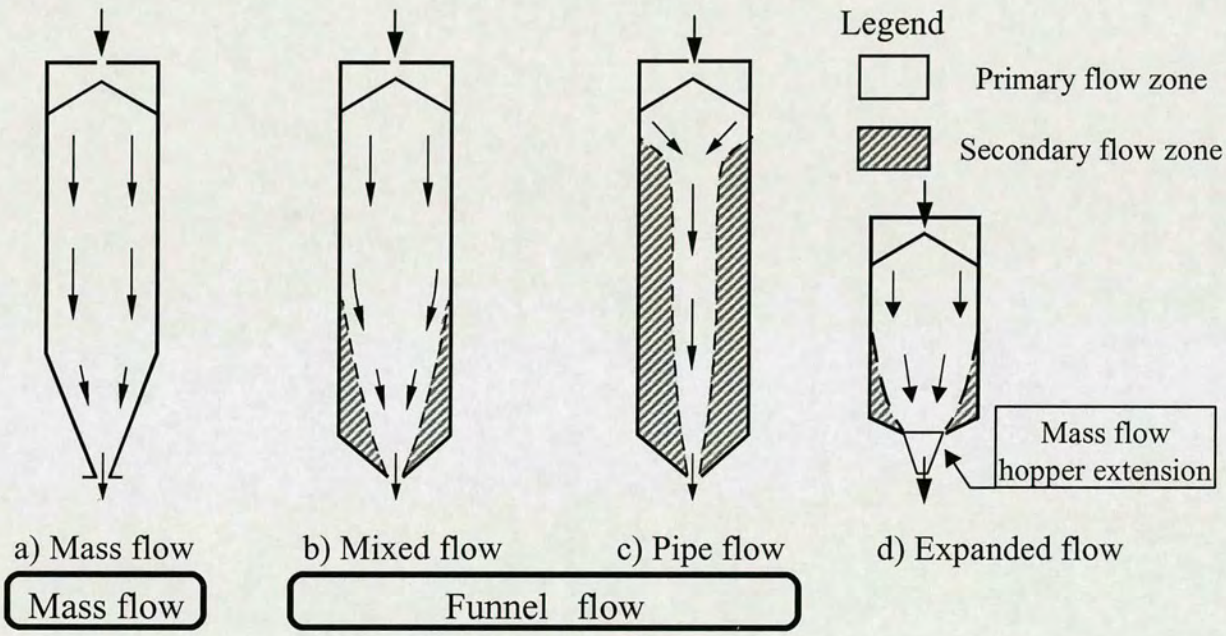

Fig. 1.3 Forms of symmetric flow patterns (after Rotter, 2001)

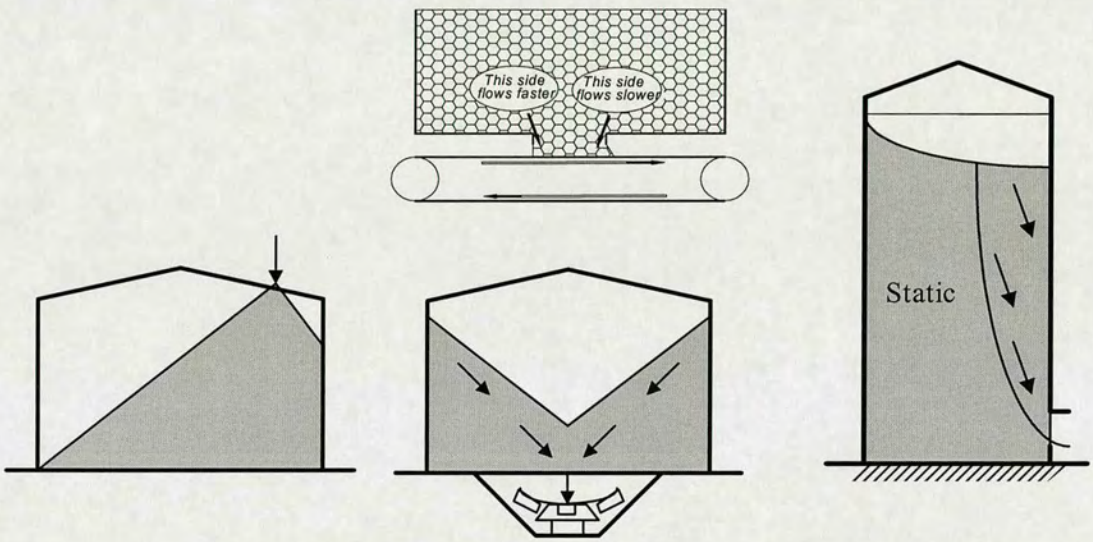

a) Eccentric filling **b) Unsymmetrical cleanout** **c) Eccentric discharge**

Fig. 1.4 Systematic causes of asymmetry in pressures (after Rotter, 2001)

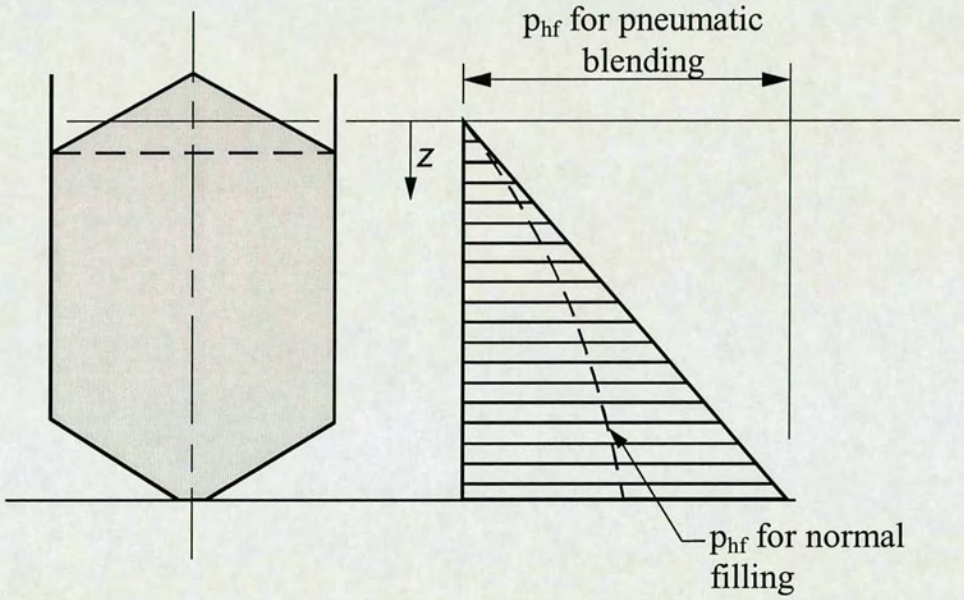

Fig. 1.5 Initial pressure modification for blending and rapid filling (after Rotter, 2001)

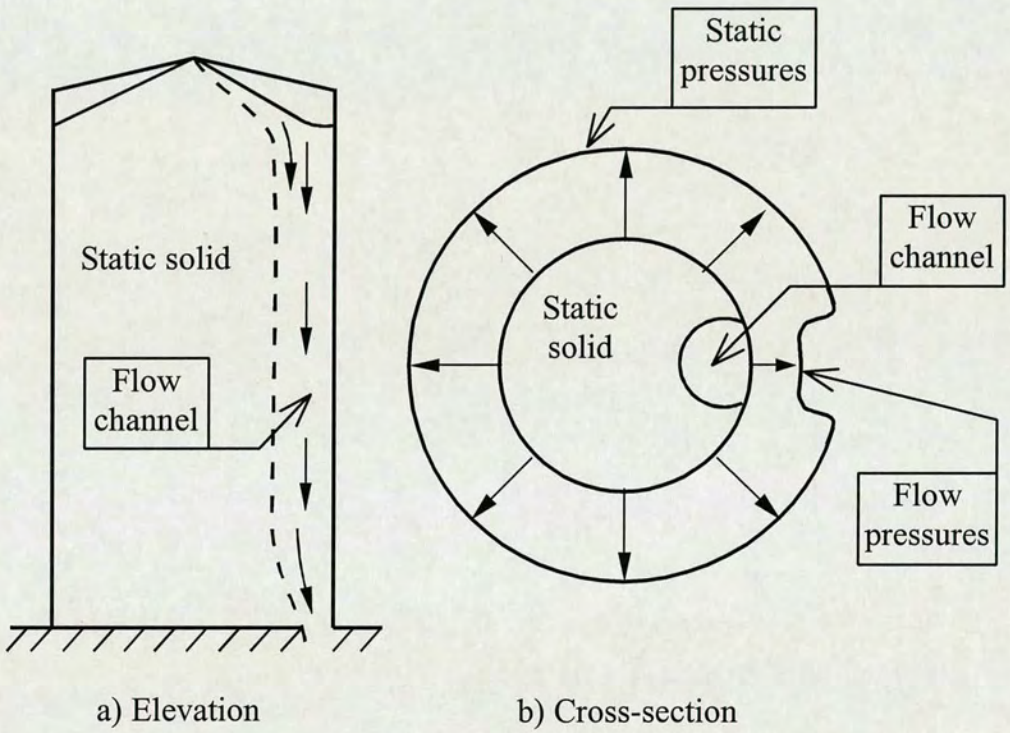

Fig. 1.6 Eccentric pipe flow discharge with stylised pressure pattern (after Rotter, 2001)

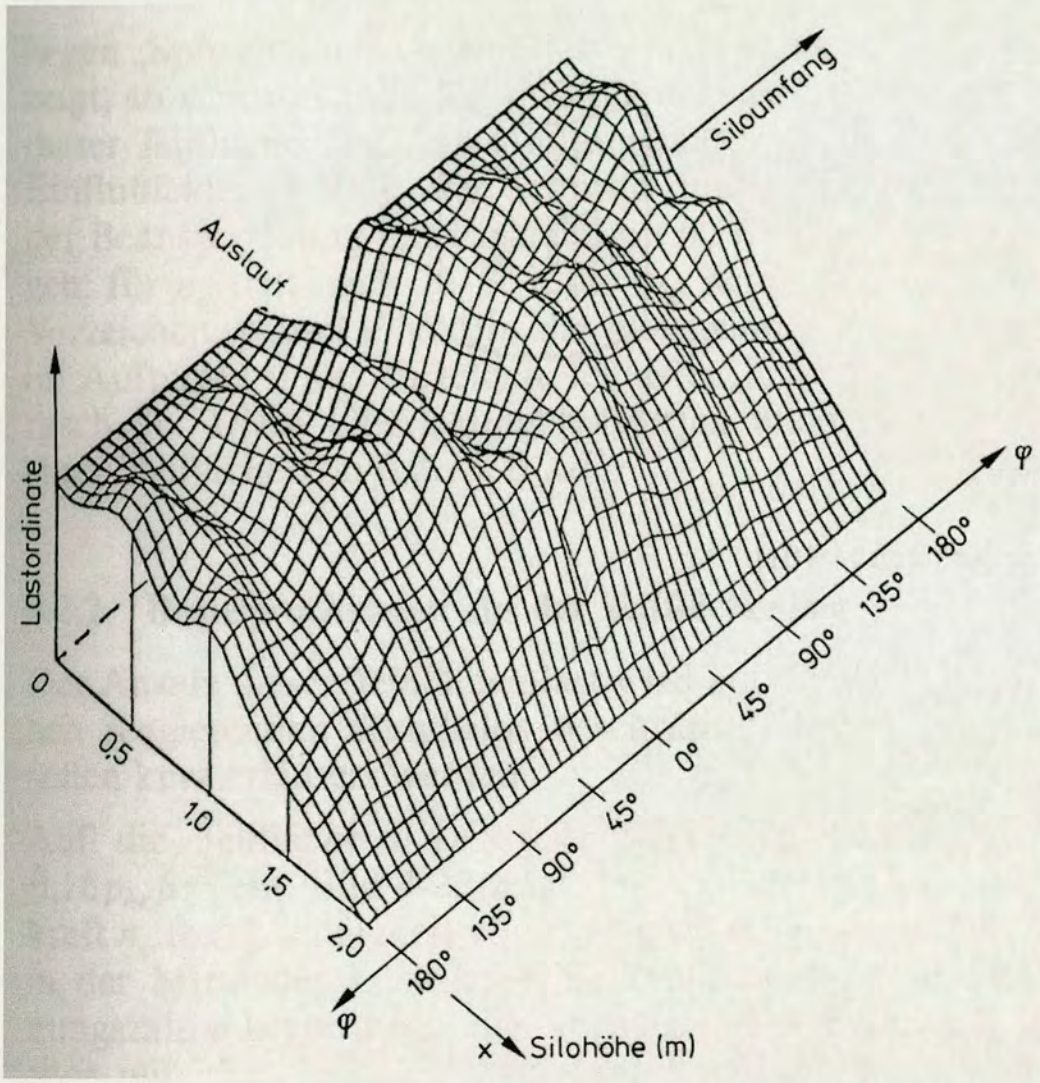

Fig. 1.7 Normal pressure on silo wall (after Stiglat, 1988)

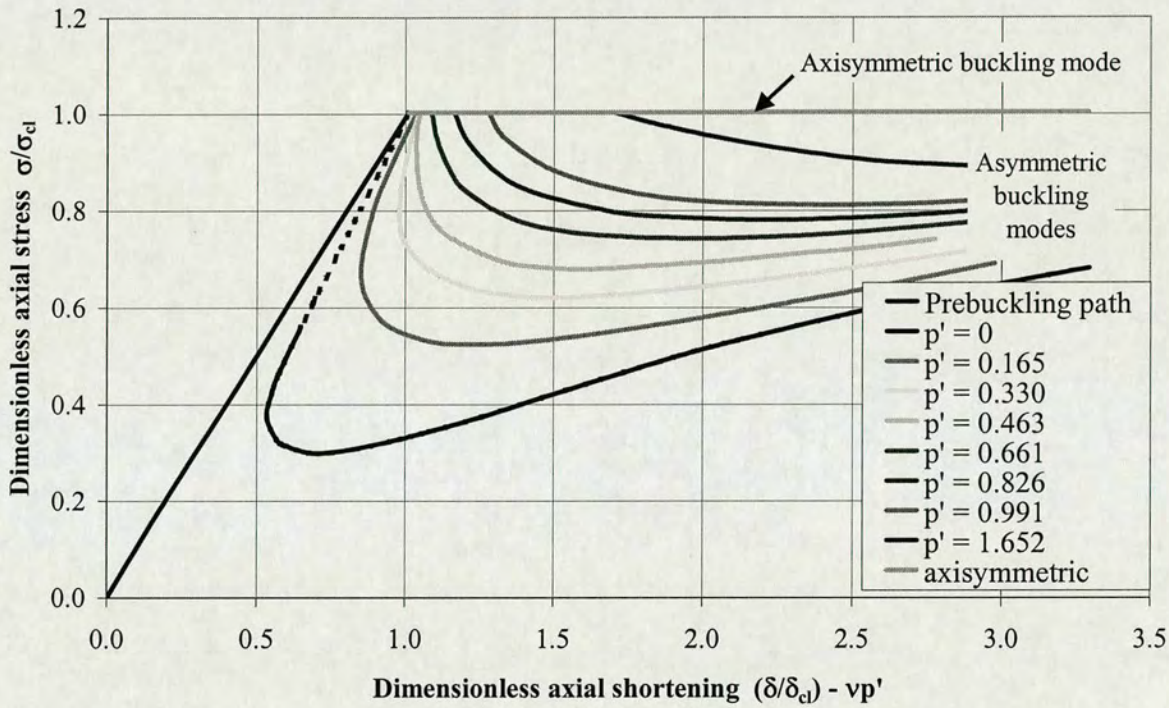

Fig. 1.8 Post-buckling paths of perfect internally pressurised elastic cylinders (after Schnell, 1959)

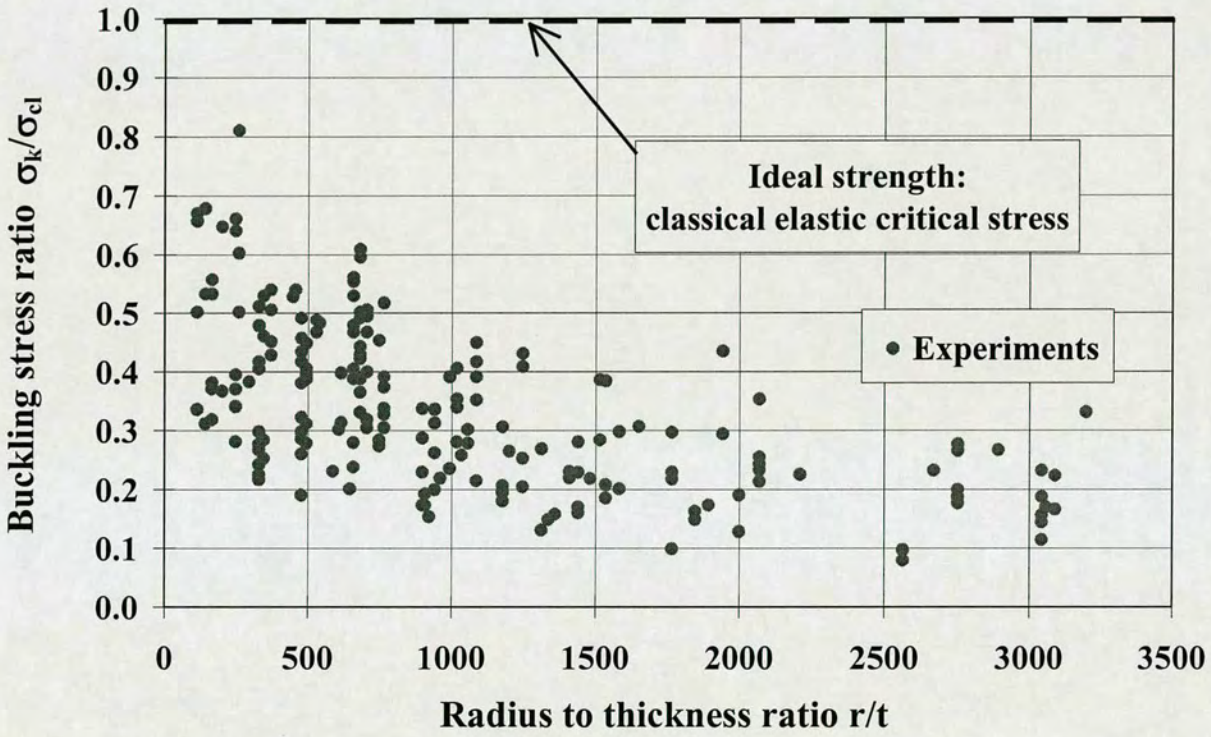

Fig. 1.9 Experimental strength of isotropic axially compressed cylinders (after Harris et al., 1957)

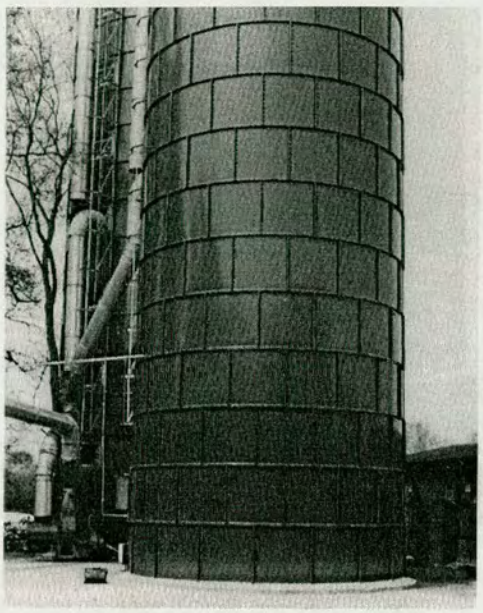

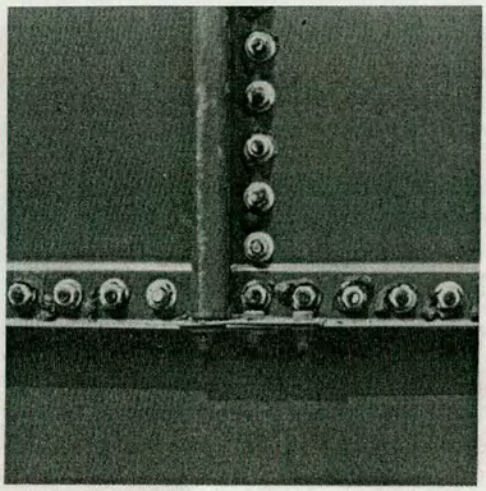

Bild 7.3-26
Aussteifung einer Silowand durch horizontale und vertikale Ab
a) Silo ∅ 5,96 m, h = 19,50 m
b) Detail

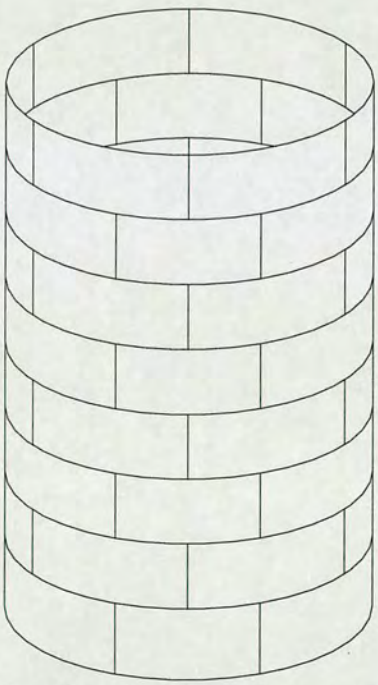

Fig. 1.10 Schematic drawing of plated silo construction (Photos after Martens, 1988)

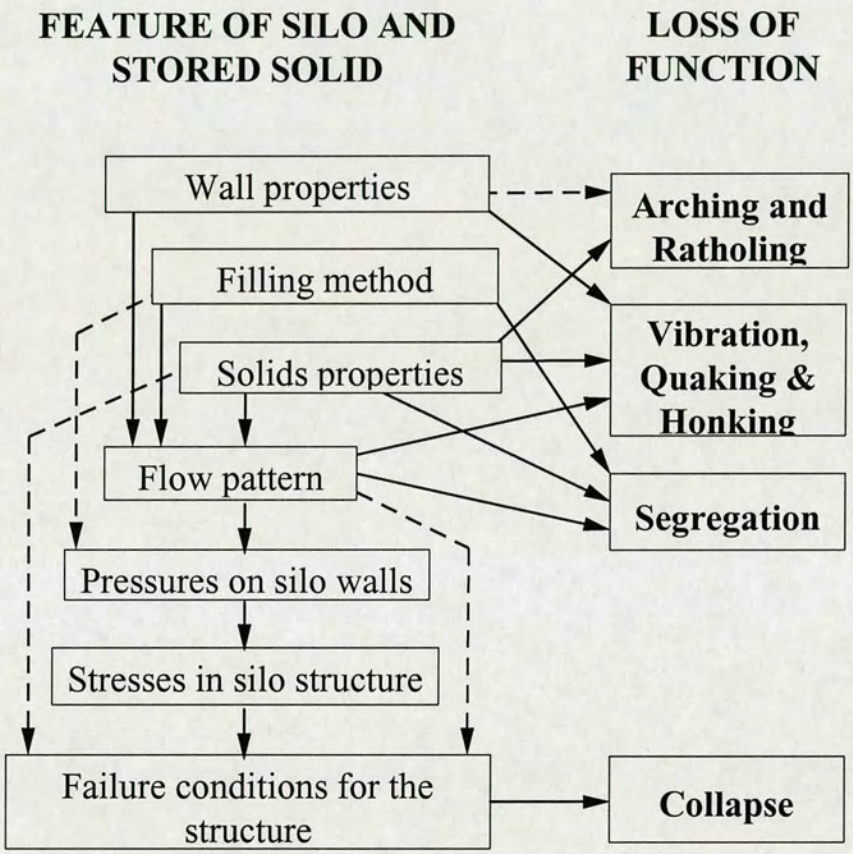

Fig. 1.11 Causes of loss of function in silos (after Rotter, 2001)

Chapter 2

LITERATURE REVIEW – BUCKLING ANALYSIS/THEORY OF THIN CYLINDRICAL SHELLS

2.1 Introduction

This chapter presents a review of current knowledge of the elastic stress states, elastic buckling, plastic collapse and elastic-plastic failure in circular cylindrical shells. The emphasis is put on locally elevated axial compression. Both the research literature and practical design codes are described.

First, the development of the classical theory of shells is outlined and some traditional classical shell theories as well as the extent of their usage are elaborated.

Second, the emphasis is put on the rapid development of this domain in the last fifty years with the application of advanced computing analyses. Different global numerical analyses types, according to the present Eurocode, which are used in the present study, are explained. Information about the ABAQUS package is also presented.

Third, available design criteria are examined carefully and the emphasis is put on the current Eurocode, which is studied later in this thesis. Particular attention is paid to the inadequacies of existing design codes for the loading case of elevated local axial compression.

2.2 Classical Theory of Thin Cylindrical Shells

2.2.1 Euler Formula

The first analysis of the phenomenon of buckling under compression is that of Euler (1757). From the very beginning, Euler's analysis of the elastic stability of slender columns under compressive loading gave the cornerstone to the further development of the theory of buckling of elastic structures with the pattern of inducing eigenvalues and

eigenvectors for the modes. Fig. 2.1 shows the initially straight, uniform column is loaded in compression, between frictionless pins bifurcating at the "Euler" load where EI is the flexural rigidity of the column for bending in the relevant plane and L is the length of the column. P_E (Eqn. (2.1)) appears as the lowest eigen-value for the linearised problem, which is defined as buckling/critical/bifurcation load, and the corresponding eigen-mode is a single half sine wave between the pins.

$$P_E = \pi^2 EI / L^2 \qquad (2.1)$$

The complicated analysis by Euler was well presented in Timoshenko's History of Strength of Materials (Timoshenko, 1953). The classic analysis is based on the assumption that the column is initially perfectly straight, an idealised column in relation to the real. If the column in its unloaded state has an initial crookedness in the form of the lowest eigenmode, the displacements grow progressively and can be represented by Equation 2.2 (Young, 1807).

$$w + w_0 = w_0 / (1 - P / P_E) \qquad (2.2)$$

where:

w_0 is the amplitude of the initial imperfection

w is the amount by which the initial imperfection is enlarged currently by the action of the applied load

P is the current axial compressive load

P_E is the Euler load

Fig. 2.2 illustrates the relationship curve between the load and displacement for the column. The perfect column can reach the classical Euler load (Eqn. (2.1)) without any deformation and then a large deformation occurs while keeping the same load support ability after reaching it. If there is an initial imperfection in column, the deformation increases with the increment of the compressive load if geometric nonlinearity is introduced:

$$(P/P_E)(w+w_0) = w - \beta w^2 \qquad (2.3)$$

where:

β is the parameter for geometric nonlinearity and β=0 if the structure is geometrical linear

When β=0, Eqn. (2.3) is the same as Eqn. (2.2) for the geometrically linear structure. If $\beta \neq 0$, the broken curve in Fig. 2.2 represents Eqn. (2.3), which shows softness of the structure compared with Yong's prediction (Eqn. (2.2)).

2.2.2 Classical Buckling Strength of Shells

During the early twentieth century, the classical analysis of elastic buckling as an eigen-value problem was extended to many examples of two-dimensional flat plates and three-dimensional curved shells. In the field of shell buckling, the classical buckling strength σ_{cl} (Lorenz, 1908; Timoshenko, 1910; Southwell, 1914) for a long perfect elastic cylindrical shell under uniform axial compression is used as a reference value for all analyses:

$$\sigma_{cl} = E\frac{t}{\sqrt{3(1-\nu^2)}R} \cong 0.605E\frac{t}{R} \qquad \text{for } \nu=0.3 \qquad (2.4)$$

Though it is restricted to perfect cylinders, simply supported boundary conditions, a uniform membrane pre-buckling stress state, elastic material domain and no practical boundary condition can reach this value even for the perfect cylinder, it is still the common reference buckling stress for the analysis and generally provides an upper bound for cylinder buckling strengths.

The load-end shortening relationship of a geometrically perfect thin elastic cylinder when axially compressed under uniform compression is shown in Fig. 2.4. Initially, the path of pre-buckling is close to a straight line, but the linear path (with verification from the analyses in Chapter 5) is suddenly terminated as the shell bifurcates into a non-symmetric

mode (Fig. 2.5b), with several full waves of buckling mode around the circumference, and several waves up the height. After buckling, the load falls very sharply (Fig. 2.4), and the cylinder actually increases in length as the displacements normal to the surface grow. The bifurcation load is usually slightly lower than the load found from a linear eigen-value calculation, because non-linearity in the pre-buckling path often leads to additional de-stabilising stresses but not much.

A noteworthy discovery is that there are a large number of different buckling modes having practically the same classical buckling load (a close examination of the analytical solution reveals that there are several hundred modes for which the critical stress is within 15% of the lowest buckling stress when a thin cylindrical shell is loaded in uniform axial compression, and sometimes over 100 modes with loads within 1%). The classical buckling strength σ_{cl} (Lorenz, 1908; Timoshenko, 1910; Southwell, 1914) assumes that the buckling eigenmode has n waves circumferentially and m half-waves longitudinally and provides a critical stress value for each combination of m and n. Many modes are possible in different "chequerboard" patterns (Fig. 2.5b) whose wavelengths in the circumferential and axial directions are related by the "Koiter circle" (Fig. 2.3a; Koiter, 1945; Calladine, 1983). Table 2.1 together with Fig. 2.3 shows the buckling modes for a long, thin, metal cylinder that is simply supported in its cross-section and loaded by a uniformly distributed compressive axial stress at its ends. For small numbers of axial half-waves (m), the critical stress changes rapidly with respect to the number of circumferential lobes (n). However, for higher values of m and n, the critical stresses are not very much higher than the lowest value and do not vary much from mode to mode. The value of n increases with the increment of value of m for the critical stresses close to the classical buckling strength σ_{cl}. This is just a general explanation of the buckling mode and in which kind of mode it does buckle (i.e. which is the minimum buckling strength) depends largely on the thickness, radius, and length of the cylinder as well as boundary conditions.

2.2.3 Buckling/Post-buckling Modes of Shells

When a perfect cylindrical shell is subjected to uniform axial compression, initial buckling can occur in two possible modes (Yamaki, 1984; Calladine, 1995):

•Symmetrical buckling

Symmetrical buckling, which the displacements along the meridional line are in the form of waves while keeping the displacements in any transverse section are constant. This is called "axisymmetric" or "ring buckling" (Fig. 2.5a). This buckling mode is related to a stable post-buckling path, and is later found to be important when the cylinder is pressurised.

•Non-symmetrical buckling

Non-symmetrical buckling, which the displacements along the meridional line are in the form of waves while the displacements in any transverse section also take on the form of waves, this gives a pattern of rectangular depressions and bulges all over the cylinder surface. Many modes are possible in different "chessboard" patterns whose wavelengths in the circumference and axial directions are related by the "Koiter circle" (Koiter, 1945; Calladine, 1983). This is hence called "chessboard" or "checkerboard buckling" (Fig. 2.5b). This buckling mode is related to a steeply falling post-buckling path.

In the post-buckling range, the deformation normal to the shell surface can no longer be regarded as infinitesimal and after having reached the initial buckling load, the cylinder snaps through into another state of equilibrium associated with a small axial load and a different pattern of buckles. This is called "diamond buckling", which is observed quite often in experiments (Fig. 2.5c). As seen from the figure, this is another extension of the chessboard-buckling mode.

2.2.4 "Misleading" Classical Buckling Strength of Shells

All the works described so far followed the assumption: the shell is assumed to be geometrically perfect and the problem of determining the buckling condition is assumed to a classical eigen-value problem. In the 1920s and 1930s, it was discovered that the

buckling strengths of the thin-walled curved panels and tubes in compression were often far less that those predicted by the classical theory (Fig. 1.9). Furthermore, the failures were unstable in the sense that the load-carrying capacity fell sharply after the buckles had appeared. This was a very important discovery (Calladine, 1995).

For the compression members used in engineering, the classical theory works well for columns and flat plates. Cylindrical shells seem to be the only exception. A lot of studies (Koiter, 1945; Ohira, 1961 &1963; Fischer, 1963 & 1965; Hoff, 1965; Hoff & Rehfield, 1965; Hoff & Soong, 1965; Almroth, 1966a; Arbocz & Babcock, 1969; Hutchinson et al., 1971; Amazigo & Budiansky, 1972; Yamaki & Kodama, 1972; Yamaki, 1984; Rotter & Teng, 1989b; Teng & Rotter, 1992) have been performed since 1930s. The following reasons may be responsible for the big difference in behaviour.

•Boundary conditions

Classical theory assumes simple boundary conditions, which are almost impossible to reach in experiments and real construction. It is also significant that clamped boundary conditions for medium length shells do not significantly alter the buckling load, which contrasts strongly with their effects in column buckling. The length of the cylinder also affects the buckling load and the classical solution ignored the influence of the cylinder height and since a relatively long cylinder is a must applying the theory.

The boundary conditions are best classified according to the system devised by Singer and used extensively by Yamaki (1984). There are two different classes of boundary conditions: Simply supported (*S*) and Clamped ends (*C*). The categories of boundary condition are shown in Table 2.3, and relate to the incremental displacements δu, δv, δw and $\delta\beta$ during buckling (Fig. 2.7b).

Where a pinned boundary condition does not restrain circumferential displacements δv during buckling (*S2, S4*), the perfect shell-buckling load falls to about half the classical value (Fig. 2.7a), but loss of restraint of other boundary has a minor effect, which is not a particularly obvious outcome. In addition, partial loss of restraint (eg. δv) will lead to the

loss of the buckling load in-between. Although the boundary conditions can affect the strength of axially compressed cylinders, the strength losses occurring from the boundary conditions are insufficient to be the cause of the very low experimental test results shown in Fig. 1.9.

•Pre-buckling deformation

Where practical restraints are taken into account, local bending due to the restraint of pre-buckling displacements near the ends can lead to a small loss of bifurcation buckling strength from the ideal one (Fig. 2.4). Classical theory assumes a uniform membrane pre-buckling stress state and ignores the pre-buckling deformation of the shell. The end conditions restrain radial displacements in the experiments and since a significant bending near the boundaries occurs as a result of the Poisson expansion of the cylinder. This causes a reduction of between 8% and 15% in the classical critical stress (Yamaki & Kodama, 1972)

•Initial Imperfections

Classical theory is limited to initially perfect cylinders, but clearly no physical cylinder is without imperfection (Fig. 2.8 and $w_0=\delta_0$ (in this study) which represents the imperfection amplitude).

Following the significant advance achievement by Koiter (1945), initial imperfections gradually became accepted as the most damaging factor for the loss of the strength. A lot of studies then attempted to solve the problem and to try to identify which is the worst imperfection form.

Though the worst initial imperfection depends on the loading pattern of the shell, it is widely agreed that an axisymmetric sinusoidal imperfection (Koiter, 1945 & 1963) is the worst, but it is not common in practice. Surveys of imperfection profile in real structures (Ding, 1992; Coleman et al., 1992) cannot easily be interpreted into the FE modelling. Despite these difficulties, a close agreement has been reached that an axisymmetric local imperfection (Amazigo & Budiansky, 1972; Bornscheuer et al., 1983; Rotter & Teng,

1989b; Teng & Rotter, 1992) is the best choice for practical design calculations in relation to full-scale structural measurements (Knoedel and Ummenhofer, 1996). More recent extensions of this concept have led to automated computer analyses (Deml and Wunderlich, 1997; Teng and Song, 2001).

Similarly, Hutchinson, Tennyson and Muggeridge (1971) and Amazigo & Budiansky (1972) also gave some prediction for the buckling strength of imperfect cylindrical shells under the uniform axially loaded cylinder without internal pressure. If the imperfection amplitude is sufficiently small and located not too close to the ends of the cylinders, results show that the lowest buckling load would usually be predicted by the local imperfection and the highest by the analyses among the modal, local and random imperfections. There are fairly good experimental verifications of the asymptotic results for local and random imperfections (Amazigo & Budiansky, 1972).

•Residual stresses

Classical theory is limited to a uniform membrane pre-buckling stress state but there will certainly be residual stresses in real cylinder, which derive from formation of shells (cold bending, finishing, straightening, flame cambering, oxygen cutting, welding, cooling after rolling and misfit of fabrication; Holst et al., 1999).

Among all the possible reasons, the initial imperfections contribute the greatest loss of the buckling strength from the classical buckling strength. This is the reason why initial geometric imperfections are so important in dealing with thin cylindrical shell buckling.

2.2.5 Classical Shell Theory

Some of the classical shell theories are noted in the following summary. No attempt is made to give a full review of the development of analytical theories for circular cylindrical shells, but only the analyses types which are of relevance to the computing analyses types presented afterwards.

•Classical linear bifurcation analysis

This analysis of buckling (Timoshenko & Gere, 1961; Brush & Almroth, 1976) is based on a linear eigenvalue problem using simplified boundary conditions. The pre-buckling stresses and deformations caused by the boundary conditions are ignored during the analyses. The buckling stress is far from the buckling load of a real construction. Nevertheless, it is an important reference value because it can always be calculated. The classical buckling load is normally used as a reference value.

•Classical elastic large deflection analysis

This analysis (Budiansky, 1959) adopts geometric non-linearity as well as the material linearity in analyses especially for the buckling strength of shallow spherical caps under pressure.

•Classical elastic-plastic small deflection analysis

The solution (Ilyushin, 1943, 1944; Hodge, 1956; Tsurkov, 1956, 1961; Klement, 1962) adopts geometric linearity as well as the material non-linearity in analyses. It leads to the plastic limit load of a structure, but can sometimes be difficult to perform.

• Classical elastic-plastic large deflection analysis

The solution (Roth, 1961; Hayes & Lee, 1970; Murphy & Lee, 1971) adopts both geometric non-linearity and material non-linearity in analyses.

• Post-buckling behaviour with geometric imperfection sensitivity

These studies (Koiter, 1945, 1963; Hutchinson, 1967; Budiansky, 1969; Amazigo & Budiansky, 1972; Budiansky & Hutchinson, 1972) process the post-buckling behaviour and imperfection sensitivity using large deflection analyses of elastic shells.

2.2.6 Cylindrical Shell Buckling under Axial Compression

This part will focus on the shell wall buckling under axial compression, especially in the area of partial axial compression, which is intensively studied in this thesis.

Cylindrical shell structures are often subjected to compressive stresses in the direction of the cylinder axis, which can be either uniform or varying throughout the cylinder. The buckling strength of a thin cylindrical shell under axial compression is particularly sensitive to imperfections in the shell, and the changing patterns of behaviour with changing geometry, loading and boundary conditions make the axially compressed cylinder a classical exemplar for behaviours that may be found in a less marked form in other structures or in shells under other loading conditions. For these reasons, the axially compressed cylinder has probably been the most extensively studied of all shell buckling conditions, giving a wealth of evidence from both experimental and theoretical work.

Many studies have explored different aspects of the buckling and post-buckling behaviour of these shells (see Timoshenko, 1936; Flugge, 1973; Brush and Almroth, 1975; Arbocz, 1983; Calladine, 1983; Yamaki, 1984; Bushnell, 1985; Teng, 1996). The complete description is the very comprehensive work of Yamaki (1984).

From the description of all the above theories in the classical way, many of the theoretical solutions can tackle shell problems though most of them are limited to very simple geometries, loading patterns and boundary conditions with less interest in the design of real constructions.

Moreover recent silo loading experimental (Pieper, 1969; Nielsen, 1983; Ooi et al., 1990) and theoretical (in both axial direction (Nanninga, 1956; Jenike et al., 1973; Walker, 1966; Walters, 1973; Rotter, 1986b; Rotter, 1998) and circumferential direction (Ooi and She, 1997)) observations show significant deviations from this classical theory, which contribute to the unsymmetrical loads on silo walls even under carefully symmetrical filling. Unsymmetrical loads on silo walls lead to local high axial compression (Rotter, 1986a; Rotter, 1998). The shell buckling strength under an axial compression (Fig. 2.6) that acts over only a part of the circumference (a typical unsymmetrical load on silo walls) may be significantly changed, but the problem has been scarcely pointed out (Rotter, 1986a; Rotter, 1986b; Ansourian, 1992; Rotter, 1997). Furthermore, the mathematics of formal algebraic solution of the governing equations is so unmanageable

that numerical analyses must dominate the field (Rotter, 2002). A more sophisticated approach is needed to deal with the above problem and this is the aim of this study.

2.3 Computer Based Analysis of Thin Cylindrical Shells

2.3.1 Introduction

The buckling analysis of the cylindrical shell has become a critical problem since the beginning of the last century and more attention has been paid after the awkward discovery of the deficiency of previous theory in 1930s. Only rough approximations were obtained owing to the excessive complexity of the problem. The geometric and material non-linearities are both very difficult to apply in classical techniques. Realistic stability and collapse analyses with geometric and material non-linearity influences as well as different loading pattern are very difficult to perform using the classical techniques pointed above. Because of the complexity of the problems in shells, more and more reliance is put on the application of advanced high-speed computer analyses especially with the advent of the more and more powerful computers from 1960s. Finite element and finite difference are the main trends developing in this area.

Only finite element analysis is discussed in the following due to its versatility. The finite element analysis package ABAQUS (HKS, 1998) is adopted in all analyses of this study. The following items: linear elastic shell analysis (LA/LEA), geometrically non-linear elastic analysis (GNA), materially non-linear analysis (MNA), geometrically and materially non-linear analysis (GMNA), geometrically non-linear elastic analysis with imperfections (GNIA), geometrically and materially non-linear analysis with imperfections (GMNIA) are reviewed according to the current Eurocode (ENV 1993-1-6, 1999; Table 2.2).

2.3.2 Different Analyses Types Based on Computing

The following analyses types according to present Eurocode (ENV 1993-1-6, 1999), which are based on computing are presented in detail.

2.3.2.1 Linear Elastic Shell Analysis (LA/LEA)

The elastic buckling analysis of a perfect shell with the assumption of small deflections is termed LA (Fig. 2.10). The linear elastic eigen-value analysis (LEA), based on LA stresses, is classed as part of the LA analysis, accurately determines the elastic critical load R_{cr} (Fig. 2.10). This is an important reference load for all analyses, since it is required in the formal definition of slenderness needed to interpret the results of other analyses and to finalise the design buckling load (Fig. 2.9). Linear bending and membrane shell theory is adopted. This critical load depends on the membrane stress and is unaffected by bending stress. Linear eigenvalue analysis cannot detect snap through buckling, so cautionary notes are given concerning problems where snap-through phenomena are known to occur.

2.3.2.2 Geometrically Non-linear Elastic Analysis (GNA)

The elastic buckling analysis of a perfect shell with the assumption of large deflection is termed GNA (Fig. 2.10). It is needed to detect elastic snap-though buckling (elastic limit loads) and is also useful for non-linear load path. It can still interpret the elastic critical buckling load R_{cr}, but it is less useful than the LA/LEA results because of the adoption of geometric non-linearity in pre-buckling state for a linear critical buckling load.

2.3.2.3 Materially Non-linear Analysis (MNA)

The plastic collapse analysis of a perfect shell with the assumption of small deflections is termed MNA (Fig. 2.10). Geometrical linearity and material non-linearity are included in the analysis. It is needed to obtain the plastic limit load. This load is treated as the reference load R_{pl}, which is needed for the definition of slenderness aiming for the characteristic elastic-plastic buckling load (Fig. 2.9) and the plateau in Fig. 2.12 (Rotter, 2002).

2.3.2.4 Geometrically and Materially Non-linear Analysis (GMNA)

The plastic collapse analysis of a perfect shell with the assumption of large deflections is termed GMNA (Fig. 2.11). Geometrical and material non-linearity is included in the analysis and it provides a good prediction for the strength of perfect structures or the structures that are not imperfection sensitive.

2.3.2.5 Geometrically Non-linear Elastic Analysis with Imperfections (GNIA)

The elastic buckling analysis of an imperfect shell with the assumption of large deflections is termed GNIA. Geometrical non-linearity is included in the analysis with the emphasis on imperfection influence. Thus the difficulty for this analysis is on the appropriate mode of the imperfection in the analysis as well as the need for a whole series of calculations with different imperfection amplitudes.

2.3.2.6 Geometrically and Materially Non-linear Analysis with Imperfections (GMNIA)

The plastic collapse analysis of an imperfect shell with the assumption of large deflections is termed GMNIA (Fig. 2.11). Geometrical and material non-linearity is included in the analysis with the emphasis on imperfection influence. The same difficulty arises as in GNIA for the imperfection profile.

2.3.3 ABAQUS Finite Element Analysis Package

HKS develops and supports the ABAQUS suite of general-purpose, non-linear finite element analysis (FEA) programs, which is used worldwide for stress, heat transfer, and other types of analyses in mechanical, structural, civil, biomedical, and related engineering applications. The theoretical formulation of ABAQUS is based on the finite element stiffness method. It is a comprehensive, general-purpose finite element analysis product.

ABAQUS/Standard uses a high-performance, parallel, sparse, multi-front equation solver to solve both symmetric and unsymmetrical systems of equations and automatically uses the unsymmetrical solution scheme when the physics of a problem demands it. For eigen-value problems ABAQUS/Standard uses a Lanczos eigen-solver that is designed for efficiency in large models. In non-linear problems the challenge is to provide a converged solution at minimum cost. This challenge is addressed by automatic control of the time incrementation, which is provided for all relevant analyses procedures. The user defines a "step" (a portion of the analysis history, such as a thermal transient, a stage in a manufacturing process, or a dynamic event), ABAQUS/Standard then automatically selects the convergence tolerances and the increments required for the step. This

approach is highly effective for nonlinear problems because the model's response may change drastically during an analysis step. Automatic control allows nonlinear problems to be run with confidence without extensive experience with the problem. This capability is a good example of the many features in ABAQUS/Standard that make it a production-oriented analysis tool and distinguishes it from other finite element programs.

ABAQUS/Standard Version 5.8 was used in all analyses within this study from the very beginning. The version was updated frequently but the format of the input files still keeps continuity, which make the old version possible to run on the current version. Analyses of several types were performed for the uniform axial compression and elevated local axial compression stresses: Linear stress analyses, linear elastic shell analysis (LA/LEA), geometrically non-linear elastic analysis (GNA), materially non-linear analysis (MNA), geometrically and materially non-linear analysis (GMNA), geometrically non-linear elastic analysis with imperfection (GNIA), geometrically and materially non-linear analysis with imperfections (GMNIA) (ENV 1993-1-6, 1999; Table 2.2). The eigenvalue extraction method was adopted in the linear bifurcation analysis (LEA) and the modified Riks method (Riks, 1979) was used in the non-linear analyses. All descriptions of the geometry modelling, material property and boundary conditions were presented in each of analyses details where the problem involved.

2.4 Structural Design of Metal Silos

For the purpose of the study, only present Eurocode (ENV 1993-1-6 & ENV 1993-4-1, 1999) is discussed here detail.

2.4.1 Membrane Theory of Shells

The membrane theory of shells has been widely used to analyse and design most smaller and medium silos in the past. It is generally adequate for design under symmetrical conditions, though the local bending effects, which occur in many places, cannot be evaluated except for special geometries where the effective sections method set out in Section 5.3.2.4 (ENV 1993-4-1) may apply. Under unsymmetrical conditions, the results of membrane theory analyses are indicative of behaviour, but they give a poor measure of real stress states except under special conditions, such as very smoothly varying

pressures. In view of the increasing awareness of unsymmetrical conditions in most silos, membrane theory should be used with some caution. A full description of the use of membrane theory for silo analyses, with many useful equations, was given by Rotter (Rotter, 1987a).

In smaller silos, the local bending effects can often be accounted for using strength assessment techniques, which include local bending without explicitly evaluating it.

2.4.2 Bending Theory of Shells

Problems (e.g. un-symmetric or local loads and discontinuities), in which local bending occurs, call for the use of the bending theory of shells. However, such an analysis undertaken by hand is very onerous (solving the coupled 4th order partial differential equations and interpretation of these results into limit state is not easy because that very high local bending stresses may/may not influence the buckling strength much if either equilibrium or boundary conditions are met). A fuller description with many useful equations is given by Rotter again (Rotter, 1987b).

2.4.3 Other Analyses Types on Computing

Other analyses types according to the code are given by the finite element analysis based on computing. Their application and content have been presented in the previous part on the computer analyses of thin cylindrical shells.

It should be recognised that such finite element analyses are difficult to perform and the results can depend strongly on assumptions made in the modelling and load path controlling parameters. Care should be taken with the following points (Rotter, 2002):

A. The shell analysis mesh should be designed with proper regard to local shell bending phenomena (several elements in each bending half wavelength near boundaries and discontinuities).
B. The analysis should be undertaken by an engineer with experience in shell finite element analysis.
C. High local bending stresses, which develop may be caused by either equilibrium phenomena or compatibility phenomena. It is not easy to distinguish between the

two, but bending stresses arising from equilibrium requirements are a serious design constraint, whilst those arising from local compatibility conditions are generally less important. Care should be taken to identify the significance of local bending stresses.

2.5 Summary

A brief review was presented of the current knowledge of thin cylindrical shell theory. The classical theory and modern analyses types based on the computing were all described with reference to the shell compression especially for the local axial compression, which is the aim of the whole study. The current Eurocode for the shell design was discussed afterwards.

Cylindrical shell structures are often subjected to non-symmetric loading as a result of eccentric filling, discharging, earthquake, wind, discrete column supports, local foundation settlement and other causes. So non-symmetric loading plays a vital role in the analyses of the shell structures.

Because industrial metal silos and tanks are frequently constructed from a set of curved panels or plates, the seam between different plates and lack of fit between plates becomes a major factor of the imperfection of the shell. The circumferential weld depression may therefore be considered to be a dominant design-relevant imperfection form for silos constructed industrially. Its effect is very serious, and an imperfection with amplitude of just one wall thickness can reduce the buckling load to just 30% of the classical value (Rotter and Teng, 1989b; Teng and Rotter, 1992; Berry, 1997).

The importance of the study examining the effect of geometric imperfections on shells subjected to non-uniform stress states is obvious. However, those classical shell theories, which most of the designers rely on, have so many limitations in application and sometimes far away from that of the real conditions. At the same time, the powerful numerical methods based on computing have little impact on silo designers. It is aim of

this study to provide a bridge — a rigorous set of recommendations from the FE shell analyses, which can be implemented in future design codes.

The following chapter will discuss the problem of this study: shell-buckling behaviour under elevated local axial compression stresses.

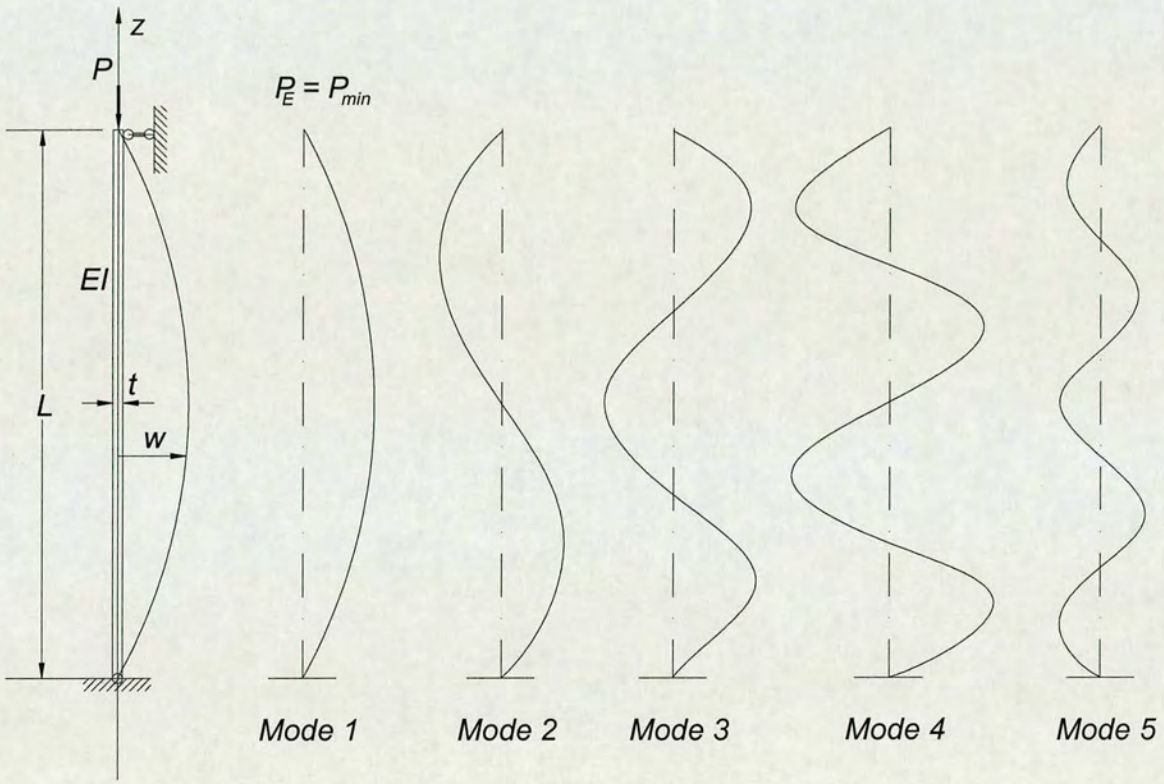

Fig. 2.1 Buckling modes of a column under compression

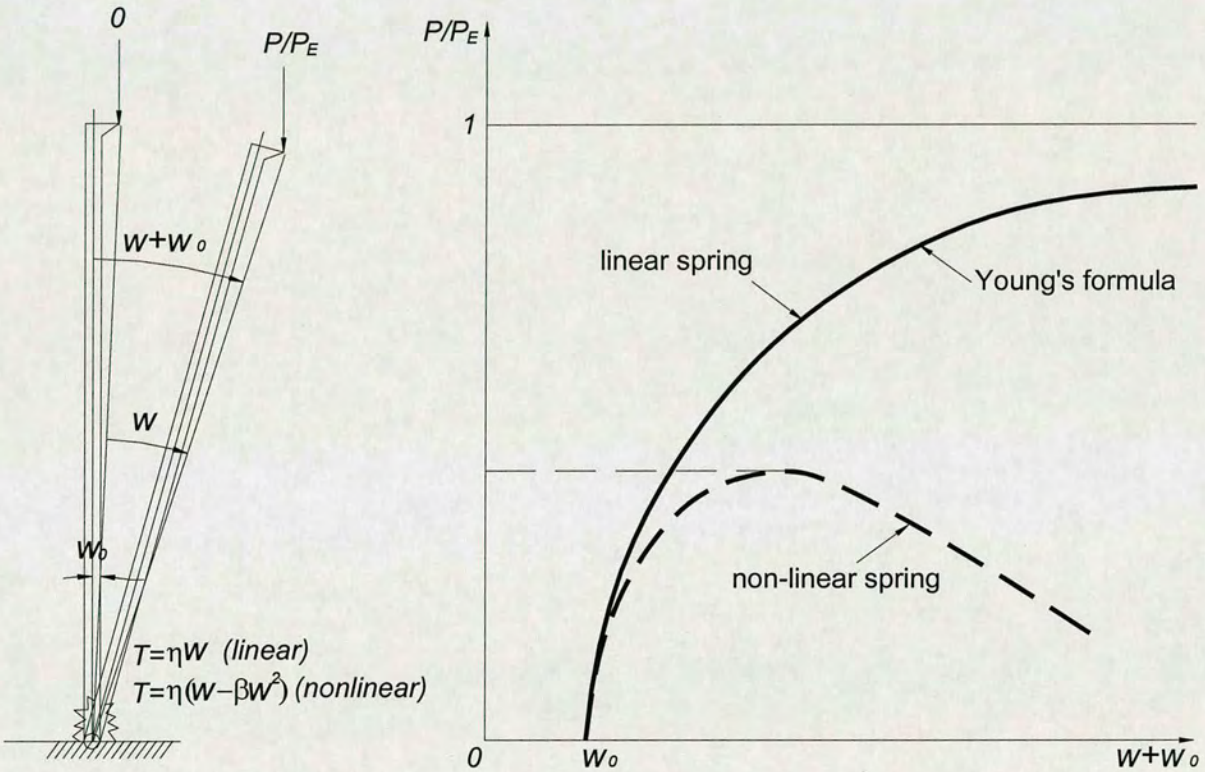

Fig. 2.2 Load-displacement plot (after Calladine, 1995)

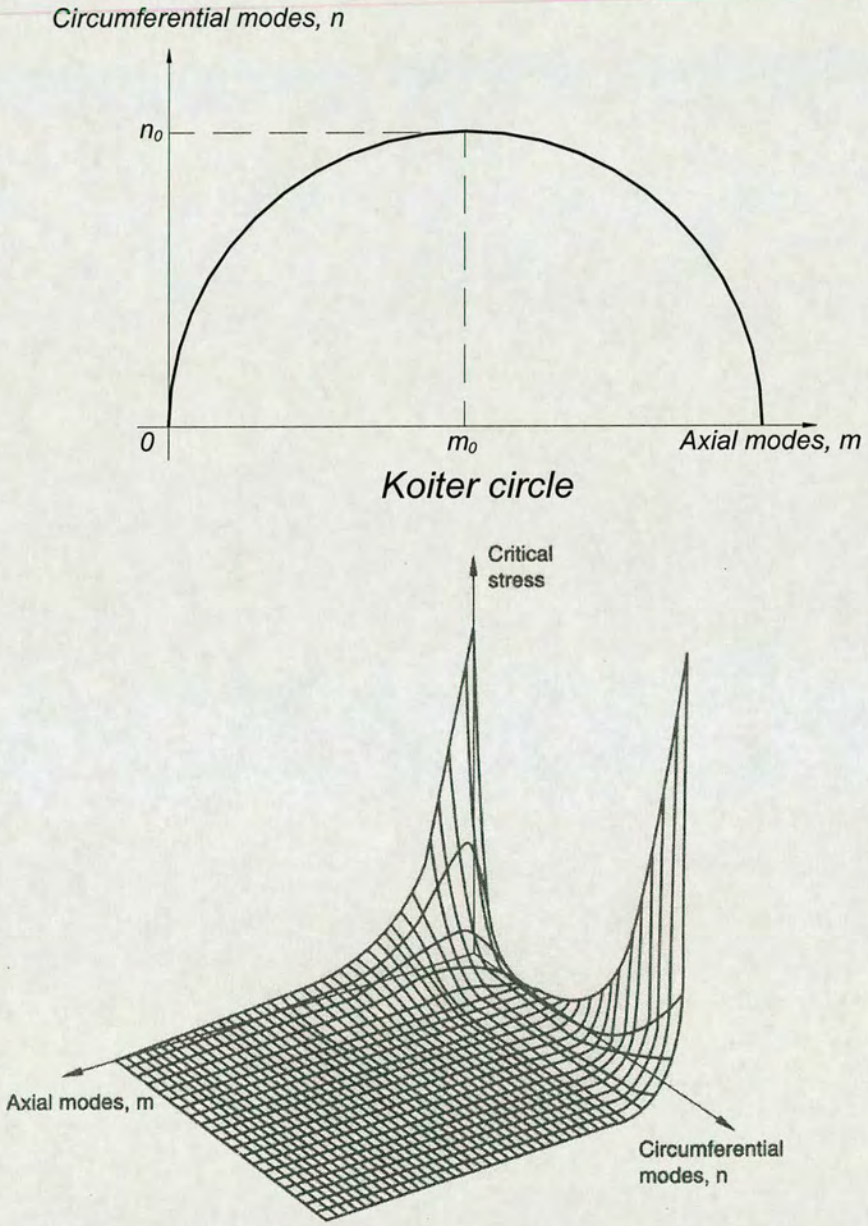

Fig. 2.3 Koiter circle and critical stress for various buckling modes (after HKS, 1998)

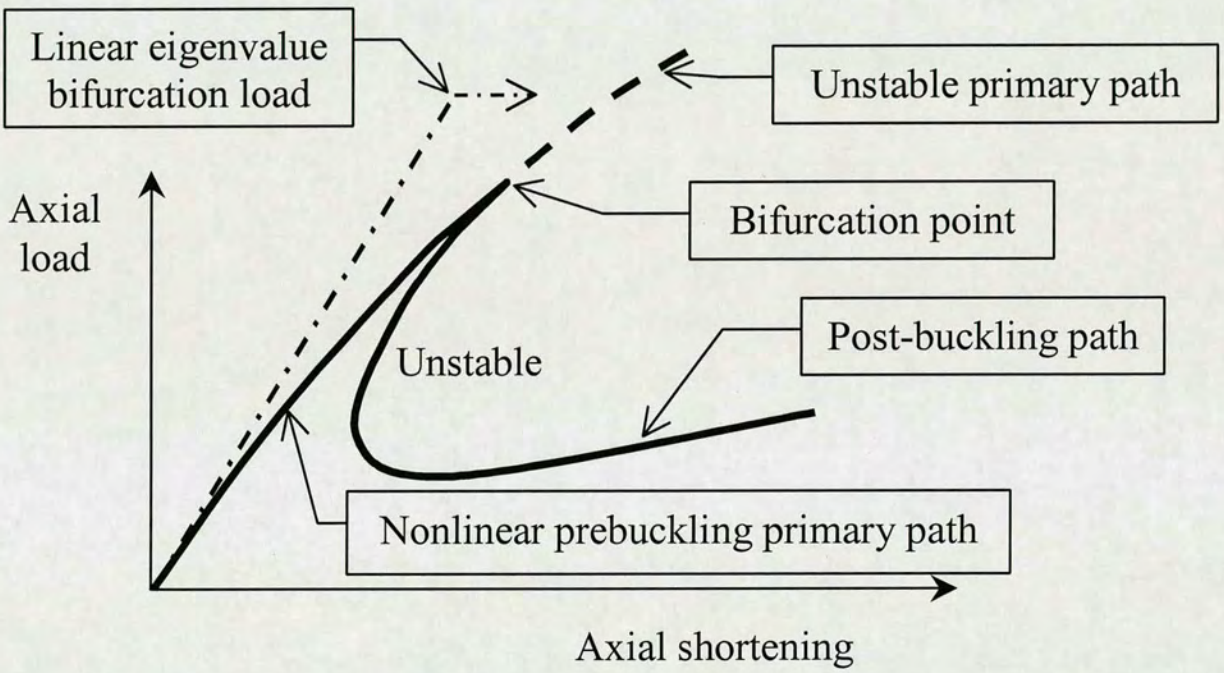

Fig. 2.4 Typical load-end shortening relationship for axially compressed cylinder (after Rotter, 2001)

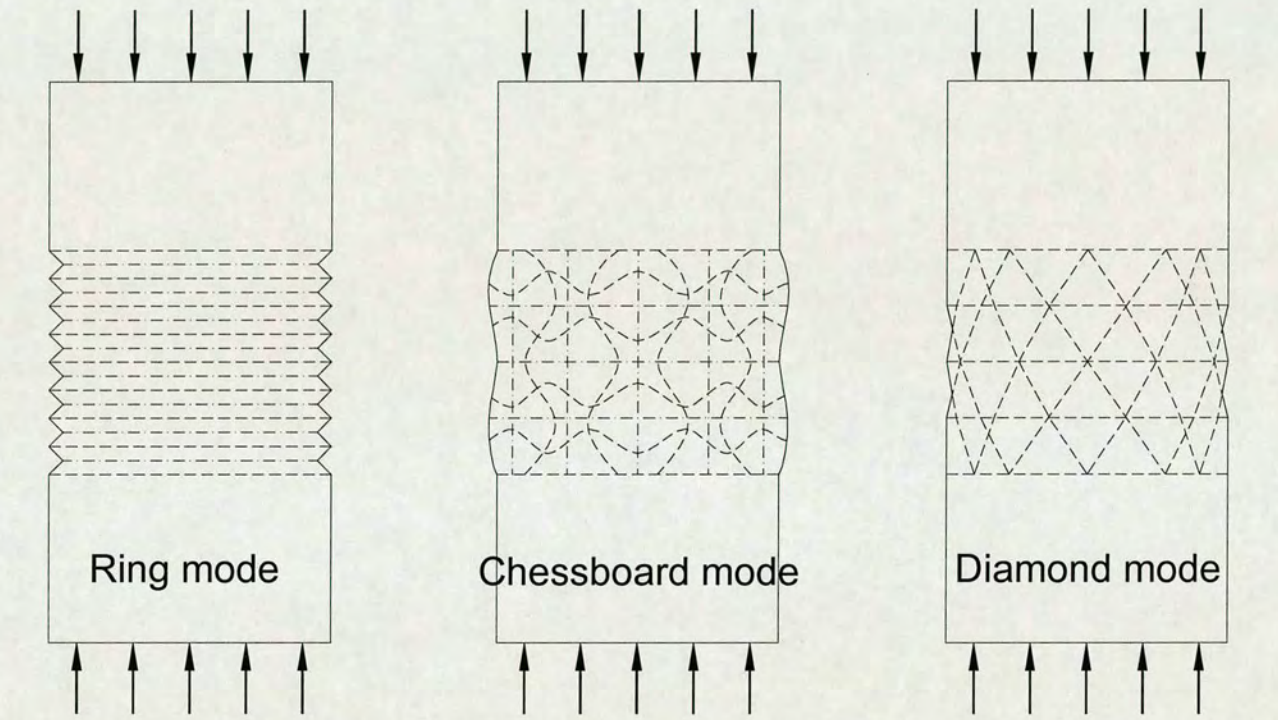

Fig. 2.5 Typical buckling modes for axially compressed perfect cylinders

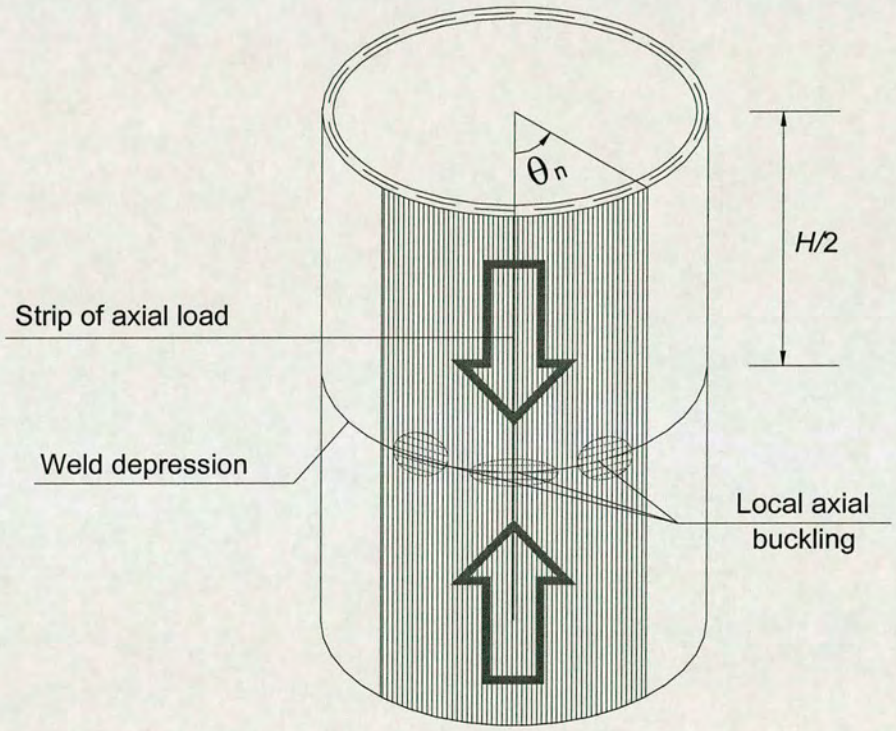

Fig. 2.6 Cylindrical shell under local axial compression

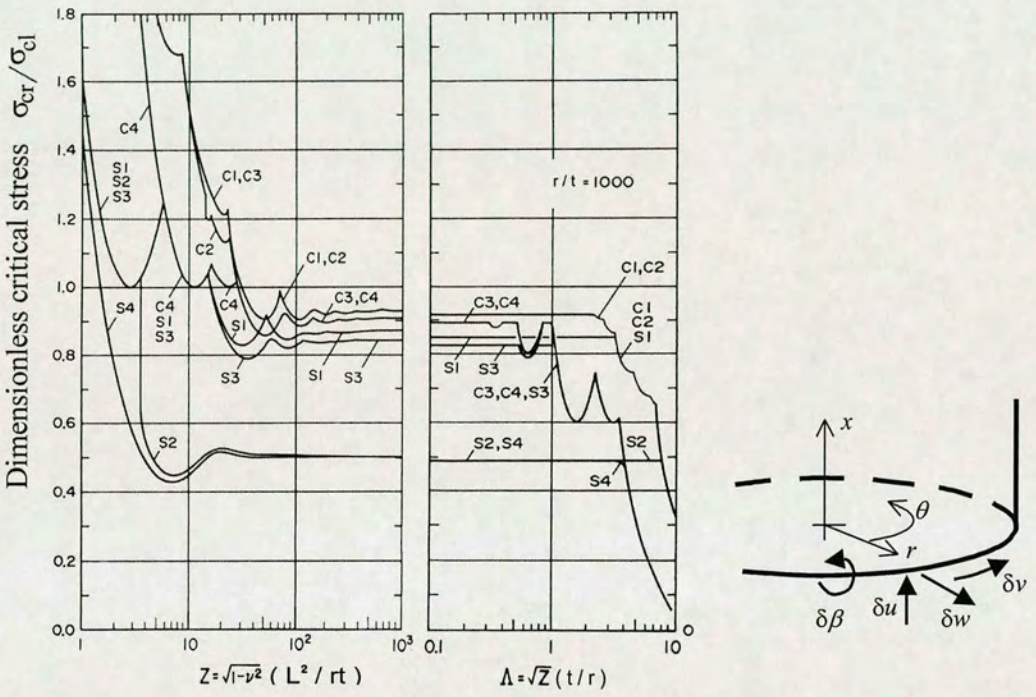

a) perfect cylinder buckling strengths

b) boundary displacements

Fig. 2.7 Effect of boundary conditions and shell length on perfect shell buckling load (after Yamaki, 1984; Figure from Rotter, 2002)

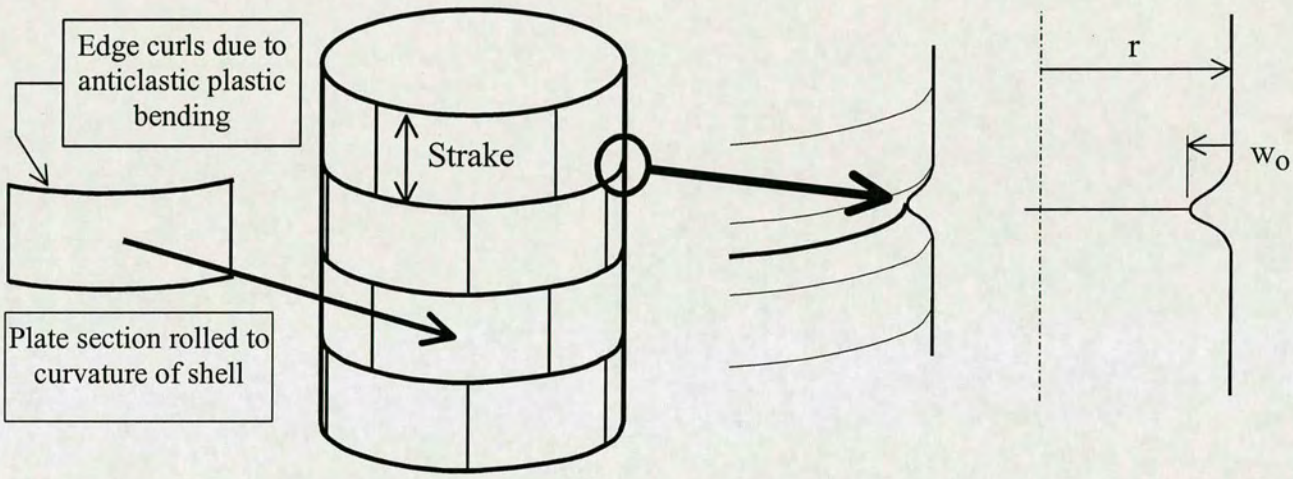

Fig. 2.8 Typical fabrication technique for civil engineering cylinders (after Rotter, 2002)

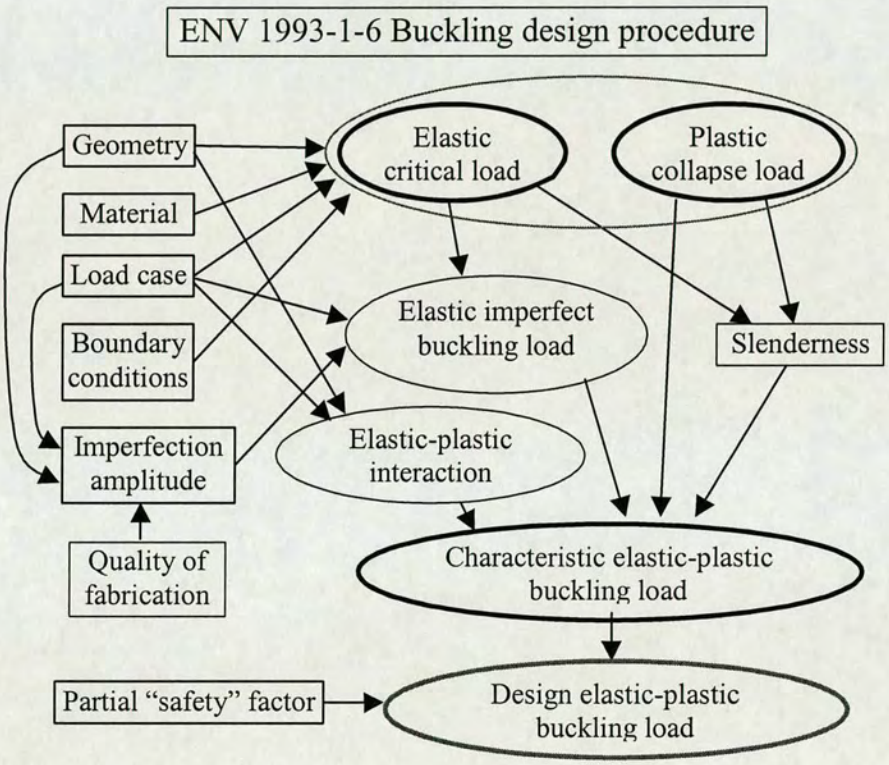

Fig. 2.9 Calculation concepts and the route to design strength (after Rotter, 2002)

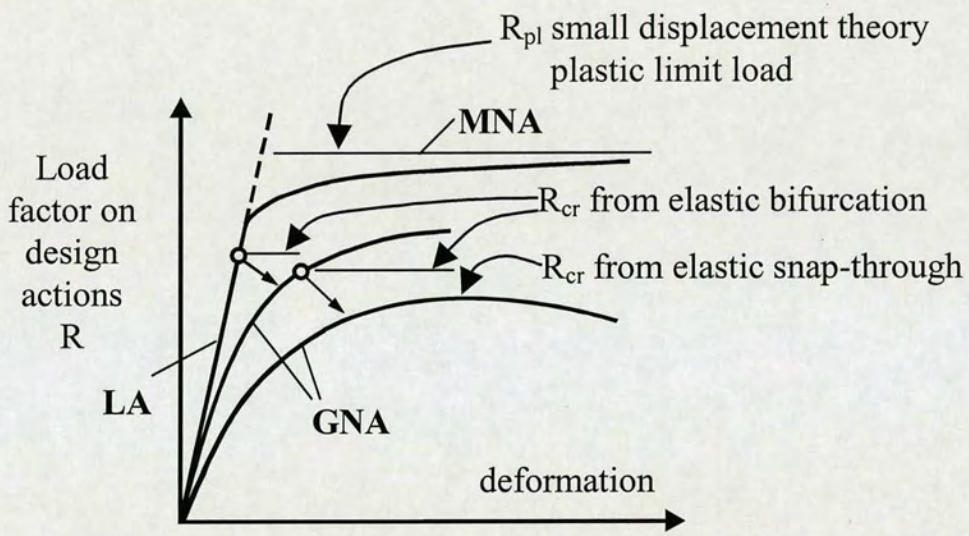

Fig. 2.10 Calculated load-displacement paths for LA, LEA, MNA and GNA analyses (after Rotter, 2002)

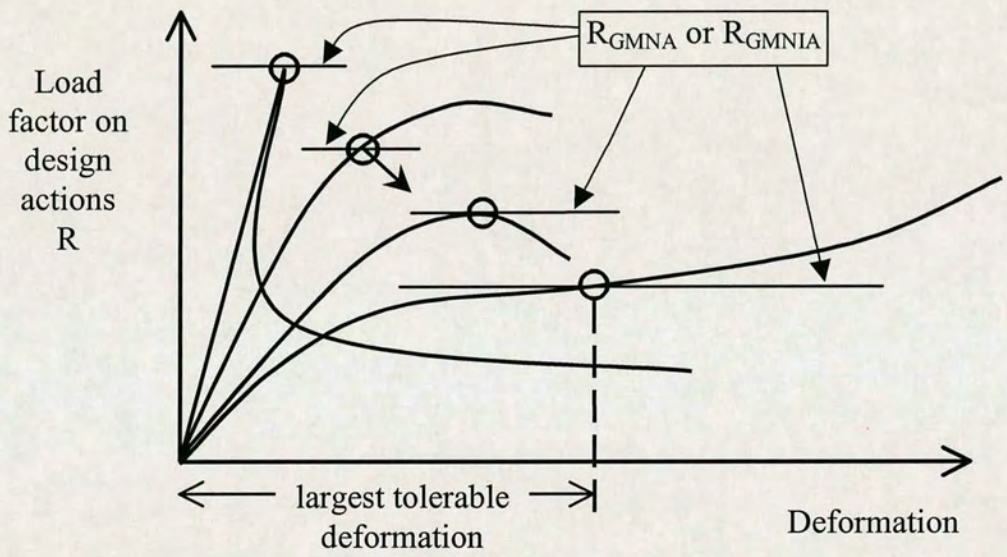

Fig. 2.11 Criteria of failure for GMNA and GMNIA analyses (after Rotter, 2002)

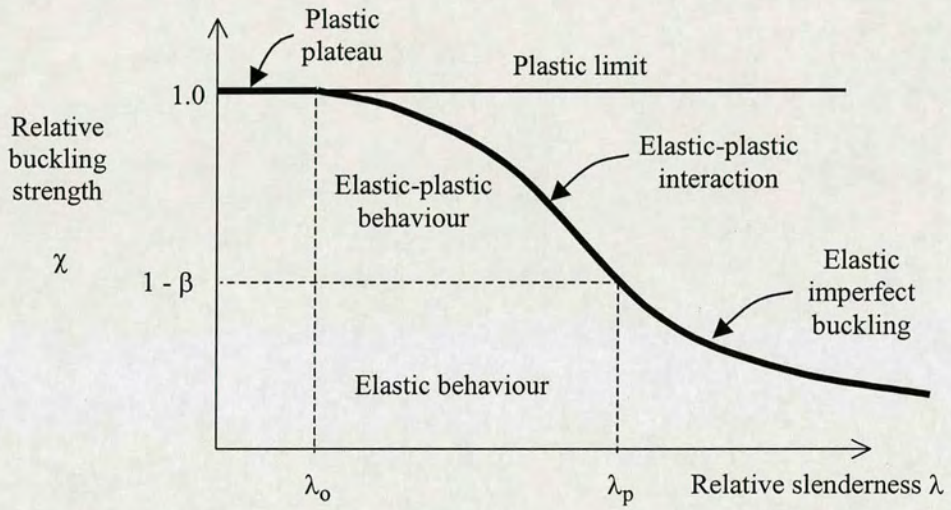

Fig. 2.12 Shell buckling capacity curve: generic form (after Rotter, 2002)

n m	1	2	3	4	5
0	**75.080**	**64.290**	**51.860**	**40.810**	**32.040**
1	**116.700**	**24.450**	**27.840**	**26.250**	**23.050**
2	**1.478**	**4.741**	**7.832**	**9.769**	**10.530**
3	**0.388**	**1.251**	**2.389**	**3.478**	**4.331**
4	**0.281**	**0.478**	**0.913**	**1.417**	**1.908**
5	**0.479**	**0.298**	**0.449**	**0.681**	**0.942**
6	**0.946**	**0.329**	**0.309**	**0.401**	**0.533**
7	**1.757**	**0.495**	**0.314**	**0.308**	**0.360**
8	**3.022**	**0.794**	**0.414**	**0.316**	**0.305**
9	**4.875**	**1.251**	**0.510**	**0.394**	**0.322**
10	**7.473**	**1.898**	**0.878**	**0.537**	**0.395**

n m	6	7	8	9	10
0	**25.370**	**20.360**	**16.590**	**13.710**	**11.480**
1	**19.680**	**16.650**	**14.100**	**11.990**	**10.270**
2	**10.470**	**9.941**	**9.190**	**8.376**	**7.577**
3	**4.886**	**5.165**	**5.228**	**5.136**	**4.945**
4	**2.328**	**2.654**	**2.878**	**3.010**	**3.064**
5	**1.197**	**1.430**	**1.625**	**1.778**	**1.888**
6	**0.680**	**0.827**	**0.966**	**1.089**	**1.191**
7	**0.437**	**0.525**	**0.616**	**0.702**	**0.782**
8	**0.332**	**0.377**	**0.431**	**0.487**	**0.544**
9	**0.305**	**0.315**	**0.339**	**0.372**	**0.407**
10	**0.333**	**0.310**	**0.305**	**0.318**	**0.336**

Table 2.1 Critical stresses versus mode shape, stresses given in GPa (after Timoshenko & Gere, 1961)

Type of analysis	Term	Shell theory	Material law	Shell geometry
Membrane theory of shells		membrane equilibrium	not applicable	perfect
Linear elastic shell analysis	LA	linear bending and stretching	linear	perfect
Geometrically non-linear elastic analysis	GNA	non-linear	linear	perfect
Materially non-linear analysis	MNA	linear	non-linear	perfect
Geometrically and materially non-linear analysis	GMNA	non-linear	non-linear	perfect
Geometrically non-linear elastic analysis with imperfections	GNIA	non-linear	linear	imperfect
Geometrically and materially non-linear analysis with imperfections	GMNIA	non-linear	non-linear	imperfect

Table 2.2 Structural analyses types

Name	δu	δv	δw	$\delta \beta$
S1	r	r	r	f
S2	r	f	r	f
S3	f	r	r	f
S4	f	f	r	f

Name	δu	δv	δw	$\delta \beta$
C1	r	r	r	r
C2	r	f	r	r
C3	f	r	r	r
C4	f	f	r	r

f = free to displace during buckling

r = restrained displacement during buckling

Table 2.3 Boundary condition terminology for cylindrical shells (see Fig. 2.7 b)

Chapter 3

PROBLEM SPECIFICATION

3.1 Introduction

3.1.1 Janssen Theory and its Deficiency

It is well known that the pressure exerted by stored bulk solid walls after filling are closely predicted by the Janssen theory (Fig. 3.1, Janssen, 1895) which can be expressed as (Rotter, 2001b):

$$p_{hf} = p_{h0}(1 - e^{-z/z_0}) \tag{3.1}$$

$$p_{wf} = \mu p_{hf} = \mu p_{h0}(1 - e^{-z/z_0}) \tag{3.2}$$

in which:

$$p_{h0} = \frac{\gamma}{\mu}\frac{A}{U} = \frac{\gamma}{\mu}\frac{r}{2} \text{ (wall pressure at infinite depth)} \tag{3.3}$$

$$z_0 = \frac{1}{\lambda\mu}\frac{A}{U} = \frac{1}{\lambda\mu}\frac{r}{2} \text{ (Janssen reference depth)} \tag{3.4}$$

where:

- A is the plan cross-sectional area of the barrel section
- U is the plan cross-sectional perimeter of the barrel section
- r is the circular silo radius
- z is the distance below the equivalent surface of the solid at maximum filling height (full condition; Figs. 3.1 & 3.2)
- γ is the characteristic value of the solid unit weight
- μ is the wall friction coefficient for the barrel section, and
- λ is the lateral pressure ratio (ratio between horizontal stress and mean vertical stress in the stored solid)

Almost all the theories and empirical approximations for predicting pressures on silo walls assume perfect silo geometry with homogeneous isotropic stored solid behaviour. This consequently predicts wall pressures, which do not vary around the circumference at a given height. However, more and more recent experimental and theoretical observations show significant meridional and circumferential deviations from the classical theory (Figs. 1.6 & 1.7) especially in filling and discharging processes, which induce extra high membrane stresses in steel silos.

No silo design code that deals with randomly occurring unsymmetrical pressure until the latest draft Eurocode (EN 1991-4, 2002). The pressures specified there follow the form defined with reference to the parameters shown in Fig. 3.2. The pressures on silo wall are defined in terms of a "fixed load" and a "free load". The fixed load means one, which is simply placed in its defined location. The free load is to be placed at any point on silo wall, notably where it is deemed to be most damaging to silo. The fixed load corresponds to traditional views of Janssen filling pressures in silos; the free load or "patch load" is a measure to ensure that the unavoidable unsymmetrical loads, which occur in all silos, are taken into account in the design. A patch of local pressure is to be applied to silo barrel (Fig. 3.3), and increased in magnitude when the filling or discharging is eccentric (Fig. 3.2). The patch pressure consists only of a normal pressure on silo wall, and all consequent changes in wall frictional traction are ignored in this design approximation. Though it is not straightforward to place the patch load according to the real loading and there is ignorance of the related change of the vertical stresses, it provides a first step into this content in silo design codes.

3.1.2 Problems with Non-uniform Axial Stresses

Cylindrical shells are subject to vertical stresses in their walls as a consequence of friction between the stored solid and the wall. It is well known that shell buckling under axial compression is normally the controlling design consideration especially for steel silo walls. Both frictional drag of the granular solid against the wall and unsymmetrical pressure cause axial compression to develop in a silo. As a result, the axial non-uniform stresses are unavoidable to the existing cylindrical shell constructions. This also gives rise to the commonest failure mode of silos in service — buckling.

The importance of the shell wall in silo construction was presented before. In practice, cylindrical shell has to sustain all the possible external loads applied to a silo in service. As discussed in Chapter 1, many different loading conditions are likely to occur. Among them, local loadings may arise from eccentric filling or discharging and attachments such as the local discrete supports and lugs, leading to local high stresses, which cannot be neglected in design.

The first attempt was taken by Bijlaard (1954, 1955) and the Donnell shell equations were used to find the displacements. The membrane and bending stresses were induced by both radial and circumferential loads as well as the external moments (represented by non-uniform pressure) in horizontal axis cylindrical pressure vessels. The shell itself was simply supported at both ends. A double-Fourier series technique was used in the study. However, axial compression was excluded in his studies though in an elevated silo, the discrete supports locally affixed to the shell wall transmit large longitudinal loads to the shell, inducing high stresses near the attached areas. The unsymmetrical filling or discharging procedure can also introduce high local axial stress. Therefore, the pattern of stresses caused by local axial loads in cylindrical shells and its influence on the buckling load needs further investigation.

Because of the limitation of the loading cases, Bijlaard (1954; 1955) and Li (1994) deduced algebraic analysis of cylindrical shells under axial local loading by using a double Fourier series technique. General formulas for the displacements induced by local

loads were derived. The boundary conditions were taken as simply supported at both ends. The corresponding expressions for stress resultants (resultant forces and bending and twisting moments) were obtained from the constitutive relations. It is a good attempt to the analysis on local buckling, though a systematic parametric study on this is needed to implement the blank of knowledge in this area. Furthermore, with the latest development of the finite element method, a more accurate result can be expected. This is the main motivation of doing this research.

3.1.3 Parameters Characterising the Buckle Size

In shell buckling analyses under uniformly axial compression, a large number of different buckling modes are all at the same/approximately same buckling load, since they are all critical. This is the difficulty of dealing with the shell buckling analyses. Some of the parameters are especially important to determine the buckle size and the scope of restraint influence from the boundary condition, which has the effect on the final buckling strength of the shell.

The boundary conditions at the end of the cylinder induce local stresses associated with the restraint of radial expansion. In pre-buckling phase, these local stresses occur in a zone, roughly limited by the linear half-wavelength of meridional bending from each end, where:

$$\lambda_0 = \frac{\pi}{[3(1-\nu^2)]^{1/4}}\sqrt{Rt} \cong 2.444\sqrt{Rt} \qquad (3.5)$$

Poisson's ratio $\nu = 0.3$ was adopted here. This parameter also defines the limits between short cylinders and medium length cylinders.

For a medium length cylinder, the critical buckling mode involves square waves (Fig. 2.5b), and can be described in terms of the number of full waves around the circumference. Wide range of possible buckling modes includes an axisymmetric mode (Fig. 2.5a) with axial half-wavelength:

$$\lambda_{cl} = \frac{\pi}{[12(1-\nu^2)]^{1/4}}\sqrt{Rt} = \frac{\lambda_0}{\sqrt{2}} \cong 1.728\sqrt{Rt} \qquad (3.6)$$

which is half the half-wavelength of the square chequerboard pattern.

3.1.4 Influence of Imperfection

Analyses without initial imperfections are insufficient and the influence of imperfection sensitivity was already introduced in Chapter 2. Due to their importance in the study, the history of imperfection in the shell buckling is still worth describing.

3.1.4.1 Trigger of Imperfection Study

The discrepancy between classical buckling stress predictions (Eqn. (2.3)) and experimental buckling strengths was first identified as predominately caused by geometric imperfections in the shell surface by Koiter (1945). His perturbation analysis explored the effect of minor deviations in the form of the axisymmetric buckling mode with λ_{cl} on the buckling stress. Eqn. (3.7) is the critical stress at bifurcation for a long cylinder with sinusoidal imperfections throughout its length from his study.

$$\sigma_{cr} = \sigma_{cl}\{1 - \psi\left|\frac{w_0}{t}\right|[(1+\frac{2t}{\psi w_0})^{1/2} - 1]\} \qquad (3.7)$$

where:

w_0 is the amplitude of the imperfection

$\psi = 0.75\sqrt{3(1-\nu^2)} \cong 1.239$ (if Poisson's ratio $\nu = 0.3$)

And this type of axisymmetric buckling mode imperfection may be regarded as the most serious for the lower strength of the shell buckling, leading to a reduction to only 24% of the classical critical stress for one wall thickness imperfection. Unfortunately, his original PhD study attracted little attention for many years.

3.1.4.2 Development of Imperfection Study in Pre-computerising Era

The influence of the imperfection sensitivity depends heavily on the forms and the length of the imperfection (the long term dispute about the "worst" imperfection in Chapter 2; Rotter, 2002). The phenomena of the elastic imperfection of the shell buckling have been widely studied ever since and a similar formula (Donnell and Wan, 1950) to the problem of column with an initial crookedness (Eqn. (2.2)) is introduced as:

$$(1-\sigma/\sigma_{cl})^2 = 4\beta(\sigma/\sigma_{cl})w_0 \qquad (3.8)$$

where:

w_0 is the amplitude of the initial imperfection

β is a constant, which is larger than zero

σ is the buckling stress

σ_{cl} is the stress predicted by the classical theory

It was rediscovered that the ultimate load at the equilibrium is far less than the classical critical load (Eqn. (2.3)). With a stiff testing machine, the perfect structure could drop from the classical load to a much lower load corresponding to the post-buckling mode. It was suspected that a small initial geometric imperfection could give a significant, disproportionately large reduction on the shell buckling. Donnell and Wan (1950) gave a confirmation of this by using a modified energy calculation method.

Koiter (1963) derived a formula for the buckling stress of a long axially compressed circular cylinder with an initial axisymmetric displacement in the trigonometric shape of the axisymmetric buckling mode:

$$(1-\sigma/\sigma_{cl})^2 = 2.6(\sigma/\sigma_{cl})w_0/t \qquad (3.9)$$

where:

w_0 is the amplitude of the initial imperfection

σ is the buckling stress

σ_{cl} is the stress predicted by the classical theory

t is the thickness of the shell

Later, the strength-imperfection relationship of two possible buckling modes in Fig. 2.5 was studied.

Amazigo and Budiansky (1972) presented asymptotic formulas for the buckling stresses of axially compressed cylinders with localized or random axisymmetric imperfections. The parameter Δ — normalised imperfection amplitude to the wall thickness ratio was used to form a set of formulae for the reduction of the buckling strength due to the imperfection magnitude. Three forms of imperfections (modal, local and random imperfections) were studied and a conclusion was reached that the lowest buckling load would usually be predicted by the local imperfection theory and the highest by the modal analysis on the condition that the imperfection only lies in a small region not too close to the ends of the cylinder.

Full non-linear analyses were performed by Yamaki (1984). Imperfections in asymmetric modes were studied and maximum loads to these imperfections were obtained. It is evident that the asymptotic expressions from this study are accurate for small amplitude imperfections if sufficient terms are included.

3.1.4.3 Development of Imperfection Study in the Computerising Era

In more recent years, with the application of fast-speed computer, more detailed and accurate analyses became possible. With the application of finite element analysis, Teng and Rotter (1992) provided the buckling of pressurized and unpressurised axisymmetrically imperfect cylinders under axial loads with different imperfection amplitudes. It was compared with the previous results of Amazigo and Budiansky (1972) for unpressurised cylinders. It was concluded that the sinusoidal imperfection from Koiter leads to the lowest unpressurised buckling strength as well as the slowest strength gains due to internal pressure among different forms of imperfections. In addition, it was also stated that the asymptotic solution for a local inward deviation by Amazigo and Budiansky (1972) was in close agreement with the finite element calculations for imperfections with amplitudes below half a wall thickness and then fell slightly below the numerical calculations. This is in agreement with the results of Yamaki (1984).

The procedure of the fabrication of the steel shell consists of a series of strakes welded together, this leads to extensive studies of this local axisymmetric depression under axial compression (Bornscheuer et al., 1983a and 1983b; Rotter and Teng, 1989b; Teng and Rotter, 1992; Rotter and Zhang, 1990; Knoedel et al., 1995 and 1996; Guggenberger, 1996; Rotter, 1996a and 1997; Berry and Rotter, 1996; Holst et al., 2000; Berry et al., 1999; Schmidt and Winterstetter, 2001) and this imperfection pattern continues to be the one of the primary resources of imperfection study.

A concise formula for the buckling of imperfect cylindrical shell under uniform axial load was introduced by Calladine (1995) as follows:

$$(1-\sigma/\sigma_{cl})^2 = C(\sigma/\sigma_{cl})w_0 \qquad (3.10)$$

where:

w_0 is a measure of the geometrical imperfection of the shell in its initial, unloaded condition

C is a numerical constant of the shell

σ is the buckling stress

σ_{cl} is the stress predicted by the classical theory

This formula tells that the reduction in buckling load below the classical value, i.e. the quantity $1-\sigma/\sigma_{cl}$, is approximately proportional to the square root of the magnitude of the imperfection for small imperfections. Thus a small imperfection leads to a disproportionately large reduction in load-carrying capacity — which introduces the concept of "imperfection sensitivity".

The buckling strength of the axial loaded imperfect cylindrical shell is very sensitive to both the amplitude and form of the imperfections, and there has been a long debate about the "worst" form of the imperfections and the most widely used interpretation of this concept is that an imperfection in the form of the prefect shell buckling eigenmode is close to the worst form. Now it appears to be relatively close agreement that an axisymmetric local imperfection is the best choice for real silo structure design in relation to full-scale structural measurements. Further discussion on the influence of imperfection amplitude and its spreading width is in the following.

3.1.4.4 Influence of Imperfection Amplitude and Spreading Width

With more and more detailed studies on the geometric imperfection, the influence of the imperfection amplitude on the shell buckling was discovered. In the comparison of the results based on computer analyses and those from pre-computerising era, the latter one can only provide accurate results in small imperfection amplitude (i.e. less than one shell thickness). A shell that is classified as medium length may move towards the short length category with an increasing imperfection amplitude (Fig. 3.4), and since the buckling strength is under estimated due to the more heavily influence from the supporting boundary conditions. The effect of geometric imperfections on the form of the load-axial shortening curve is shown in Fig. 3.5, where it can be seen that the imperfection slightly modifies the pass of the shell from the pre-buckling path to the post-buckling path, but the proximity of these paths causes minor imperfection to have a disproportionate effect on the buckling strength. Furthermore, large amplitude imperfections produce a smooth transition from pre-buckling to post-buckling without the dramatically dropping curve as the perfect or small amplitude imperfections (Fig. 3.5).

Berry and Rotter (1996), who examined "axisymmetric" imperfections extending around a small part of the circumference, showed that most of these caused the same dramatic loss of strength as a fully axisymmetric imperfection, and even quite a short length of imperfection in the axisymmetric form, extending only slightly further around the circumference than one full wavelength of the critical buckle, produced buckling strength losses comparable with a fully axisymmetric imperfection. This means that a relatively local imperfection that remains stable in form over a small part of the circumference is as detrimental as a fully axisymmetric imperfection.

From all different forms of imperfections studied above, the local axisymmetric imperfection (Amazigo & Budiansky, 1972; Bornscheuer et al., 1983; Rotter & Teng, 1989b; Teng & Rotter, 1992; Fig. 3.8) was adopted in this study according to the real imperfection measurement of the shell structures and the specification of this will be discussed in the following.

3.2 Geometry and Imperfection Specification

In order to make a meaningful comparison to the existing research, and of course due to the difficulties arising in the lack of close agreement between the experimental and numerical results, a particular case (local axisymmetric imperfection) was selected to study using the same model dimension as suggested by Teng and Rotter (1992) because of its wide application in the research study of the imperfect shell buckling.

3.2.1 Geometry and Load Definition

The cylinder model height H is 30 m, the radius R is 10 m, and the shell thickness t is 10 mm. Thus, the radius to thickness ratio for the shell R/t is 1,000:1 and H/R equals to 3 (Fig. 3.6 shows the local axial compression cases with different configurations of boundary conditions as well as different dimension are also adopted). These dimensions make it a relatively tall and moderately thin cylinder, with the aim of eliminating the influence of boundary conditions on the calculated buckling stress. An isotropic material with Young's modulus E of $2*10^5$ MPa and Poisson's ratio ν of 0.3 corresponding to mild steel was selected. Fig. 3.7 presents the convention of the resultants used in the shell.

Turning to the loads studied in this thesis, several items that need to be mentioned. First, the term "strip load" is used here to refer to a local distributed axial loading applied to the shell, causing local axial compression. This local load is different from the local pressure (termed as "patch load"), which is normal to the shell defined by silos loading standard (ENV 1991-4, 1995; Fig. 3.6). Second, the strip load applied in the model induces stresses that increase approximately linearly (Fig. 5.1). The combination of this load with the symmetry in the mid-plane of the cylinder permits a range of local high-elevated stresses states to be generated, which is the main focus of this study.

Explorations of different load heights and widths were performed to form a full parametric study, from which several simple formulae were summarised for engineering usage and the possible implementation in future shell and silo design codes.

3.2.2 Imperfection Specification

Because of the importance of the initial imperfections in the shell buckling analyses, the local axisymmetric imperfection (Amazigo & Budiansky, 1972; Bornscheuer et al., 1983; Rotter & Teng, 1989b; Teng & Rotter, 1992) was used in the analyses. Fig. 3.8 describes the details of the local axisymmetric inward imperfect cylinder outline near the mid-plane, with one cylinder wall thickness as the maximum imperfection amplitude. It gives an identical description in FE modelling with comparison of the Eqn. (3.11) (Rotter and Teng, 1989b): the two types of the local inward/outward axisymmetric imperfections (Eqn. (3.11) and Eqn. (3.12)) are shown as the following (Rotter and Teng, 1989b):

$$\delta = \delta_0 e^{(-\pi z/\lambda)}[\sin(\pi z/\lambda) + \cos(\pi z/\lambda)] \qquad \text{Type A} \qquad (3.11)$$

$$\delta = \delta_0 e^{(-\pi z/\lambda)} \cos(\pi z/\lambda) \qquad \text{Type B} \qquad (3.12)$$

$$\lambda_{cl}/\lambda_0 = 1/\sqrt{2} \approx 0.707 \qquad (3.13)$$

where the parameter λ_0 (Eqn. (3.5)) is the linear bending half-wavelength and the imperfection half-wavelength $\lambda_{cl}=\lambda$ is given by Eqn. (3.6) above; δ is the amplitude of the imperfection at axial coordinate z; δ_0 is the maximum imperfection amplitude used to characterise this imperfection. In the study, dimensionless imperfection parameter δ_0/t varies between 0 and 2.0 to illustrate the influence of the imperfection amplitude on different load cases.

3.3 Summary

This chapter opened with the introduction of the Janssen theory for silo loading. The source of the non-uniform loads comes from the flowing patterns of the solids inside and the supporting system of the shell (Chapter 1). Unsymmetrical loads on silo walls lead to local high axial compression (Rotter, 1986a; Rotter, 1998). There are several investigations on the influence of the non-uniform pressure (normal direction) on the buckling strength, but little appears to be on the influence of the non-uniform friction drag distribution (axial direction). The shell buckling strength under an axial compression that acts over only a part of the circumference (a typical unsymmetrical load on silo

walls) may be significantly changed, but the problem has been scarcely explored at all (Rotter, 1986a; Rotter, 1986b; Ansourian, 1992; Rotter, 1997).

Geometric imperfections in silo wall play a key role in reducing the cylinder buckling strength. The buckling strength of a thin cylindrical shell under axial compression is known to be very sensitive to geometric imperfections in the wall (Yamaki, 1984; Calla dine, 1995) and one particularly detrimental nature and well-defined imperfections is a local depression due to the rolling process of the steel plate and shrinkage of the weld (Amazigo, 1969; Hutchinson et al., 1972; Amazigo and Budiansky, 1972; Bornscheuer et al., 1983a and 1983b; Rotter and Teng, 1989b; Teng and Rotter, 1992; Rotter and Zhang, 1990; Knoedel et al., 1995 and 1996; Guggenberger, 1996; Rotter, 1996a and 1997; Berry and Rotter, 1996; Holst et al., 1999 and 2000; Berry et al., 1999; Schmidt and Winterstetter, 2001). Some important features of the imperfection (forms, amplitude and spreading width) and their influence were also stated from previous studies. A representative idealised local axisymmetric inward imperfection (Type A) was introduced (Rotter and Teng, 1989b), which was used in the studies throughout the whole thesis.

The importance of the elevated local axial compression and local axisymmetric inward imperfection of shell buckling study is significant. Reliable quantification of the above effects presents a considerable challenge. This study is the first known study to examine this problem systematically. To be consistent with the draft European Standard for Metal Shells (ENV 1993-1-6, 1999), the analyses types used to predict shell buckling strength are Linear Analysis (LA), Geometrically Non-linear Analysis (GNA), and Geometrically Non-linear Analysis with Imperfections (GNIA). The influence of the material non-linearity is also under consideration.

Furthermore, it is well known that the internal pressure from the stored material reduces the detrimental effects of the imperfections (Harris et al., 1957; Seide, 1962; Weingarten, 1962; Rotter, 1986a; Rotter and Teng, 1989b), and the stiffness of the solid also increases shell buckling strength further (Trahair et al., 1983; Rotter and Zhang, 1990). The buckling strength of the imperfect cylinder is commonly related to the classical elastic

critical stress, the internal pressure can even increase the buckling strength in a perfect cylinder (Lo et al, 1947; Harris et al, 1957; Weingarten et al, 1965; Rotter & Seide, 1987), but the increase depends heavily on the form of the imperfection which caused this effect in pressurised cylinders. This was thoroughly documented by Rotter & Teng (1989b) and the relationship between local inward, local outward and sinusoidal imperfections were also investigated by Teng & Rotter (1992). However, since this is the first study of the problem, these strengthening effects are ignored.

The other half of the chapter focuses on the study itself: specify the problem of the shell buckling under elevated local axial compression stresses, the geometry of the model and the load definition as well as the imperfection profile. All these contribute to the opening of the computer modelling chapter next.

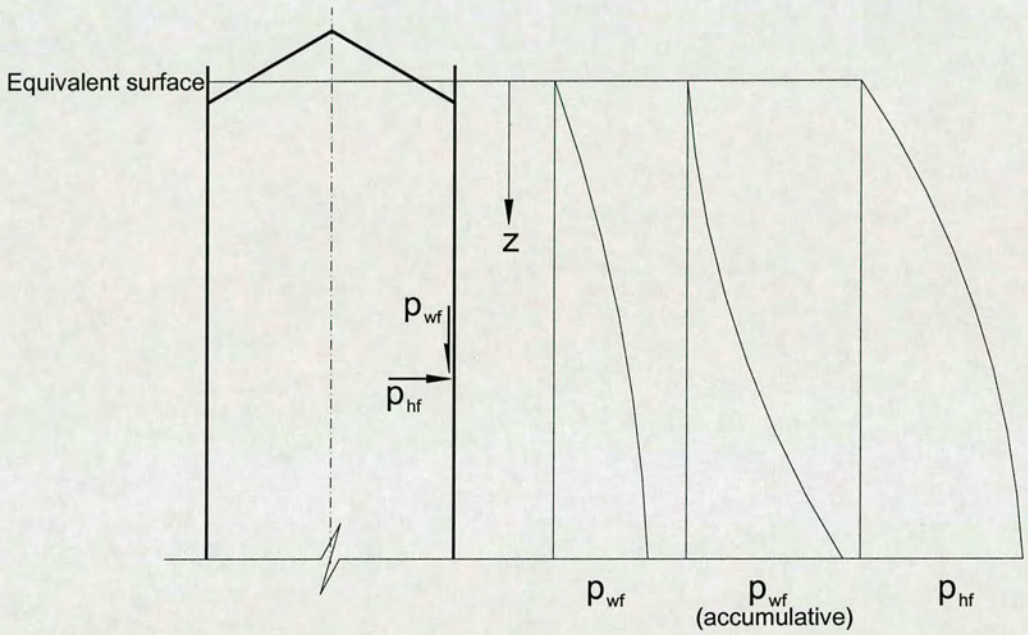

Fig. 3.1 Janssen distribution on silo walls

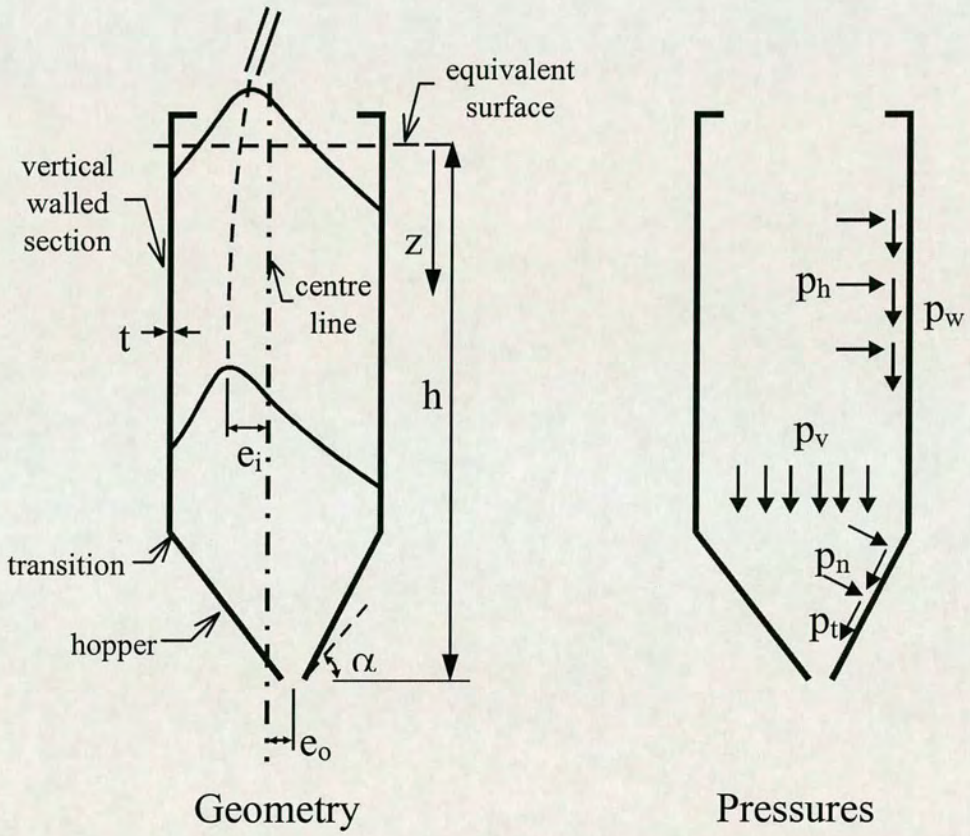

Fig. 3.2 Geometry definitions used in Eurocode (after ENV 1993-4-1, 1999)

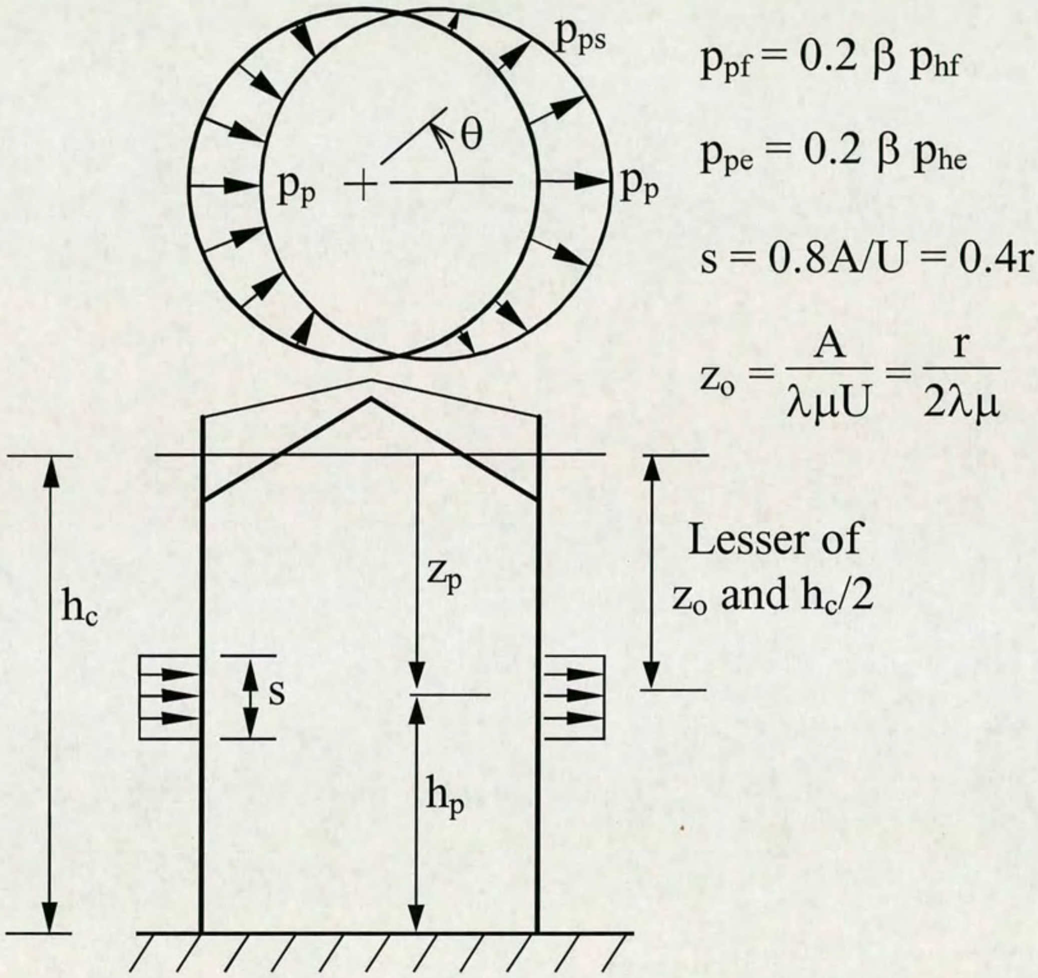

Fig. 3.3 Unsymmetrical local patch pressure

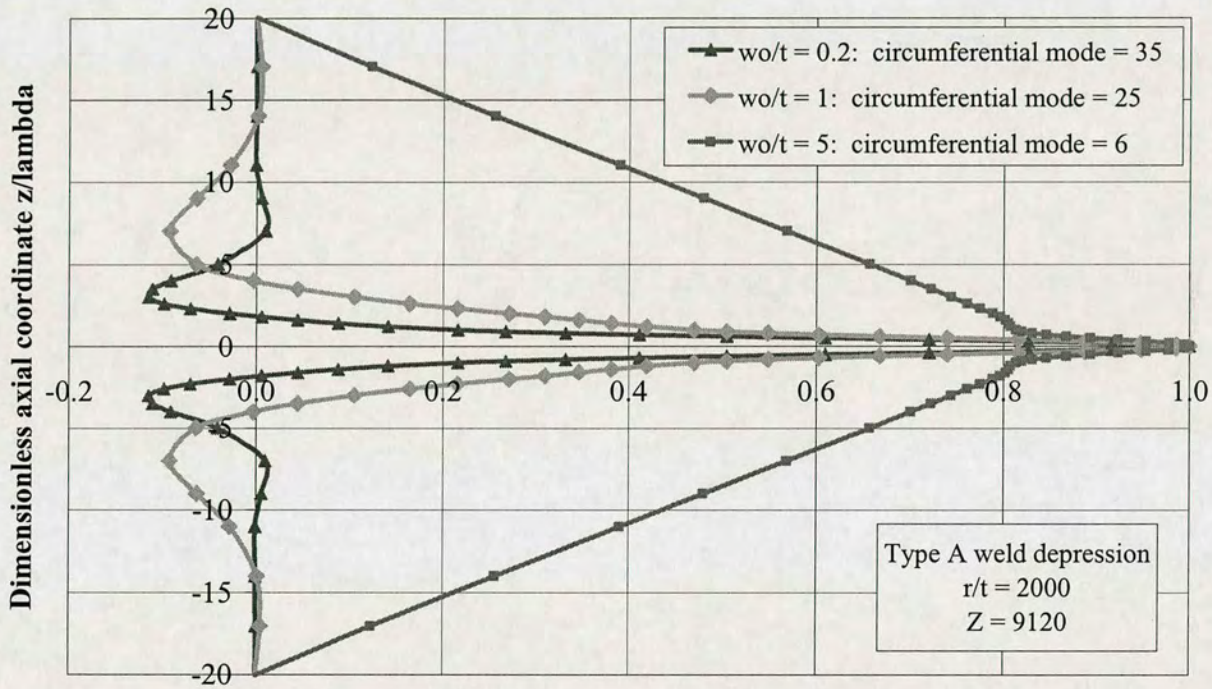

Fig. 3.4 Changing axial mode of buckling as imperfection amplitude w_0/t rises (after Rotter, 2002)

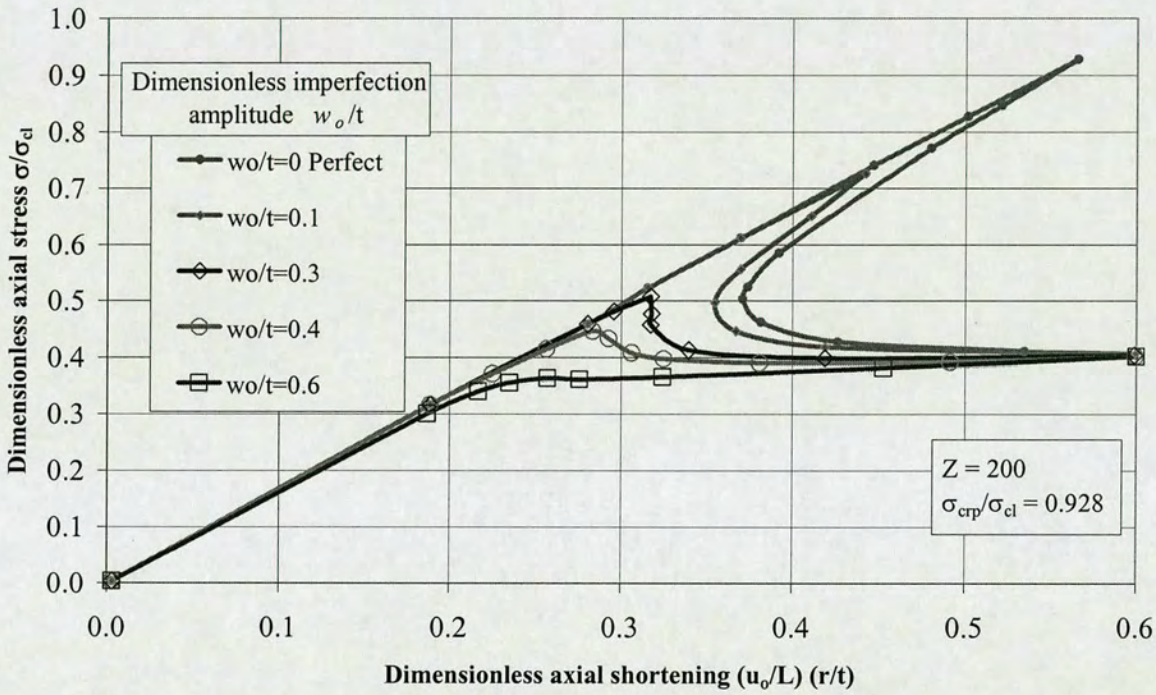

Fig. 3.5 Load-axial shortening relationships for cylinders with circumferentially asymmetric imperfections (after Rotter, 2002)

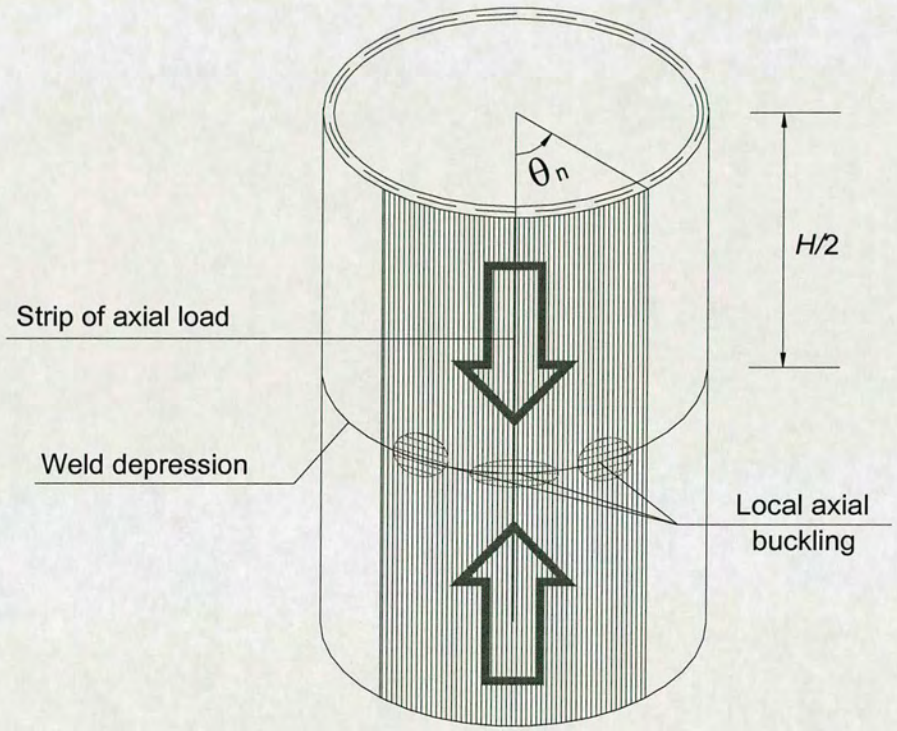

Fig. 3.6 Cylindrical shell under local axial compression

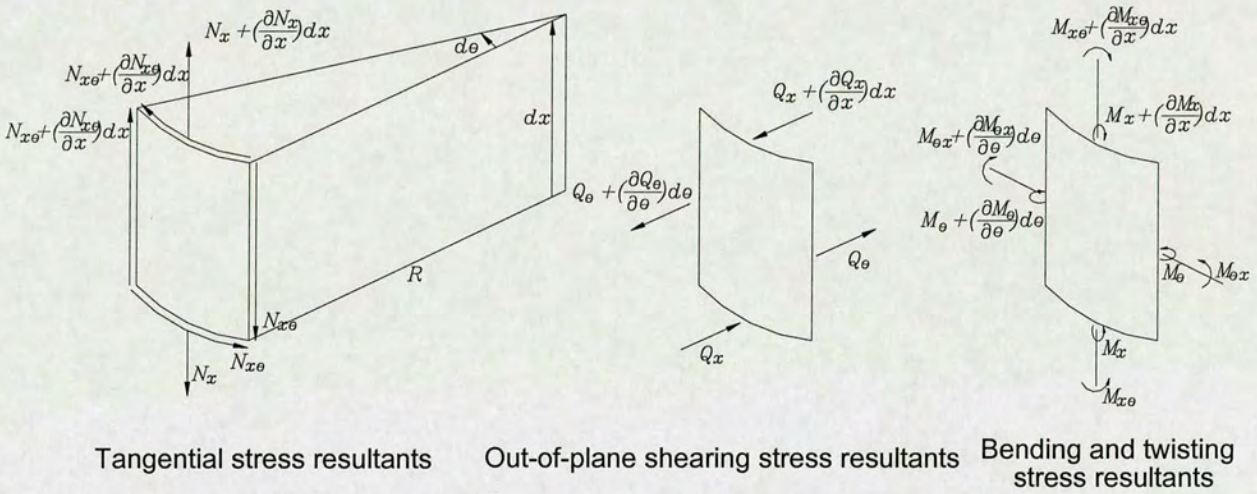

Fig. 3.7 Convention of the shell element

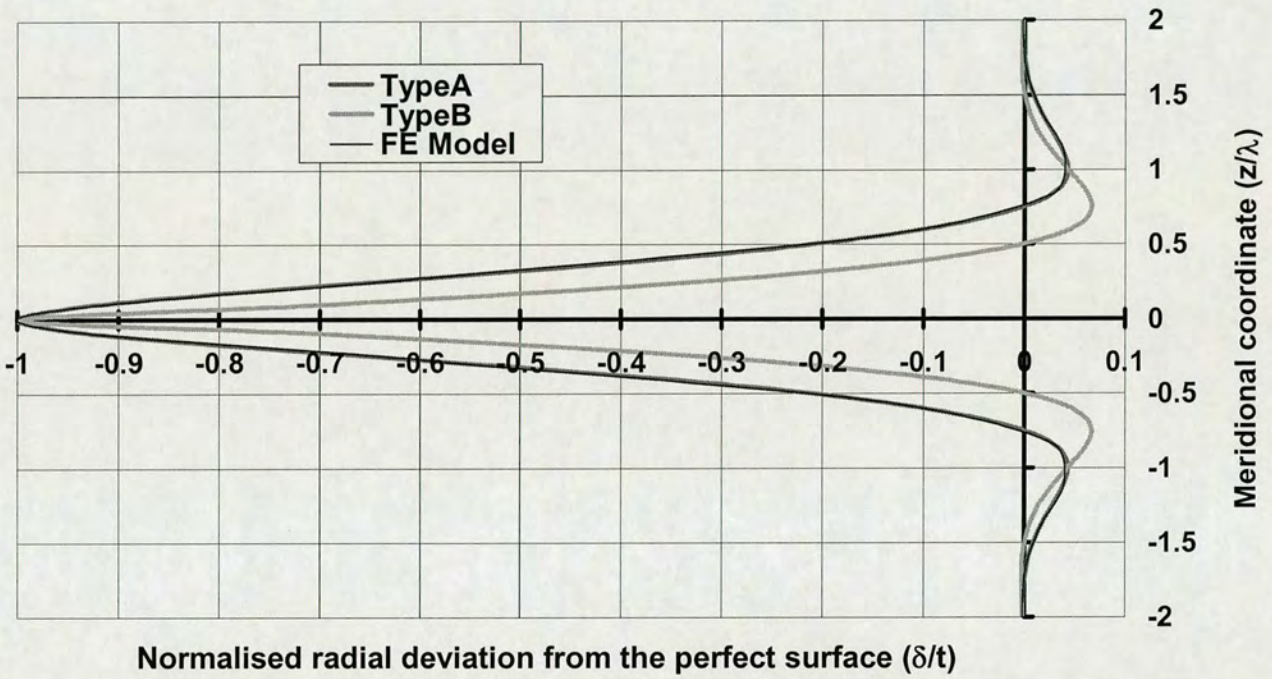

Fig. 3.8 Local axisymmetric inward imperfection

(Note: FE model stands for the model used in the Finite Element Analysis and Type A & B for the axisymmetric local inward deviation (Rotter & Teng, 1989b; Teng & Rotter, 1992). The curve shows the half shape of the local inward imperfection, which is axisymmetric. Only the domain close to imperfection is shown here in detail.)

Chapter 4

COMPUTER MODELLING

4.1 Background Knowledge

A large number of commercial and public-domain finite element software for buckling and nonlinear analyses are currently available. Some popular general-purpose software with this capabilities are ABAQUS, ADINA, ANSYS, COSMOS, NIKE3D, DYNA2D, DYNA3D, MSC/NASTRAN, NISA, PATRAN, STARDYNE and GTSTRUDL. Among these, ABAQUS was chosen because of its large number of validation problems (over 5,000) and its wide application in the field of thin-walled structures as well as the availability for this study.

4.1.1 Principle of FE Analysis

This chapter presents the background to the numerical calculations of the study, which was performed using the finite element package ABAQUS (HKS, 1998).

The whole analysis is based on a static procedure, which assumes that an instantaneous state of stress is developed so as to be in static equilibrium with the force applied. The general equations of static equilibrium may be written as the following:

$$Ka = R \tag{4.1}$$

where K is the structure stiffness matrix, a is the vector of nodal displacement and R is the structure force vector.

The structure stiffness matrix for an individual element consists of two parts: D is a matrix of elastic constants and B is the strain-displacement matrix:

$$K^e = \int_v B^{eT} D^e B^e dV \tag{4.2}$$

where e stands for element, V refers to the whole structure volume and T is transpose of the matrix.

The exact integration of the element stiffness matrix is often replaced with an approximate numerical integration (quadrature method) such as Gaussian integration, using a summation over (n) sampling positions: $K=\sum_{e=1}^{n} K^e$.

Each individual element stiffness matrix is assembled in its place according to its node numbering into the global stiffness matrix. It is this topological connectivity, which accounts for the well-conditioned nature of the equations.

For efficiency, only a symmetric half of the non-zero band is stored. The half-bandwidth is therefore an important problem statistic. Using the leading diagonal (pivot) terms to manipulate each equation row, the matrix is converted to upper/lower triangular form. And the last step is to solve the equation (Eqn. (4.1)) via progressively back-substituted to solve each previous equation. Essentially, finite element analysis forms the matrix equilibrium via the stiffness, displacement and load matrix and then follows by the solution of the equation, which is "repeatedly" done by the massive computer calculation ability. Because that the displacement is solved initially from the equation, this method is since termed a "displacement approach" (Zienkiewicz, 1967).

In a standard procedure in ABAQUS, the analysis of a problem consists of three stages: Pre-processing (forming the geometry/mesh/material/support/loading) in the input file, followed by the processing of a standard solving procedure by solving the displacement matrix via the standard matrix equation (Eqn 4.1) using different analyses types according to different models and specification which are specified in the input file. The last step is the post-processing in order to extract the relevant results (stain/stress) from the analysis by outputting/printing/plotting/contouring in a diagram or in a data format (Fig. 4.1).

4.1.2 Unstable Collapse and Post-buckling Analysis

A non-linear analysis is needed if the load displacement curve is non-linear. There are three types of non-linearity (Fig. 4.2): non-linear softening response, non-linear stiffening response and snap-through buckling response. Non-linear responses might be in an ill-conditioned equation following the previous procedure. In order to solve some ill-conditioned problems, a new method (Riks, 1979) is introduced to deal with the limit load problems or almost unstable softening problems and more complicated buckling problems which is the focus of the shell study.

The sources of non-linearity come from the following factors listed in table 4.1. Among all the three major sources, only two — material non-linearity and geometric non-linearity have been taken into accout in this study. Because of the large deformation and rotation occur in the shell buckling, the geometric non-linearity is considered. The material non-linearity is studied because of its elasto-plastic property of the mild steel studied but within the limitation of the elasto-perfectly plastic range in aim of simplicity and very limited application of material nonlinearity in the shell buckling (no hardening slope, see Fig. 4.3).

4.1.3 Different Methods in Non-linear Analysis

There are three methods applied in the computer analysis in the non-linear range: pure iteration, pure incrementation and incremental-iteration (Fig. 4.4).

•Pure iteration, which total load is applied and initial stiffness used exclusively and since there is no path history.

•Pure incrementation, which load is applied incrementally with no iterative correction and stiffness updated incrementally and since there is a path history available though not accurate.

•Incremental-iterative, which load is applied incrementally with iterative correction restoring incremental equilibrium and stiffness updated incrementally or iteratively and since a relative accurate path history is available.

What should be pointed out is that there is a special method in incremental-iterative methods. It is termed "Newton-Raphson" method. This method adopts a tangent stiffness matrix which is computed at each iteration of each increment continually and since needs few iterations and provides a rapid convergence to solve the non-linear equilibrium equations. There are also other methods derived from Newton-Raphson method which adopts either the initial stiffness matrix (K_0) and only the first stiffness matrix (K_1) for the rest of the whole procedure or even the single K_0 in order to make this method more computational economical.

Fig. 4.5 shows the summary of a traditional non-linear analysis, and it is a dynamic process which adjusts its stiffness matrix according to its individual method. The loading increases with the development of the iteration loop for the balance at current loading level. In summary, non-linear analysis is a multi-step procedure and this makes the big different to the linear analysis.

4.2 Problem Modeling

This part describes the details of computer modelling on the problem which was introduced in Chapter 3.

4.2.1 Co-ordinate System and Element Type

The cylinder model geometry was introduced in Chapter 3. For efficiency, the cylindrical system (r, θ, z) was induced in the definition of the model (Fig. 4.6). As pointed out before, due to the majority of applications in civil engineering is thin shell in which transverse shear deformation can be ignored, a rectangular 4-node doubly curved thin shell element, with reduced integration, hourglass control and 5 degrees of freedom per node (*S4R5*) was adopted.

The shell normal remains orthogonal to the shell surface through all process (Kirchhoff constraint) in this type. It can provide arbitrarily large rotations but with small strains (the change in thickness is ignored). With the reduced integration, it provides more accurate results if the in-plane bending can be ignored which is not a problem for the shell buckling. At the same time, the mass matrix and distributed loading are still integrated exactly. All these contribute to more efficient but still acurate according to nature of the problem if transverse shear flexibility can be ignored.

4.2.2 Introduction of Geometric Imperfection in the Analysis

There are two kinds of methods inducing the imperfection in the ABAQUS analysis: The first method defines the imperfection by means of a sub-routine that is used to generate the perturbed mesh, using the data either stored on the results file written during the previously performed eigenvalue analysis or the specified imperfection mode for its profile. The meshes for the buckling prediction analysis and the post-buckling analysis are identical. The postbuckling analysis is performed using the *STATIC, RIKS analysis procedure. The second method uses the *IMPERFECTION option to define the imperfection directly.

Since the specified local inward axisymmetric imperfection is used for all analyses and for the convinence of the comparison later, the first method is used and its detailed description was already mentioned in Chapter 3.

4.2.3 Mesh Convergence Study

As a very important step in the finite element analysis, a mesh convergence study was performed initially to ensure the accuracy of the analyses results.

Step by step, there are three steps into the final modelling of the shell buckling analysis under the localised partial axial compression with imperfections. The linear eigenvalue analysis is adopted thoroughout these studies.

4.2.3.1 Mesh Convergence Study under Uniform Axial Compression

For the particular problem under study, the critical buckling mode will be a displacement pattern with n circumferential waves and m longitudinal half-waves and the key point is to determine the combination of the two values representing the lowest possible stress — the critical strength of the shell buckling.

Eigenvalue buckling analysis is performed within ABAQUS by first storing the stiffness matrix at the state corresponding to the "base state" loading on the structure, then applying a small perturbation of a "live" load. The initial stress matrix resulting from the live load is calculated, and then an eigenvalue calculation is performed to determine a multiplier to the "live" load at which the structure reaches its instability according to its linearity.

Only one-fourth of the cylinder was studied in order to reduce the amount and time for computation: symmetry conditions were applied at the mid-plane section and the top section of the shell was fully restrained against the translation in radial direction, but free to move axially; a combination of anti-symmetry and symmetry boundary conditions at two longitudinal edges of this model were adopted during the eigenvalue extraction allows this one-fourth model to represent the entire cylinder for all possible buckling modes both in the circumferential and longitudinal direction. In short, a simply supported case (*S3* in Singer's notation) as stated in Eqn. (4.3) (Fig. 4.7; Yamaki, 1984) was used for this analysis from the view of whole cylinder.

$$S3: \quad W_l = W_{l,xx} = N_{xl} = V_l = 0 \tag{4.3}$$

The reason of this choice is that it can provide a reliable and stable classical buckling strength in the range of "medium" length for the perfect cylinder buckling analysis (Yamaki, 1984).

The mesh convergence study is taken in two directions: circumferential (Fig. 4.8) and meridional (Fig. 4.9). The mesh can be easily converged in the longitudinal direction comparing with that of the circumferential one.

4.2.3.2 Mesh Convergence Study under Uniform Axial Compression with Imperfection

To reduce the size of the problem further, a smaller portion of the shell was used in the analysis to obtain a converged mesh. The mesh (Fig. 4.10) used for this phase of the study consists of 15 elements of *S4R5* in the circumferential direction in one row with symmetry boundaries at 15° and 7.5° and with 1° (174.53*mm*) and 0.5° (87.27*mm*) divisions repectively. In the meridional direction, the mesh dimension is 150mm giving 100 rows between the end boundary and the symmetry boundary. All these make mesh sizes in both directions less than one fourth of the linear bending half-wavelength λ_0 ($0.25\lambda_0 = 0.611\sqrt{Rt} = 193.22mm$).

The imperfection (Type A) is specified in Chapter3 and only amplitude of one quarter of the shell thickness was performed and the result shows the converged mesh is accurate enough to present both the buckling mode (n=24) and buckling strength of cylindrical shell as Teng & Rotter (1992). Fig. 4.11 shows the result that the analysis with the converged mesh is just over 1% deviation to the finest mesh with the same buckling. So this mesh type is indeed efficient and acurate enough to be implemented in the future analyses.

4.2.3.3 Mesh Convergence Study under Non-uniform Axial Compression with Imperfection

For analysis of shell buckling under non-uniform axial compression, there is concern about geometric nonlinearity prior to buckling and its possible unstable postbuckling response. A nonlinear load-deflection analysis (especially with the influence from some sort of imperfections) is performed to investigate the problem further.

The sudden change of buckling mode(s) at collapse causes the elasto-plastic response to switch from elastic to yielding in some parts of the model and from yielding to elastic unloading at other points due to their individual stiffness at that time. The steeply falling post-buckling path (Fig. 4.14) is associated with the proximity of these modes. Linear eigenvalue analysis is therefore most usefully employed only in establishing the finite element mesh and in producing a reference value for the true (GMNIA) buckling strength. An imperfection with an amplitude of only one wall thickness, which may be only a thousandth part of the radius, has a dramatic effect on the peak load, and thus a local inward imperfection with δ_0/t = 1.0 was included in the model. The boundary condition is identical to the previous two cases.

The mesh refinement (Fig. 4.12) was pursued in two directions: circumferential ("circumferential reconvergenced" in the figure legend) and meridional ("fine meridional division", "2*fine meridional division", "converged meridional-1" and "converged meridional-2"). The "final adopted mesh" was the one with the combination of the mesh refinement results from the above two directions, which shows that the analysis using a converged mesh deviates by only 0.5% from the extrapolated result. The model uses a very fine mesh (less than ¼ λ_0) within the local imperfection, and in the boundary area and the area of local axial compression; the mesh size increases step by step in the neighbourhood of the local imperfection as well as the place where local axial compression was applied (Fig. 4.13).

The master input file of the ABAQUS analysis is used to make the parametric study more efficiently. The related FORTRAN files constructing the node, element and the load elements are all attached in Appendix for details.

4.3 Analysis Procedure

In Chapter 2, all different analyses types based on computing according to the current Eurocode (ENV 1993-1-6, 1999) have been stated. The following details the normal procedure of the analyses which will be used in the parametric study of this project.

4.3.1 Linear Elastic Analysis (LA/LEA)

In general, a first eigenvalue analysis is used to obtain estimates of the buckling loads and modes. Such studies also provide guidance in mesh design because mesh convergence studies are required to ensure that the eigenvalue estimates of the buckling load have converged: this requires that the mesh be adequate to model all possible buckling modes, which are usually more complex than the pre-buckling deformation mode. Furthmore, its critical role in determining the buckling strength of the cylinder according to the current Eurocode (ENV1993-1-6, 1999) will be explanined in detail later.

As discussed in Chapter 2 (Table 2.1, Fig. 2.3), for small numbers of axial half-waves (m) the critical stress changes rapidly with respect to the number of circumferential lobes (n). However, for higher values of axial half-waves, the critical stresses are not very much higher than the classical critical stress (Eqn. (2.3), m=1, n= 4**)** and do not vary much from mode to mode. ABAQUS (HKS, 1998) estimates the eigenvalues in ascending order, from the lowest eigenmode to the highest (in theory, only if the mesh is fine enough to model the mode) with the eigenvalue varying from large number to zero, unless a shift point is defined. Since the critical stresses for all of these high-order longitudinal eigenmodes are so similar, the eigenmode is rather indeterminate. The finite element mesh, however, has a fixed number of nodes longitudinally and cannot represent very high numbers of half-waves with any amount of clarity. Thus, the eigenvector plots show many longitudinal modes — too many for the mesh to represent accurately. And that is also the reason why there is a tiny difference in the n/m numbers between different studies.

4.3.2 Load-displacement Analysis

Linear eigenvalue analysis might be sufficient for some problems. But a non linear analysis is needed to investigate the problem further if there is concern about geometric nonlinearity prior to buckling, material nonlinearity, or unstable post-buckling response (with associated imperfection sensitivity). Fig. 4.14 shows a modal load-displacement curve for both perfect and geometrically imperfect cylinder under uniform axial compression. In order to have an apparent view of the whole buckling process in each of

the different load cases, a Riks analysis (Riks, 1979) was performed first to examine its non-linear behaviour.

Only part of the cylinder was under study again with a combination of different boundary conditions. Different analysis types have different limitation(s) on the use of boundary conditions in ABAQUS. In the eigenvalue analysis, antisymmetry boundary conditions were permissible, which made this one-eighth model represent every possible buckling mode as the whole cylindrical shell (Fig. 4.15). But the antisymmetry assumption was no longer applicable in the load-deflection study. This is the reason why an eigenvalue analysis was performed first to get the probable buckling mode, then a minimum size of the partial model with the modified symmetric boundary conditions is run accordingly for the non-linear analysis.

Moreover, a full load-displacement curve of a specific problem can provide a general view of the whole energy increasing and decreasing procedure and hence the possible reason for the mechanism can be detected from this.

4.3.3 Geometrically Non-linear Elastic Analysis (GNA)

A geometrically non-linear analysis is a dynamic process, some important controlling parameters (step reduction, iteration number, convergence tolerance etc.) can only be better "controlled" after several tries. So it is very difficult to conduct a full parametric study using only the individual load-displacement paths for both time and cost reasons. A newly defined scheme adopting the Riks method (arc-length) is used in all the non-linear analyses (geometrically and materially non-linear analyses).

First, an incremental load-deflection analysis is performed using the modified Riks method with few coarse increments, and a slack convergence tolerance to check initial plasticity and the possible buckling mode. This is followed by two additional Riks analyses with refined load increments and tight convergence tolerance at the top of a preload from the previous relatively coarse analysis to get a result closer to the "real" buckling load. Finally, the process uses an eigenvalue buckling analysis applied using the

current result as the base state. Since the current result is already very close to the "real" buckling load after three "coarse" non-linear analyses, the difference between linear analysis and non-linear analysis in the last step is tiny. This provides a rapid determination of the buckling load compared with the whole dynamic process of a traditional load-displacement analysis and how fast it can improve the analysis all depends on the coarsing extent of the two Riks analyses, how big the nonlinearity is as well as the experience accumulated from the previous analysis. But a complete non-linear path is needed in the first of a series parametric study of a new configuration of geometry and loading to verify the accuracy and a comparision study was also undertaken since.

4.3.4 Geometrically Non-linear Elastic Analysis with Imperfections (GNIA)

Due to the shells' relatively thin thickness, the elastic buckling strength governs many of these designs. In some cases the buckling may be only a local effect in the whole response: the shell may subsequently become stiffer again and reach higher load levels usefully with respect to its design objective; sometimes there are many possible collapse modes into which the shell may buckle. These analyses would typically study imperfection sensitivity by perturbing the perfect geometry with different magnitudes of imperfection in the most important buckling modes and investigating the effect on the response. So several series of analyses on this are studied to examine the influence from the geometric imperfection. The method used in GNA is still applicable for this analysis type.

4.4 Summary

This chapter has described the details about the computer modeling of the study. The basics of computer analyses were mentioned together with the introduction of pre-buckling, buckling and post-buckling analyses in the shell study. The application of each individual analyses types was mentioned according to its usage. Among all these, the focus was put on the mesh study due to the sensitivity of the mesh refinement in the finite element analysis. Some techniques used in the study were stated and the following is a summary of the study done in this chapter.

From the mesh convergence study, the mesh refinement in the meridional direction is much faster than that of longitudinal counterpart for this shell problem. This would assist future studies of the mesh convergence under more complicated geometry and loading configurations.

In addition, a mesh for the study of shells under local axial compression with/without imperfections, with reasonable total elements, which can still provide a satisfactory buckling load through the convergence study was obtained and this is the main purpose of the study in this chapter.

Furthermore, a newly defined scheme with the combination of Riks and eigenvalue procedure was devised aiming for the geometrically nonlinear analysis, which can further reduce the computing time, but still provides acurate results.

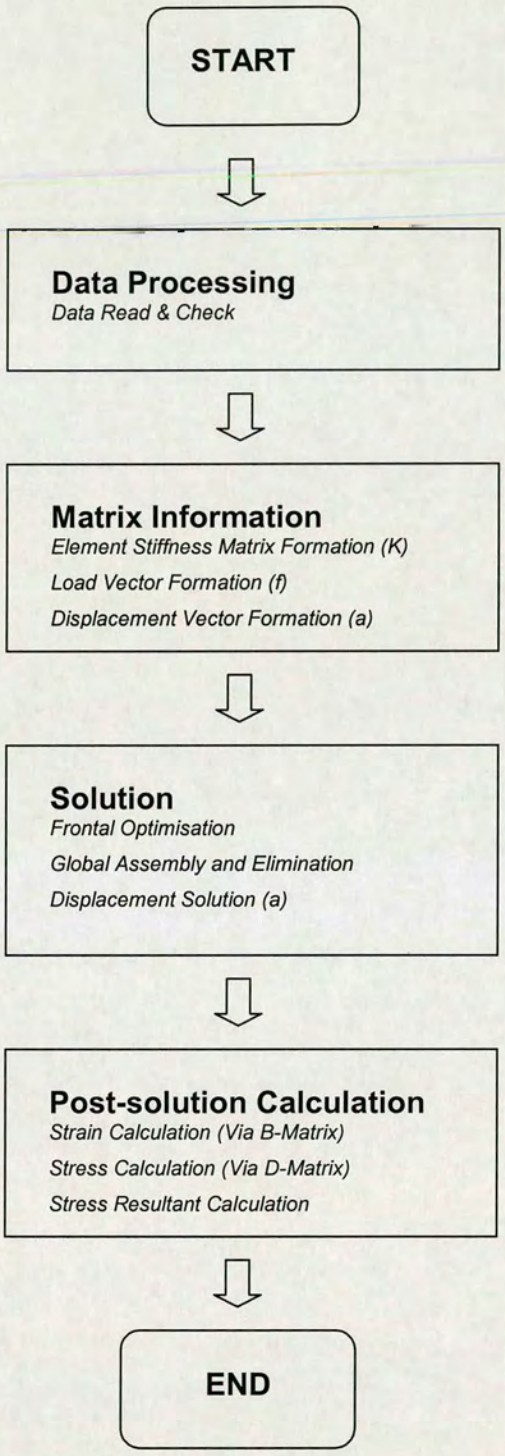

Fig. 4.1 Procedure of finite element analysis

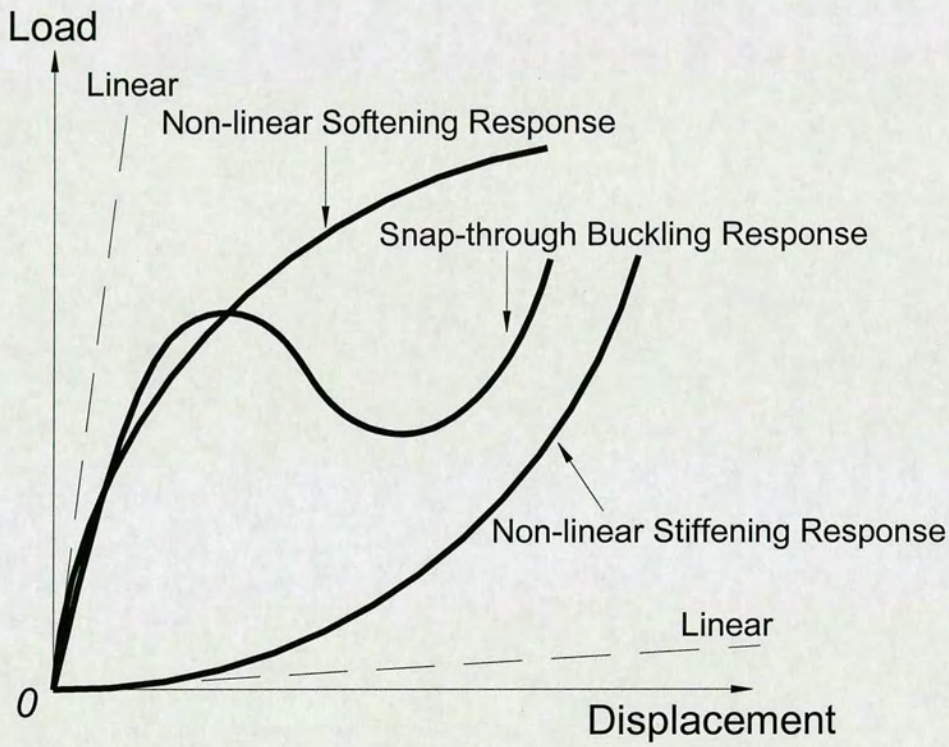

Fig. 4.2 Non-linear behaviour in the load-displacement curve

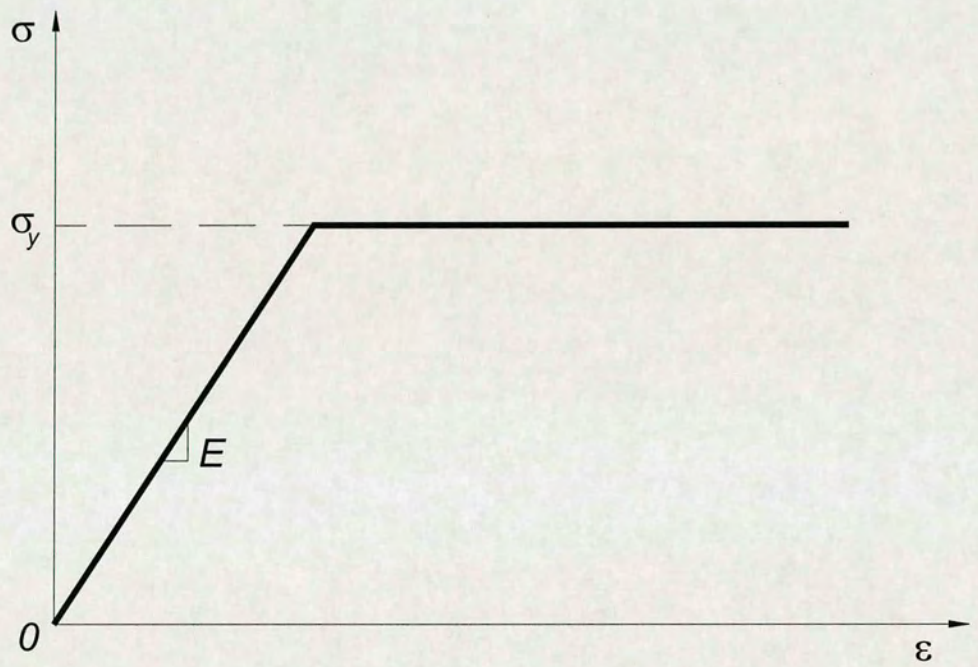

Fig. 4.3 Material non-linearity

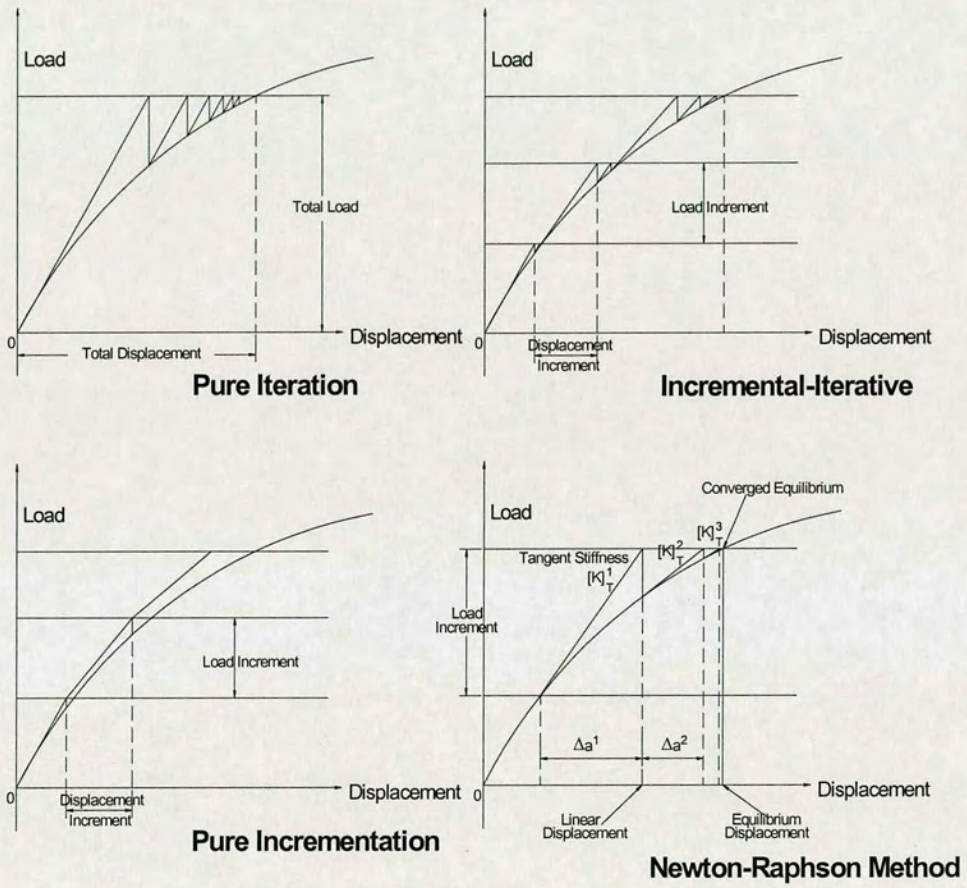

Fig. 4.4 Non-linear analyses methods (after FEA, 2002)

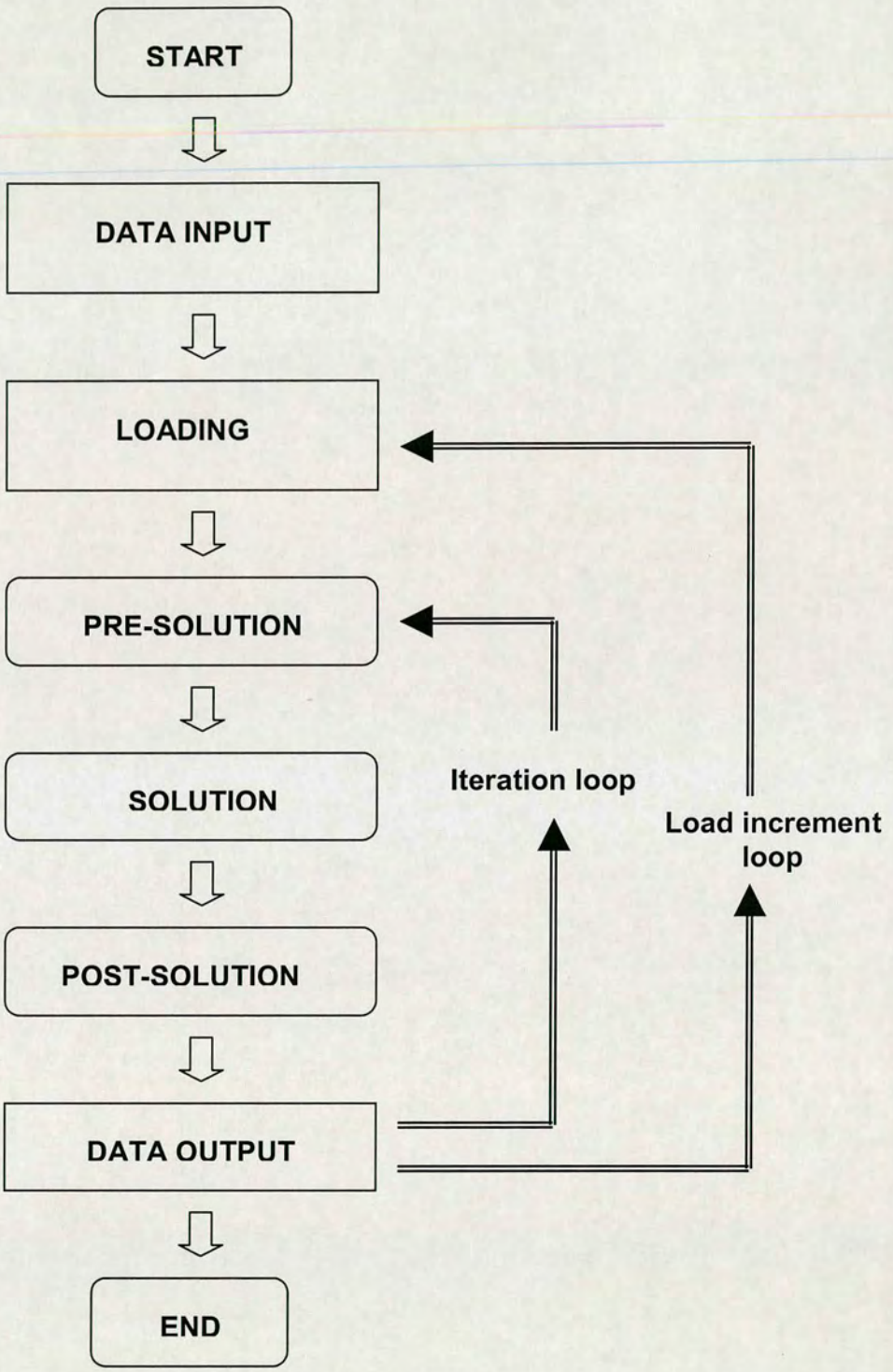

Fig. 4.5 Non-linear analysis procedure

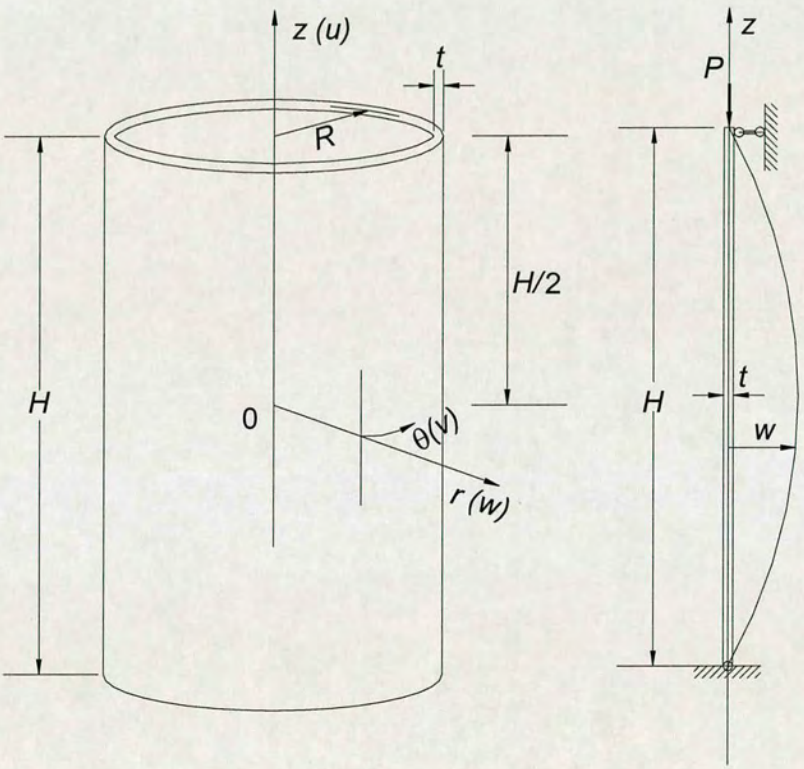

Fig. 4.6 Cylindrical coordinate system

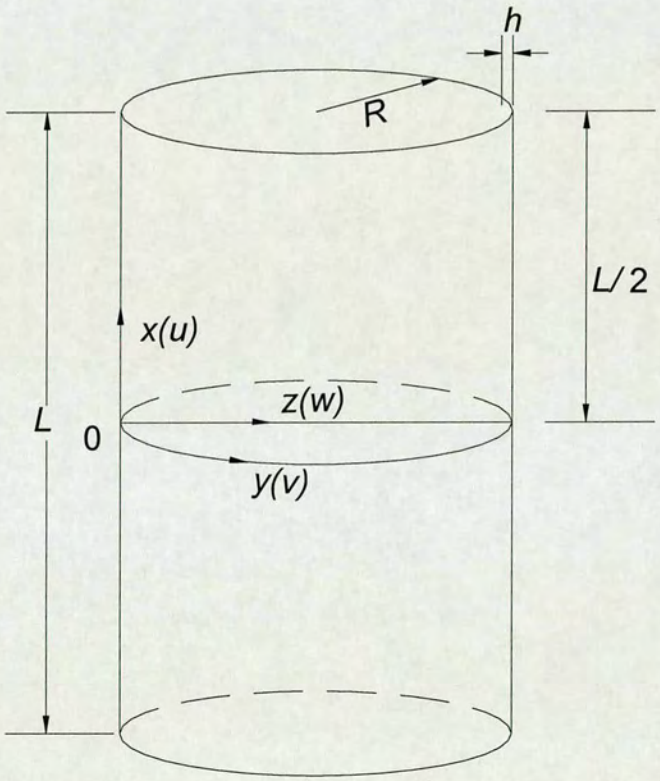

Fig. 4.7 Cylindrical coordinate system (Yamaki, 1984)

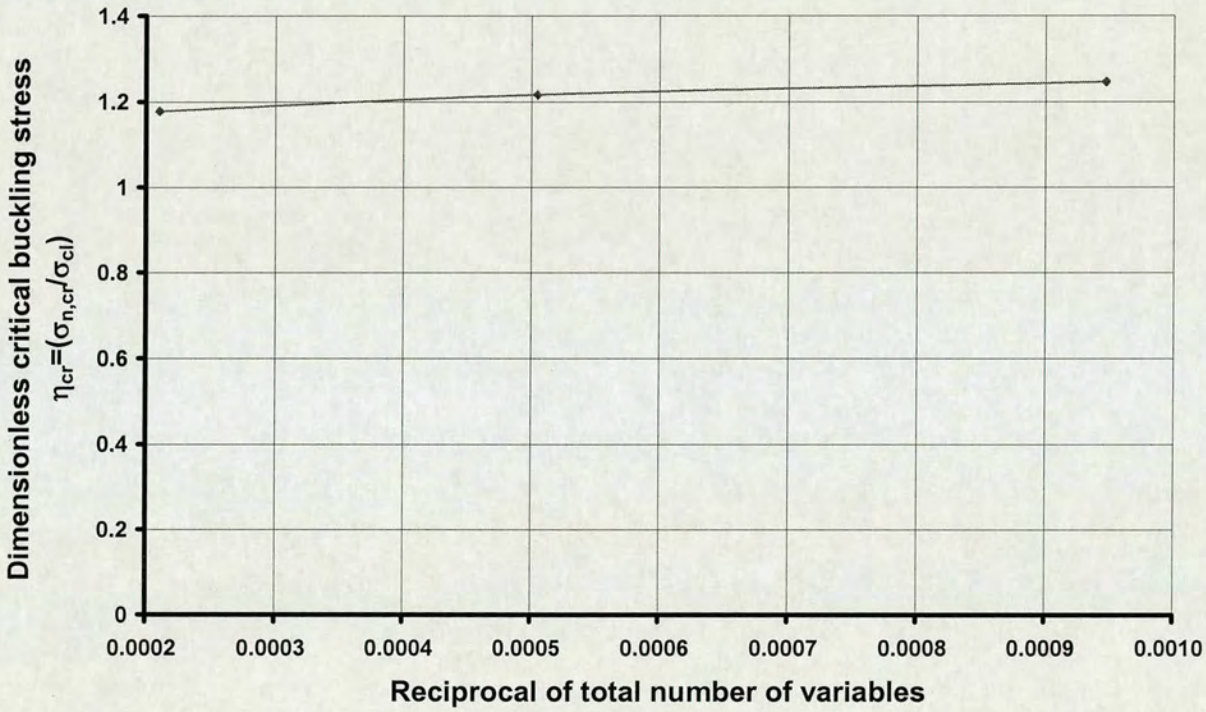

Fig. 4.8 Mesh convergence in circumference for the perfect shell under uniform axial compression

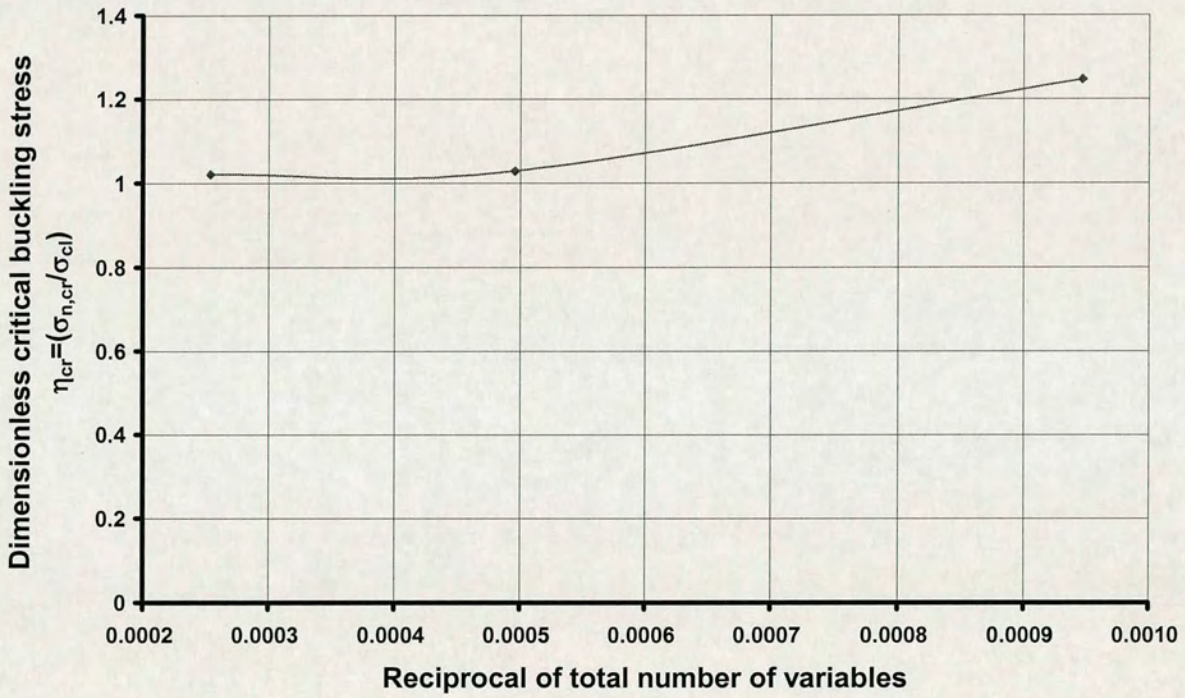

Fig. 4.9 Mesh convergence in meridian for the perfect shell under uniform axial compression

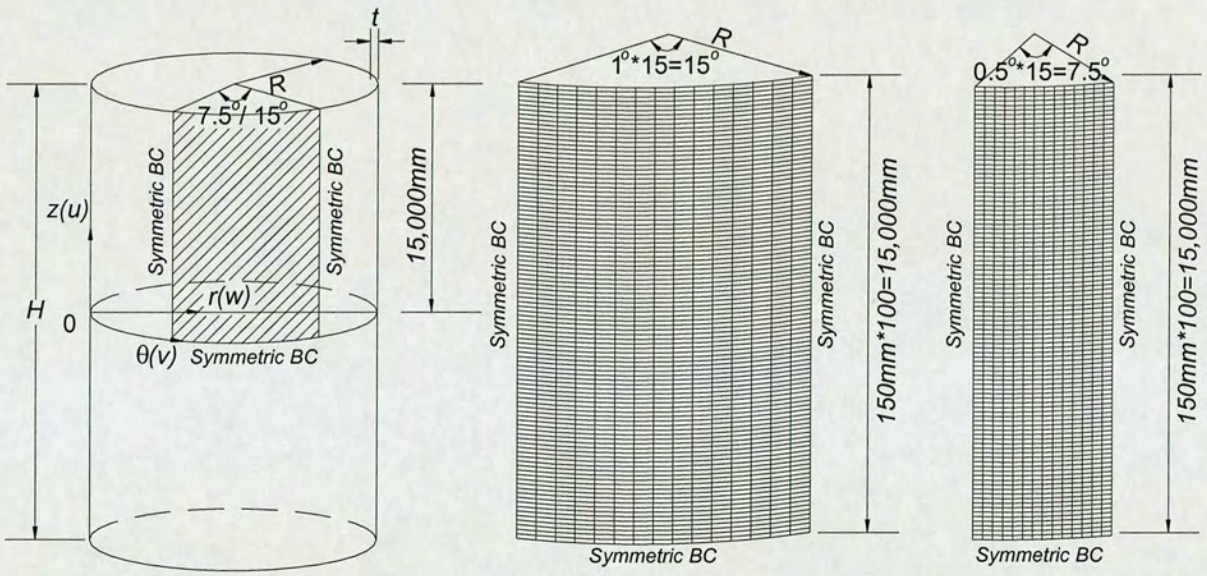

Fig. 4.10 Mesh for imperfect cylinder

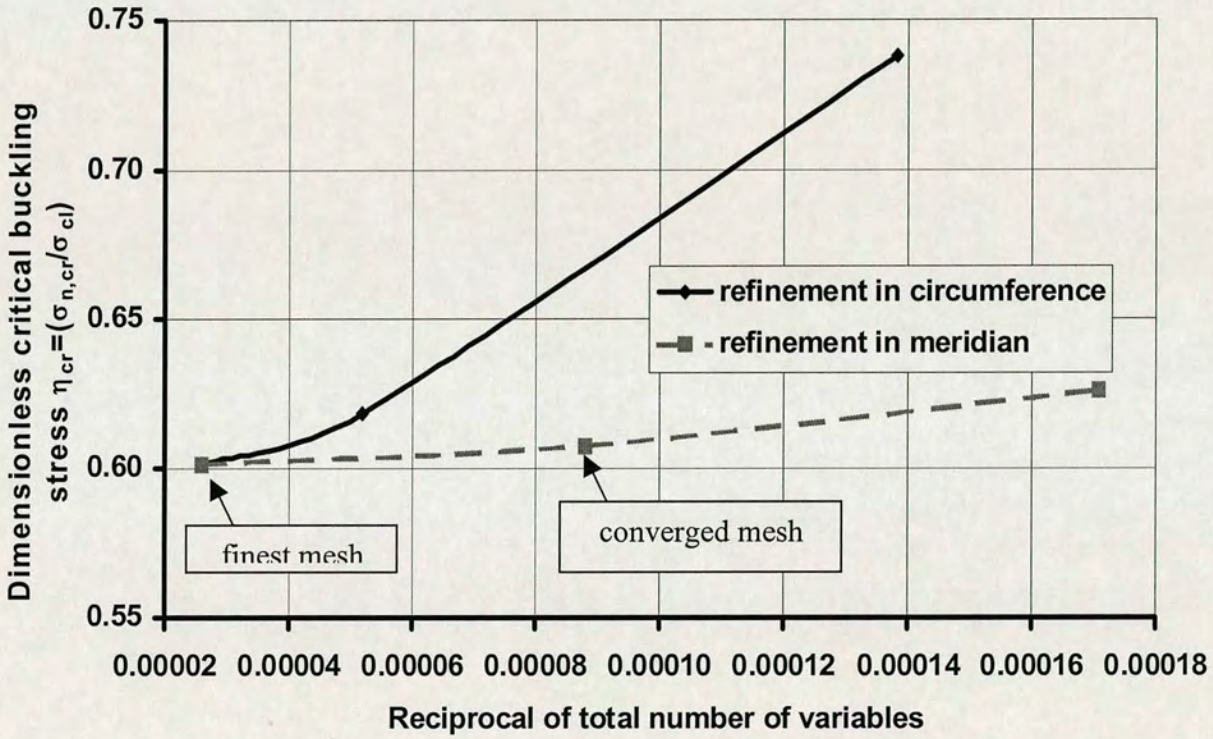

Fig. 4.11 Mesh convergence study for the imperfect shell under uniform axial compression

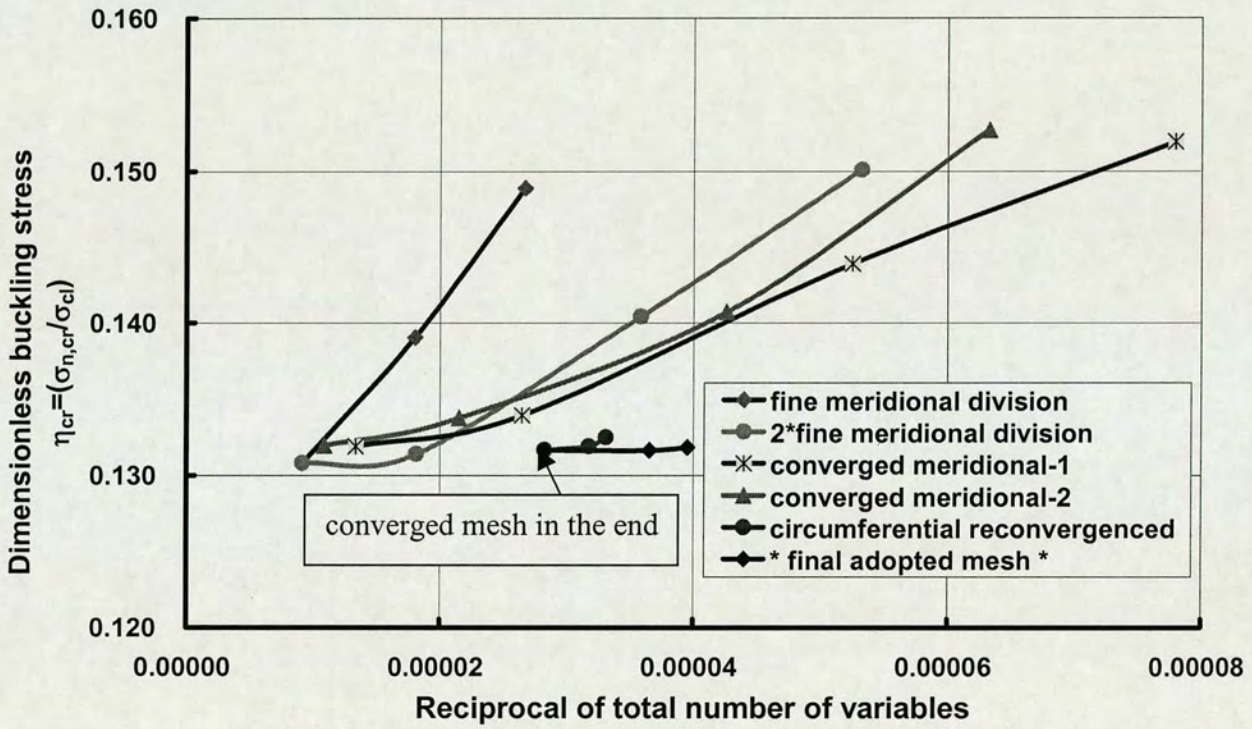

Fig. 4.12 Mesh convergence study for the imperfect shell under non-uniform axial compression

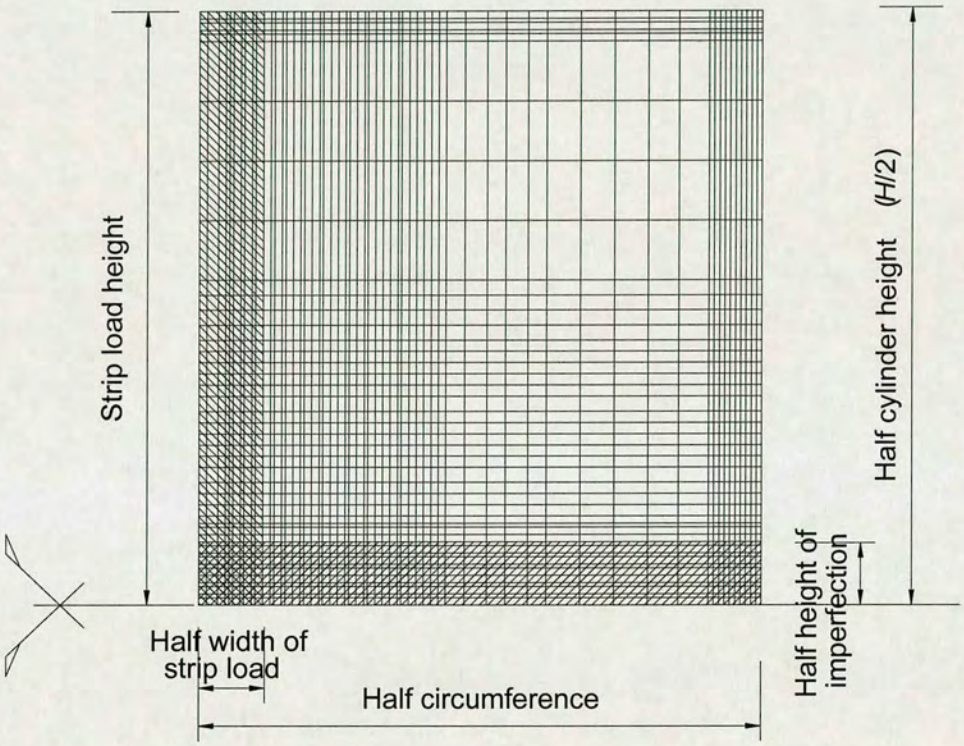

Fig. 4.13 Model mesh

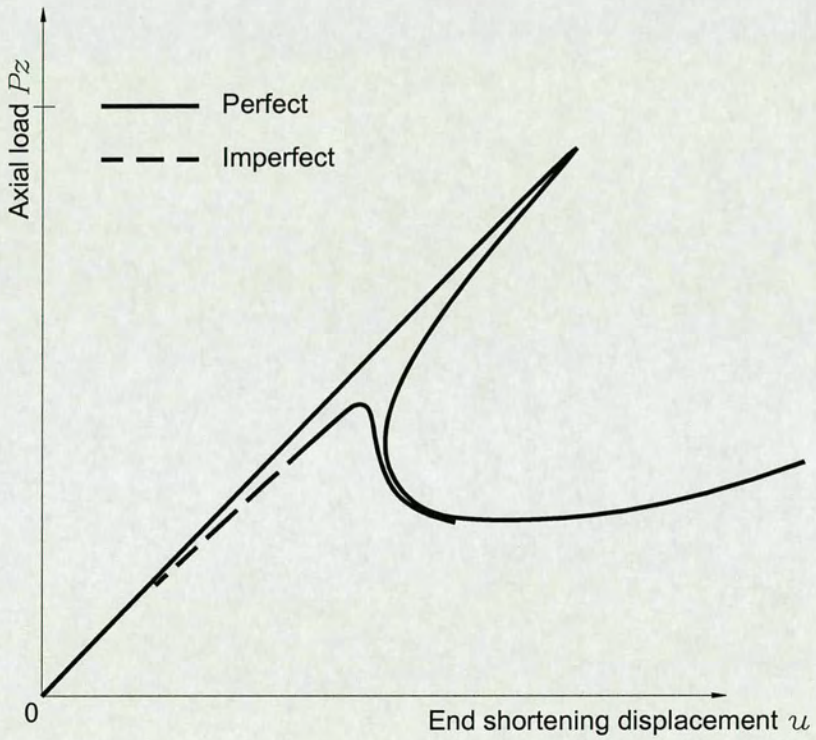

Fig. 4.14 Behaviour of cylindrical shells under axial compression (after Donnell & Wan, 1950)

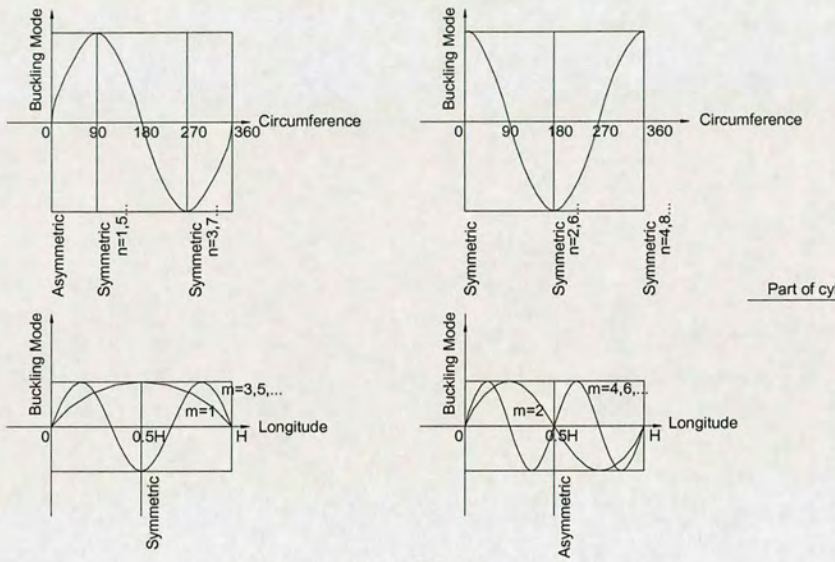

B.C. combination of 1/8 cylinder model

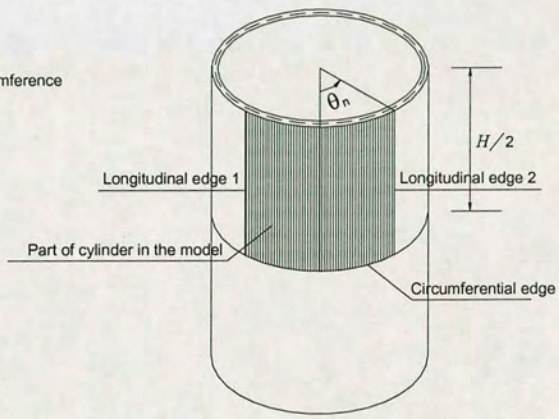

Modelling part in the whole silo

Circumferential edge		Longitudinal edge 1		Longitudinal edge 2		n	m
Sym	Asym	Sym	Asym	Sym	Asym		
√		√			√	1,3,5...	1,3,5...
√		√		√		2,4,6...	1,3,5...
	√	√			√	1,3,5...	2,4,6...
	√	√		√		2,4,6...	2,4,6...

Fig. 4.15 Combinations of the boundary conditions

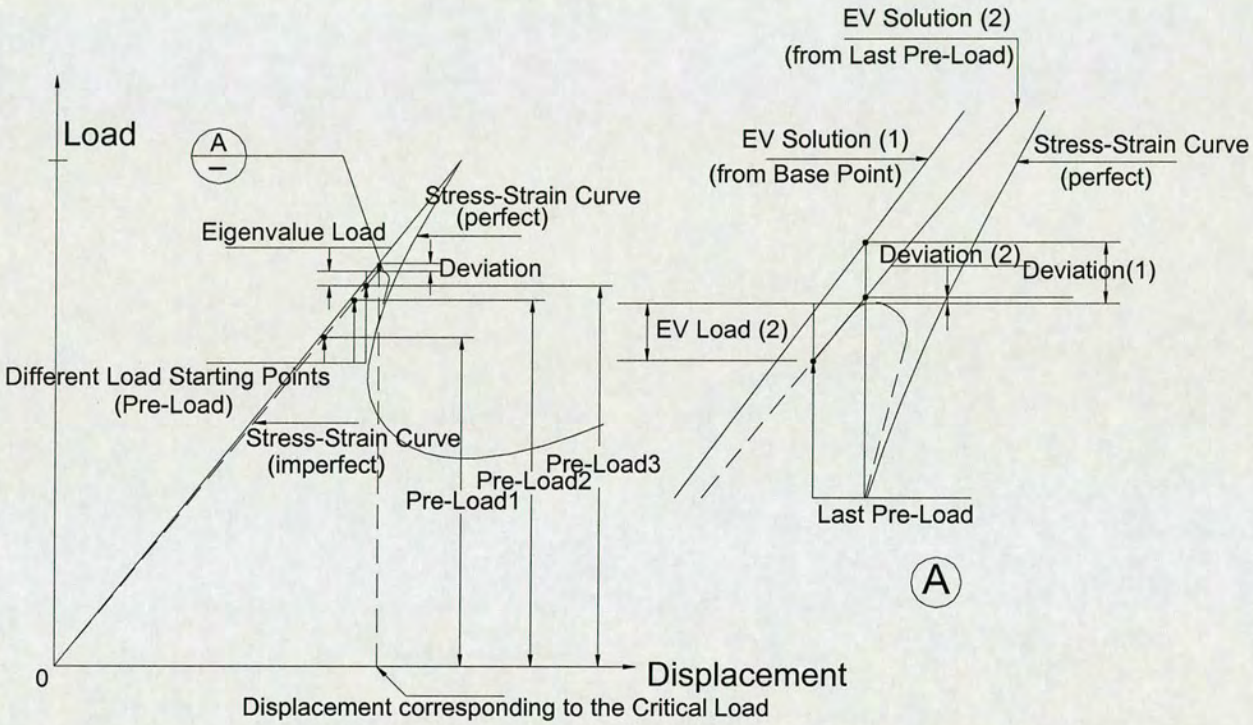

Fig. 4.16 Load-displacement curves

Name	Sources
Material Non-linearity	Plasticity
	Fracture/Cracking
	Damage
	Creep
	Volumetric Crushing
	Rubber
Geometric Non-linearity	Large Deflection/Rotation
	Large Strain
	Non-conservative Loading
Boundary Conditions	Lift-off Supports
	General Contact
	Compressional Load Transfer
	Dynamic Impact

Table 4.1 Sources of non-linearity

Chapter 5

SHELL BUCKLING BEHAVIOUR UNDER ELEVATED LOCAL AXIAL COMPRESSION STRESSES

5.1 Introduction

The thin cylindrical shells of storage structures are often subjected to axial compressive stresses that can cause buckling failures. In silos, the primary sources of such axial compression are friction between the stored solid and the wall together with the more complicated effects of circumferentially non-uniform normal pressures. Axial compressive stresses arise also in tanks under wind loading and in horizontal tanks that are partially filled with fluid. Buckling under axial compression is normally the controlling design consideration for such structures.

Unsymmetrical loads on silo walls (Nielsen, 1983, 1998; Ooi et al, 1990) lead to local high axial compression (Rotter et al, 1986; Rotter, 1998) (Fig. 5.1), which is a common cause of buckling failures in service (Fig. 5.2). The magnitude of local stress that can be sustained before buckling depends very much on the stress distribution in which it occurs, and high stresses that act over only a small part of the circumference may be expected to reach much higher values (Rotter, 1986, 2000; ENV 1993-4-1, 1999) than the value for uniform axial compression buckling. However, the conditions that lead to buckling under unsymmetrical stresses have received very little attention (Rotter, 1998, 2001). The few studies that address this problem either deal with linear buckling (Bijlaard and Gallagher, 1959; Libai and Durban, 1977; Peter, 1974) or deal only with buckling above a support (Guggenberger et al, 2000). This study is the first to consider axial compression buckling using a geometrically nonlinear analysis, considering geometric imperfections, and exploring the buckling strength under a stress regime that is distant from boundary conditions.

Geometric imperfections in silo wall play a key role in reducing the cylinder buckling strength. The buckling strength of a thin cylindrical shell under axial compression is

known to be very sensitive to geometric imperfections (Yamaki, 1984; Rotter, 1985b; Calladine, 1995) and one of the most detrimental and well-defined imperfections is a local depression due to the rolling process of the steel plate and shrinkage of the weld (Bornscheuer et al, 1983; Rotter and Teng, 1989; Teng and Rotter, 1992; Rotter, 1996, 1997; Holst et al., 1999, 2000). The rationally-based local axisymmetric inward (Type A) imperfection of Rotter and Teng (1989), which has been used in many later studies, was adopted.

Reliable quantification of the effects of high local stresses and geometric imperfections presents a considerable challenge. To be consistent with the draft European Standard for Metal Shells (ENV 1993-1-6, 1999), this study obtained predictions using the following analysis types: Linear Analysis (LA/LEA), Geometrically Non-linear elastic Analysis (GNA) and Geometrically Non-linear elastic Analysis with explicit modelling of Imperfections (GNIA). In addition, a few calculations adding material non-linearity (GMNA and GMNIA) were performed to check on its impact.

It is well known that the internal pressure from a stored solid or fluid in a cylinder can reduce the detrimental effects of the imperfections (Harris et al., 1957; Weingarten et al, 1965; Rotter and Teng, 1989; Rotter, 1997), and that the stiffness of a stored solid also increases shell buckling strength further (Trahair et al., 1983; Rotter and Zhang, 1990). However, since this is the first study of the problem of local high stresses, these strengthening effects were ignored here.

The aim of this study is to use a load case that produces local high stresses in the cylinder where can be predicted easily, the geometry imperfection to be positioned and since the effect of geometry imperfections as well as the high local stresses can be explored simultaneously. It is also important that the effects of the high axial stresses should not be confused with those that would be associated with local bending stresses and their accompanying membrane stresses if local loads normal to the wall exist. This study consequently chose a load case that leads to high local axial compression at the centre of the shell, in a well-defined position, and substantially free of local bending. It is not

proposed as a typical practical load case, but one that permits a clear scientific study to be conducted without ambiguity.

5.2 Modeling and Coordinate System

The majority of the model dimensions were described in Chapter 3. However, a slightly different shell model which has a height $H = 30\ m$, radius $R = 5\ m$, and thickness $t = 10$ mm giving $R/t = 500$ and $H/R = 6$ was used for the check of the boundary conditions and their influence. These dimensions still make it a relatively tall and moderately thin cylinder, in which the boundary conditions do not affect the calculated buckling stress. A schematic drawing of a cylinder under local axial compression was already shown in Fig. 3.6.

With the mesh convergence study under non-uniform axial compression with imperfections in Chapter 4, the edge of the strip load and the four boundaries (including the area nearby) were modelled using a very fine mesh, where the element sizes were chosen to be all less than $0.25\lambda_0$. A smooth variation in the element sizes was used elsewhere (Fig. 4.11).

A cylindrical coordinate system was used, where a point on the shell middle surface is defined by the circumferential coordinate θ, radial coordinate r and axial coordinate z (Fig. 4.6). The half angle that defines the circumferential width of the strip load is θ_n. The full strip width is $2\theta_n$; twice that appearing on the mesh (Fig. 3.6). Two different strip widths (θ_n=10° & 45°) were analysed to explore the behaviour under moderately local and highly local loads.

5.3 Buckling Stress Characterising and Validation

The axial stress pattern derived from membrane shell theory was compared with the stress pattern from a non-linear elastic calculation, incorporating bending effects and geometric non-linearity (GNA & GNIA) in Fig. 5.3. The maximum membrane theory axial stress (at the mid-plane) was used to define the applied load and termed the nominal stress σ_n here. When the load displacement curve of a thin-cylindrical shell under local axial compression reaches the first peak value after just passing the elastic linear period, the curve drops, which starts the decrease of the whole support ability. This critical point is termed "at buckling" (Fig. 5.10). At buckling, this nominal stress reaches the value $\sigma_{n,cr}$, which is used to characterise the buckling stress state in all analyses. The stresses in Fig. 5.3 are shown at the instant of buckling and the bending effects that cause a significant smoothing of the applied stress pattern.

To validate this analysis procedure, it was tested by comparing the buckling strength of axisymmetrically imperfect cylinders under uniform axial load with other study (Teng and Rotter, 1992; Fig. 5.4). Because the imperfection shape was defined using different half-wavelengths in these analyses (the linear bending half-wavelength λ_0 was used in Teng and Rotter, 1992; the classical axisymmetric buckling mode half-wavelength λ_{cl} was used in this analysis and the ratio of $\lambda_0/\lambda_{cl}=\sqrt{2}:1$), differences can be observed between two series of analyses and the influence of the imperfection half-wavelength in the buckling strength was verified again: the most critical wave-length increases with the increment of the imperfection amplitudes and shorter half-wavelength provides a higher buckling stress (Fig. 5.5, Rotter, 1997). This trend is also influenced by the imperfection type adopted (Teng and Rotter, 1992). Furthermore, with different half-wavelength, the number of half-waves around the circumference is also changed. Overall, a satisfactory match can be observed between the four FE solutions (This analysis provides slightly higher buckling strength predictions than Teng and Rotter, 1992).

5.4 Boundary Conditions and their Influences

To reduce the problem to a manageable size, only one quarter of the whole cylinder was analysed with the combination of different boundary conditions. This is one of the most important cases for the validity of the whole analyses results and the following boundary conditions were applied in the analyses:

5.4.1 Boundary Conditions

Symmetry conditions were used at the mid-plane section and the top end section of the shell was fully restrained against the translation in radial direction, but free to move axially and rotate about the circumference. This is aimed for the elevated high local stress status in the mid-plane, which stays the focus of this study. A symmetry boundary was placed along the two meridional edges as well, which was verified in Chapter 4, to provide the lowest buckling load. In short, a simply supported case (*S3* in Singer's notation) as stated in Eqn. (4.3) (Yamaki, 1984) was used for this analysis from the view of whole cylinder.

5.4.2 Stresses Distributions in Boundaries

Dimensionless axial and circumferential membrane stress distributions around the half circumference in the mid-plane of the cylinder of two different strip loads (a wide strip load and a narrow strip load for comprehensive representations) are shown in Figs. 5.6 & 5.7 and the spread of the strip load width can be represented roughly from the distribution of the axial membrane stress. The stress distribution at the top section is about 1% of that in the mid-plane, which means that it can move freely in the axial direction at the top section as defined in *S*3 (Eqn. (4.3)).

In addition, it will be beneficial to examine the deformation of all boundaries to explore if they fit just as planned.

5.4.3 Deformations on Boundaries

The following diagrams of deformation (Figs. 5.8 & 5.9) illustrate the variation of the boundaries used in the analyses, in which one line shows the initial shape of the cylinder and another line shows the deformed shape when the load has been applied. The mid-plane section is a plane of symmetry about the plane z=0 which means that the displacement is restrained in the z direction while keeping the rotation of r and θ unstrained.

With the combination of the top and mid-plane sections together with symmetry of the two side bounds, all above diagrams illustrate the possibility of a large deformation of the cylinder in the buckling. Most of all, this boundary configuration does not restrain global bending of the whole cylinder, which is unavoidable under the asymmetric loading.

5.4.4 Summary

The boundary conditions adopted in the modelling permit a possible global bending no matter from the observation of the cylinder deformation as well as from the stress distribution. The discrepancy between the model boundaries and the desired simply supported condition — *S3* (Yamaki, 1984) is very limited.

5.5 Methodology of Analysis

As discussed in Chapter 4, there are several different analyses types available in the static analysis of the finite element analysis and the adoption of each type depends heavily on the corresponding part in the code (ENV 1993-1-6, 1999).

5.5.1 Analysis Procedure

Elastic shell buckling stability analyses may be performed using either geometrically linear or non-linear theory. A linear eigenvalue analysis (LEA) was used first on the geometrically perfect structure to obtain estimates of the elastic buckling load and the buckling modes, which are very useful for further study. Moreover, if the results of the present study are to be interpreted into the conceptual framework of the Euro-code for shell structures (ENV 1993-1-6, 1999), the critical stress of a linear eigenvalue analysis is needed as a key element of the description. It locates the structure correctly in the elastic-plastic interaction space by means of a slenderness parameter. The critical load from a linear eigenvalue analysis depends only on the membrane stresses and is unaffected by bending stresses (Rotter, 2002). Geometrically non-linear analyses (GNA & GNIA) with bifurcation tests were used next, to obtain the elastic perfect and imperfect buckling strengths. The load-displacement curve was obtained from this analysis type using Riks method (Riks, 1979). Geometric imperfections of different amplitudes were introduced to exploit the sensitivity of the buckling strength to imperfections.

5.5.2 Load-displacement Curve

A typical load-displacement curve/path for a thin-walled shell buckling under local compression with two different strip widths is shown in Fig. 5.10 to explore the phenomenon first. The main common trend is: during the period of the post-buckling, the load and/or the displacement may decrease as the solution evolves, and the modified Riks method (Riks, 1979) is an algorithm that allows effective solution for such cases. Due to this special strength response of the shell, the GNA and GNIA analyses were needed to determine the pre-buckling, buckling and post-buckling equilibrium curves.

5.6 Typical Behaviour of Perfect Cylindrical Shells

5.6.1 Deflected Shapes

Two different strip load angles (θ_n=10° and 45°) were studied first. Fig. 5.11 shows the different buckling modes with θ_n=10° and 45°. The deformed shape of the cylinder down the centre of the strip in the pre-buckling, buckling and post-buckling stages are shown in Figs. 5.13 & 5.14. The deformations plotted in Figs. 5.13 & 5.14 are from a non-linear analysis and Fig. 5.11 describes the buckling mode from LEA analysis, which makes the deformation depends heavily on the scale of the show. To demonstrate the suitability of the meridional boundary adopted in the analyses, a full circumference of the shell was studied in two load cases and the same shapes were obtained (Figs. 5.11 & 5.12). A few other combinations of meridional boundaries were also analysed which led to the same conclusion: the symmetry meridian down the centre of the strip loading gives the lowest buckling mode.

From the deflected shape around the circumferential line at the midplane (Fig. 5.14), two different phenomena can be identified: the shape for a narrow strip (R/t = 500, θ_n = 10°) shows a buckle in the middle of the strip. This contrasts with the wide strip (R/t = 500, θ_n = 45°), which buckles close to the strip edge. Furthermore, the narrow strip (R/t = 500, θ_n = 10°) retains the same buckle shape from initial buckling to post-buckling, though the displacement is increased due to the lost of stability after buckling. By contrast for the wide strip (R/t = 500, θ_n = 45°), a significant change of mode occurs in the post-buckling range.

The membrane stress distribution for different loading patterns is recorded in the following to examine this phenomenon further in detail.

5.6.2 Membrane Stress Distribution

The changing stress patterns down the centre of the strip and around the circumference at the midplane were examined next for these two cases.

From the diagrams (Figs. 5.15 – 5.18), it can be observed that in the pre-buckling state the compression stress zone is consistent with the loading extent though the upper part near the top section shows a little expansion due to the fact that the linear varying strip load is not big enough at the very top of the shell. The membrane axial stress distribution shapes of two cases are very similar and furthermore in the buckling state, they still keep this similarity, which presents a linear response prior to the buckling. This can also be seen in the load-displacement curve (Fig. 5.10).

In the post-buckling state, the situation is very different. The wide strip (R/t = 500, θ_n = 45°) shows the big discrepancy compared with the previous two states: the compression shape around the circumference changes into two peaks instead of one and the compression stress down the centre of the strip loading shows a reduction, which is caused by the re-distribution of the stress circumferentially in the post-buckling stage, works in concert with its corresponding deformation in Fig. 5.13. Furthermore, compression itself reduces a lot, which means the supporting ability decreases a lot after it buckles. By contrast, the narrow strip (R/t = 500, θ_n = 10°) also shows the big discrepancy compared with pre-buckling: The initial compression zone moves outside from the direct load applying area and occupies the former expansion extent, and correspondingly the majority of the load applied area is controlled by the expansion stress which means the instability in this area. This is consistent with the observation from the buckling mode.

5.6.3 Summary

From the comparison of deflected shapes and membrane stress distributions above, it is evident that there are two possible and distinct buckling phenomena for a cylindrical shell under local compression — the narrow strip (R/t = 500, θ_n = 10°) displays a buckle in the middle of the strip and so is termed as strip centre buckle (local load effect). By contrast, the wide strip (R/t = 500, θ_n = 45°) buckles close to the strip edge and so is called here a strip edge buckle (uniform load effect).

Strip centre buckles is dominated by the axial compression, but strip edge buckles is predominantly caused by the high membrane shear stress that develops due to the incompatibility of axial deformations at the edge of the strip.

Based on the above observations, the hypothesis was formulated that narrow loaded strips lead to strip centre buckles, but wide loaded strips cause strip edge buckles. If the axial membrane stress is high over an area far larger than a typical buckle, it may be supposed that conditions similar to uniform compression buckling will pertain and the local high shear will precipitate strip edge buckles. By contrast, where high stresses cover a zone smaller than a typical buckle, axial compression buckling with strip centre buckles will occur, at a much higher peak stress than for uniform compression. Further parametric study is needed to verify this for a general conclusion.

5.6.4 Effect of Non-linearity

To illustrate the geometric non-linearity of shell buckling under local axial compression, the following two diagrams (Figs. 5.19 & 5.20) are provided to show this characteristic. They show the axial membrane stress distribution at the mid-plane circumference at the point of buckling. It compares the results from a linear analysis (LA/LEA) with those from a geometrically non-linear analysis (GNA). The stress distribution according to membrane theory is shown for comparison. The effect of non-linearity is comparatively tiny in these two cases and this conclusion is found in all other cases considered here.

Material non-linearity is later examined in the parametric study.

5.7 Imperfect Cylindrical Shells

An axisymmetric imperfection may be regarded as the practical form that is most deleterious to the buckling strength under axial compression (Koiter, 1963; Bornscheuer, Häfner and Ramm, 1983; Rotter and Teng, 1989; Teng and Rotter, 1992; Rotter, 1996; Rotter, 1997; Holst et al., 1999; Holst et al., 2000) and therefore it is adopted as a typical type of imperfection in silo design. Many studies have explored this type of imperfection (for example: the shape of the axisymmetric buckling mode, modal, local, random imperfections) in the previous study (Koiter, 1945; Amazigo and Budiansky, 1969; Rotter and Teng, 1989; Teng and Rotter, 1992) and a local axisymmetric inward imperfection 'Type A', derived from the weld depression (Rotter and Teng, 1989; Teng and Rotter, 1992), is now regarded as one of the most critical imperfection types for the buckling of the realistic cylinders, greatly reducing the buckling strength even if the imperfection amplitude is only one wall thickness (Knoedel et al., 1995; Berry and Rotter, 1996). Thus it was adopted in all the imperfection analyses here.

5.7.1 Imperfection Characterisation

Fig. 3.8 describes the details of the local axisymmetric inward imperfect cylinder outline near the mid-plane, with one cylinder wall thickness as the maximum imperfection amplitude. The shape of the local inward axisymmetric imperfection has been stated before in Eqn. (3.11-3.13) (Rotter and Teng, 1989).

5.7.2 Influence of Imperfections

Figs. 5.21 and 5.22 show the changing axial mode of shell buckling under uniform compression subjected to imperfection amplitude changes for both local inward and outward axisymmetric imperfection 'Type A' (Rotter and Teng, 1989). The size of the critical buckle can rise to the whole height of the shell with an increase in imperfection amplitude, which in consistent with Rotter's results (Rotter, 2002). These figures also show the influence of this phenomenon on different forms of imperfections: an outward imperfection displays a slow increase of buckle size with the increase of imperfection amplitude.

As mentioned before, a comparison of the buckling strength of axisymmetrically imperfect cylinders under uniformly axial load among different procedures (Koiter, 1945; Amazigo & Budiansky, 1972; Teng and Rotter, 1992) is shown in Fig. 5.4. The results show the imperfection sensitivity of axially compressed cylinders: The asymptotic solutions for a local inward deviation by Koiter (1945) and Amazigo & Budiansky (1972) are slightly lower than the finite element calculations at large imperfection amplitudes.

Load-displacement curves are shown in Figs. 5.23, 5.24 and 5.25 for strip loads of circumferential extent $2\theta_n$=20° & $2\theta_n$=90° corresponding to strip centre buckles and strip edge buckles (Figs. 5.23 and 5.24 show the same node at the mid-plane while Figs. 5.23 and 5.25 show the maximum displaced node at the mid-plane). Different amplitudes of the imperfection have been used to obtain these curves.

To make the expression of buckling strength simple and clear in future analyses, dimensionless membrane stress (η, Eqn. (5.1)) was induced as an important strength index.

$$\eta = \sigma_{n,z} / \sigma_{cl} \qquad (5.1)$$

where $\sigma_{n,z}$ is nominal axial membrane theory stress and σ_{cl} is the classical solution for uniform axial compression (Eqn. (2.3)).

Initially, the behaviour is linear but at a larger load and for a larger imperfection the behaviour becomes moderately non-linear before the buckling load is reached. With the increase of imperfection amplitudes, the buckling load gradually decreases. For larger imperfections a post buckling plateau is reached at η = 0.53 and 0.31 accordingly.

From all the diagrams of axial membrane buckling stress distribution with different amplitudes of imperfections (Figs. 5.26 – 5.29), with the increase of the imperfection amplitude, either the buckling stress reduces or the compression zone shrinks. Furthermore, the critical buckling stress for R/t = 500, θ_n = 10°, δ_0/t=1.0 can only reach

circa 53% of its perfect case (also from Fig. 5.23), while correspondingly the critical buckling stress for $R/t = 500$, $\theta_n = 45^\circ$, δ_0/t=1.0 reaches only 37.2% of its perfect case.

The influence of the imperfection on the buckling strength is important and since this is critical issue in the analyses. What should be noted further is that the strip centre buckles cases seem to be more sensitive to the geometric imperfections than the strip edge buckles.

5.8 Conclusions

5.8.1 Summary

This chapter explored a typical thin cylindrical shell under local axial compression. The influence of geometric imperfections has been considered and different amplitudes of imperfection have been taken into account. Two different buckling phenomena were identified with corresponding, and distinct, buckling mode forms by using the deflected shapes and axial membrane stress distribution. Based on the content above, the following conclusions can be drawn:

5.8.2 Conclusions

A. Two possible and distinct buckling phenomena have been identified for a wide range of shell geometries subject to a wide range of strip loads;
B. For narrow strips, a strip centre buckle occurs caused by the axial compression, but for wider strips, a strip edge buckle is caused by the high shear induced by membrane incompatibility at the strip edge;
C. The influence of imperfection amplitude has been examined and shown to have a moderate effect;
D. Geometric non-linearity seems to have a minor effect on the stress distribution at buckling;
E. The influence of boundary conditions in the finite element analyses has also been explored in order to prove the validity of such analyses results here and afterwards.

After the initial explorations of the shell buckling under local compression, there is an urgent need to do a full series of parametric study on different geometry and loading configurations to examine this problem further aiming for the possible general rule(s).

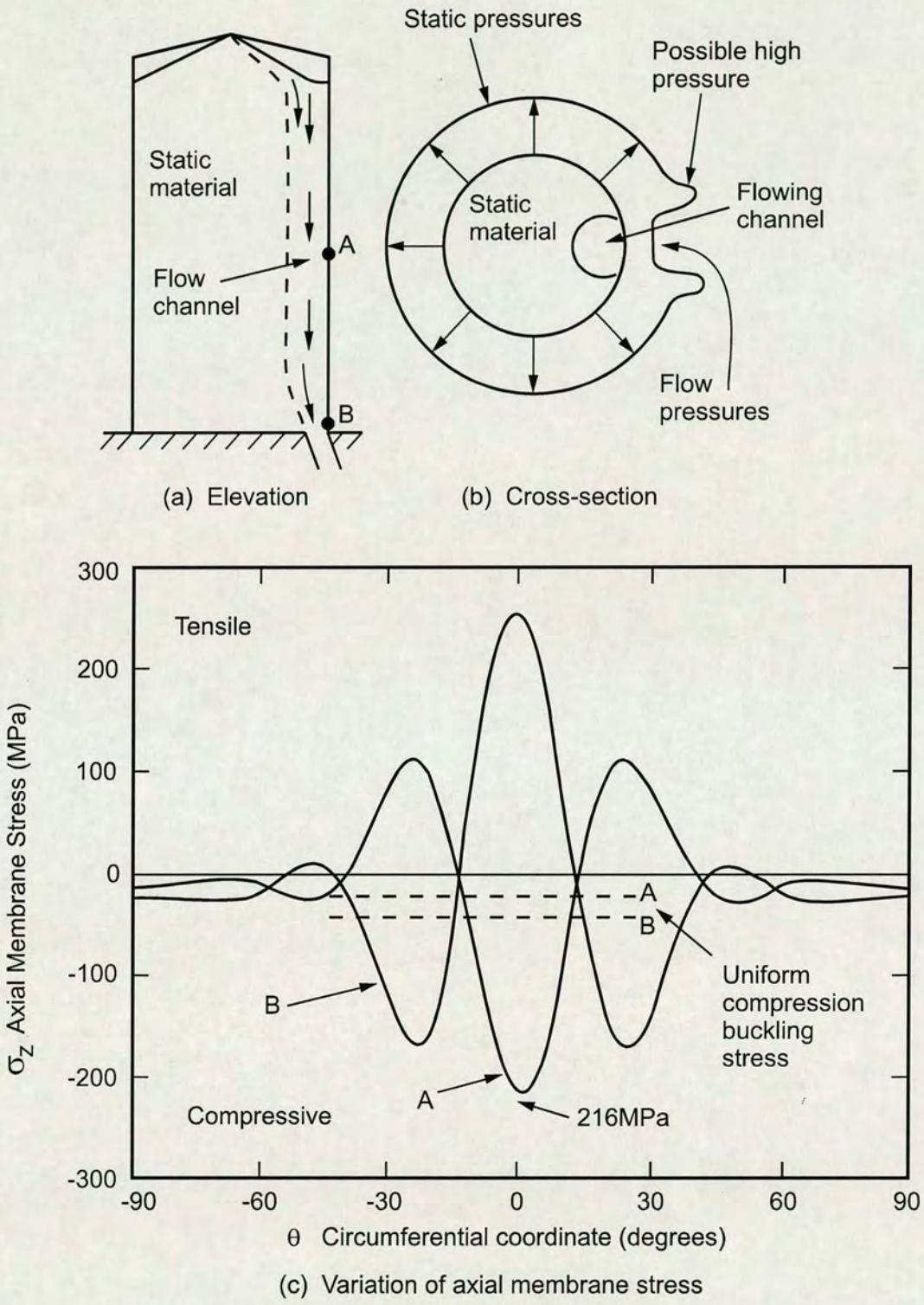

Fig. 5.1 Eccentrically discharged silo (after Rotter, 1986b)

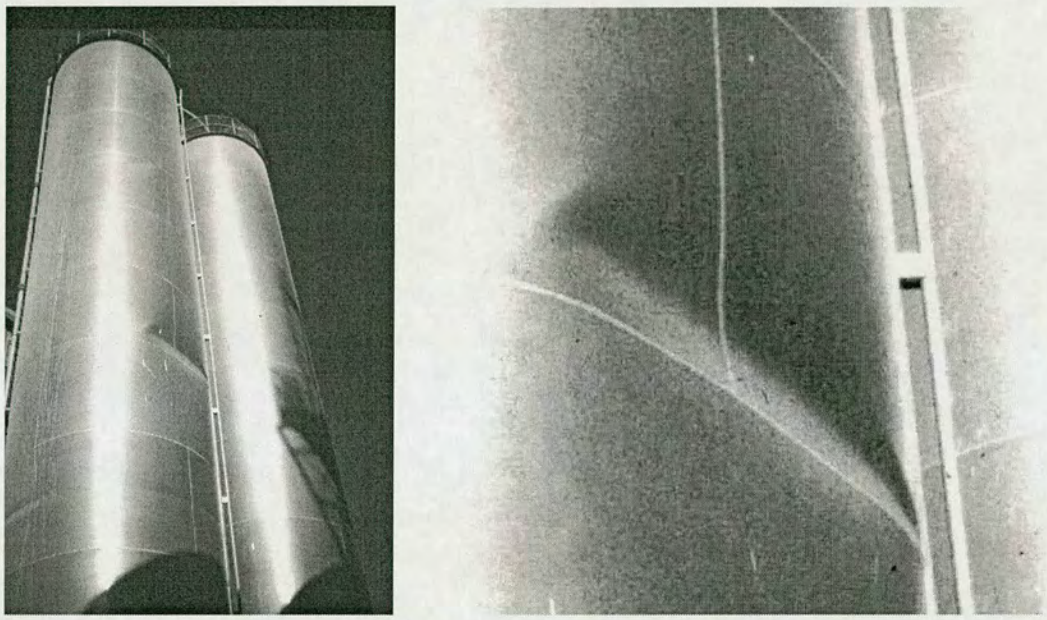

Fig. 5.2: Typical buckling failure under eccentric discharge (after Rotter, 2001)

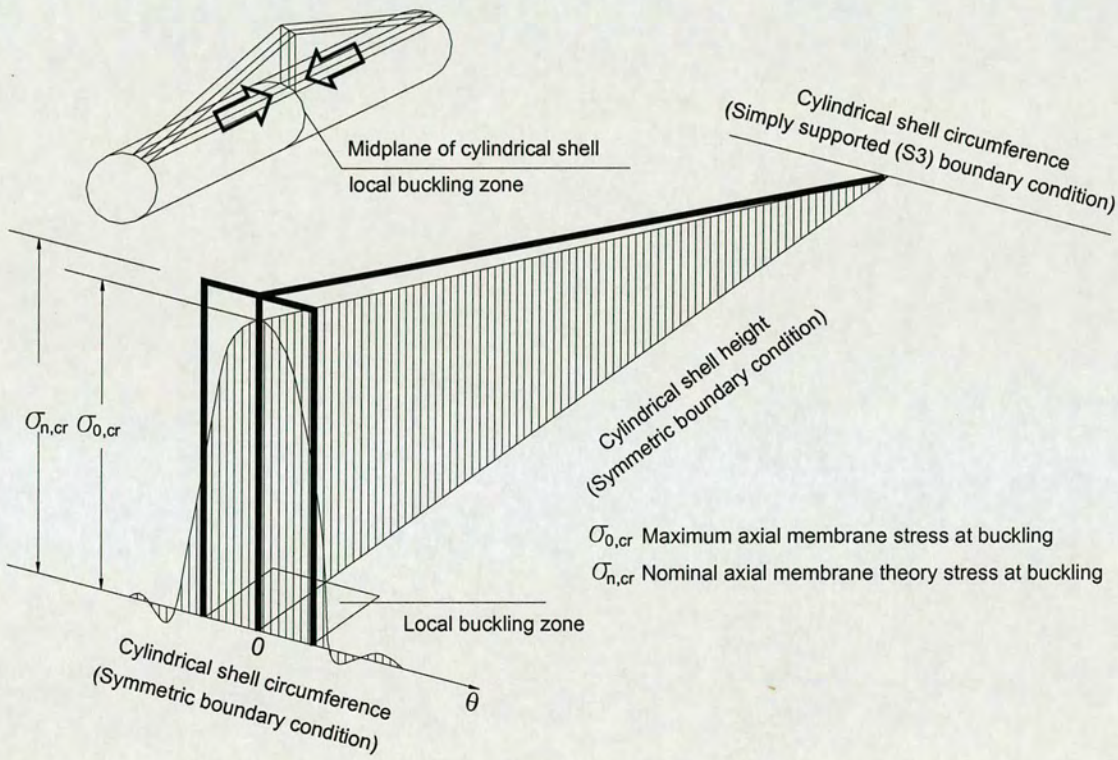

Fig. 5.3: Stress pattern at buckling

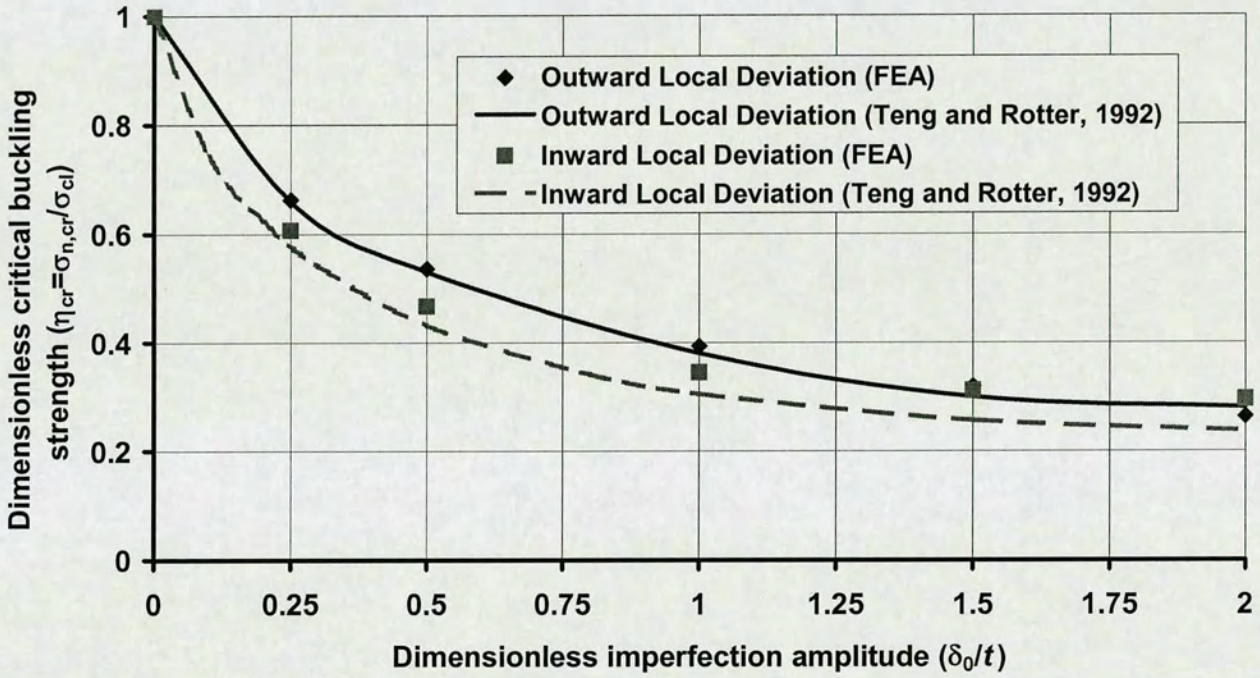

Fig. 5.4: Imperfection sensitivity of axially compressed cylinders

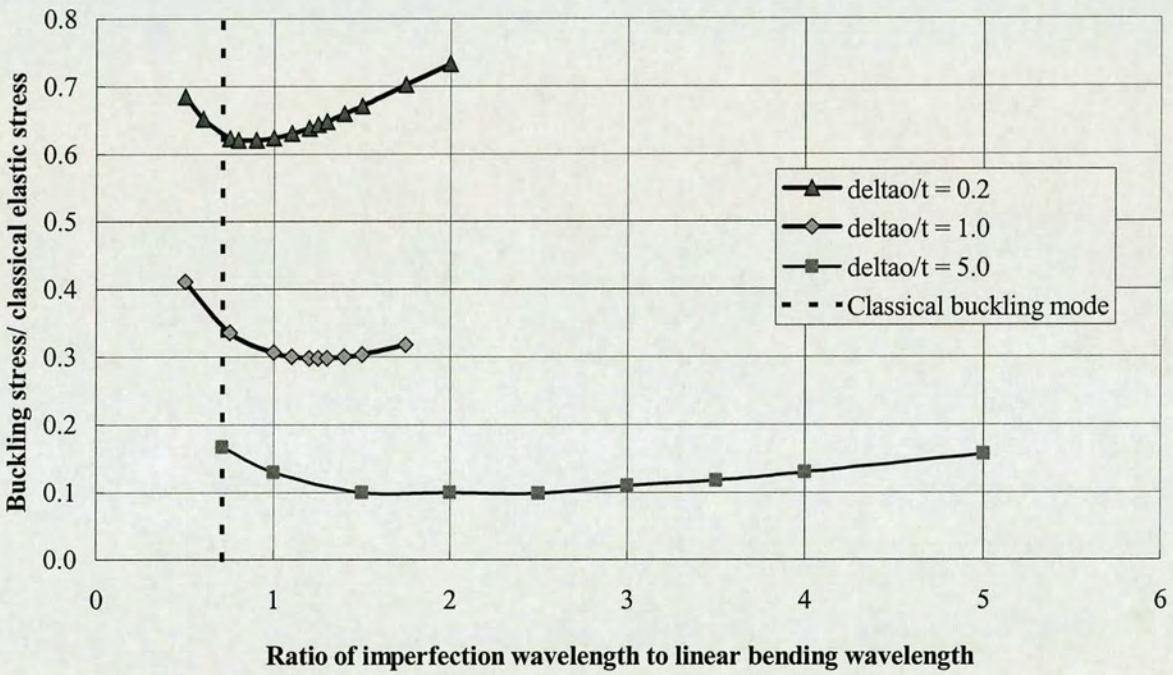

Fig. 5.5: Imperfection sensitivity varies with the half wavelength λ (after Rotter, 1997)

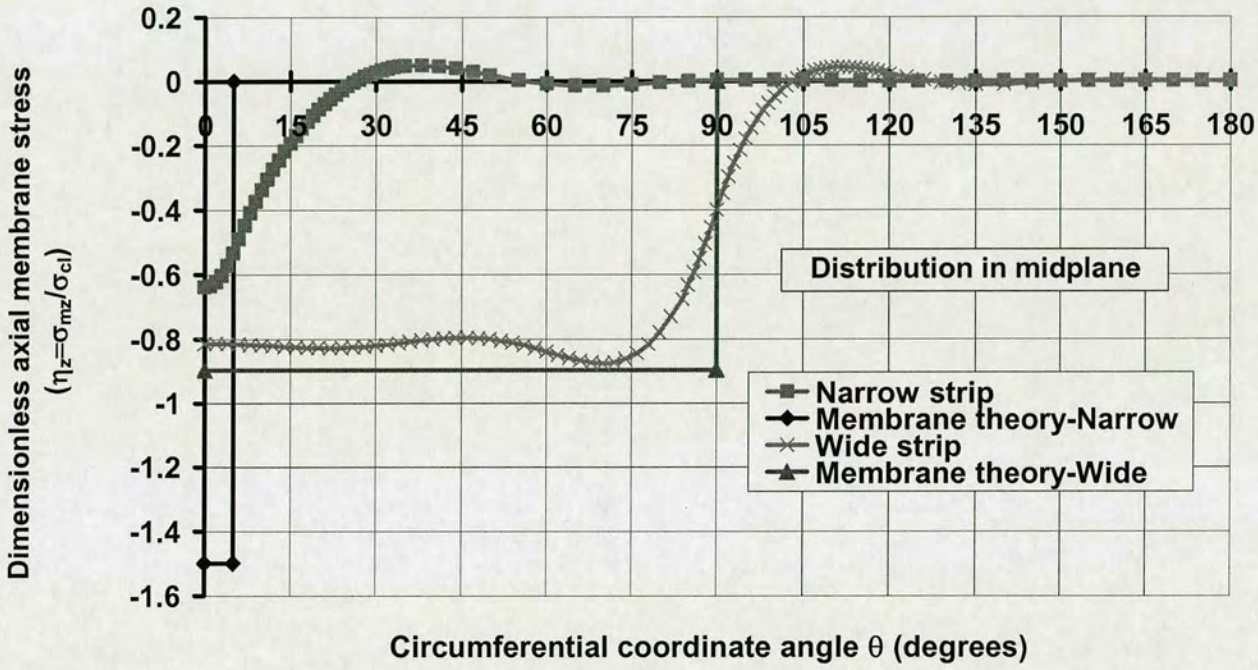

Fig. 5.6: Comparison of axial membrane stress distribution between wide strip (strip edge buckles) and narrow strip (strip centre buckles)

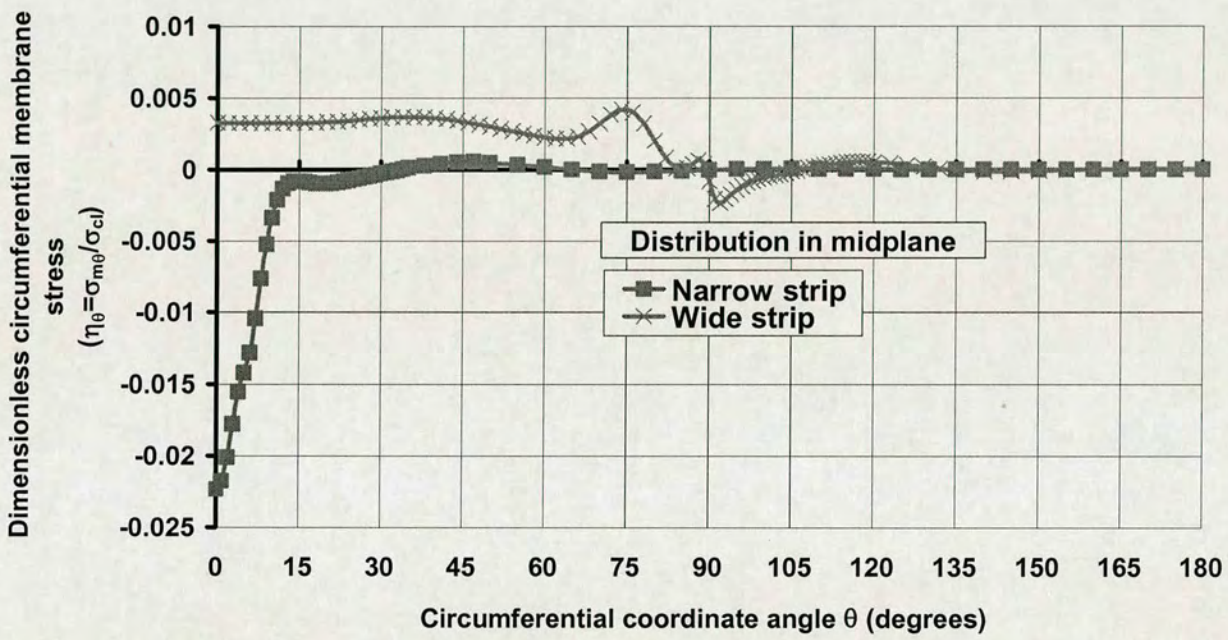

Fig. 5.7: Comparison of circumferential membrane stress distribution between wide strip (strip edge buckles) and narrow strip (strip centre buckles)

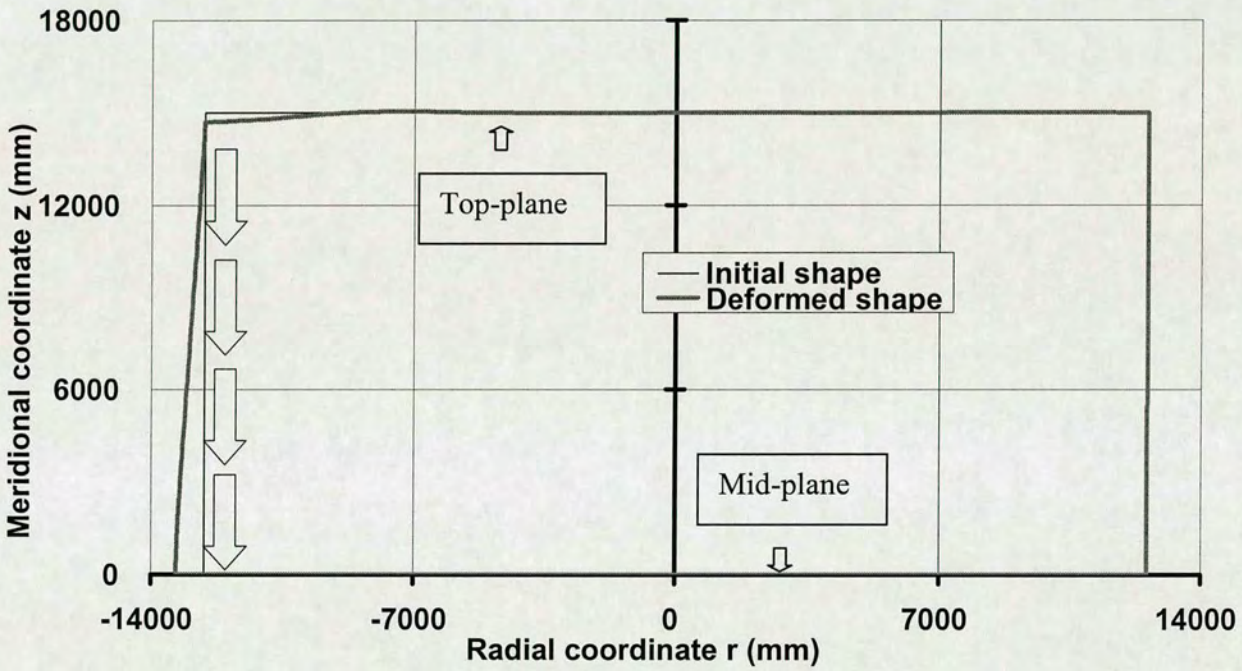

Fig. 5.8: Cylinder initial outline vs. deflected shape

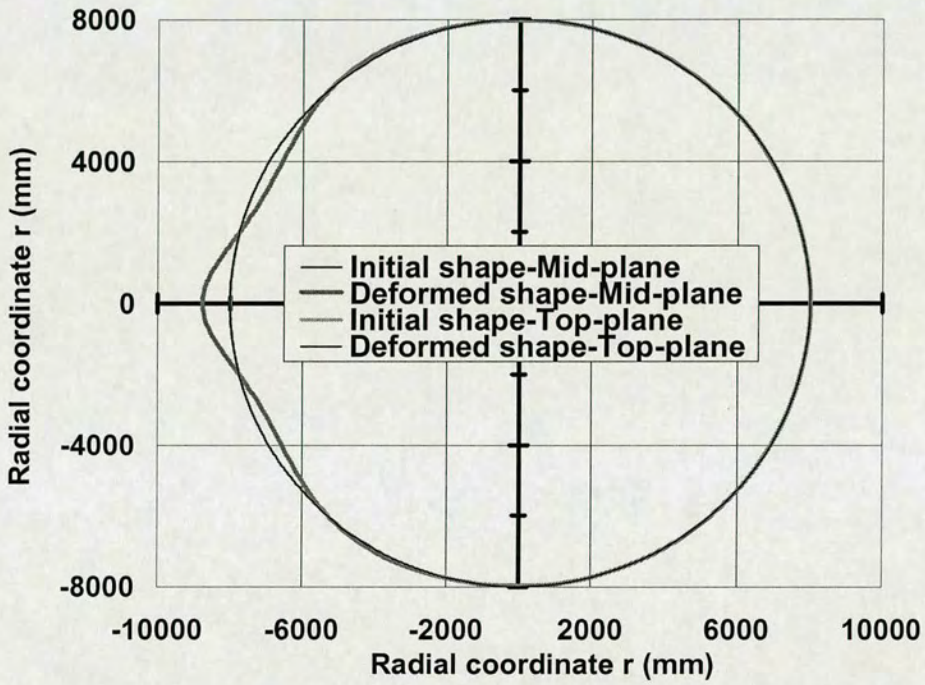

Fig. 5.9: Cylinder mid-plane section deflected shape

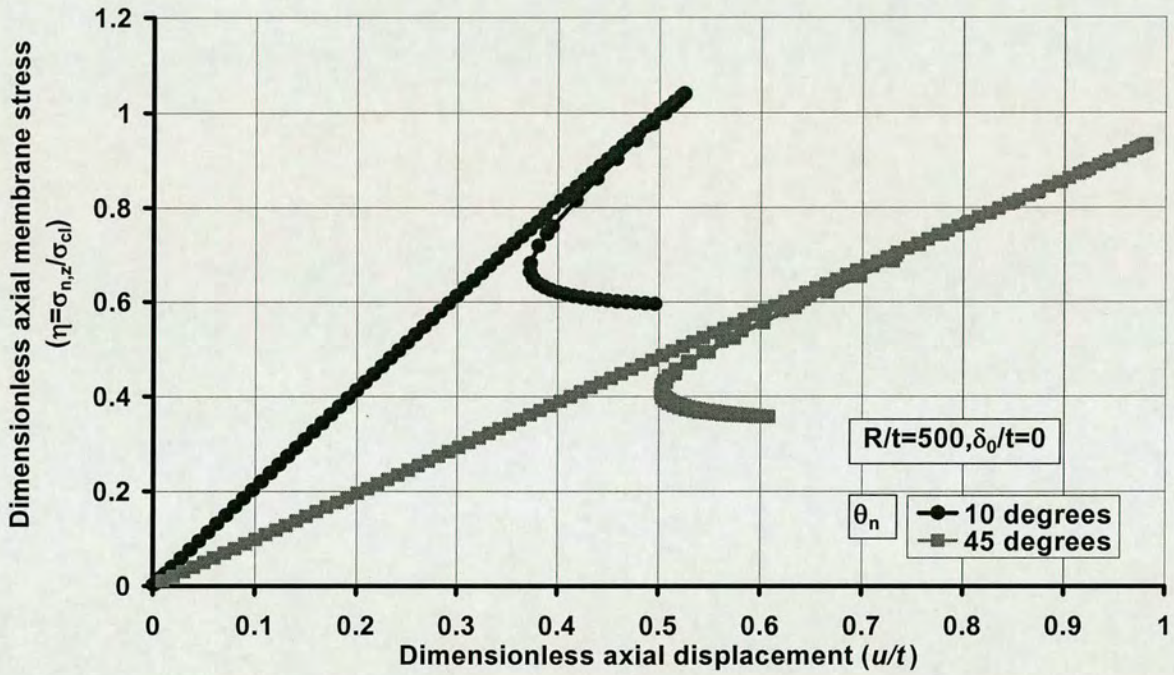

Fig. 5.10: Load-displacement curve of a thin-cylindrical shell under local axial compression with the influence of strip load width

(Note: δ_0/t refers to the ratio of cylinder imperfection amplitude to its thickness.)

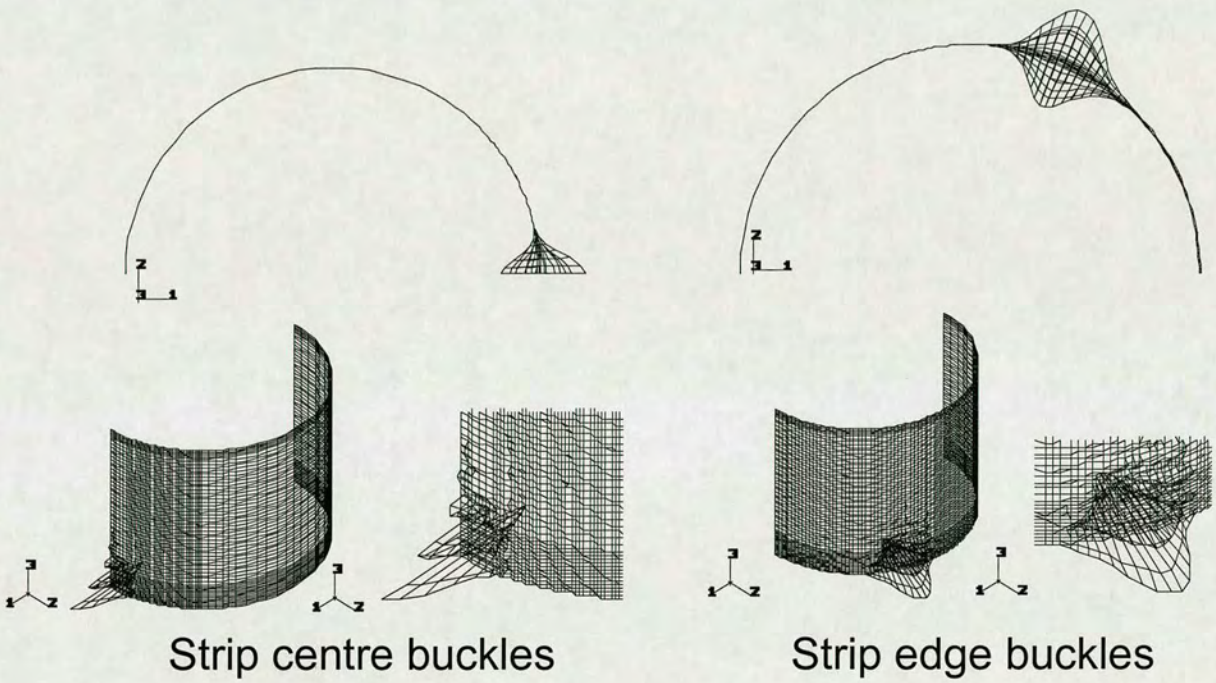

Fig. 5.11: Two different buckling modes (half circumference)

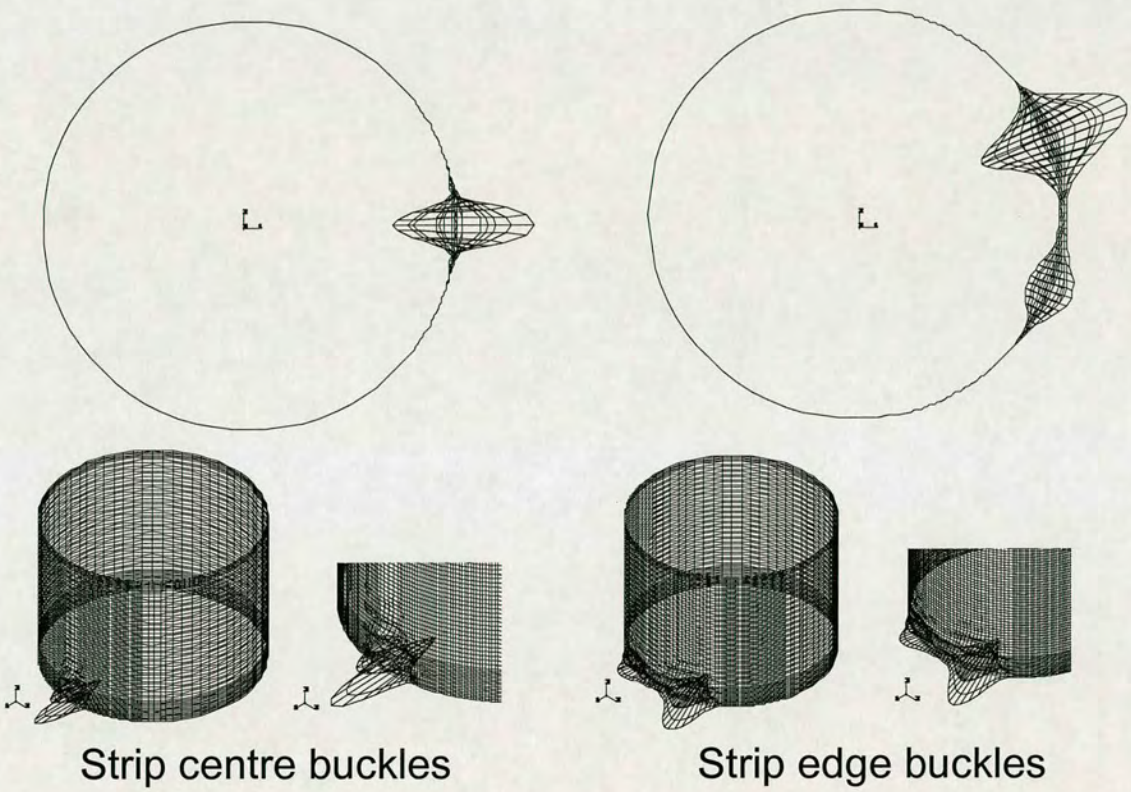

Fig. 5.12: Two different buckling modes (full circumference)

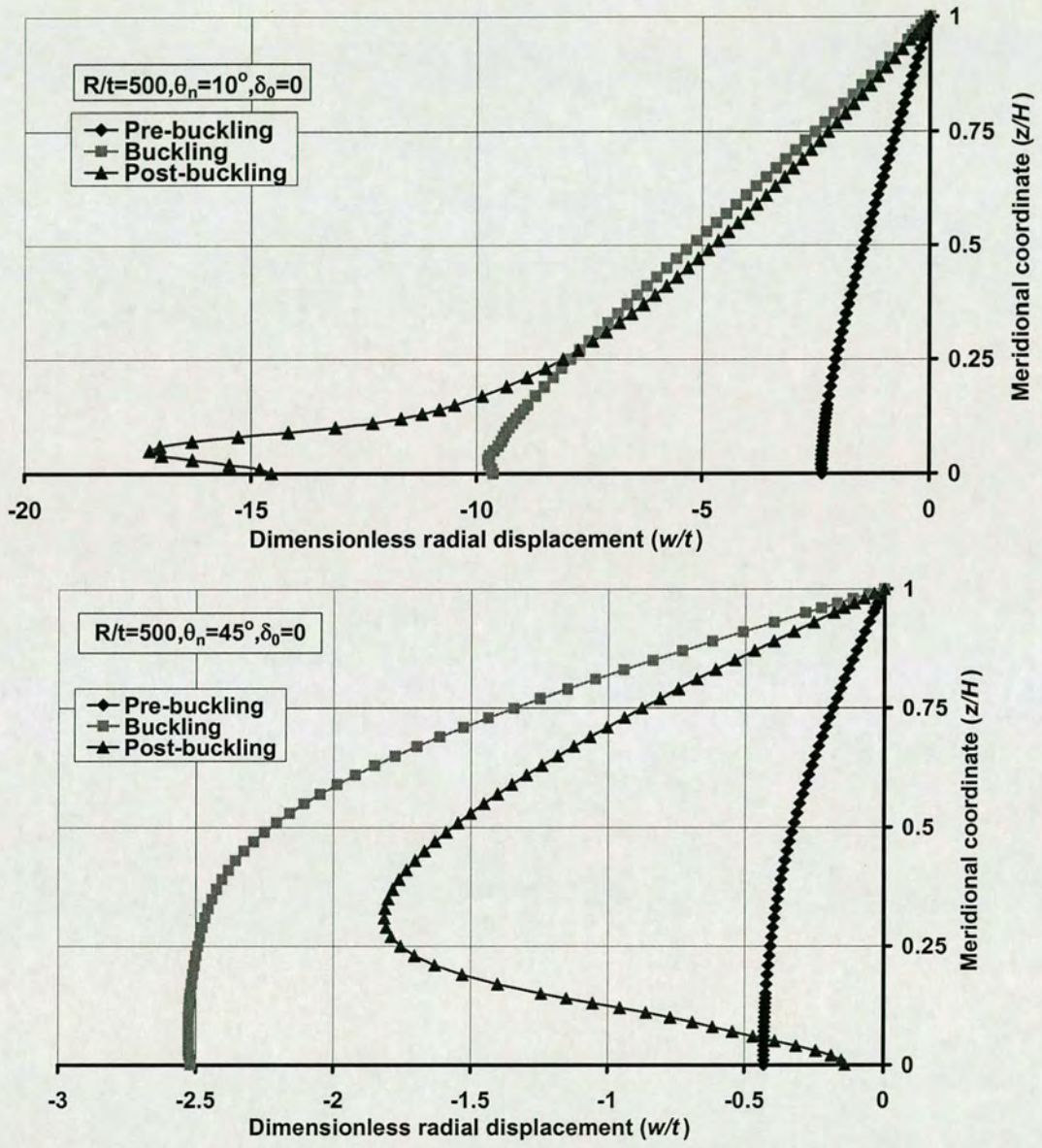

Fig. 5.13: Deflected shapes in pre-buckling, buckling and post-buckling states (along the meridional line at the centre of strip load)

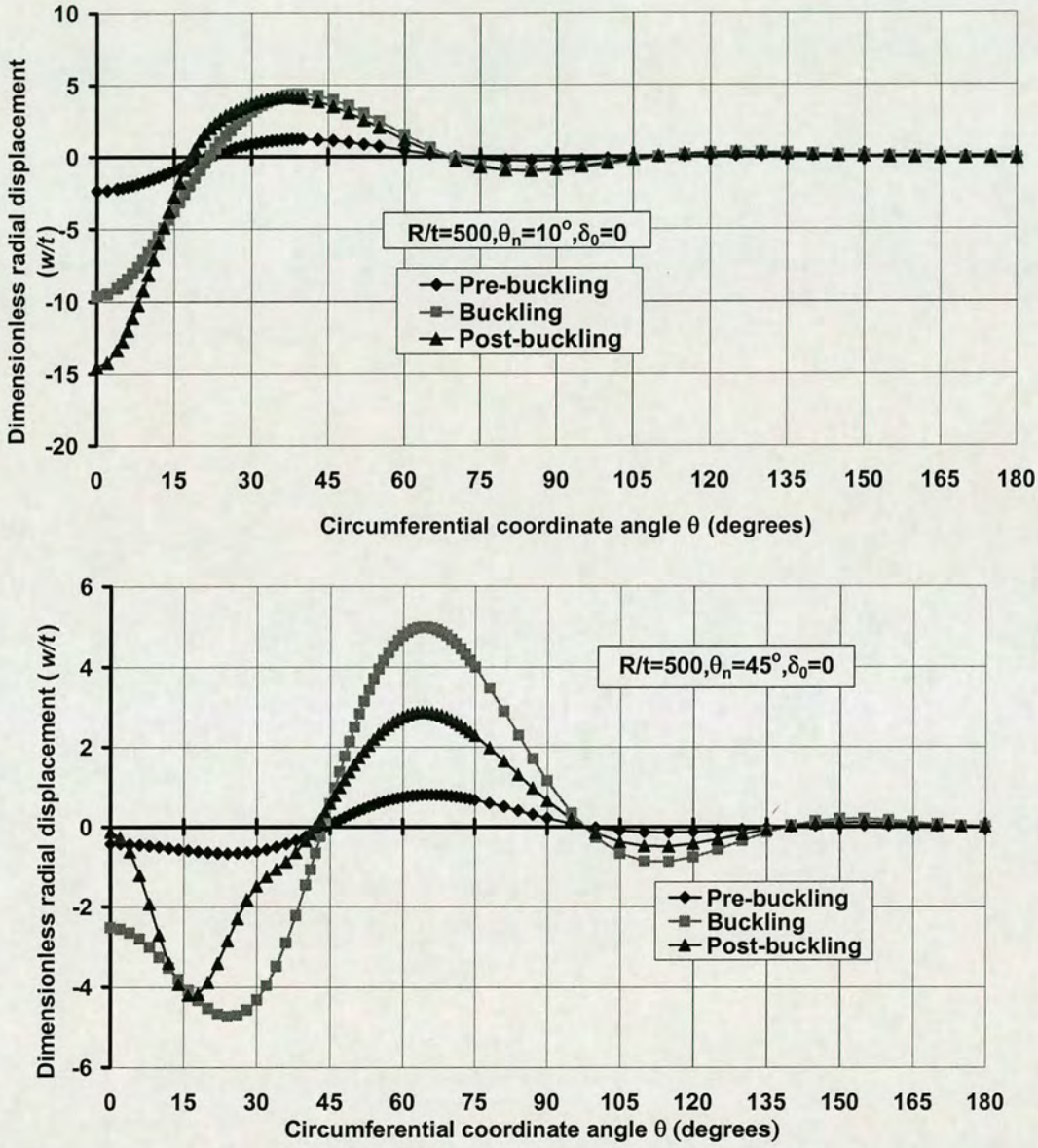

Fig. 5.14: Deflected shapes in pre-buckling, buckling and post-buckling states (around the circumferential line at mid-plane)

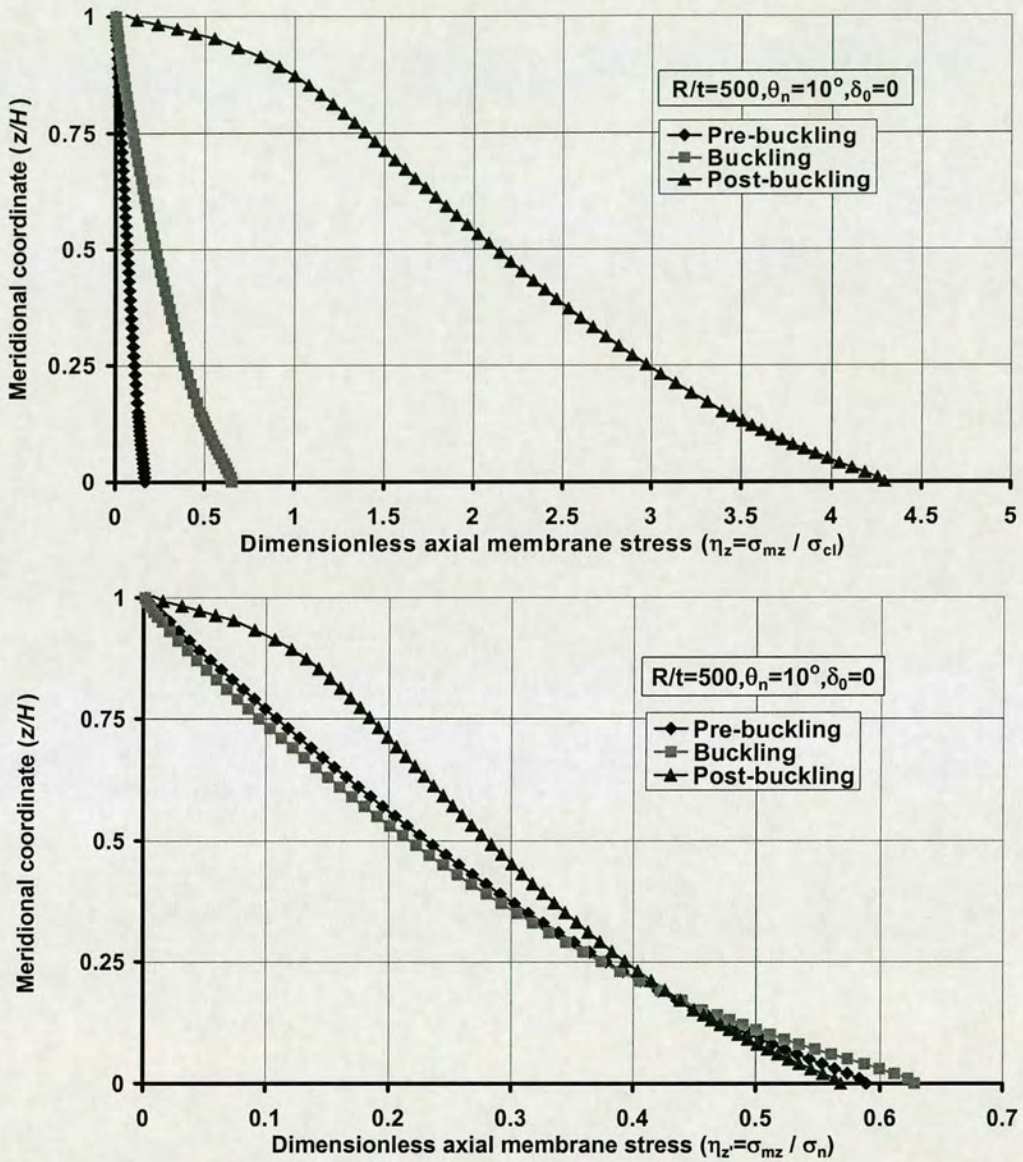

Fig. 5.15: Axial membrane stress in pre-buckling, buckling and post-buckling states (along the meridional line at the centre of strip load, strip centre buckles)

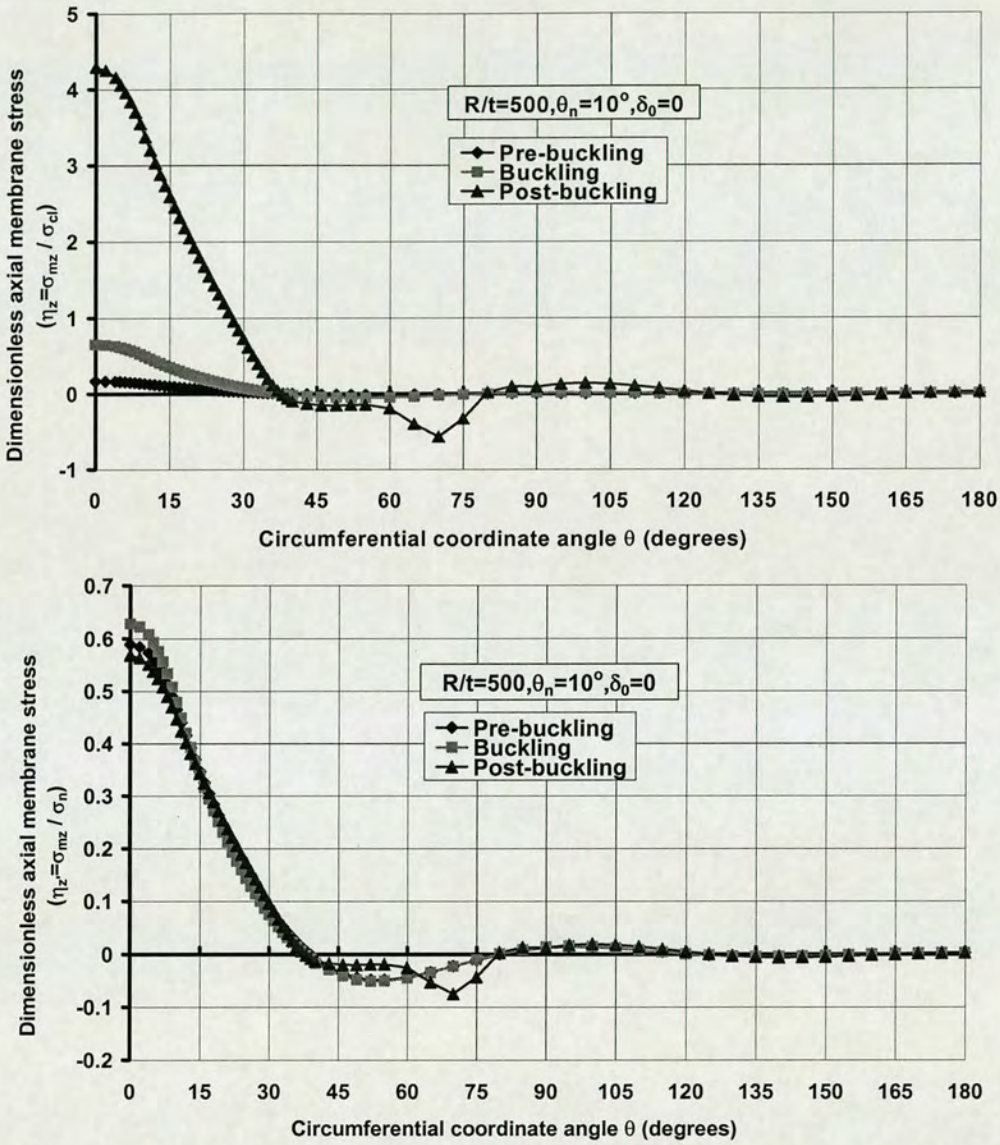

Fig. 5.16: Axial membrane stress in pre-buckling, buckling and post-buckling states (around the circumferential line at mid-plane, strip centre buckles)

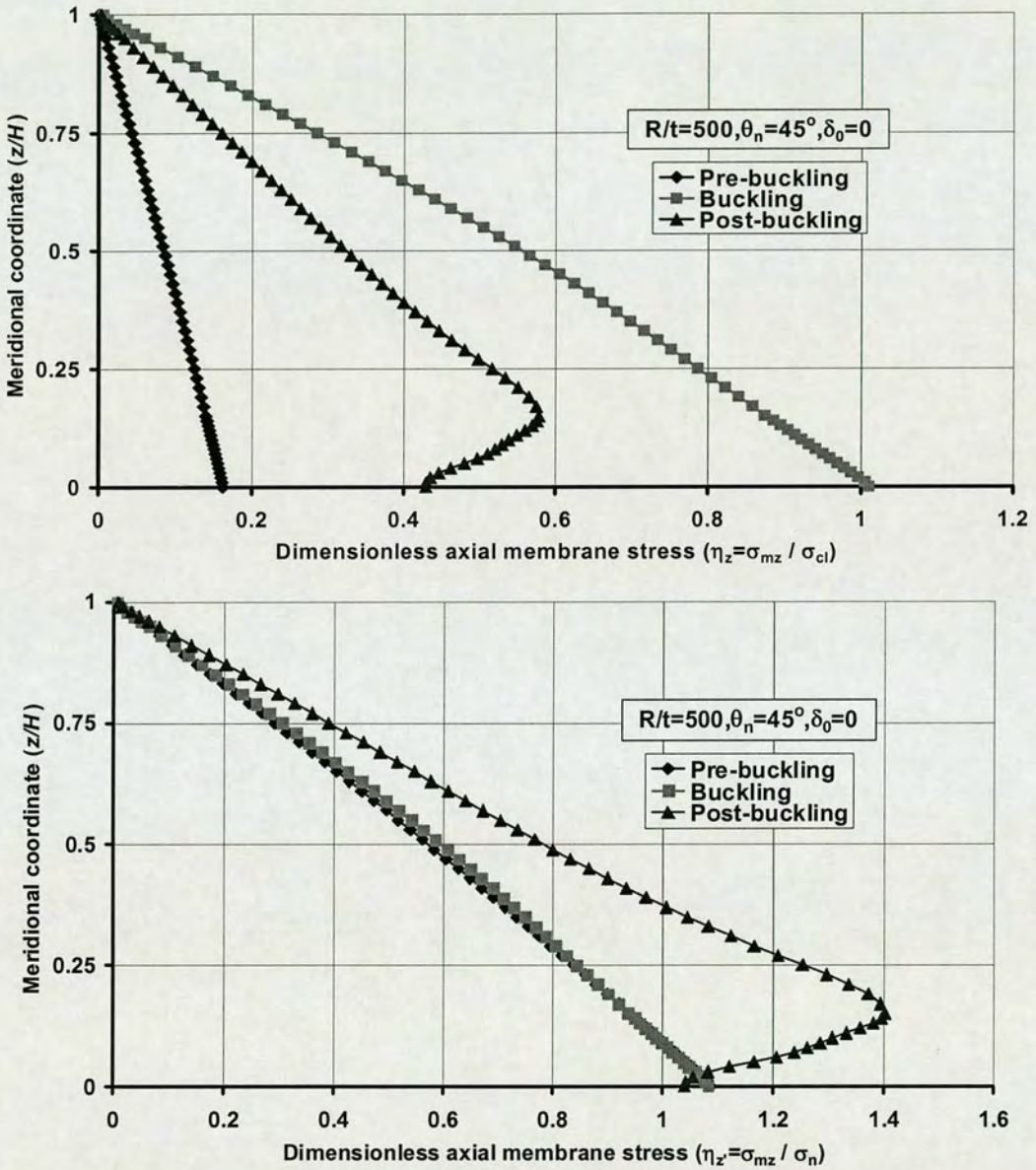

Fig. 5.17: Axial membrane stress in pre-buckling, buckling and post-buckling states (along the meridional line at the centre of strip load, strip edge buckles)

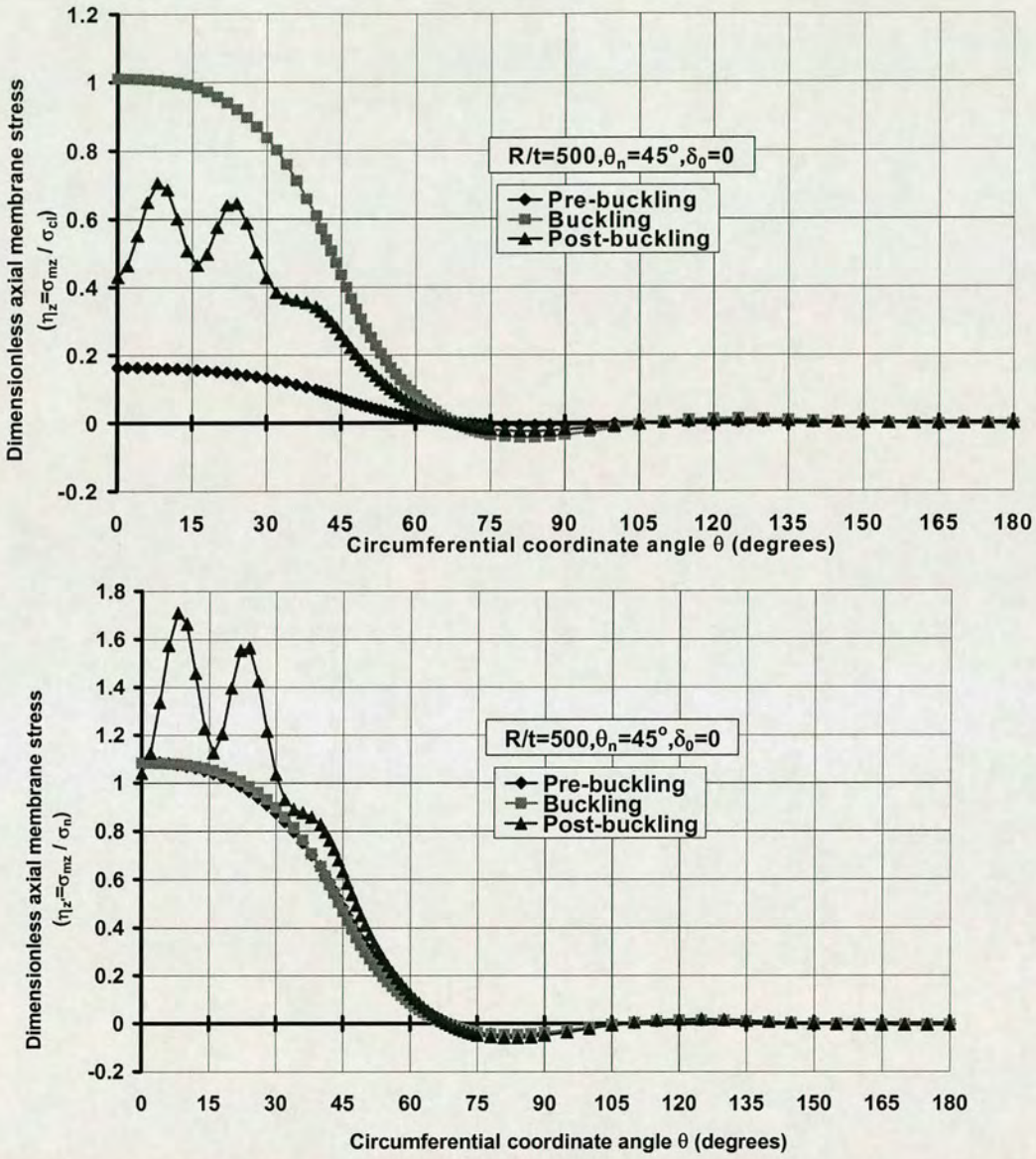

Fig. 5.18: Axial membrane stress in pre-buckling, buckling and post-buckling states (around the circumferential line at mid-plane, strip edge buckles)

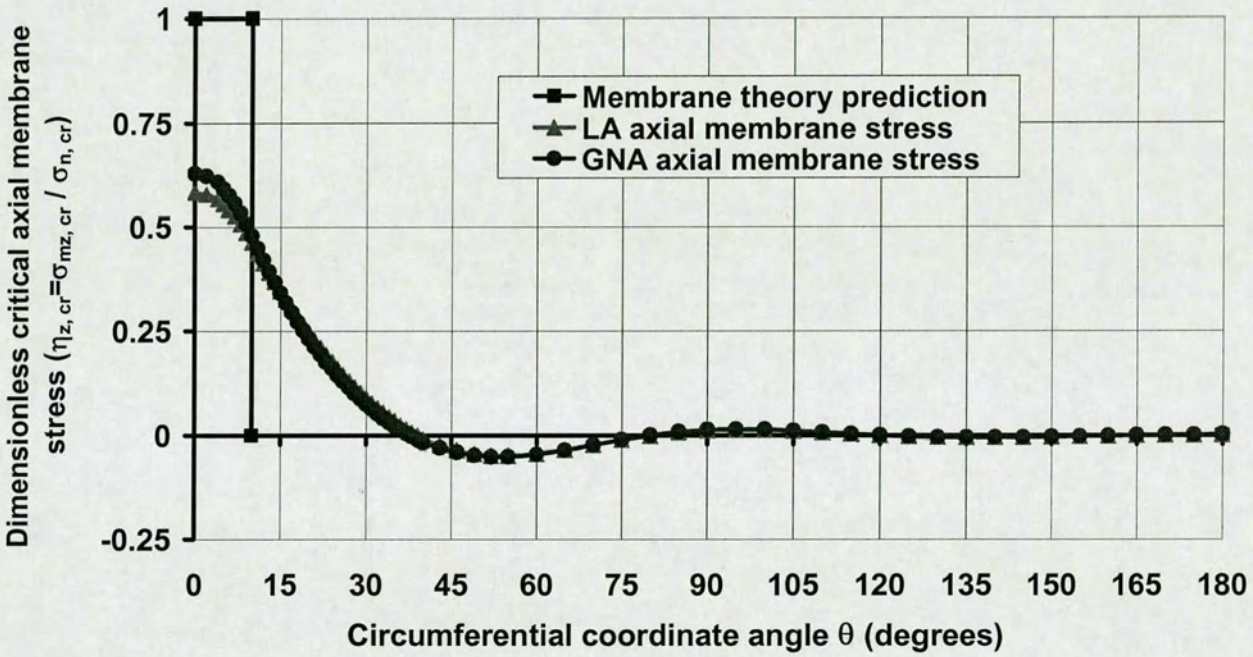

Fig. 5.19: Effect of geometric non-linearity on the stress distribution at buckling (LA & GNA, strip centre buckles)

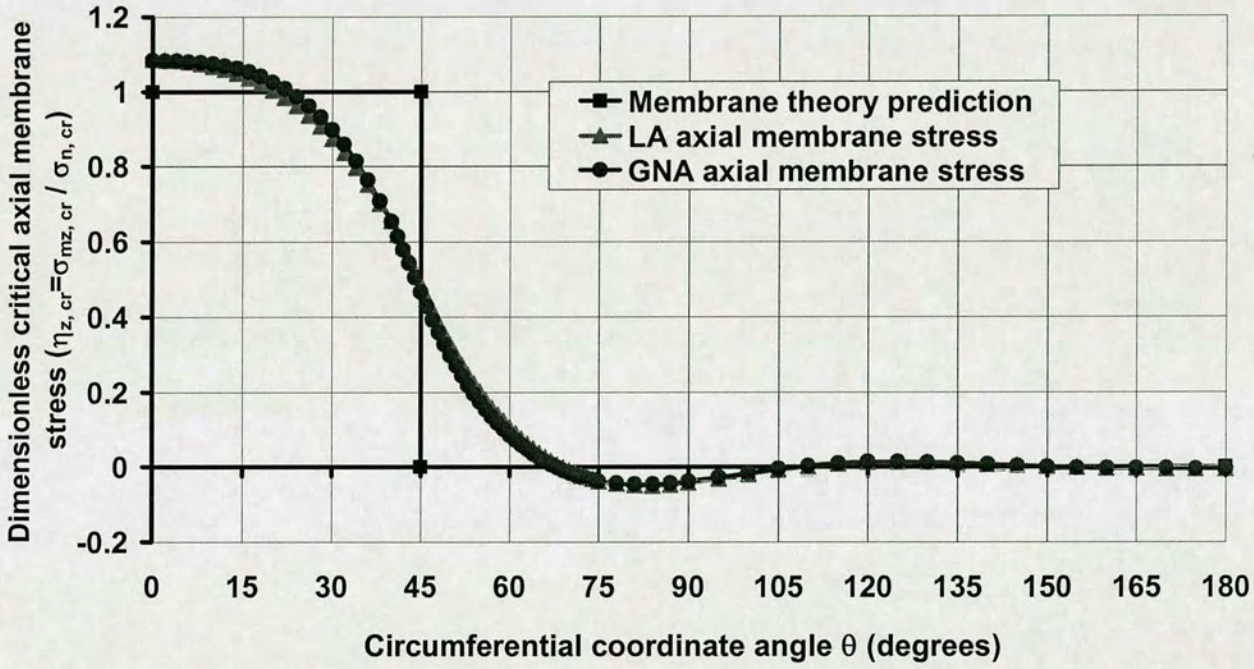

Fig. 5.20: Effect of geometric non-linearity on the stress distribution at buckling (LA & GNA, strip edge buckles)

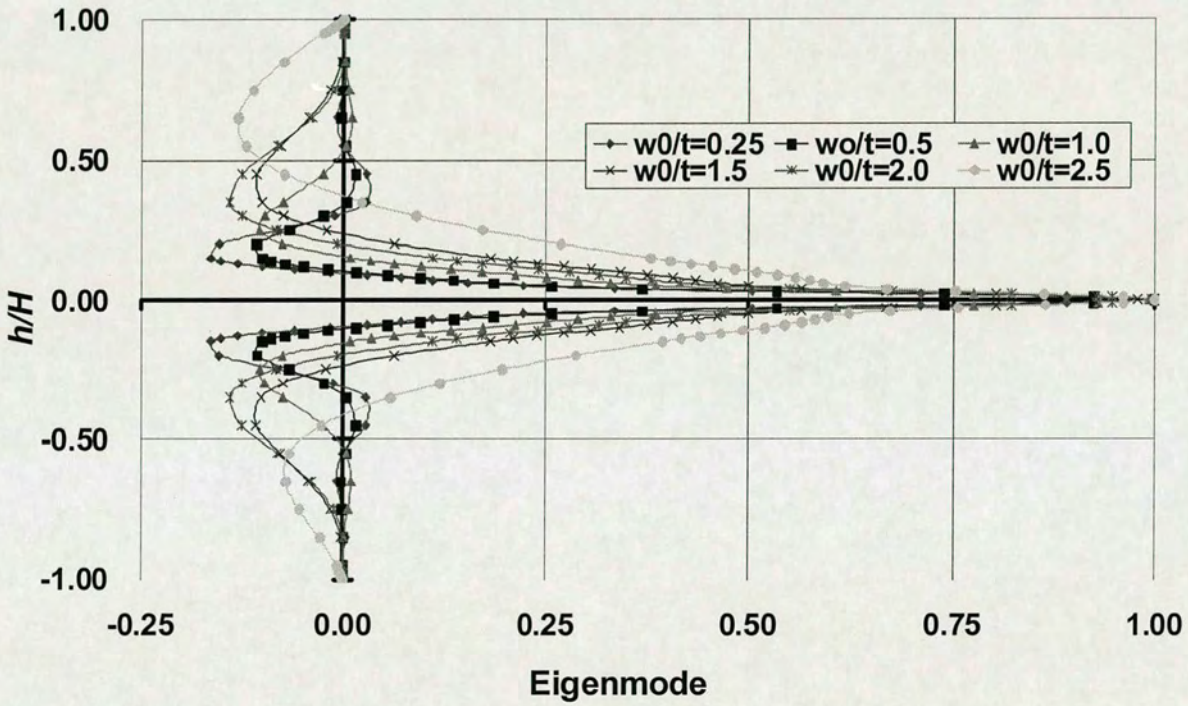

Fig. 5.21: Changing axial mode of buckling with the changing of imperfection amplitude w_0/t (local inward Type A)

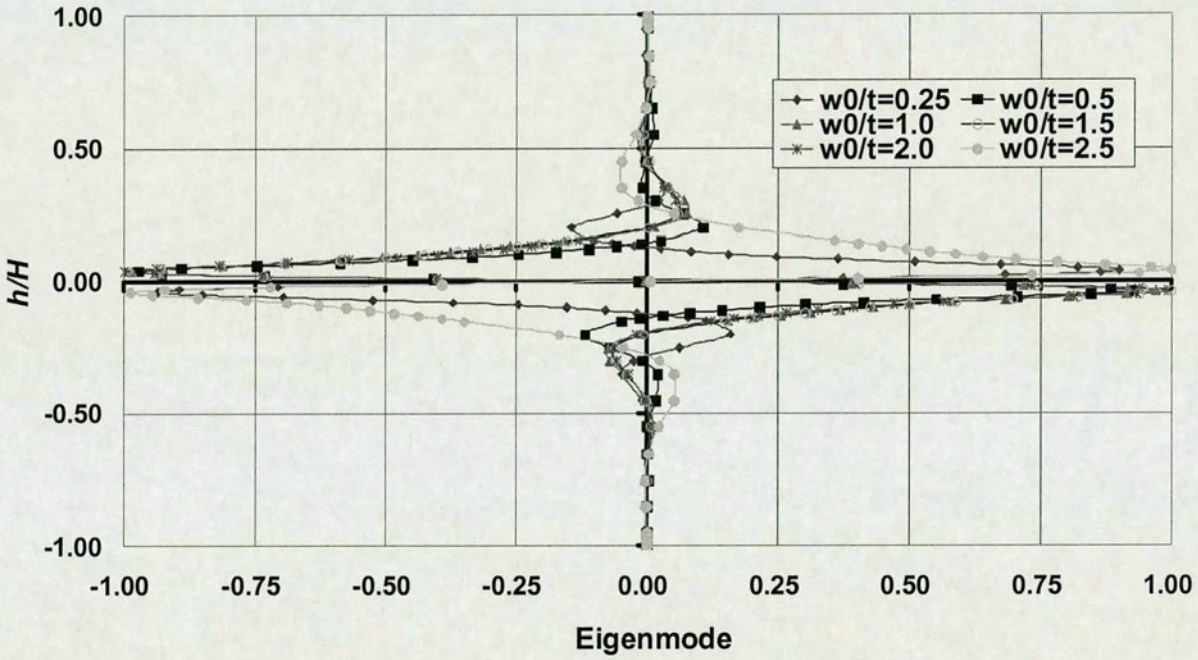

Fig. 5.22: Changing axial mode of buckling with the changing of imperfection amplitude w_0/t (local outward Type A)

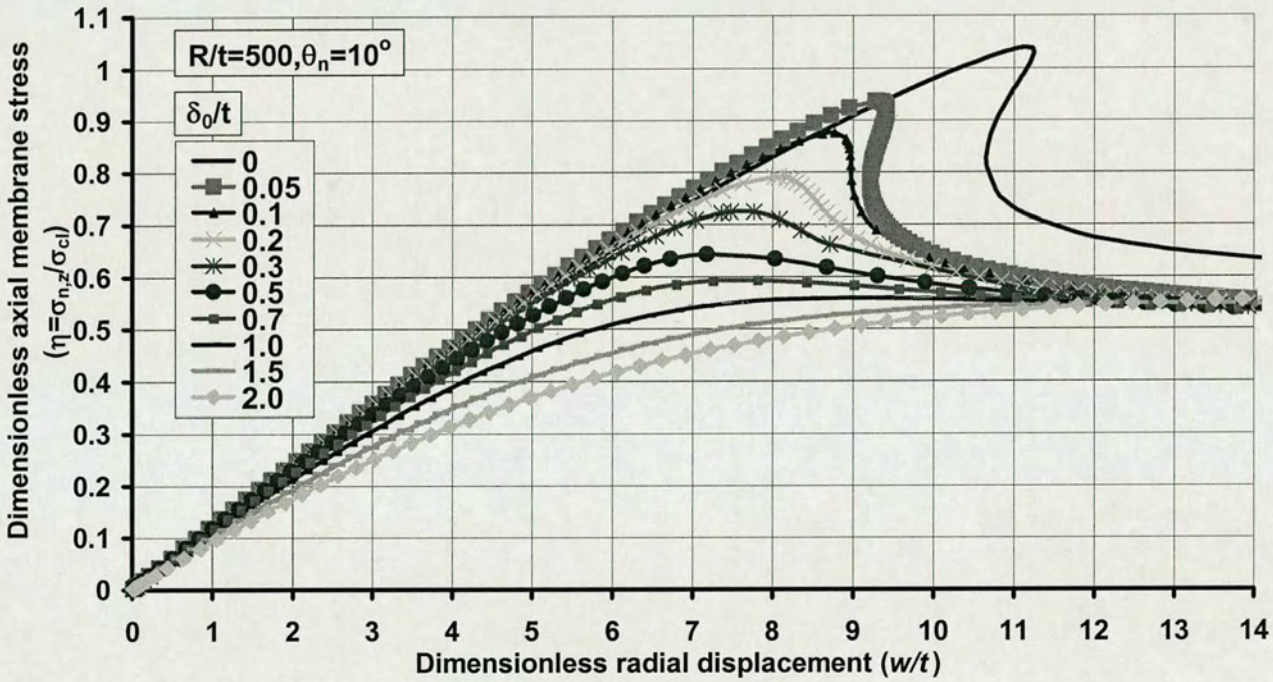

Fig. 5.23: Load-displacement curve of a thin-cylindrical shell under local axial compression with the influence of different imperfection amplitudes – Strip center buckles

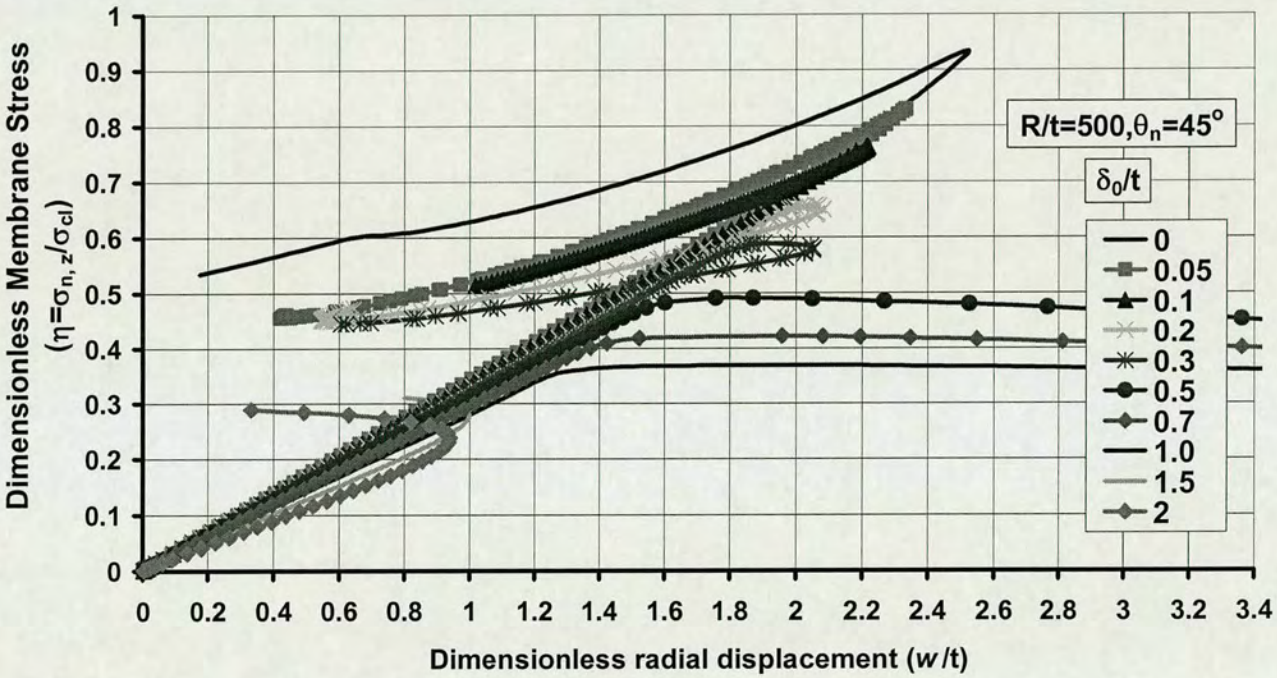

Fig. 5.24: Load-displacement curve of a thin-cylindrical shell under local axial compression with the influence of different imperfection amplitudes – Strip edge buckles

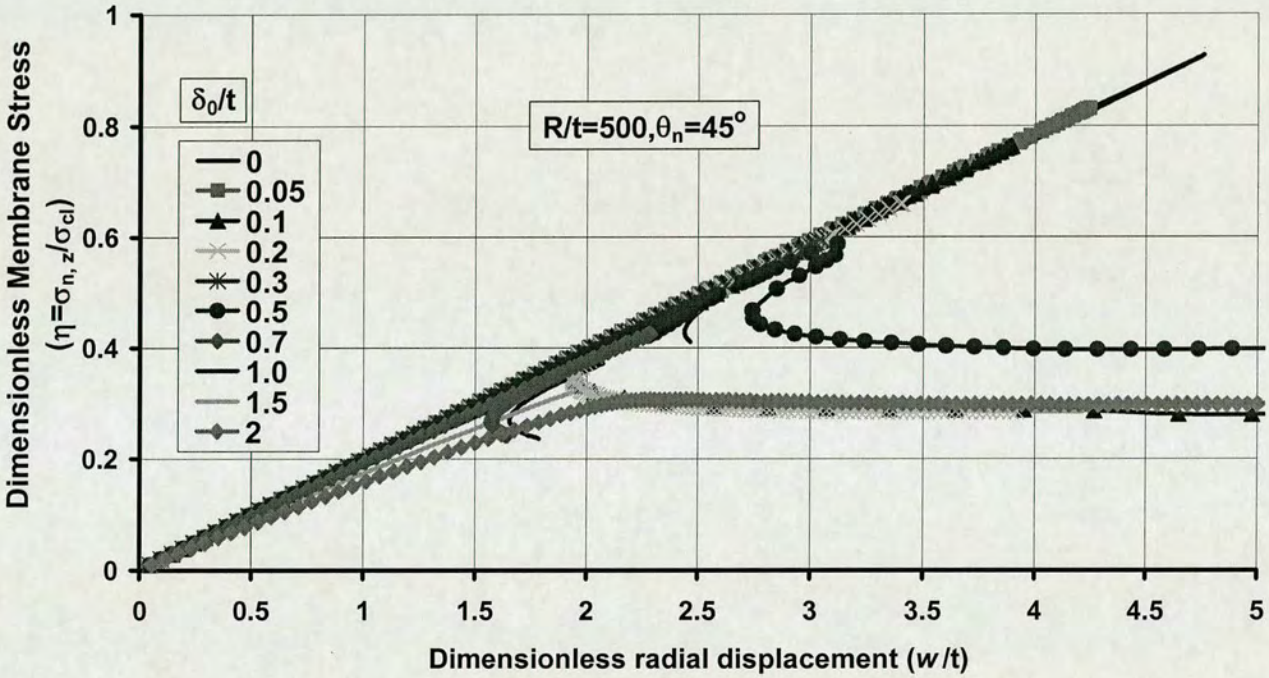

Fig. 5.25: Load-displacement curve of a thin-cylindrical shell under local axial compression with the influence of different imperfection amplitudes – Strip edge buckles

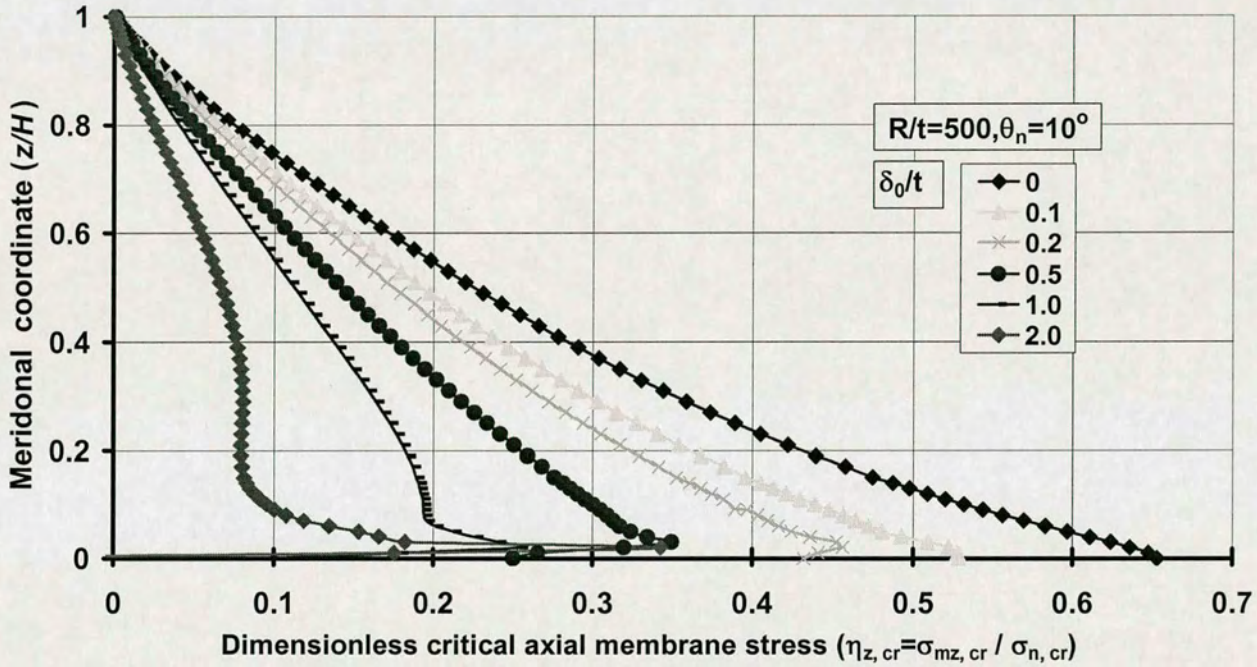

Fig. 5.26: Axial membrane stress distribution along the meridional line at the centre of strip load at buckling with the influence of imperfection sensitivity (strip centre buckles)

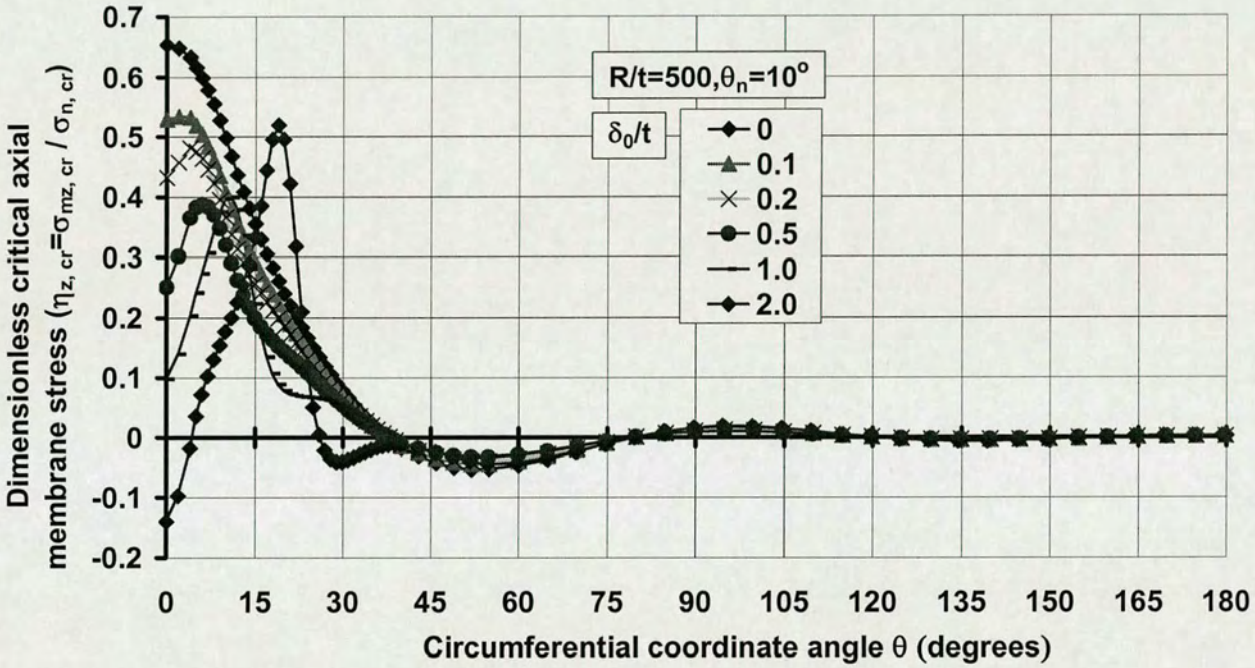

Fig. 5.27: Axial membrane stress distribution around the circumferential line at mid-plane at buckling with the influence of imperfection sensitivity (strip centre buckles)

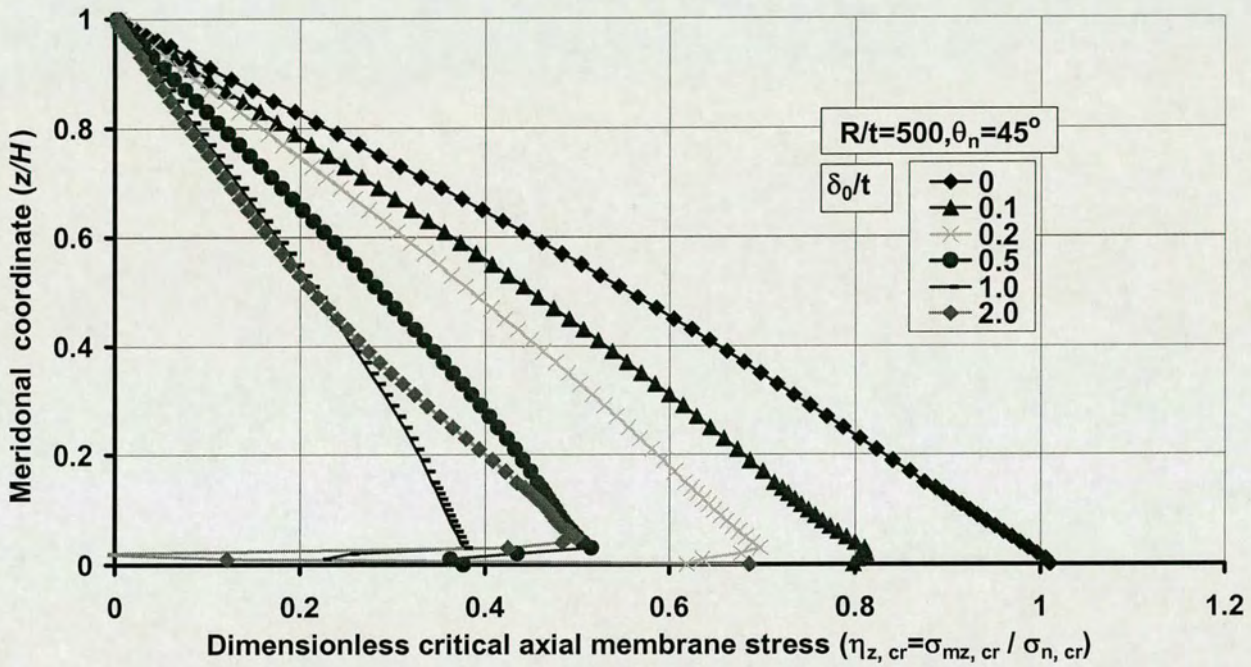

Fig. 5.28: Axial membrane stress distribution along the meridional line at the centre of strip load at buckling with the influence of imperfection sensitivity (strip edge buckles)

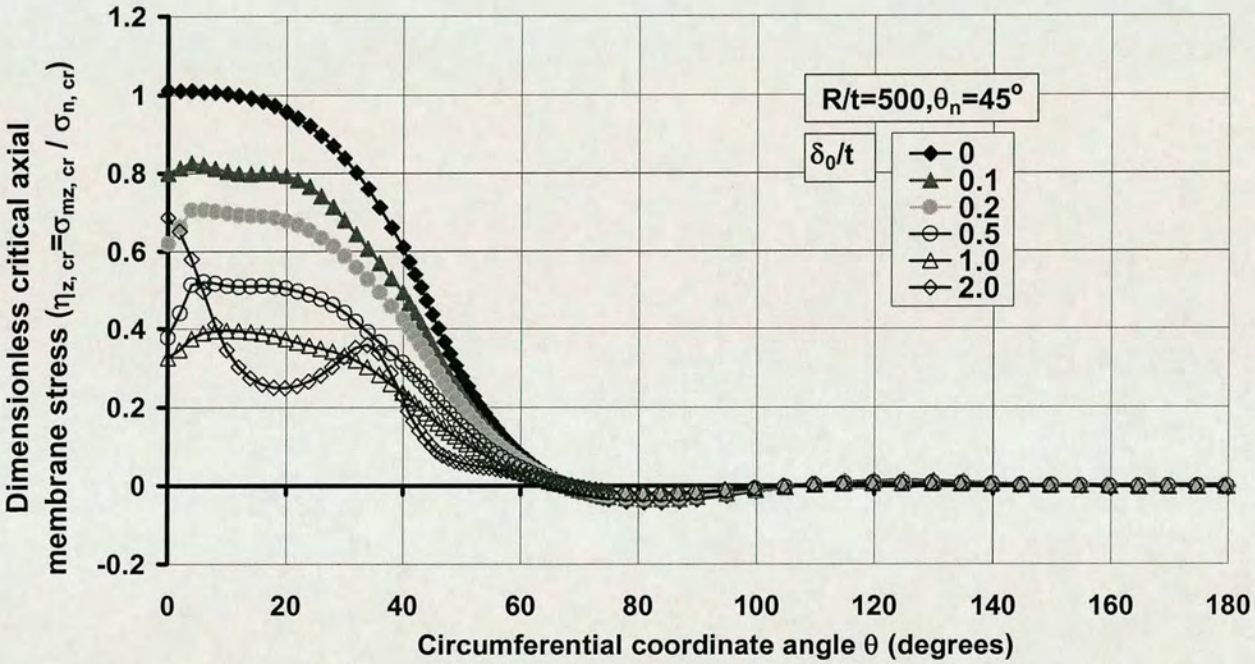

Fig. 5.29: Axial membrane stress distribution around the circumferential line at mid-plane at buckling with the influence of imperfection sensitivity (strip edge buckles)

Chapter 6

SHELL BUCKLING STRENGTH UNDER LOCALISED AXIAL COMPRESSION: EFFECT OF LOAD ZONE WIDTH

6.1 Introduction

Localised compression is a result of non-symmetry pressures on the wall (Rotter, 1997). Highly local non-uniform stresses (both in-plane and out-plane) are unavoidable in real cylindrical shells during an eccentric filling and discharging process, overhead conveyors supported on the cylinder wall and on discrete supports. In addition, the buckling strength is very sensitive to geometric imperfections in the wall, which are common in real structures. Reliable quantification of these effects is still challengingly difficult. From Chapter 5, two different buckling modes have been discovered and a parametric study on this field is needed to develop it further, devising an empirical equation aiming for a possible modification on predictions of that according to the current code.

6.2 Model

Different parameters of the circular cylinders have been investigated in order to provide enough data for the analyses. The radius R varies from 1 m to 10 m and the half angle of the load strip θ_n changes from 0.2° to 90°. The wall thickness t is kept at 10 mm and the cylinder height H at 30 m, which makes the radius to thickness ratio R/t between 100 and 1,000. The variation of the corresponding parameters of the model is shown in Fig. 6.1.

The converged mesh was obtained from the previous study in Chapter 4. The model descriptions including the properties of the material, the co-ordinate system, boundary conditions as well as its influence on the analyses results, geometric imperfection and analysis procedure were also presented in Chapter 5.

The parametric study includes linear bifurcation analysis, non-linear analysis and non-linear analysis with local inward imperfections. This plan has been developed in order to find a full set of shell buckling strength predictions for all different analyses types according to the present code (ENV 1993-1-6, 1999).

Of all different kinds of numerical analyses of elastic buckling strength, the LA/LEA analysis, which predicts the behaviour of a thin-walled shell structure on the basis of small displacement and linear elastic shell bending theory, is the simplest/easiest. This is an important reference load for all analyses because it contributes to the vital parameter 'slenderness' which is needed to interpret the results of other analyses types (ENV 1993-4-1, 1999; Rotter, 2002). Other analyses types are not always easily accessible to practical design engineers and since the LA/LEA results are more popular in practice especially for comparatively simple projects. Furthermore, geometric non-linearity in the pre-buckling behaviour is not obvious from the study of the Chapter 5. For all these reasons, the prediction of the LA/LEA is under study first.

6.3 Linear Eigenvalue Analyses (LEA)

6.3.1 Buckling Strength Prediction

The classical buckling stress σ_{cl} (Eqn. (2.3); Lorenz, 1908; Timoshenko, 1910; Southwell, 1914) and the nominal axial membrane stress at buckling $\sigma_{n,cr}$ (Fig. 5.3), were used here as reference values to describe the results of all the analyses simply and clearly. The results are again expressed in terms of dimensionless buckling strength parameter $\eta_{cr}=\sigma_{n,cr}/\sigma_{cl}$.

The analyses results display the following trends (Figs. 6.2 & 6.3):

First, if the *R/t* ratio is fixed, the buckling strength rises as the strip load angle decreases and it increases dramatically for small strip load angles.

Second, if the angle of the strip load θ_n is fixed, the buckling strength decreases with an increase in the *R/t* ratio. The variation of smaller strip load angles is sharper than that of larger angle ones.

From the figures, the bucking strength of the cylinder is clearly related to the *R/t* ratio and the width of the strip load is applied. But the relationships are quite complicated, and

difficult to use in any design process. From observations, the calculated buckling strength for a small angle strip load applied to relatively stocky cylinders is much higher than the classical solution and therefore impractical (with the influence of restraint from the boundary conditions). The cases with dimensionless critical buckling strength ($\eta_{cr}=\sigma_{n,cr}/\sigma_{cl}$) higher than 5.0, which are of little interest in practice, since have been omitted from the figures shown below. However, the curves found for predicting the buckling strength are still relatively accurate even for this omitted range.

The ratio of *R/t* and the width of the strip load are representations of the model and the stress applied, but it is difficult to apply the results directly. All the related parameters (*R/t* and *H/R* ratio, half strip angle θ_n) have been taken into account to achieve a better representation with an appropriate connection in-between. Finally, a dimensionless parameter (Eqn. 6.1) has been formed to predict the clear picture of the buckling strength (Eqns. 6.2 & 6.3, Fig. 6.4). Both the *R/t* ratio and the half strip angle θ_n were incorporated into this parameter — the dimensionless inverse strip half angle ξ — which maps the analysis results onto two separate straight lines:

$$\begin{aligned} &\eta_{cr} = \sigma_{n,cr} / \sigma_{cl} \\ &\xi = \theta_n^{-1} (R/t)^{-2/3} \\ &\theta_n \quad in \quad radians \end{aligned} \tag{6.1}$$

In Fig. 6.4, dimensionless critical buckling strength η_{cr} is plotted against dimensionless inverse strip half angle ξ. The eigenvalue results obtained can be closely mapped onto two straight lines if an appropriate parameter of ξ has been chosen. (Eqn. (6.2) and (6.3))

$$\eta_{cr} = 18.312\xi + 0.316 \tag{6.2}$$

and

$$\eta_{cr} = 1 \tag{6.3}$$

The relative error bounds are given by (-7.99%, +5.58%) for Eqn. (6.2) and (-5.20%, +5.25%) for Eqn. (6.3).

A comparison of two sets of numerical results with Eqn. (6.2) and (6.3) was shown in Fig. 6.5. The empirical equations match well with FE results though in the region approaching dimensionless critical buckling strength η_{cr}=1.0, a big deviation occurs. But it can be easily modified by the second prediction line (Eqn. (6.3)). Because of the two different prediction lines, it is very important to distinguish the bounds between these two modes.

6.3.2 Bound Between Two Buckling Modes

Before going to the bound between these two modes, it is vital to see how this prediction works. The method used for prediction can be seen from the diagram (Fig. 6.6). From the figure, curve fitting gives two separate curves to model the analyses results and each curve relates to a distinct buckling phenomenon – strip centre buckles and strip edge buckles (Chapter 5). On approaching this boundary, the prediction buckling strength lies slightly below FE results (Fig. 6.6) and thus it is a lower bound approximation. Therefore this prediction equation is a good, applicable and safe prediction in engineering.

The bound distinguishing these two modes is determined by the following Eqn. (6.4).

$$\theta_{cr} = 26.760\left(\frac{R}{t}\right)^{-2/3} \quad in \quad radians \tag{6.4}$$

$\theta_n > \theta_{cr}$	Strip edge buckles	Eqn. (6.3)
$\theta_n < \theta_{cr}$	Strip centre buckles	Eqn. (6.2)

This equation has been improved by a converged study and the results are shown in Fig. 6.7. It shows the bound between these two modes for different strip half angle θ_n and its corresponding *R/t* ratio.

6.3.3 Summary

Following the same idea from Chapter 5, the prediction of the buckling strength in linear elastic buckling analysis can be divided into two modes: Strip centre buckles and Strip edge buckles. In strip centre buckles, the local buckle forms at the centre of the strip load while in strip edge buckles, the uniform-load-effect buckle constructs somewhere near the strip load edge. In both phenomena, the stress localisation and uniformity are obvious from their buckling modes (Chapter 5). From the previous part, the buckling strength of Strip edge buckles is almost identical with the case where a uniform load is applied to the whole circumference though it is still a local buckle compared with that of the uniform loading case with an axisymmetric buckle. By contrast, the other case where the buckles form somewhere near load centre is very different (explanation in Chapter 5).

In conclusion, if the R/t ratio lies between 100 and 1,000, and the strip half angle θ_n lies between 0.2° and 90° (i.e. (0.4°, 180°) for the whole cylinder), the linear buckling analyses results can be accurately predicted by one of the these two predictions: Strip edge buckles and Strip centre buckles.

The buckling strength can be predicted using the formulae described above and the separation of the two modes can also be controlled by one equation, which is also shown there. The predictive error of the simple formulae (Eqn. (6.2) & (6.3)) is generally less than $\pm 5\%$, which is adequate for prediction in engineering applications.

Because the LEA analysis is generally an upper bound to the elastic critical buckling strength, it will be useful to know the influence of geometric nonlinearity on the buckling strength. This is explored in the following section. Geometrically nonlinear analysis is also important to capture snap-through, which cannot be detected by the LA/LEA.

6.4 Geometrically and Materially Non-linear Analyses (GNA & GMNA)

6.4.1 Buckling Strength Prediction

Following the same idea from that of buckling analysis, the GNA (geometrically non-linear elastic analysis) buckling strength prediction can also be divided into two sub-sections: Strip edge buckles and Strip centre buckles. The variations in the buckling strength are almost identical to those of the eigenvalue buckling strengths.

First, if the *R/t* ratio is fixed, the buckling strength rises with a decrease in the strip-load angle in the narrow strip-load angles ($<10^{o}$) and keeps less variable in rest of the wider strip angles. (Fig. 6.8)

Second, if the angle of strip load is fixed, the buckling strength decreases with an increase in the *R/t* ratio for the narrow strip angle ($\theta_n=10^{o}$). For wide strip angle ($\theta_n=45^{o}$), the buckling strength keeps almost the same level regardless of the *R/t* ratio variation. (Fig. 6.9)

Again, from both figures, the bucking strength of the cylinder is clearly related to the *R/t* ratio and the width of the strip load is applied. But the relationships are quite complicated and difficult to use in any design process.

A better representation is best described in terms of a dimensionless parameter, which is defined as the dimensionless inverse strip half angle ξ (Eqn. 6.1) in the linear bifurcation analyses. Both the *R/t* ratio and the half strip angle θ_n were brought into the analyses to form a dimensionless inverse strip half angle ξ to map the analyses results onto two separate lines (Eqn. (6.5) and (6.6)). The cases with dimensionless buckling strength η_{cr} higher than 5.0 have been omitted during the analyses for the same reason as that of eigenvalue results though the formula found are still quite accurate in this range.

In Fig. 6.10, dimensionless critical buckling strength η_{cr} is plotted against dimensionless inverse strip half angle ξ. The analyses results obtained can be closely mapped onto two straight lines if an appropriate parameter of ξ has been chosen. (Eqn. (6.5) and (6.6))

$$\eta_{cr} = 9.101\xi + 0.215 \tag{6.5}$$

and

$$\eta_{cr} = 0.7 \tag{6.6}$$

The relative error bounds are given by (-9.33%, +5.56%) for Eqn. (6.5) and the maximum occurs only somewhere near the boundary of two modes because of the scatter of the analyses results in the uniform likely loading range (comparatively wide strip load angles).

Unfortunately the prediction of the GNA analysis, which shows a similarity with the curve of the eigenvalue solution for relatively large angles of strip load θ_n, Eqn. (6.6) has a big deviation in relatively small angles of strip loads, which is very different to that of eigenvalue results. But it still provides a lower bound of buckling strength.

The relative error bounds here are not included for the reason that there are big deviations from this prediction and the analyses data are widely scattered in this extent due to the instability of the axial symmetric cylinders under the axial symmetry uniform loading (Fig. 6.11 & 6.12 for the details below). But, what should be pointed out here is that there will be less scattered if additional imperfections are introduced to such cases. The reason for this is that the perfect cylindrical shell assumed here cannot be realised experimentally and practically (Arbocz and Babcock, 1969) — there must be some geometric imperfections in real existing cases and with the introduction of such imperfections, the big deviation is generally diminished, at least for uniform axial compression.

With the comparison above, this equation provides a good and safe prediction in the range other than that of Strip centre buckles and it is still applicable in engineering but its use is somewhat limited (ENV 1993-1-6, 1999; Rotter, 2002).

6.4.2 Bound Between Two Buckling Modes

The dividing bound between the Strip edge buckles and Strip centre buckles is determined by the following Eqn. (6.7), which is the intersection between Eqn. (6.5) & (6.6).

$$\theta_{cr} = 18.747\left(\frac{R}{t}\right)^{-2/3} \quad in \quad radians \tag{6.7}$$

$\theta_n > \theta_{cr}$	Strip edge buckles	Eqn. (6.6)
$\theta_n < \theta_{cr}$	Strip centre buckles	Eqn. (6.5)

This equation has again been obtained from a converged study and the results are shown in Fig. 6.13. It shows the bound between these two modes on different parameter combinations of strip half angle θ_n and R/t ratio using GNA predictions.

6.4.3 Mechanism of Two Modes

In order to know the mechanism of the buckling in the non-linear analysis with and without local inward imperfection, a load-displacement curve is shown in the following two diagrams: Figs. 6.14 and 6.15 show the load-displacement curves for different modes with and without local imperfections using the nominal stress — dimensionless axial membrane stress $\eta=\sigma_{n,z}/\sigma_{cl}$ plotted against dimensionless radial displacement parameter w/t.

From Fig. 6.14, the Strip edge buckles curve is similar to that of the uniform compression case which has been widely published in a lot of corresponding studies and textbooks (HKS, 1998). By comparing the cases with and without imperfection, the perfect cylinder can reach $0.8\sigma_{cl}$ while the imperfect one can reach only $0.5\sigma_{cl}$ for δ_0/t=0.5 and $0.4\sigma_{cl}$ for

δ_0/t=1.0 but the decrease in strength is milder and smoother than in the case of the uniform loaded cylinder.

From Fig. 6.15 of the Strip centre buckles curve, which is the focus of the study here, it is apparent that these kinds of cases develop much larger radial deflections than the case of the uniformly compressed cylinder (roughly 10 times of cylinder thickness for the imperfect case (δ_0/t =0.5 & δ_0/t =1.0) and 13 times of thickness for perfect cylinder) in order to reach the maximum load. Comparing the cases with and without imperfection, the perfect cylinder can reach $\sigma_{n,z}$=1.5 σ_{cl} and the imperfect one can still reach as far as $\sigma_{n,z}$=0.95 σ_{cl} for δ_0/t =0.5 and $\sigma_{n,z}$=0.85 σ_{cl} for δ_0/t =1.0. It should be noted that the postbuckling decrease in the strength of the imperfect cylinder is milder and smoother than in the perfect cylinder no matter which buckle location is involved. Thus the imperfect cylinder can sustain the peak value longer and in a more stable stage than the perfect cylinder, though in general, it reached a lower peak due to the introduction of imperfections.

From Fig. 6.17, it is observed that the Strip centre buckles produce a much larger deformation than deflections of the Strip edge buckles before reaching its maximum load.

6.4.4 Material Non-linearity

Material yielding usually occurs in the post-buckling range for very thin cylindrical shells. Further, it occurs especially in regions of local bending, which has little influence on the buckling load. However, the elevated local stress state may cause an even more severe situation on the local bending which causes geometric instability (forming a mechanism) before the majority part of the material can reach its buckling strength. Since this is the first time that local load patterns like this have been studied, it is worth exploring the influence of the material non-linearity in the analyses.

For simplicity, the material non-linearity is introduced using a yield stress of 250*MPa* and the Young's modulus keeps the same as before: $2*10^5 MPa$. The model adopted an elasto-perfectly plastic behaviour whose plastic hardening is ignored.

$\sigma_{n,cr}$ is the nominal buckling stress introduced from Chapter 5 and $\sigma_{n,cr,m}$ is the nominal buckling stress considering material non-linearity. Fig. 6.16 shows the relationship between *R/t* ratio and the reduction of the buckling strength for each of the corresponding strip half angle, and the material non-linearity can increase the buckling strength with the reduction of *R/t* ratio (thicker shell) because that yielding develops in thicker shell before buckling and since more energy absorbed. With an increase of the strip angle, the buckling stress considering material non-linearity also decreases into a stable flat line, which indicated Strip edge buckles (wide strips) is more sensitive to material nonliearity.

Because of limited data available for the plasticity analyses, a possible lower buckling strength of 0.4, instead of 0.7 (Eqn. 6.6), might be a good approximation for the strip edge buckles. Further study is needed.

6.4.5 Summary

In conclusion, if *R/t* ratio lies between 100 and 1,000 and the strip half angle θ_n lies between 0.2° and 90°, the geometrically non-linear analyses results can be accurately predicted by Eqn. (6.5) & (6.6) for Strip centre buckles and Strip edge buckles respectively. The boundary between the two modes is easily found from Eqn. (6.7). The eigenvalue and the Riks solutions can provide a satisfactory prediction for the linear and non-linear analysis which require substantial computational time to obtain and the deviation, which can still be controlled within a extent of ±5%. Thus this prediction is a very simple and good reference for the perfect cylindrical shell strength prediction in engineering.

The reason for the separation of these two cases of strip loading comes from the buckling mechanics.

The influence of the material non-linearity is included in this study and a full parametric study could be executed but is of little practical value without introduction of geometric imperfections.

To continue the previous discussion, it is important to know the non-linear analysis prediction with some imperfections, which are unavoidable in practical usage. The local inward imperfection is introduced as a typical form. Although some cases with local inward imperfections have been stated before exploring the mechanism, a full parametric study on the influence of this imperfection is needed.

6.5 Geometrically and Materially Non-linear Analyses with Imperfection (GNIA & GMNIA, δ_0/t =1.0)

Since the imperfection plays a very important role in the buckling strength as well as the post-buckling behaviour, it is necessary to investigate its influence in the present study. As in Chapter 5, the imperfection introduced refers to the local inward deviation of Type A (Rotter and Teng, 1989; Teng and Rotter, 1992), which is among the most deleterious forms to the buckling strength under uniform axial compression (Koiter, 1963; Bornscheuer, Häfner and Ramm, 1983; Yamaki, 1984; Rotter and Teng, 1989; Teng and Rotter, 1992; Holst et al., 1999; Holst et al., 2000).

6.5.1 Imperfection Feature

The imperfection feature has been mentioned in Chapter 3 and what should be pointed is that for the purpose of simplicity, only one imperfection amplitude (δ_0/t = 1.0) is used here.

6.5.2 Buckling Strength Prediction

As with the treatment method of the LA/LEA and the GNA analyses prediction, the prediction of GNIA (geometrically non-linear elastic analysis with imperfections) analyses can be divided into two modes: Strip centre buckles and Strip edge buckles. The buckling strength variation is found to follow the same trends as those of the other two analyses. (Figs. 6.18 & 6.19)

First, if the R/t ratio is fixed, the buckling strength rises dramatically with a decrease in the strip half angle θ_n.

Second, if the angle of strip load is fixed, the buckling strength decreases with an increase in the *R/t* ratio.

The buckling strength of the cylinder is clearly related to the *R/t* ratio, the strip width over which the strip load is applied. But the relationships are quite complicated, and difficult to use in any design progress. Both the *R/t* ratio and the half strip angle θ_n were brought into the analyses to form a dimensionless inverse strip half angle ξ to map the analyses results onto two separate straight lines. For the same reason as above, dimensionless critical buckling strength of the GNIA (η_{cr}) analyses higher than 5.0 is omitted during the analysis procedure although the formula found here is still very accurate. All the observations above are similar to those of the LA/LEA and GNA analyses before.

As in the previous study, the dimensionless buckling stress η_{cr} is plotted against dimensionless inverse strip half angle ξ in Fig. 6.20. The results obtained can be closely mapped onto two straight lines if an appropriate parameter of ξ has been chosen (Eqn. (6.8) and (6.9)).

$$\eta_{cr} = 5.633\xi + 0.046 \tag{6.8}$$

and

$$\eta_{cr} = 0.35 \tag{6.9}$$

The deviation for Eqn. (6.8) is between (-16.34%, +3.91%). By contrast with the GNA results, the huge deviation does not exist here. This shows that the introduction of a local imperfection, which is common in civil engineering, avoids the big scatter in the strengths seen in nonlinear bifurcation analyses of perfect shells.

The relative error bounds for Eqn. (6.9) are given by (-7.11%, +2.31%) and the maximum deviation occurs also near the bound dividing the two modes due to the difference between the combination of two curves and one single curve as indicated in Fig. 6.6.

A comparison of Eqns. (6.8) and (6.9) with FE results is shown in the two diagrams — Figs. 6.21 & 6.22 for details. It is a good and safe prediction, even in the region where a change occurs between buckling modes, and thus it is applicable in engineering.

6.5.3 Bound Between Two Buckling Modes

The separation between the Strip centre buckles and Strip edge buckles can be determined by the following Eqn. (6.10). As before, it has been obtained from a converged study (Fig. 6.23).

$$\theta_{cr} = 18.535\left(\frac{R}{t}\right)^{-2/3} \quad in \quad radians \tag{6.10}$$

$\theta_n > \theta_{cr}$	Strip edge buckles	Eqn. (6.9)
$\theta_n < \theta_{cr}$	Strip centre buckles	Eqn. (6.8)

The comparison of the LA/LEA, GNA and GNIA bounds is shown by Fig. 6.24.

From Fig. 6.24 above, it is clear that the bound between the two buckling modes is identical for GNA and GNIA, whether imperfections are present or not and thus there will be only two separate bounds in the end: one for linear buckling analysis and one for non-linear analysis. This also means that it is not necessary to explore the effect of different imperfection amplitudes, since these will also be the same, at least for moderate imperfection amplitudes.

6.5.4 Imperfection sensitivity

To investigate the imperfection sensitivity of buckling strength, both buckling modes were analysed. The range of imperfection amplitude (δ_0/t) was in-between (0, 2.0). Fig. 6.25 shows that Strip centre buckles almost keeps constant after reaching the imperfection of one shell thickness while the Strip centre buckles also shows little variation after reaching that point. All these keep the same pace as that of uniformly compressed cylinder (Fig. 5.4): one shell thickness of imperfection amplitude contributes the most of the strength reduction from the geometric imperfection influence.

6.5.5 Material Non-linearity

The material non-linearity is the same as for the GMNA analysis.

Fig. 6.25 shows the effect of R/t on the reduction of the buckling strength for each of the corresponding strip half angle. Material non-linearity only reduces the buckling strength slightly for cylinders thinner than R/t=400, the reduction from plasticity is less than 5%. In conclusion, the influence of material non-linearity can be ignored for industrial applications if appropriate load factor or safety factor is used in design.

6.5.6 Summary

In conclusion, if the R/t ratio lies between 100 and 1,000, and the strip half angle θ_n between 0.2° and 90° and one wall thickness of local axisymmetric inward imperfection is present, the GNIA results can be accurately predicted by one of the these two simple equations: Strip edge buckles and Strip centre buckles. The separation of the two cases can also be controlled by one equation. This prediction depends only on the well-known classical solution and this is the same as that of LA/LEA, GNA analyses. The critical strength prediction, whose deviation can be controlled within a range of ±5%, could be a good reference for prediction in engineering. Only an imperfection of one wall thickness (δ_0/t=1.0) was taken into account here, but other imperfection amplitudes will have similar relationship with different coefficients.

The reason for the separation of two typical cases in the strip loading comes from the buckling mechanics.

Material non-linearity has little influence on the shell buckling strengths applicable in practical use, due to its R/t ratio and the quality of real construction.

6.6 Conclusions

6.6.1 Summary

A parametric study has been presented which examined the effect of local axial compression on the buckling strength of geometrically perfect and imperfect cylindrical shells. Emphasis was placed on the influence of the width of the compressed zone. Design rules have been given based on calculations, in which geometric imperfections were adopted. Predictions for different analyses types (LA/LEA, GNA, GNIA) have been obtained and the influence of material non-linearity has been taken into account (GMNA, GMNIA).

LEA: $\eta_{cr} = 18.312\xi + 0.316$ (6.2)

$\eta_{cr} = 1$ (6.3)

GNA: $\eta_{cr} = 9.101\xi + 0.215$ (6.5)

$\eta_{cr} = 0.7$ (6.6)

GNIA: $\eta_{cr} = 5.633\xi + 0.046$ (6.8)

$\eta_{cr} = 0.35$ (6.9)

All the equations above show the similar variation: the buckling strength decreases with the introduction of geometric non-linearity and local inward imperfection and the trend of buckling strength also keeps more constant accordingly.

The results of a full set of parametric analyses presented in this chapter support the hypothesis from Chapter 5: the prediction of shell buckling strength under local axial compression with or without geometric imperfections can be divided into two distinguishing buckling modes because of their corresponding buckling mechanism – Strip centre buckles and Strip edge buckles and a full set of simple predictive equations have been provided accordingly. A summary of conclusions is as follows.

6.6.2 Conclusions:

A. Parametric studies led to simple predictive equations;
B. Predictions were obtained using three different analyses types, conforming to the requirement of draft European Standard for Metal Shells (ENV 1993-1-6, 1999);
C. Two different buckling modes have been found;
D. The boundaries between the buckling modes have been summarised in the form of empirical formulae;
E. Material non-linearity has little influence on the practical application due to its *R/t* ratio and the quality of real construction;
F. A comparison of the boundaries between the two modes shows that the bounds for GNA and GNIA analyses cannot be distinguished because they are very close to each other. Hence only two empirical expressions are given for these boundaries: one for linear eigenvalue and the other for non-linear analysis.

The effect of the meridional extent of the load zone in the localized axial compression of the shell buckling needs to be explored correspondingly. The following chapter will be focus on this question.

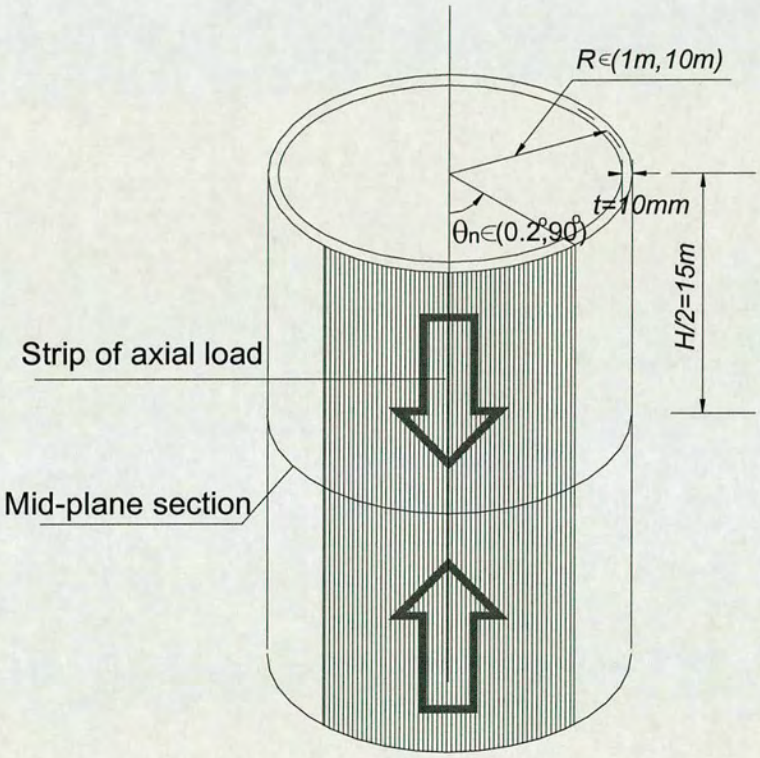

Fig. 6.1: Cylinder under local compression with varying strip load width

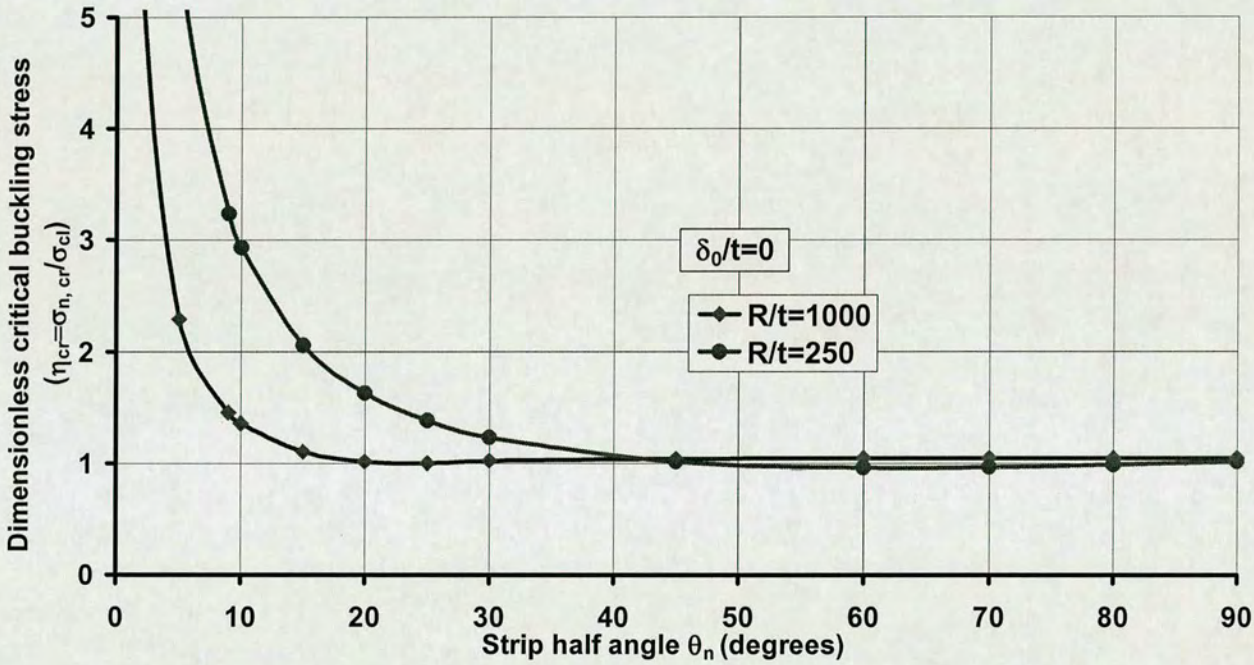

Fig. 6.2: Effect of strip half angle on linear bifurcation buckling strength of perfect cylinders (LA/LEA)

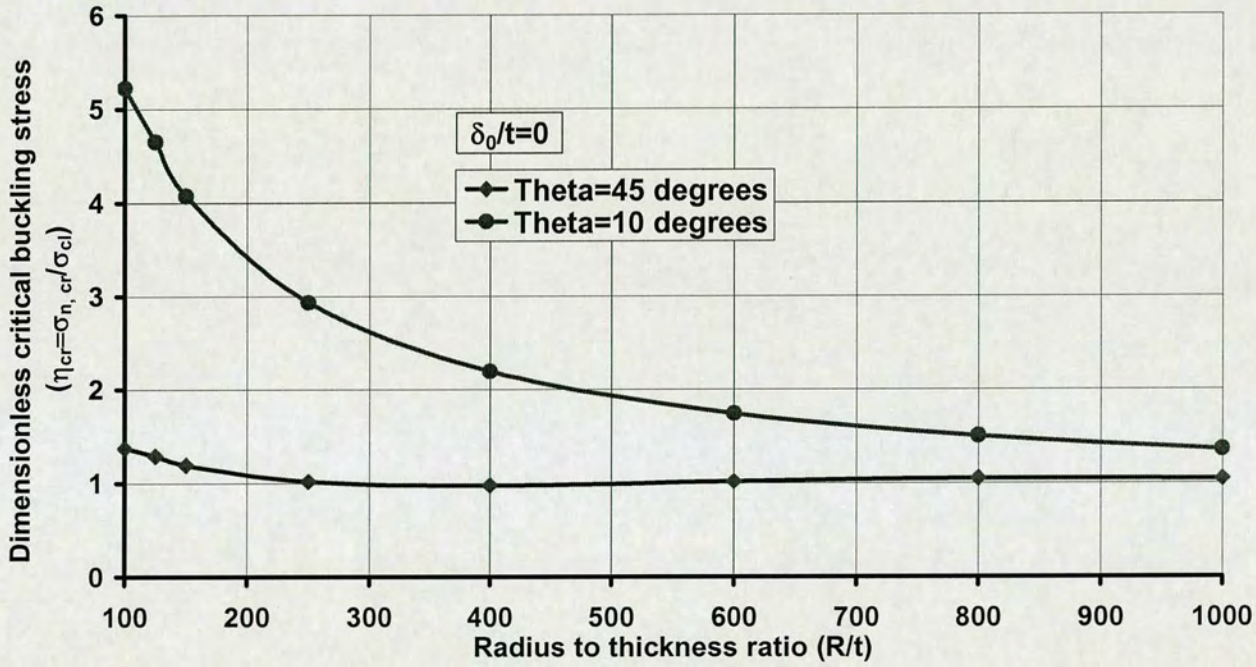

Fig. 6.3: Effect of *R/t* ratio on linear bifurcation buckling strength of perfect cylinders (LA/LEA)

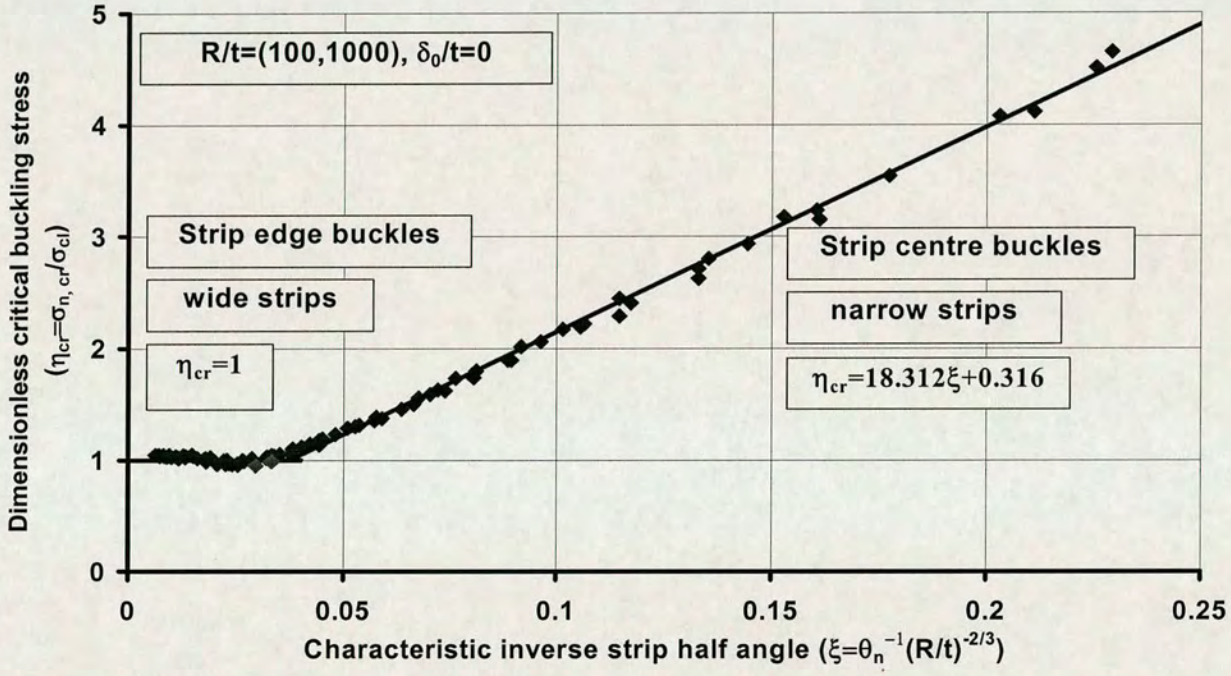

Fig. 6.4: Linear bifurcation buckling strength for all strip load (all *R/t* and θ_n included)

(Note: The continuous line shows the empirical fit, nodes show FE analyses results)

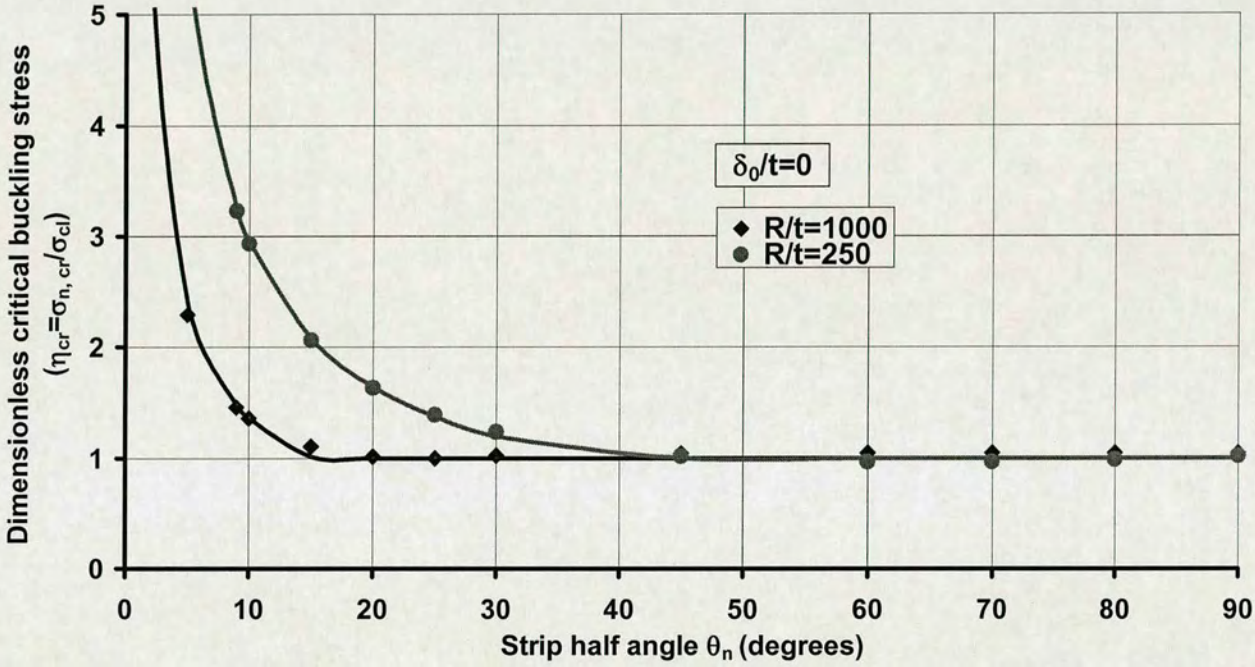

Fig. 6.5: Comparison between FE and empirical equation of LA/LEA
(Note: The continuous line shows the empirical fit, nodes show FE analyses results)

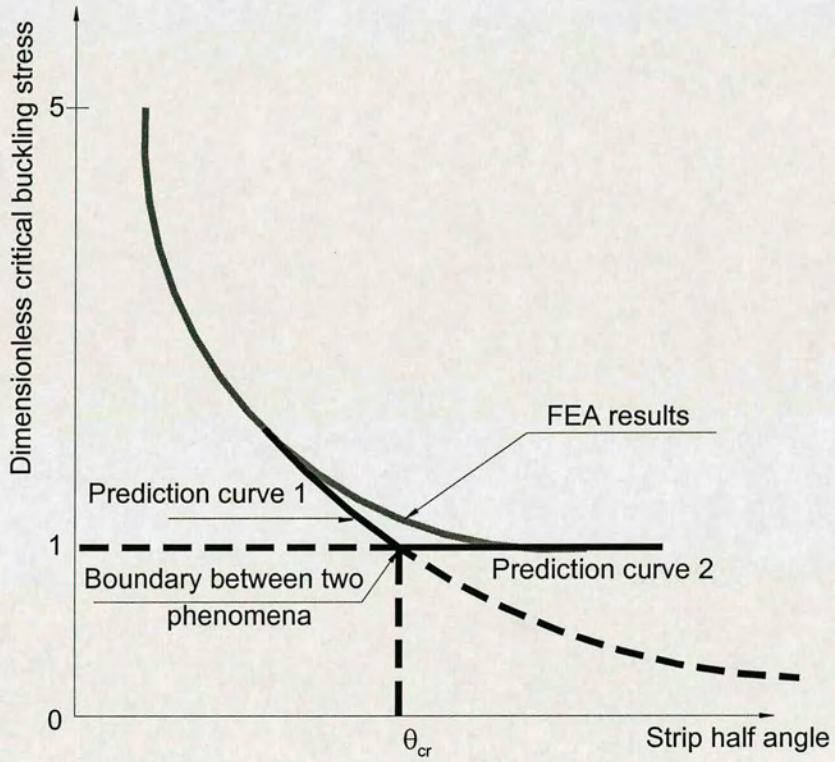

Fig. 6.6: Prediction method explanation

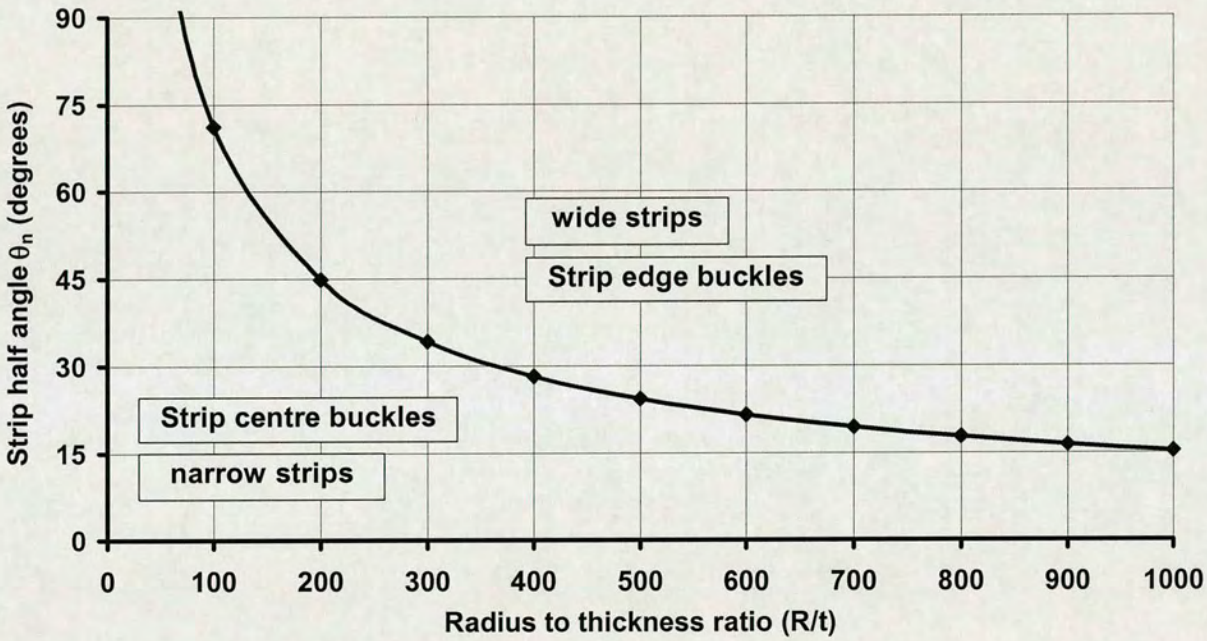

Fig. 6.7: Bound for LA/LEA empirical equations

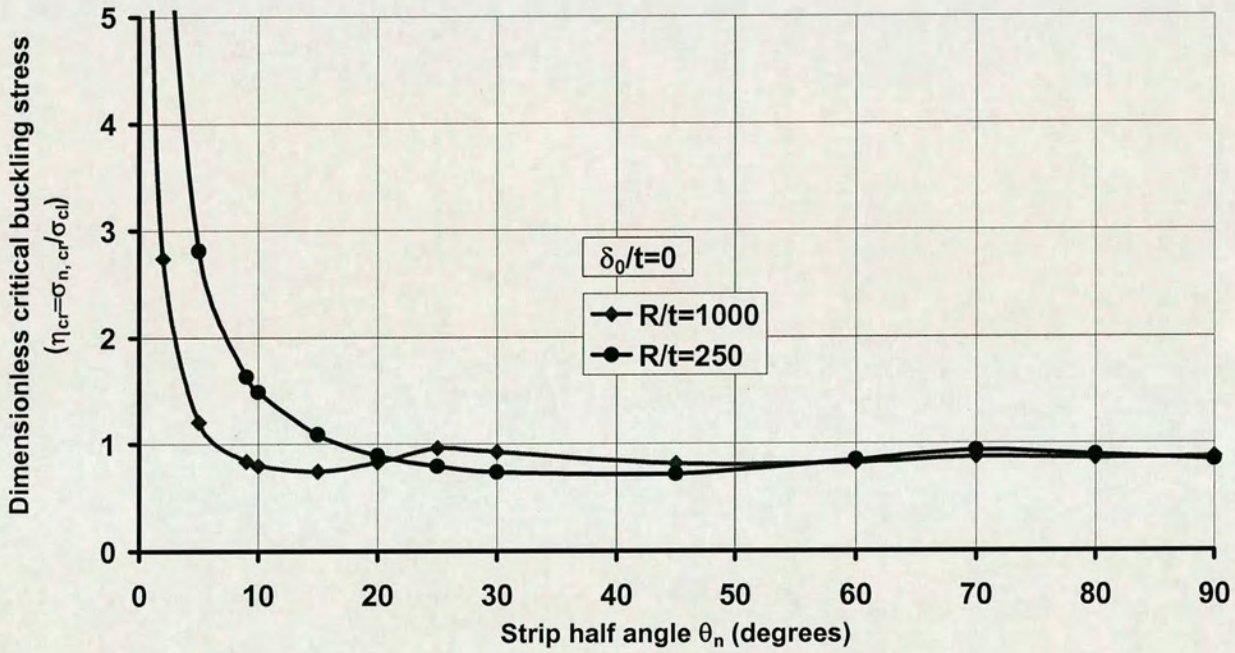

Fig. 6.8: Effect of strip half angle on non-linear buckling strength of perfect cylinders (GNA)

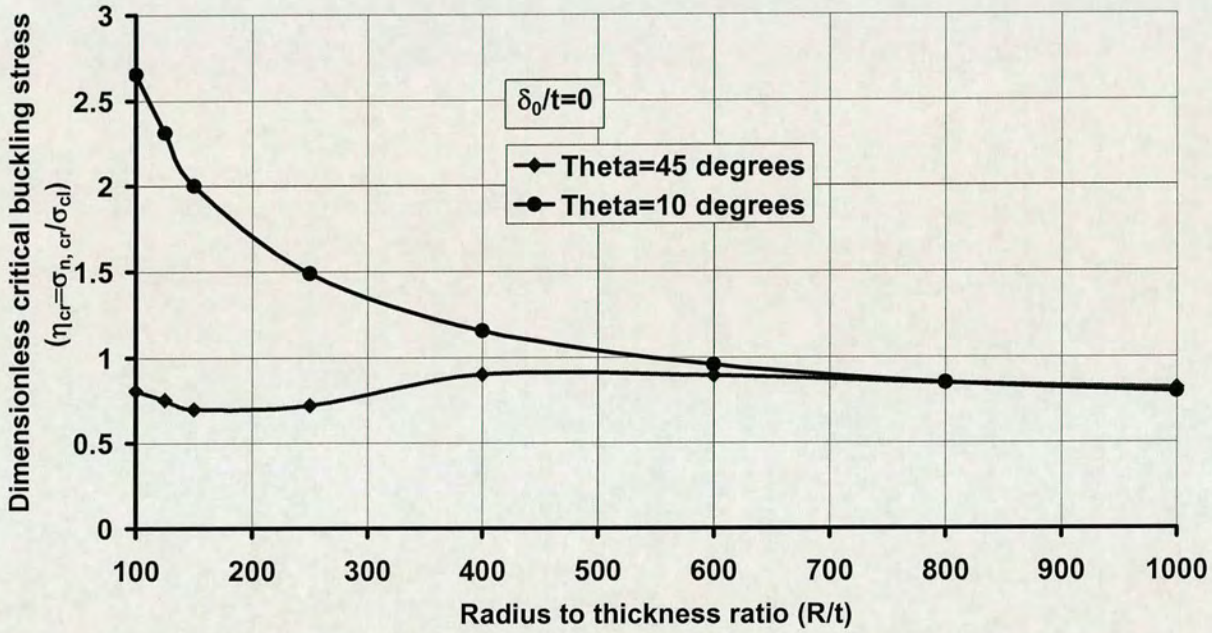

Fig. 6.9: Effect of *R/t* ratio on non-linear buckling strength of perfect cylinders (GNA)

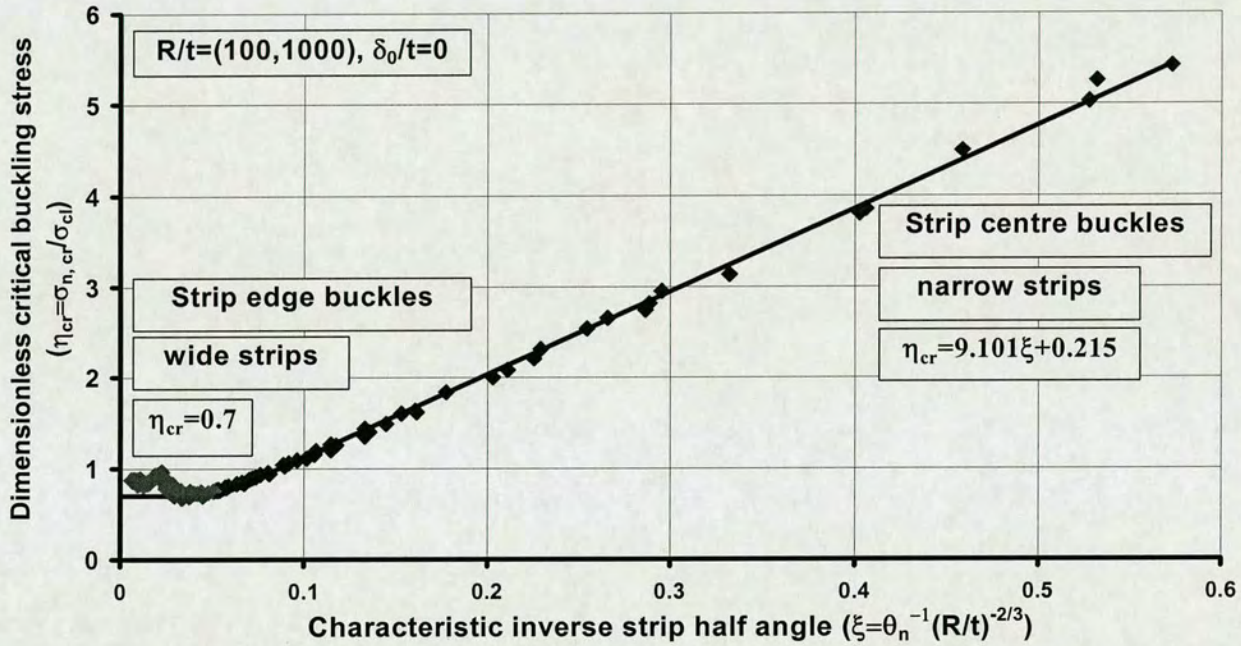

Fig. 6.10 Non-linear buckling strength for all strip load (all *R/t* and θ_n included)

(Note: The continuous line shows the empirical fit, nodes show FE analyses results)

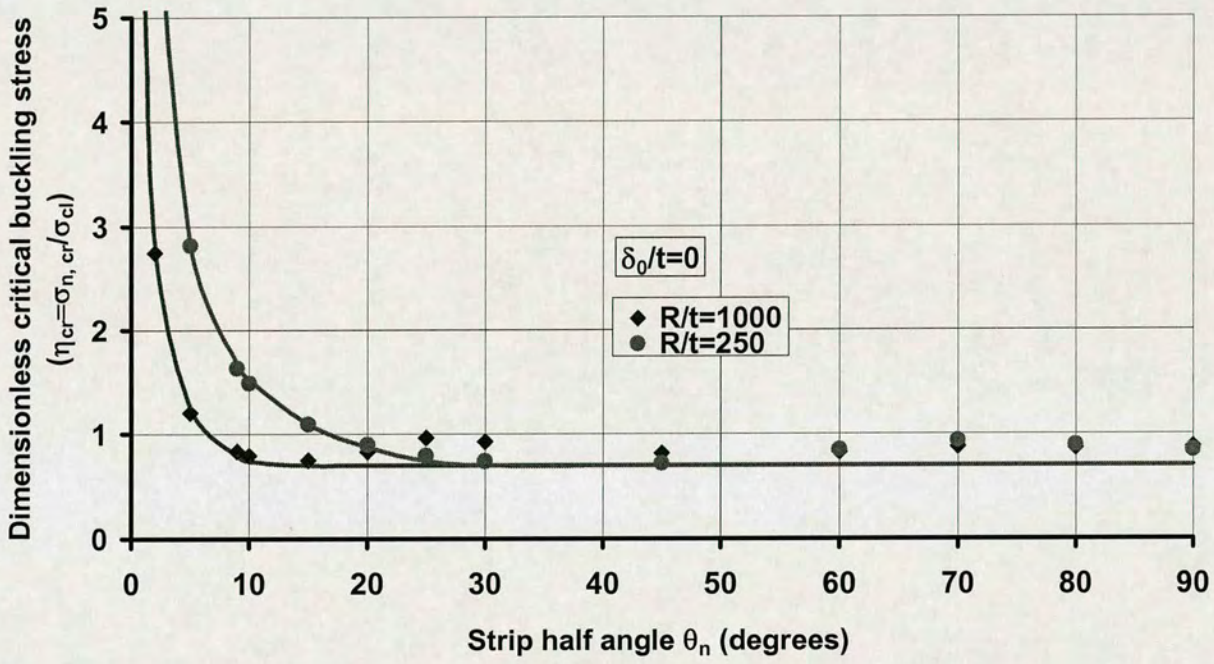

Fig. 6.11: Comparison between FE and empirical equation of GNA
(Note: The continuous line shows the empirical fit, nodes show FE analyses results)

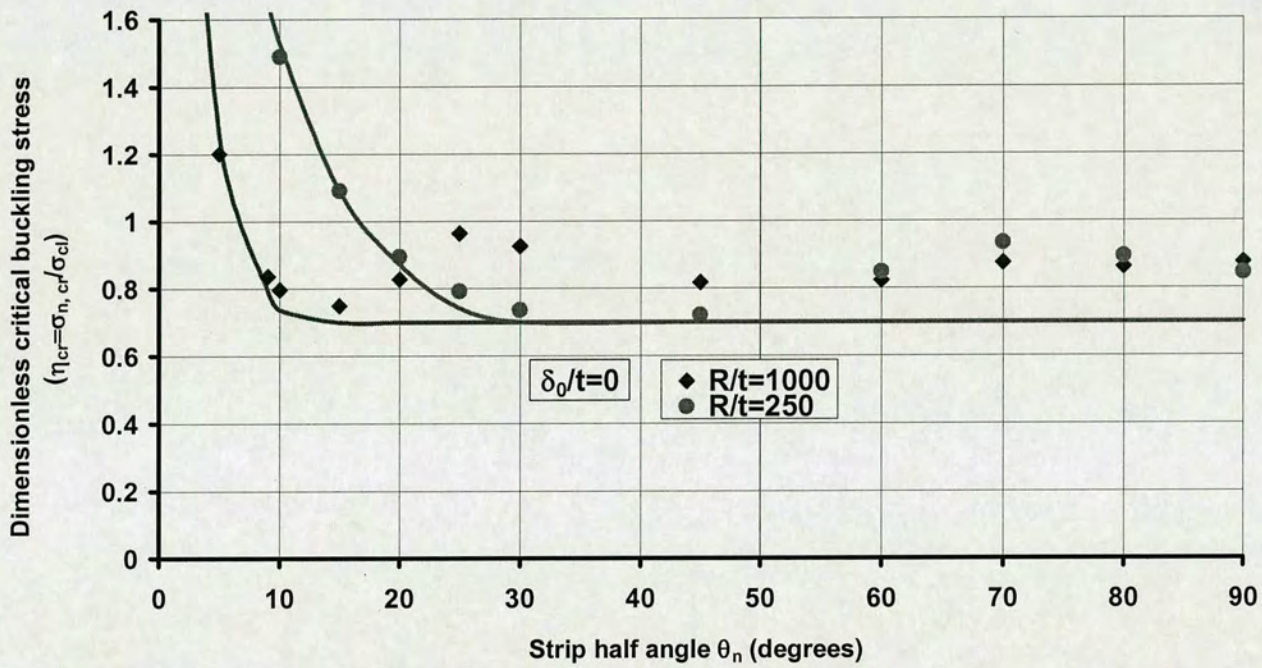

Fig. 6.12: Comparison between FE and empirical equation of GNA (in detail)
(Note: The continuous line shows the empirical fit, nodes show FE analyses results)

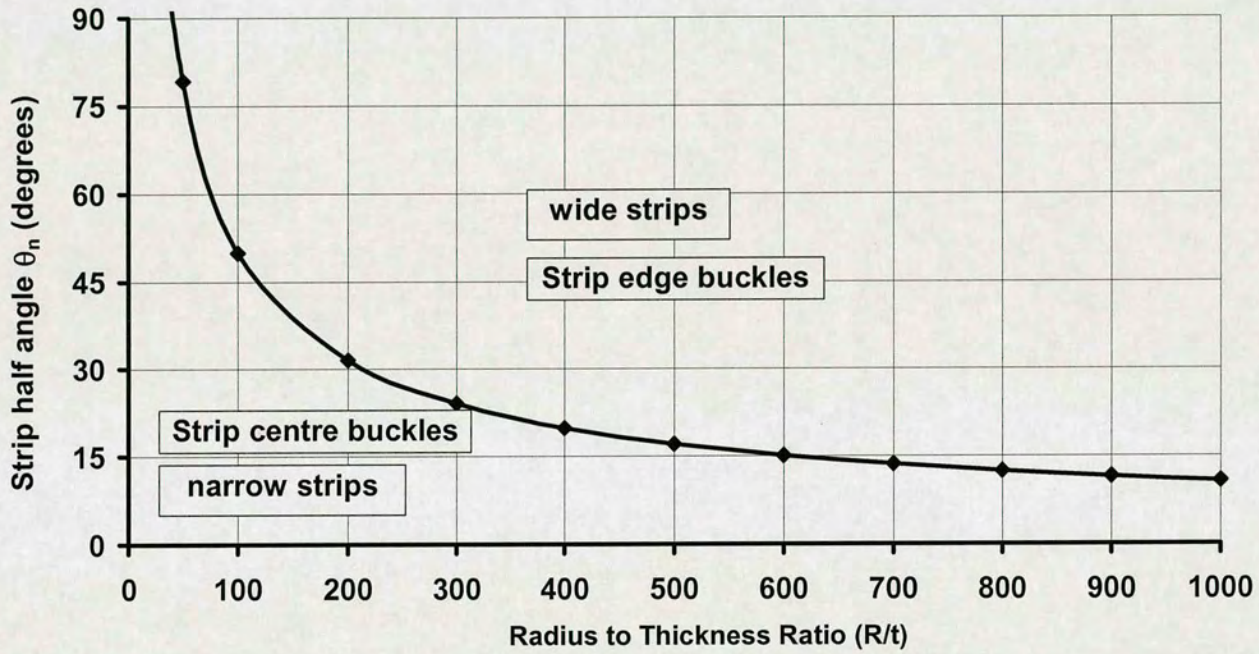

Fig. 6.13: Bound for GNA empirical equations

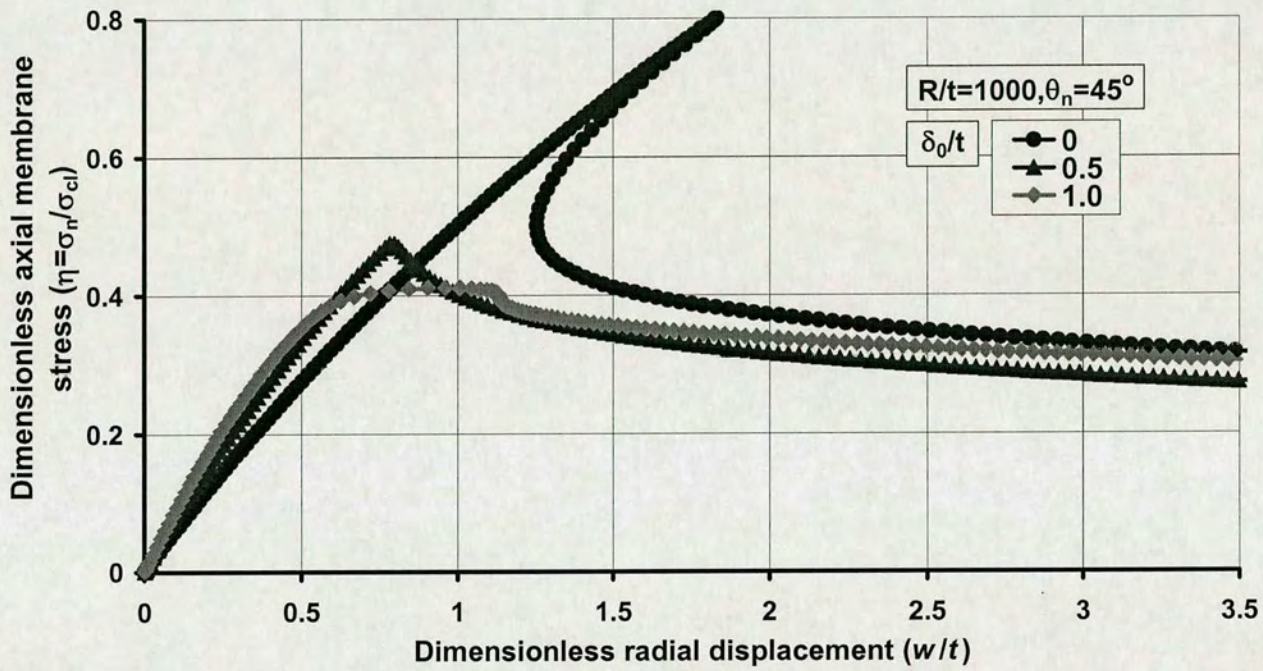

Fig. 6.14: Load-displacement curve for strip edge buckles

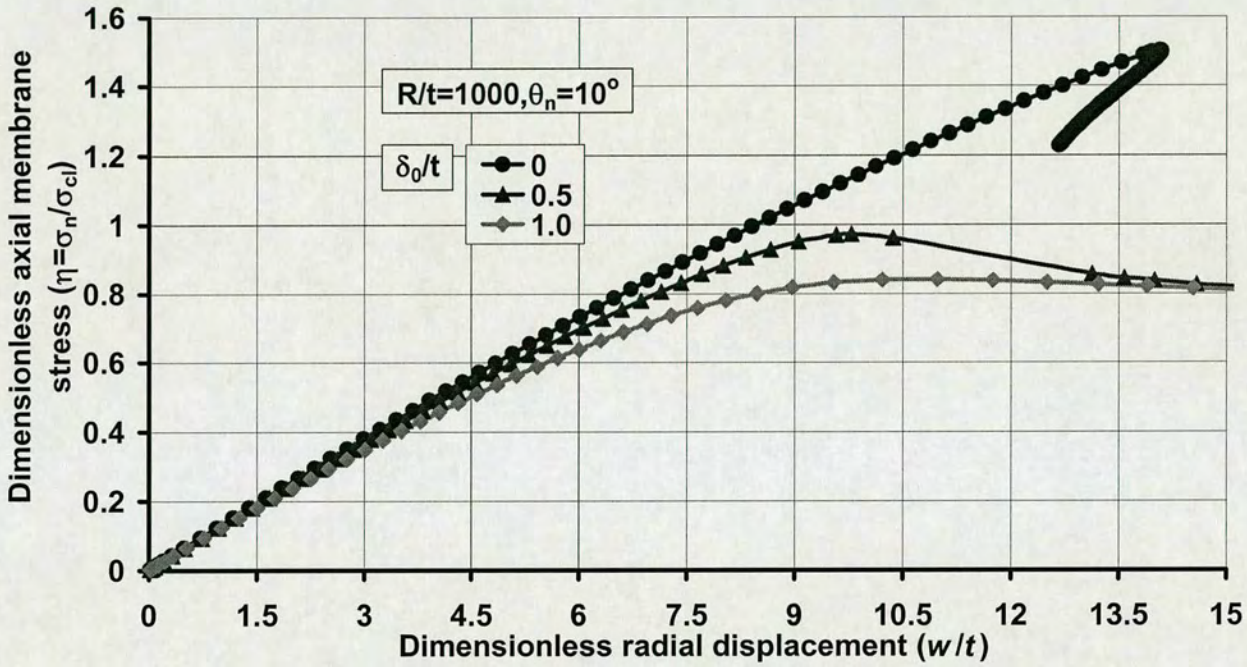

Fig. 6.15: Load-displacement curve for strip centre buckles

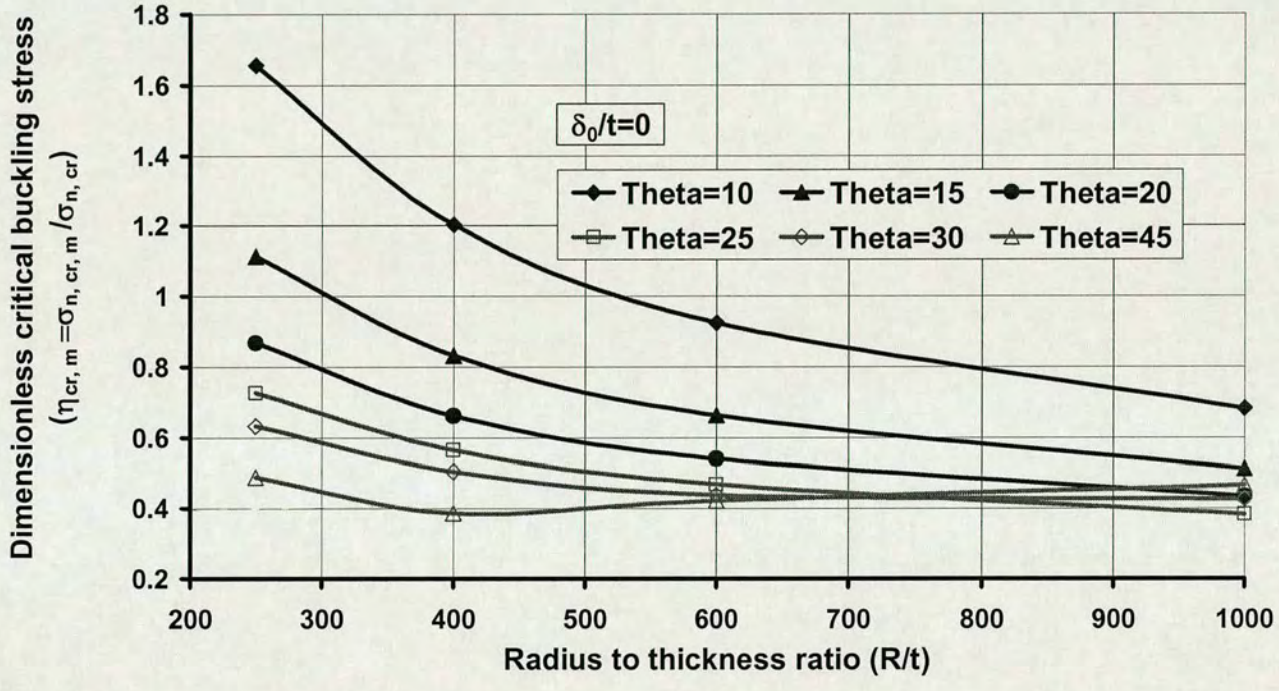

Fig. 6.16: Effect of *R/t* ratio on material non-linearity (GMNA/ GNA)

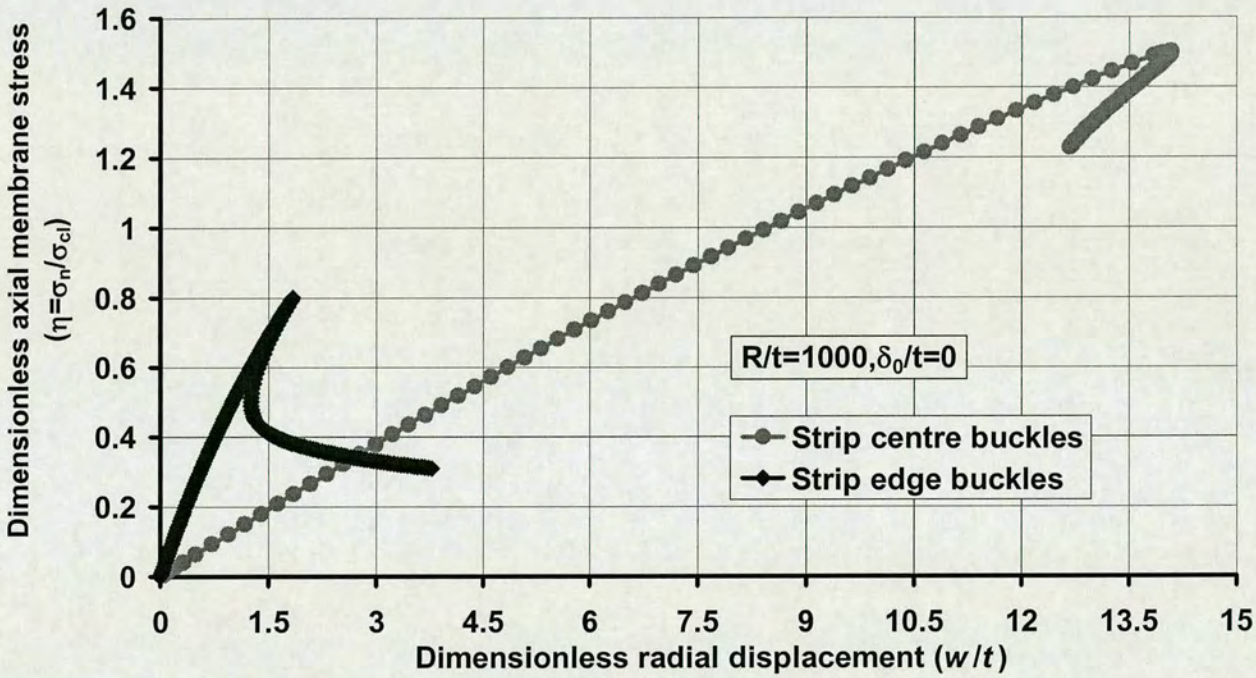

Fig. 6.17: Comparison of two load-displacement curves

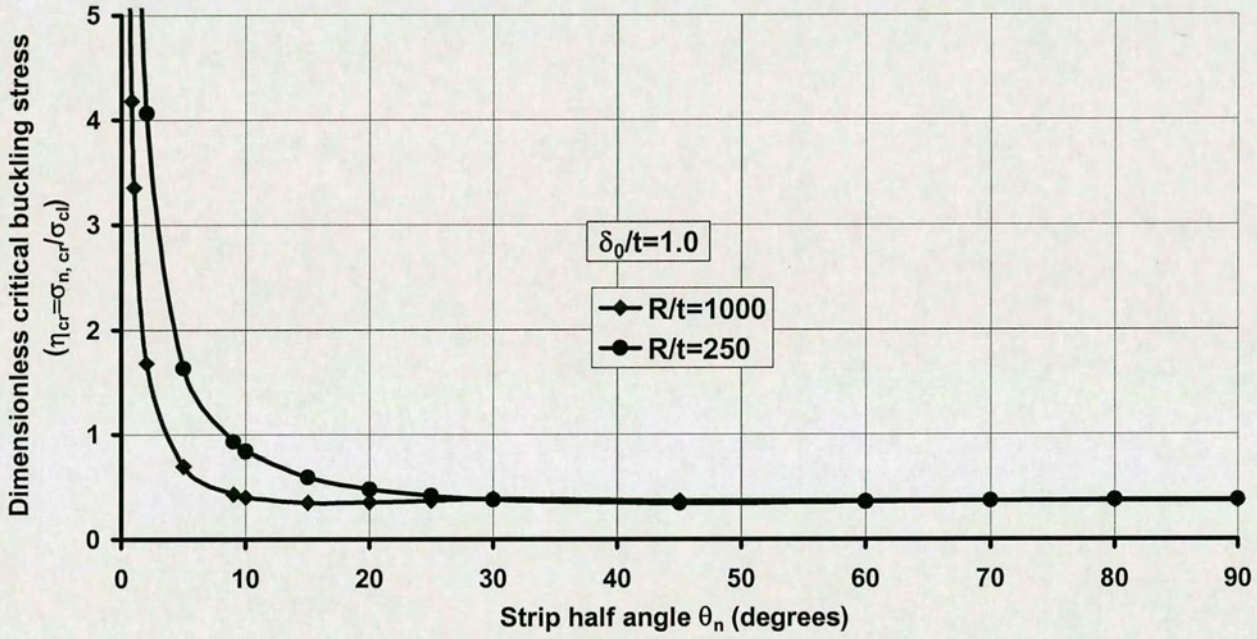

Fig. 6.18: Effect of strip half angle on non-linear buckling strength of imperfect cylinders (GNIA)

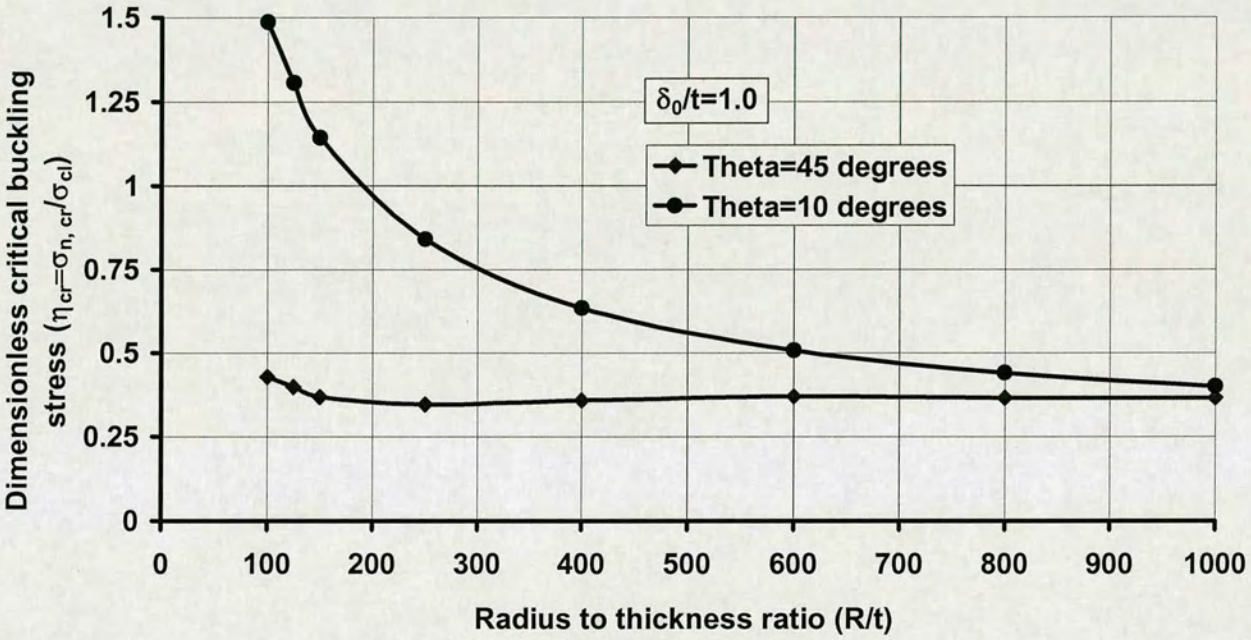

Fig. 6.19: Effect of *R/t* ratio on non-linear buckling strength of perfect cylinders (GNIA)

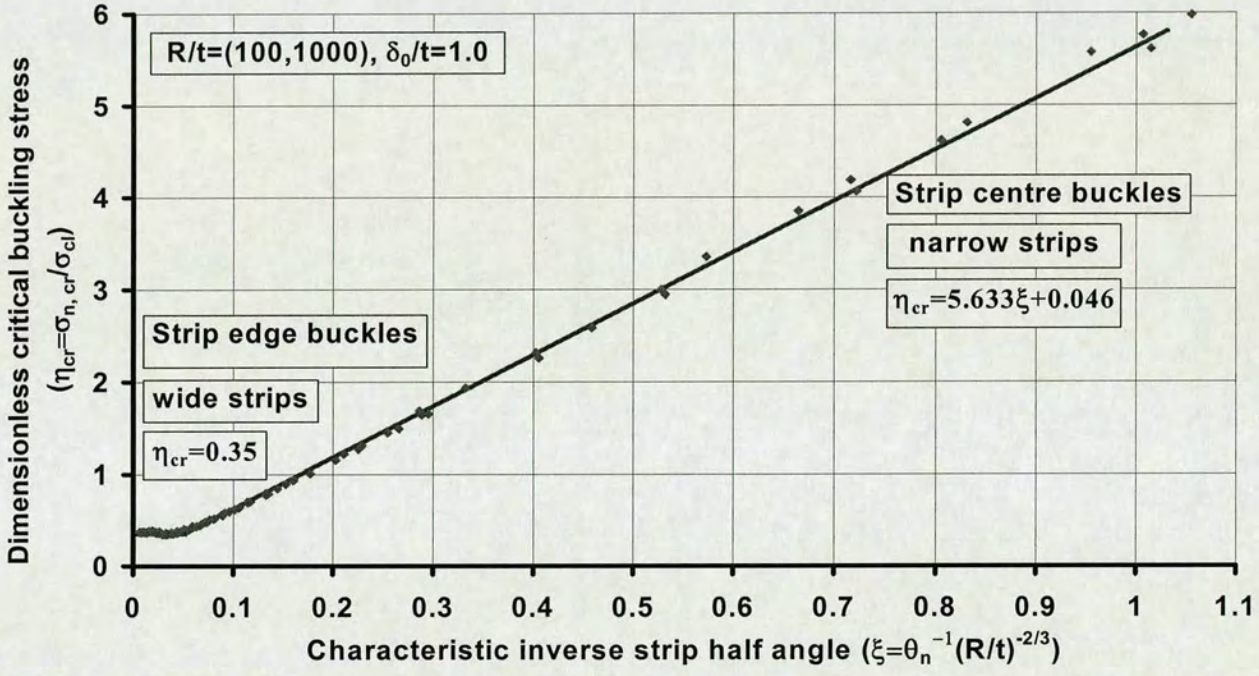

Fig. 6.20: Non-linear buckling strength of imperfect cylinders for all strip load (all *R/t* and θ_n included)

(Note: The continuous line shows the empirical fit, nodes show FE analyses results)

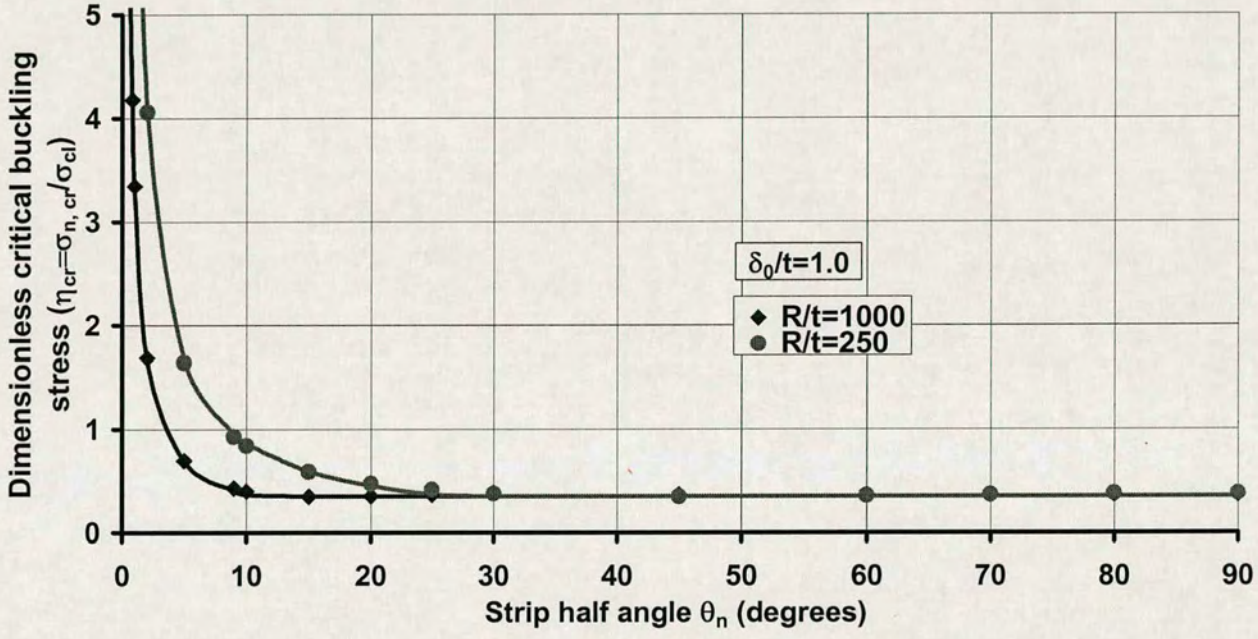

Fig. 6. 21: Comparison between FE and empirical equation of GNIA
(Note: The continuous line shows the empirical fit, nodes show FE analyses results)

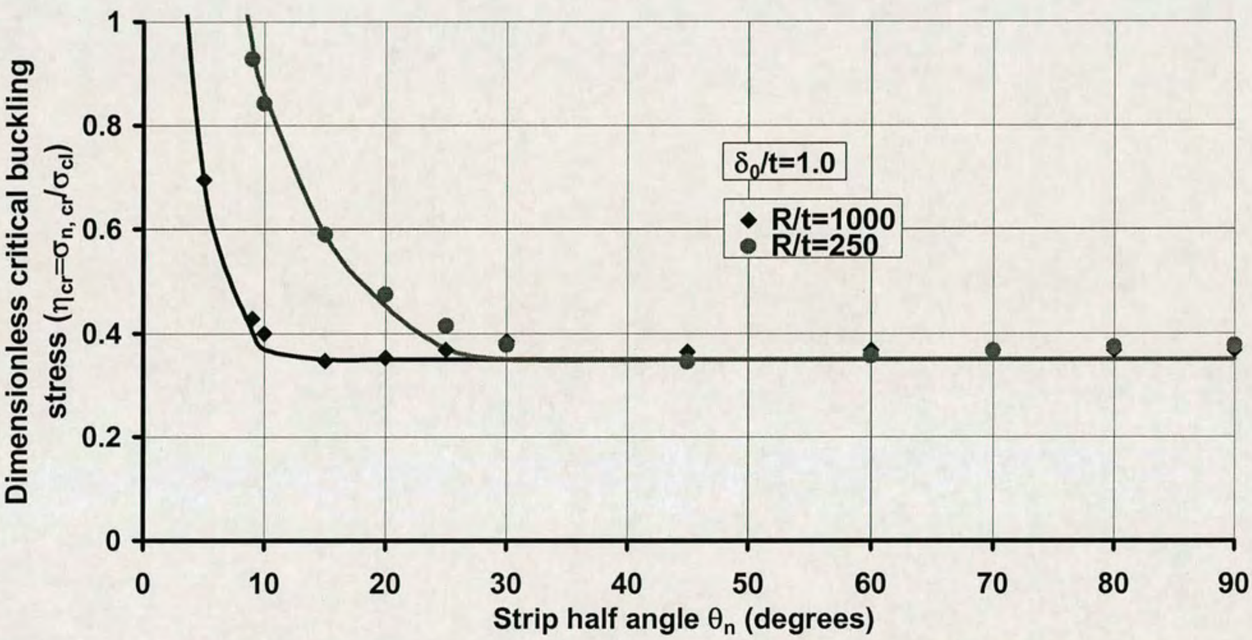

Fig. 6.22: Comparison between FE and empirical equation of GNIA (in detail)
(Note: The continuous line shows the empirical fit, nodes show FE analyses results)

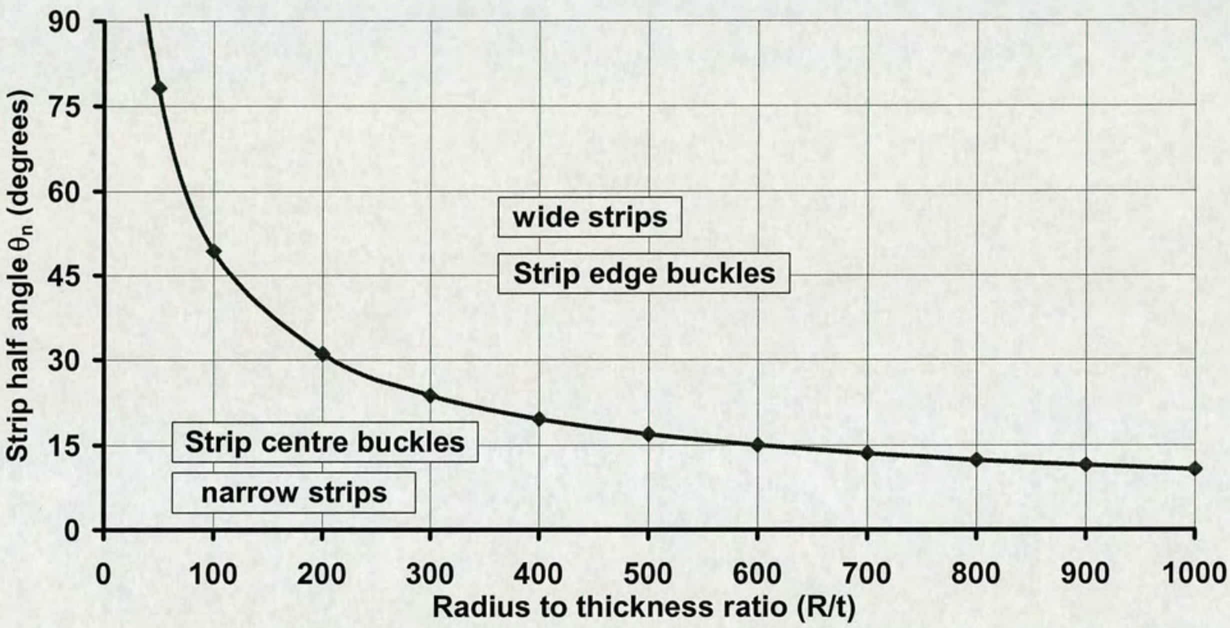

Fig. 6.23: Bound for GNIA empirical equations

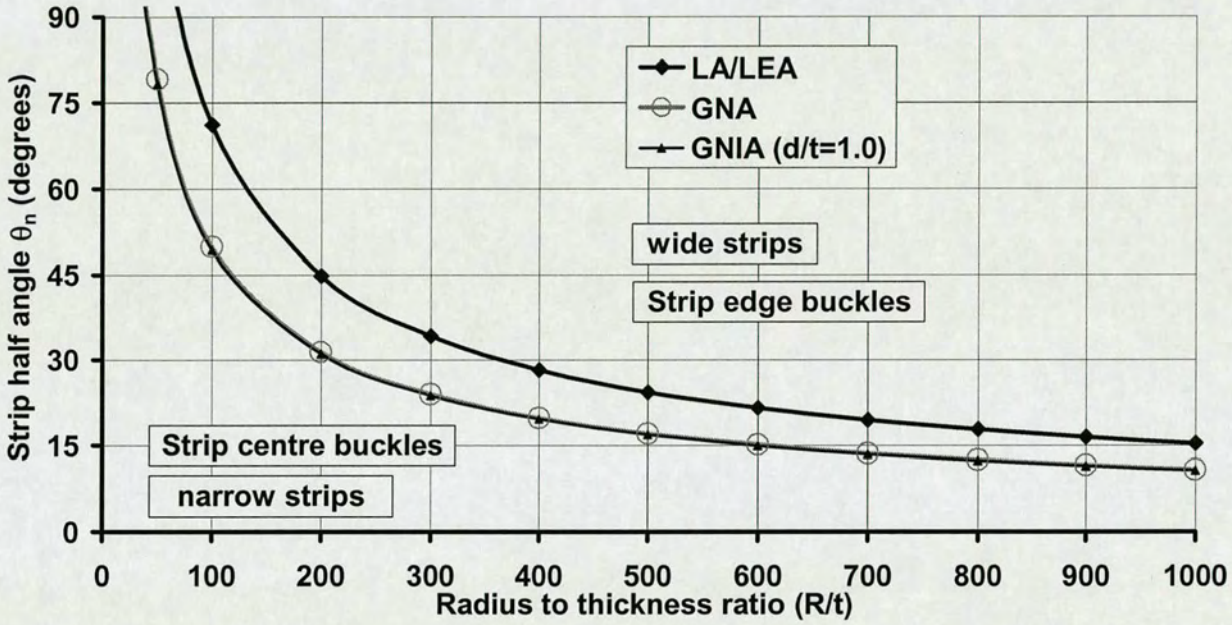

Fig. 6.24: Comparison of different analyses bounds

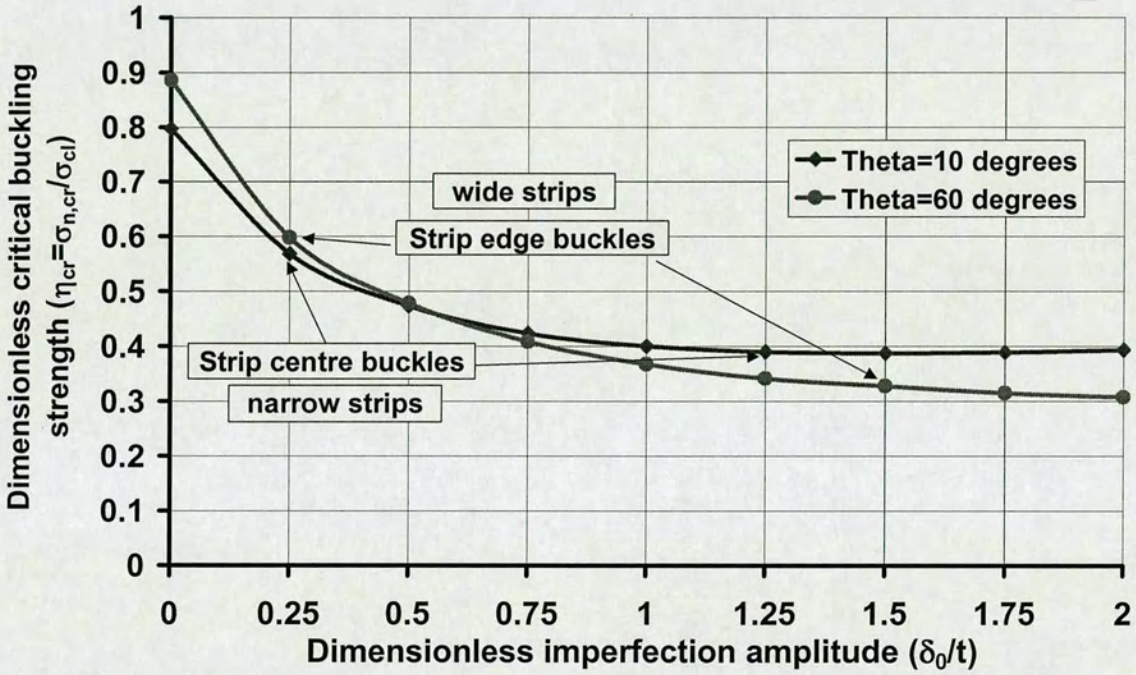

Fig. 6.25: Imperfection sensitivity of partially compressed cylinders

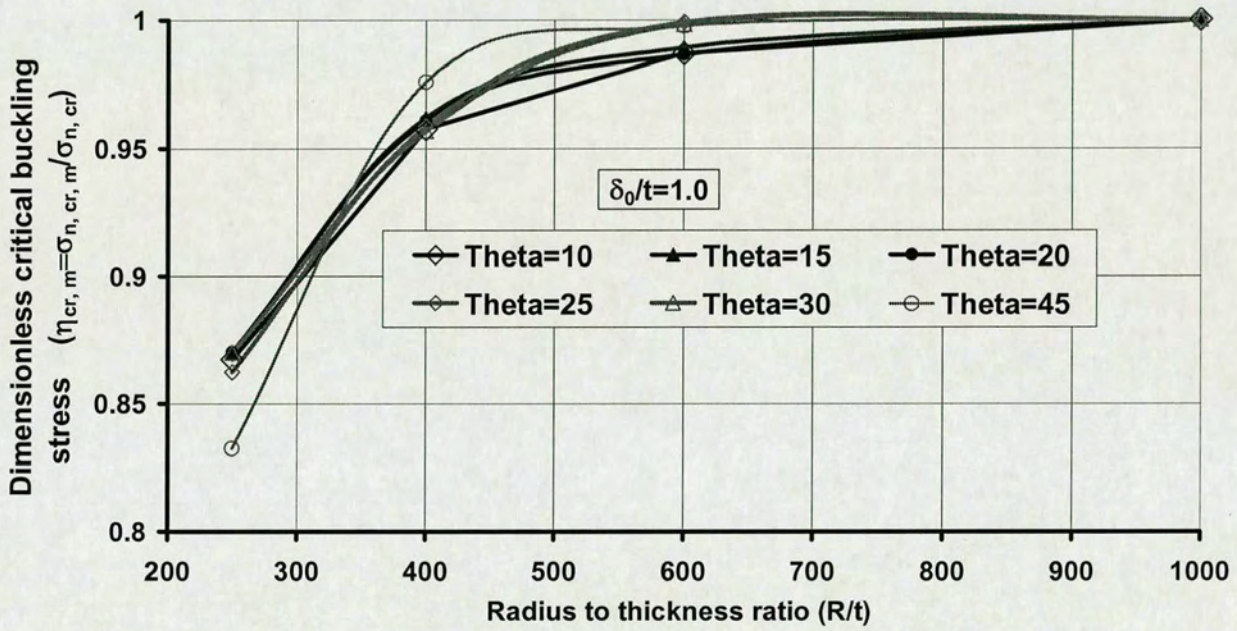

Fig. 6.26: Effect of *R/t* ratio on material non-linearity of imperfect cylinders (GMNIA/ GNIA)

Chapter 7

SHELL BUCKLING STRENGTH UNDER LOCALISED AXIAL COMPRESSION: EFFECT OF LOAD ZONE HEIGHT

7.1 Introduction

As stated in the previous chapters: reliable quantification of highly local non-uniform stress effects on the buckling of a cylindrical shell is still challengingly difficult. Special emphasis was placed here on understanding the effect of the meridional extent of the load zone. In addition, analyses with geometric imperfections in the wall were done to explore the imperfection sensitivity of thin-walled cylindrical shells under these conditions.

7.2 Model

Two distinguishable strip angles with a wider content of the circular cylinders (compared with Chapter 6) have been investigated. The radius R varies from 1 m to 20 m with two half angles of strip load θ_n 10° and 60°. Strip height changes from 1/100 H to the whole cylinder height H. The wall thickness t is 10 mm and the height of cylinder H is 30 m, which makes the ratio of R/t between 100 and 2,000. The variation of the corresponding parameters of the model is shown in Fig. 7.1. The change of the axial stress can be expressed by $d\sigma_{n,z}/dz$ and the extremes can be interpreted as $d\sigma_{n,z}/dz=0$ when the compression is at the top and $d\sigma_{n,z}/dz=\propto$ when the theoretical edge compression is applied in the mid-plane. The introduction of the axial stress gradient (Eqn. 7.1) to make it dimensionless for the rate of change of nominal axial stress in the elevated axial stress region.

A converged mesh was again obtained from the previous study (Chapter 4). The model descriptions, including the properties of the material, the co-ordinate system, boundary condition as well as its influence on the analyses results, geometric imperfection and analysis procedure were also presented before (Chapter 5).

The parametric study includes linear bifurcation analysis, non-linear analysis and non-linear analysis with local inward imperfections. This is consistent with the previous study on the load zone width effect, and should produce a full set of shell buckling strength predictions for all the analyses types mentioned above in the area of local axial compression and give enough data support for possible design rules.

For the reason given in Chapter 6, the predictions of the LA/LEA analysis, based on small deflection and linear elastic shell bending theory, is a key reference load in the framework of all analyses types (ENV 1993-4-1, 1999; Rotter, 2002) and is under study first.

7.3 Linear Eigenvalue Analyses (LA/LEA)

7.3.1 Buckling Strength Prediction

In the previous study on the effect of the width of the load strip, two buckling modes were found. To be consistent with the previous study, the notion of dividing the buckling modes into two groups was used in describing all the analyses on the influence of the axial stress gradient. To achieve this, two typical strip load half angles were used: θ_n=10° and 60° were selected as they caused strip centre and strip edge buckles respectively in the study in which the full height of the modelled shell was loaded.

The classical buckling stress σ_{cl} (Eqn. (2.3); Lorenz, 1908; Timoshenko, 1910; Southwell, 1914) and the nominal axial membrane stress at the mid-plane section $\sigma_{n,cr}$ (Fig. 5.3), were again used here as reference values to describe the results of all the analyses. The results are again expressed in terms of dimensionless buckling strength parameter $\eta_{cr}=\sigma_{n,cr}/\sigma_{cl}$.

7.3.1.1 Buckling Strength Prediction for Strip Centre Buckles

Following the same step used in Chapter 6, the results of the analyses are shown for θ_n=10° in Fig. 7.2. For thin shells (R/t=2,000), the buckling load progressively decreases for all strip load heights, which indicates that a higher stress gradient (shorter strip height)

always produced a higher buckling strength. However in stocky cylinders (R/t=200), the buckling load decreases for very small strip load heights, but quickly reaches a minimum and rises for most larger strip load heights. This indicates that, for most of the analysed conditions, a higher stress gradient (shorter strip height) produces a lower buckling strength.

The buckling strength of the cylinder is clearly related to the R/t ratio, the strip width and height over which the strip load is applied. But the relationships are quite complicated, and difficult to use in any design process.

The ratio of strip height to the total height of the modelled cylinder h/H is a represetation of the stress gradient, but it is of limited application because it is special to this model. A better representation is to use the axial stress gradient in the zone where the buckles are forming. This is best described in terms of a dimensionless parameter, which is here defined as the dimensionless axial stress gradient g (Eqn. 7.1). This parameter g describes the rate of change of nominal axial stress in the buckle region:

$$g = \frac{d\sigma_{n,z}}{dz}\frac{R}{\sigma_{n,cr}} \tag{7.1}$$

In Eqn. 7.1, $\sigma_{n,cr}$ is the maximum nominal stress introduced by the axial compression stress and is here the stress in the middle plane (Fig. 7.1). With the application of dimensionless axial stress gradient g, Figs. 7.3 & 7.4 show a set of curves with different height on the drawing representing different R/t ratio respectively. The results appear differently, but are still not simply describable. To achieve a simple description, it is necessary to devise a new dimensionless parameter that simplifies the description. This was achieved the same manner as in the study of the effect of the width of the load strip. Both the R/t ratio and the half strip angle θ_n were brought into the analyses to using a new dimensionless strip load extent parameter ϕ (Eqn. 7.2) to map the analyses results onto a single straight line:

$$\phi = \theta_n^{-1}(R/t)^{-2/3}(\frac{d\sigma_{n,z}}{dz}\frac{R}{\sigma_{n,cr}})^{-1/3} = \theta_n^{-1}(R/t)^{-2/3} g^{-1/3} \qquad (7.2)$$

The dimensionless buckling stress η_{cr} is plotted against dimensionless strip load extent parameter – characteristic inverse strip half angle ϕ in Fig. 7.5 for strip angle θ_n=10°. The buckling analyses results obtained can be closely mapped onto one straight line if an appropriate parameter ϕ has been chosen (Fig. 7.6; Eqn. (7.3)):

$$\eta_{cr} = 5.342\phi + 0.969 \qquad (7.3)$$

The appropriate parameter here refers to $\phi \geq 0.07$, $R/t \leq 1{,}000$ and $\eta \leq 5$ (From the analyses done in Chapter 5, the influence of local buckling can be expanded into a wider/higher content if the rigidity of the whole structure is changed (related closely to the *R/t* ratio, the content of the load) and since the influence from the boundary conditions is unavoidable. Such analyses results should be ignored for the empirical equations aiming for medium length of cylinder). These limitations exclude results for very short zones and very thin cylinders ($R/t \leq 1{,}000$). The relative error bounds of this formula are given by (-6.68%, +5.14%). The empirical equations give a close match to FE results (Fig. 7.6).

From Fig. 7.5, it is also evident that there is a minimum buckling stress $\eta_{cr,\,min}$ for each *R/t* and this can provide a reasonable lower bound for the empirical equation of each *R/t* ratio. The following Eqn. (7.4) was used for this purpose (obtained from Fig. 7.7):

$$\eta_{cr,\min} = 6.528\phi + 0.858 \qquad (7.4)$$

where the parameter ϕ is defined in Eqn. (7.2) but $\eta_{cr,min}$ refers to the minimum dimensionless buckling stress of each *R/t*. There is no strict limitation on this formula (Eqn. 7.4) which means that it is valid for $100 < R/t < 2{,}000$. The relative error bounds are (-4.23%, +3.89%).

Furthermore, it is important to interpret the relationship between R/t ratio and stress gradient $d\sigma_n/dz$ where its own minimum buckling stress lies. In Fig. 7.8, all the nodes show the cylinder R/t ratio of the minimum linear buckling strength with different axial stress gradient g, and the following Eqn. (7.5) is account for this:

$$(R/t)_{cr,\min} = 627.99g^4 \qquad (7.5)$$

Due to the discontinuity of the analyses data (more continuous variation of analyses data needed), only relative continuous data have been selected to approach this formula and since the applicable extent will be $250<R/t\leq1{,}000$ (for civil engineering practice) and the relative error bounds are given by (-4.28%, +4.67%).

7.3.1.2 Buckling Strength Prediction for Strip Edge Buckles

The results of the analyses are shown for $\theta_n=60^\circ$ in Fig. 7.9. For all the shells analysed ($100\leq R/t\leq2{,}000$), the buckling load sharply falls for all strip load heights in higher axial stress gradient (shorter strip height), which indicates that a higher stress gradient always produced a higher buckling strength. The buckling strength stabilised in a level after reaching a relatively lower axial stress gradient (longer strip height).

Again, the buckling strength of the cylinder is clearly related to the R/t ratio, the strip width and height over which the strip load is applied. But the relationships are quite complicated, and indirect to use.

A general representation is to use the axial stress gradient g (Eqn. 7.1) in the zone where the buckles is forming, which replaces the ratio of strip height to the total height of the modelled cylinder h/H.

With the application of dimensionless axial stress gradient g, Figs. 7.10 & 7.11 show a set of curves with different height on the drawing representing different R/t ratio respectively. The results appear differently, but are still not simply describable as the strip centre buckles. To achieve a simple description, it is necessary to devise a new

dimensionless parameter that with simplifies the description via the same manner as in the study of the effect of the width of the strip load. Both the *R/t* ratio and the half strip angle θ_n were brought into the analyses to using a new different dimensionless strip load extent parameter – characteristic inverse strip half angle Π (Eqn. 7.6) to map the analyses results onto a single straight line:

$$\Pi = \theta_n^{-1}(R/t)^{-1/3}(\frac{d\sigma_{n,z}}{dz}\frac{R}{\sigma_{n,cr}})^{4/3} = \theta_n^{-1}(R/t)^{-1/3}g^{4/3} \qquad (7.6)$$

The dimensionless buckling stress η_{cr} is plotted against dimensionless strip load extent parameter Π in Fig. 7.12 for strip angle θ_n=60°. The buckling analyses results obtained can be closely mapped onto one straight line if an appropriate parameter Π has been chosen (Fig. 7.13; Eqn. (7.7)):

$$\eta_{cr} = 0.682\prod+1.08 \qquad (7.7)$$

The appropriate parameter here refers to $0.01 \leq \Pi \leq 1$ (which eliminates the applications of stocky cylinders (small *R/t* ratio) with lower stress gradient), $100 < R/t < 2000$ and $\eta \leq 5$. These limitations eliminate the results from very short or extremely large load zones (It is difficult to find very short load zone in practice and very large load zone were covered by the previous Chapter 6). The relative error bounds of this formula are given by (-8.99%, +7.97%).

7.3.2 Summary

From the analyses above, the exploration the effect of axial stress gradient on these two buckling modes gives a wider validity to the previous study on shell buckling under local axial compression on load zone width.

Introducing only one additional parameter, the axial stress gradient $d\sigma_n/dz$, into the previous corresponding study of the local compression, can easily solve the buckling strength in the case of both strip centre buckles and strip edge buckles. The common

adoption of the relevant parameters into the two analyses reveals a close relationship existing between this chapter and the previous chapter. And what is more important is that both ways can give a satisfactory prediction of the buckling strength, which is applicable in engineering.

The influence of geometric non-linearity due to possible large deflections during the loading procedure (GNA) is considered in the following section.

7.4 Geometrically Non-linear Analyses (GNA)

7.4.1 Buckling Strength Prediction

Following the same ideas as used for the linear buckling analysis prediction, the GNA analysis is divided into two sections too: strip centre buckles and strip edge buckles.

7.4.1.1 Buckling Strength Prediction for Strip Centre Buckles

The results of the analyses are shown for θ_n=10° in Fig. 7.14. For thin shells (R/t=2,000), the buckling load progressively falls for all strip load heights, which indicates that a higher stress gradient (shorter strip height) always produced a higher buckling strength. However in stocky cylinders (R/t=200), the buckling load falls for very small strip load heights, but quickly reaches a minimum and rises for most larger strip load heights. This indicates that, for most of the analysed conditions, a higher stress gradient (shorter strip height) produces a lower buckling strength.

The buckling strength of the cylinder is clearly related to the R/t ratio, the strip width and height over which the strip load is applied. But the relationships are quite complicated, and difficult to use in any design process.

The dimensionless strip height h/H is a limited representation of the stress gradient, and a better representation — the axial stress gradient in the zone where the buckles is forming was introduced in Figs. 7.15 & 7.16, which is defined as the dimensionless axial stress gradient g (Eqn. 7.1). This parameter g describes the rate of change of nominal axial

stress in the buckle region. Both figures show a set of curves with different height on the drawing representing different R/t ratio respectively. The results appear differently, but are still not simply describable. A simplified description is devised again to achieve a simple description. Both the R/t ratio and the half strip angle θ_n were brought into the analyses to using a new dimensionless strip load extent parameter ϕ (Eqn. 7.2), which is introduced in the linear bifurcation analyses to map the analyses results.

The dimensionless buckling stress η_{cr} is again plotted against dimensionless strip load extent parameter – characteristic inverse strip half angle ϕ in Fig. 7.17 for strip angle θ_n=10°. The non-linear analyses results obtained can be closely mapped onto a single straight line if an appropriate parameter ϕ has been chosen (Fig. 7.18; Eqn. (7.8)):

$$\eta_{cr} = 2.359\phi + 0.646 \qquad (7.8)$$

where the corresponding parameter ϕ is defined in Eqn. (7.2).

The same assumption has been adopted in order to get a satisfactory result. It limits the analyses results into a relative gentle stress gradients ($0.01 \le \phi$) and thicker cylinders ($R/t \le 1000$). Again this assumption is applicable to real structures. The relative error bounds of this formula are given by (-13.99%, +8.69%). Not surprisingly, like previous study on the influence of strip width, the big deviation occurs due to the instability of the axial symmetric cylinders under the load type approaching the axial symmetric uniform loading and it will be more meaningful if geometric imperfections are introduced. The reason for this is that perfect cylindrical shells assumed here cannot be realised experimentally and practically (Arbocz and Babcock, 1969) — there must be some geometric imperfections in real existing cases and with the introduction of such imperfections, the huge deviation might be diminished again as that of the load zone width cases.

Like before, the minimum buckling stress $\eta_{cr,min}$ provides a reasonable lower bound for the empirical equation of each R/t ratio. The following Eqn. (7.9) was used for this purpose (obtained from Fig. 7.19):

$$\eta_{cr,\min} = 2.451\phi + 0.637 \tag{7.9}$$

where the corresponding parameter ϕ is defined in Eqn. (7.2). The limitation for this formula is $100<R/t<2000$ and the relative error bounds are (-5.94%, +5.64%).

In Fig. 7.20, all the nodes shows the cylinder R/t ratio of the minimum non-linear buckling strength with different axial stress gradient g, and the following Eqn. (7.10) is account for this:

$$(R/t)_{cr,\min} = -1110g + 1160 \tag{7.10}$$

where the corresponding parameter g is defined in Eqn. (7.1). Due to the discontinuity of the analyses data (enormous analyses data needed), only relative continuous data have been selected to approach this formula and since the applicable extent will be $250\leq R/t<1{,}000$ (for civil engineering practice) and the relative error bounds are given by (-6.00%, +5.00%). Another obvious disadvantage of this form lies in the fact there it can only predict the R/t ratio to a maximum of R/t=1,000, which is not enough in theory but sufficient in real cylinder practice.

7.4.1.2 Buckling Strength Prediction for Strip Edge Buckles

The results of the analyses are shown for θ_n=60° in Fig. 7.21. For all the shells analysed ($100\leq R/t\leq 2{,}000$), the buckling load sharply falls for all strip load heights in higher axial stress gradient (shorter strip height), which indicates that a higher stress gradient always produced a higher buckling strength. The buckling strength stabilised again in a level after reaching a relatively lower axial stress gradient (longer strip height).

Again, the buckling strength of the cylinder is clearly related to the *R/t* ratio, the strip width and height over which the strip load is applied. But the relationships are indirect to use.

A general representation of dimensionless axial stress gradient *g* is to describe the variation of axial stress (Eqn. 7.1) in the zone where the buckles is forming, which replaces the ratio of strip height to the total height of the modelled cylinder *h/H*. Fig. 7.22 & Fig. 7.23 show a set of curves with different height on the drawing representing different *R/t* ratio respectively. The results appear differently, but are still not simply describable as the strip centre buckles. To achieve a better description, dimensionless strip load extent parameter – characteristic inverse strip half angle Π (Eqn. 7.6), defined in linear bifurcation analyses, is devised to simplify the description via the same manner as in the study of the effect of the width of the load strip.

The dimensionless buckling stress η_{cr} is plotted against dimensionless strip load extent parameter Π in Fig. 7.24 for strip angle θ_n=60°. The non-linear strength analyses results obtained can be closely mapped onto one straight line if an appropriate parameter Π has been chosen (Fig. 7.25; Eqn. (7.11)):

$$\eta_{cr} = 0.694\prod + 0.947 \qquad (7.11)$$

This expression is slightly different from that of the LA/LEA. The appropriate parameter here refers to the same as LA/LEA: $0.01 \le \Pi \le 1$ (which eliminates the applications of stocky cylinders (small *R/t* ratio) with lower stress gradient), $100 < R/t < 2{,}000$ and $\eta \le 5$. The relative error bounds of this formula are given by (-12.79%, +16.35%).

7.4.2 Summary

Here again the value of two divided buckling modes was verified. Like the linear buckling analysis, with the stress gradient $d\sigma_n/dz$, the buckling strengths in both strip centre buckles and strip edge buckles were simply expressed by empirical equations, which adopted only the assumptions of civil practice.

In summary, the critical buckling strength of GNA can be predicted by using the formulae described above and the separation of these two approaches can be achieved from the previous study. This empirical equation uses only on the classical buckling stress and the nominal membrane stress, which are early evaluated. Within a small error bounds and engineering applicable limits, this empirical equation is a very simple and good reference for the perfect cylindrical shell strength prediction in engineering.

To continue the previous discussion, it is important to know the non-linear analysis prediction with some imperfections, which are unavoidable in engineering practice, and the widely accepted local inward imperfection is introduced as a typical form.

7.5 Geometrically Non-linear Analyses with Imperfection (GNIA, with δ_0/t =1.0)

Since imperfections play a very important role in their strength as well as the post-buckling behaviour, it is necessary to investigate influence. As in the previous study, the imperfection introduced here is a local inward deviation of Type A (Rotter and Teng, 1989; Teng and Rotter, 1992), which is among the most deleterious types to the buckling strength under axial compression (Koiter, 1963; Bornscheuer, Häfner and Ramm, 1983; Yamaki, 1984; Rotter and Teng, 1989; Teng and Rotter, 1992; Holst et al., 1999; Holst et al., 2000).

7.5.1 Imperfection Feature

The imperfection feature has been mentioned in Chapter 3 and for the purpose of simplicity, only an imperfection of one wall thickness (δ_0/t=1.0) was taken into account here.

7.5.2 Buckling Strength Prediction

Like the treatment method of the LA/LEA and the GNA analysis prediction, the prediction of the GNIA (geometrically non-linear elastic analysis with imperfection) results can be treated separately according to their own buckling modes: strip centre buckles and strip edge buckles.

7.5.2.1 Buckling Strength Prediction for Strip Centre Buckles

The results of the analyses are shown for θ_n=10° in Fig. 7.26. For all shells ($100 \leq R/t \leq 2{,}000$), the buckling load progressively falls for all strip load heights, which indicates that a higher stress gradient (shorter strip height) always produced a higher buckling strength. However in very long strip height (lower stress gradient), the buckling load rises for most stocky shells. This indicates that, for most of the analysed conditions, a lower stress gradient (longer strip height) produces a higher buckling strength. This effect was not anticipated. There might two possible reasons for this: one from the converged mesh which is not suitable for a very high strip load and the other is that the buckle size may increase a lot in the stocky shells with local imperfection (comparative to the cylinder height) and since the influence from the boundary conditions are unavoidable. Fortunately, the extreme cases (very long strip height) were stated in Chapter 6 already.

The buckling strength of the cylinder is clearly related to the *R/t* ratio, the strip width and height over which the strip load is applied. But the relationships are quite complicated, and difficult to use in any design progress.

A dimensionless parameter, which is here defined as the dimensionless axial stress gradient *g* (Eqn. 7.1) was introduced in both Figs. 7.27 & 7.28. This parameter *g* describes the rate of change of nominal axial stress in the buckle region.

With the application of dimensionless axial stress gradient *g*, Figs. 7.27 & 7.28 show a set of curves with different height on the drawing representing different *R/t* ratio respectively. The results appear differently, but are still not simply describable. Following the ideas from the two analyses for perfect cylinder, the same dimensionless parameter – characteristic inverse strip half angle ϕ (Eqn. 7.2) were applied to achieve a simple description.

The dimensionless buckling stress η_{cr} is plotted against dimensionless strip load extent parameter ϕ in Fig. 7.29 for strip angle θ_n=10°. In Fig. 7.29, the results are more widely scattered than the LA/LEA or GNA analyses. The reason for this might arise because of

the size of buckles and mesh design, which were stated before. But, with the limits of a relatively high load zone (comparatively lower stress gradient) ($0.07 \leq \phi$) and excluding very thin cylinders ($R/t \leq 1{,}000$), the results (Fig. 7.30) can be accurately mapped by the following empirical Eqn. (7.12):

$$\eta_{cr} = 1.472\phi + 0.314 \tag{7.12}$$

Just like LA/LEA and GNA, those assumptions limited the analyses results into a relative high load zone within excluding very thin cylinders ($R/t \leq 1{,}000$) and so are applicable in real structures. The relative error bounds by this formula are given by (-4.99%, +8.22%).

The minimum non-linear buckling strength for each R/t is plotted again the characteristic inverse strip angle in Fig. 7.31. The following Eqn. (7.13) is used to map this:

$$\eta_{cr,\min} = 1.531\phi + 0.291 \tag{7.13}$$

The limitation for this formula is $100 < R/t < 2{,}000$ and the relative error bounds are (-5.67%, +6.35%).

The relationship between R/t ratio and stress gradient $d\sigma_n/dz$ when it reaches its own minimum buckling stress provided a poor mapping and the same reason with discontinuity contributes to this.

7.5.2.2 Buckling Strength Prediction for Strip Edge Buckles

The results of the analyses are shown for $\theta_n = 60^\circ$ in Fig. 7.32. For all the shells analysed ($100 \leq R/t \leq 2{,}000$), the buckling load sharply falls for all strip load heights in higher axial stress gradient (shorter strip height), which indicates that a higher stress gradient always produced a higher buckling strength. The buckling strength stabilised in a level or even slightly decreases with the lower axial stress gradient after reaching a relatively longer strip height.

In addition, there is no much influence from the boundary conditions in the large strip height range (lower axial stress gradient) like that of the strip edge buckles. This can be explained that different buckling modes in these two buckling phenomena cause the different degree of boundary influence due to different height of buckle zones (Figs. 5.11 & 5.12).

Again, the buckling strength of the cylinder is clearly related to the *R/t* ratio, the strip width and height over which the strip load is applied. But the relationships are quite complicated, and indirect to use.

A general representation is to use the axial stress gradient *g* (Eqn. 7.1) in the zone where the buckles is forming, which replaces the ratio of strip height to the total height of the modelled cylinder *h/H*.

With the application of dimensionless axial stress gradient *g*, both Figs. 7.33 & 7.34 show a set of curves with different height on the drawing representing different *R/t* ratio respectively. The results show a trend of convergence in higher axial stress gradients, but are still not simply. Like that of the perfect cylinder analyses, dimensionless strip load extent parameter – characteristic inverse strip half angle Π (Eqn. 7.6) was used to interpolate this further: the dimensionless buckling stress η_{cr} is plotted against dimensionless strip load extent parameter Π in Fig. 7.35 for strip angle θ_n=60°. The GNIA analyses for δ_0/t=1.0 can be represented by the lower bound empirical equation if an appropriate parameter Π has been chosen (Fig. 7.36; Eqn. (7.14)):

$$\eta_{cr} = 0.224\prod + 0.376 \qquad (7.14)$$

This equation is different from that of previous analyses types (Eqn. (7.7) & (7.11)), it shows more flat variation with the strip load height, which means that the GNIA results are less sensitive to the axial stress variation (gradient). The equation was based on $\Pi \leq 1$ (eliminates the applications of stocky cylinders (small *R/t* ratio) with lower stress

gradient), $100<R/t<2{,}000$ and $\eta \leq 5$. These limitations eliminate the results from very short or extremely large load zones. The relative error bounds of this formula are given by (-11.86%, +9.38%).

7.5.3 Summary

Like that of LA/LEA and GNA analyses, two different approaches according to their different buckling mechanism give another test on the validity of these equations. All these assumptions do not hinder the application in engineering as before, which validate the feasibility of practical usage.

The critical buckling strength of GNIA can be predicted by using the formulae described above and the separation of these two approaches can be achieved from the previous study on strip load width. This empirical equation, with a small error bounds and engineering applicable limits, is expressed in terms of parameters that can be easily evaluated and provides a good and simple reference for the imperfect cylindrical shell strength prediction in engineering. Only an imperfection of one wall thickness ($\delta_0/t=1.0$) was taken into account here, but other imperfection amplitudes will have similar relationship with different coefficients.

7.6 Conclusions

7.6.1 Summary

This chapter has presented a comprehensive parametric study, which examined the effect of non-uniform loading on the buckling strength of geometrically perfect and imperfect shells. The non-uniform loading is set up by applying shear stresses to the shell wall over a limited extent. Special emphasis is placed on understanding the effect of the meridional extent of the load zone. Local axisymmetric weld depression imperfections are used in conjunction with several different analyses types. The chapter defines a revised set of buckling empirical equations for different analyses types:

LA/LEA	(Strip centre buckles): $\eta_{cr} = 5.342\phi + 0.969$	(7.3)
	(Strip edge buckles): $\eta_{cr} = 0.682\prod + 1.08$	(7.7)
GNA	(Strip centre buckles): $\eta_{cr} = 2.359\phi + 0.646$	(7.8)
	(Strip edge buckles): $\eta_{cr} = 0.694\prod + 0.947$	(7.11)
GNIA	(Strip centre buckles): $\eta_{cr} = 1.472\phi + 0.314$	(7.12)
	(Strip edge buckles): $\eta_{cr} = 0.224\prod + 0.376$	(7.14)

All the equations above show the similar variations of the buckling strength with the changing of each individually selected parameter (ϕ or Π). In strip centre buckle cases, the buckling strength decreases with the introduction of geometric non-linearity and local inward imperfection and the trend of buckling strength also keeps more constant accordingly. In strip edge buckle cases, the buckling strength does not varies much with the changing of the parameter Π like the strip centre buckle case does, but the buckling strength still decreases with the introduction of geometric non-linearity and local inward imperfection.

The results of the parametric analyses presented in the current chapter support the hypothesis from the previous chapters that the prediction of shell buckling strength under local axial compression, no matter emphasis is placed on the meridional extent of the load zone or on the circumferential extent of it, with or without geometric imperfections, can be divided into two buckling modes due to their corresponding buckling mechanism and a full set of simple empirical equations have been provided accordingly. A summary of conclusions is as follows.

7.6.2 Conclusions

A. Parametric studies lead to a simple empirical equation for the shell buckling strength under non-uniform axial compression gradient;
B. Empirical equations are obtained using three different analyses types conforming to the requirement of draft European Standard for Metal Shells (LA/LEA; GNA; GNIA; ENV 1993-1-6, 1999);

C. The notion of two different buckling modes in the local axial compression has been proved again.

Real loading in silos is different to the idealised loading used in the analyses here and it is worthwhile to interpret the above results in terms of characterising the shape of a local axial stress peak in a shell at a key point (Rotter, 1986; ENV1993-4-1).

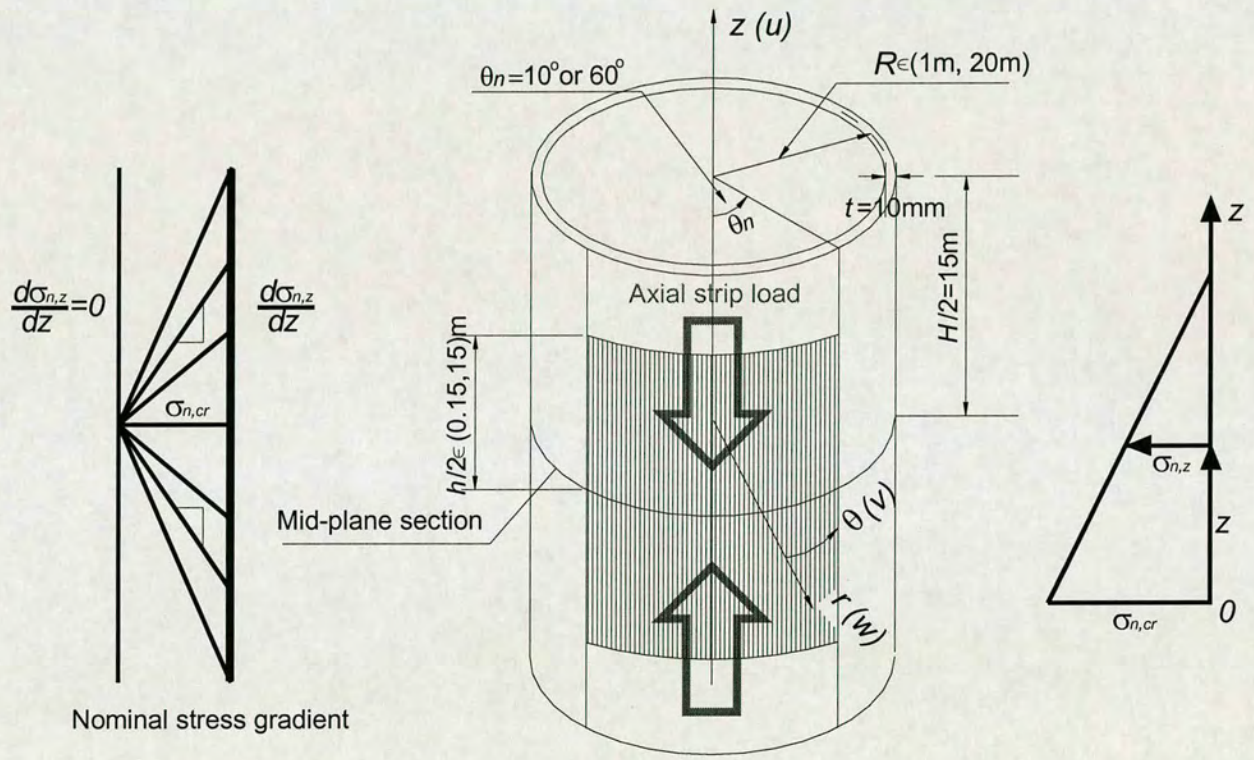

Fig. 7.1: Cylinder under local compression with varying strip load height, causing changes in the axial stress gradient at the buckle

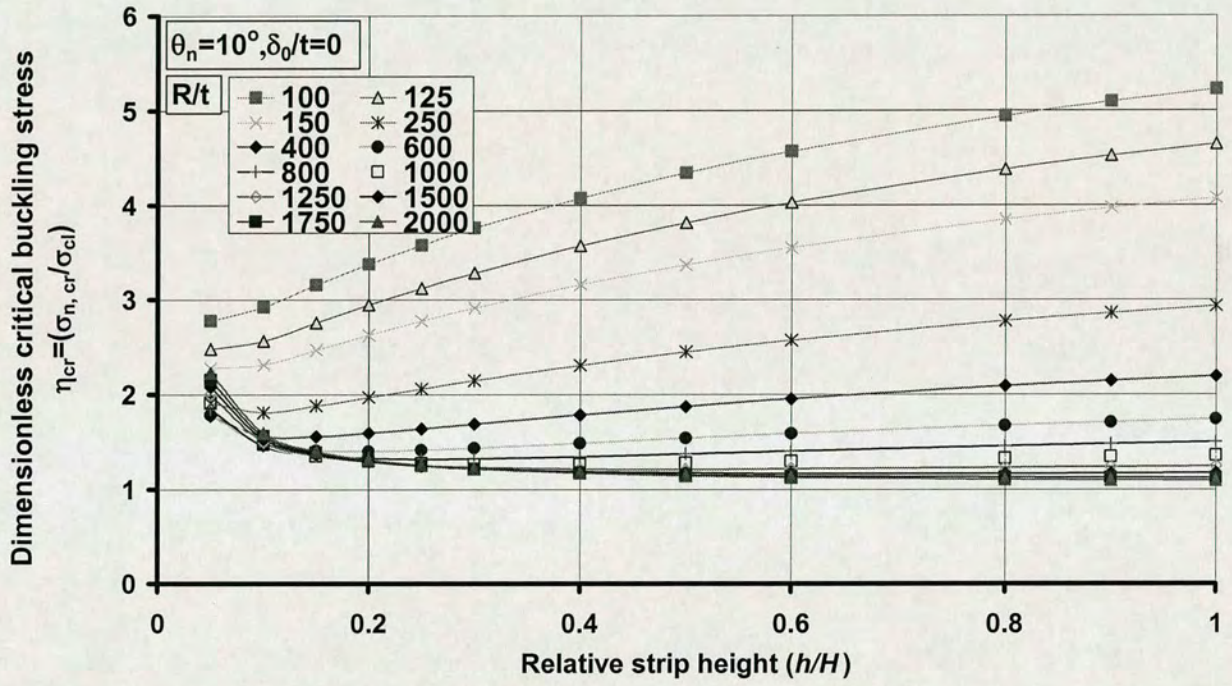

Fig. 7.2: Effect of strip load height h on the linear bifurcation buckling strength of perfect cylinders for strip angle θ_n=10° (LA/LEA, Strip centre buckles)

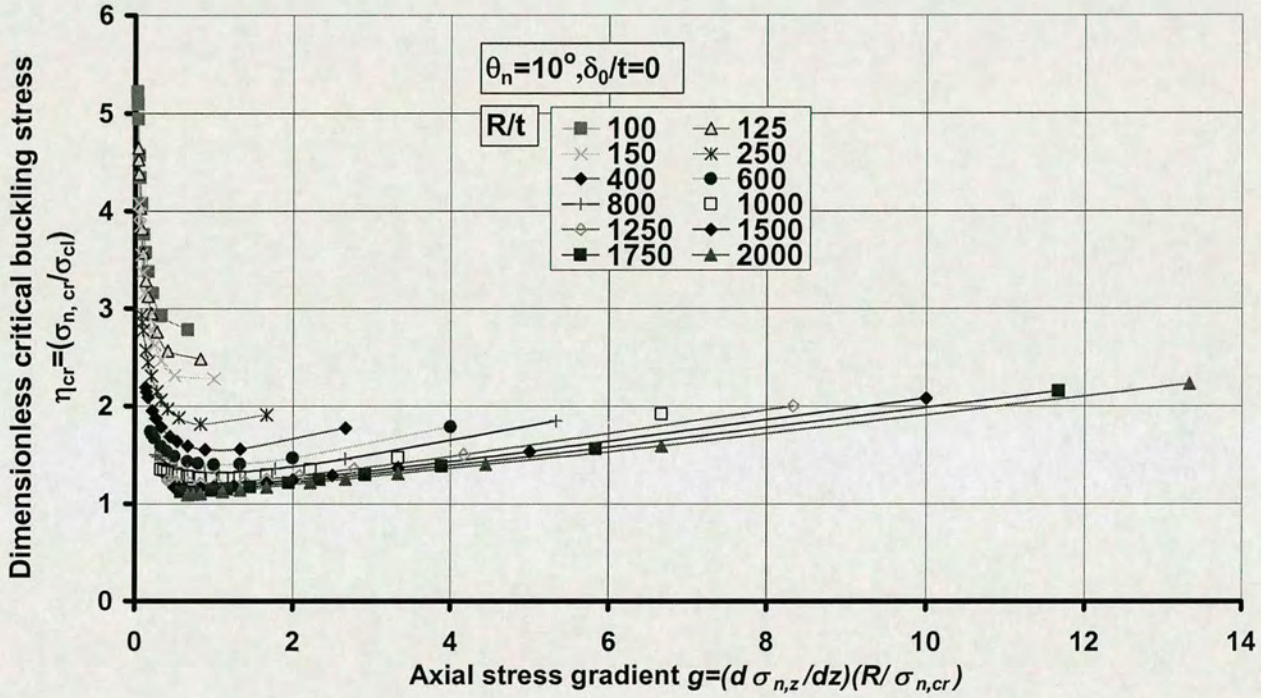

Fig. 7.3: Effect of axial stress gradient on linear buckling strength of perfect cylinders with strip centre buckles (LA/LEA)

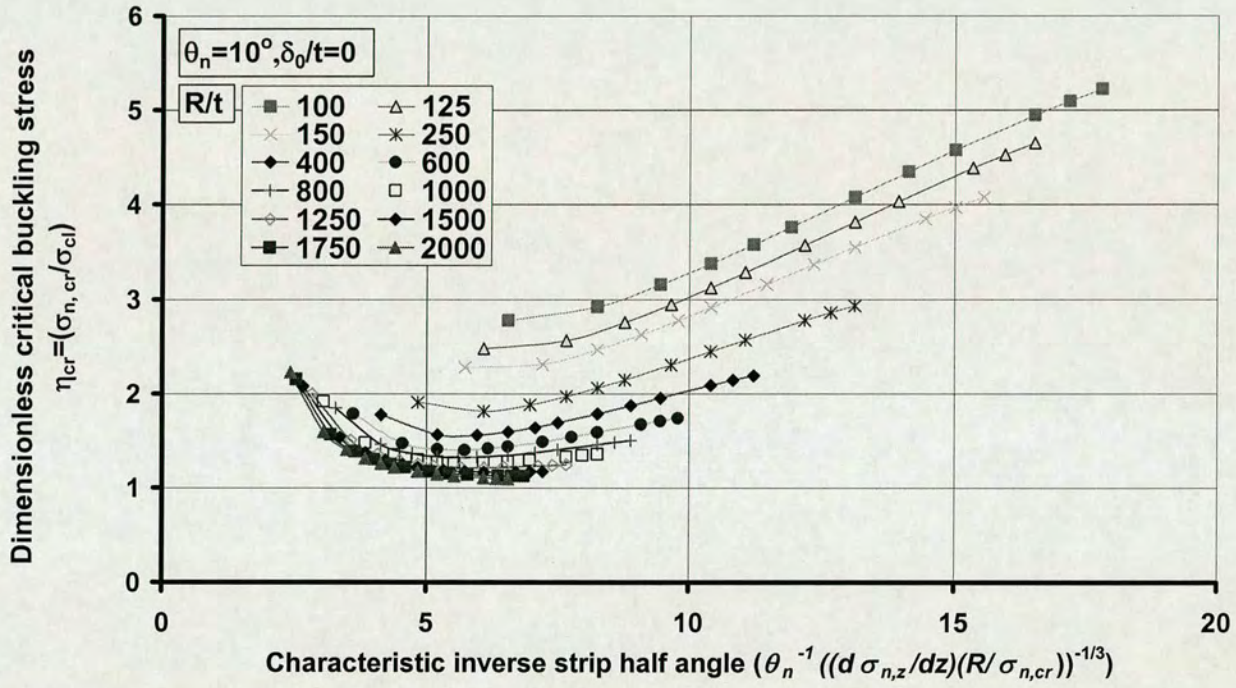

Fig. 7.4: Effect of modified inverse axial stress gradient on linear buckling strength of perfect cylinders with strip centre buckles (LA/LEA)

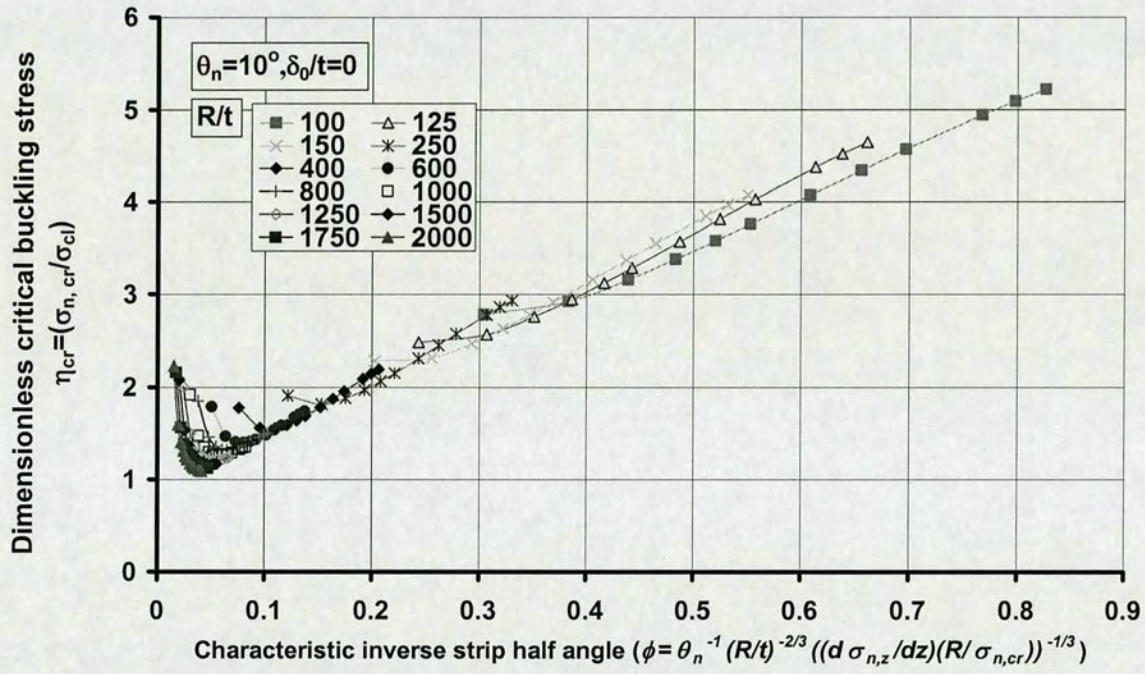

Fig. 7.5: Effect of characteristic inverse strip half angle on linear buckling strength of perfect cylinders with strip centre buckles (LA/LEA)

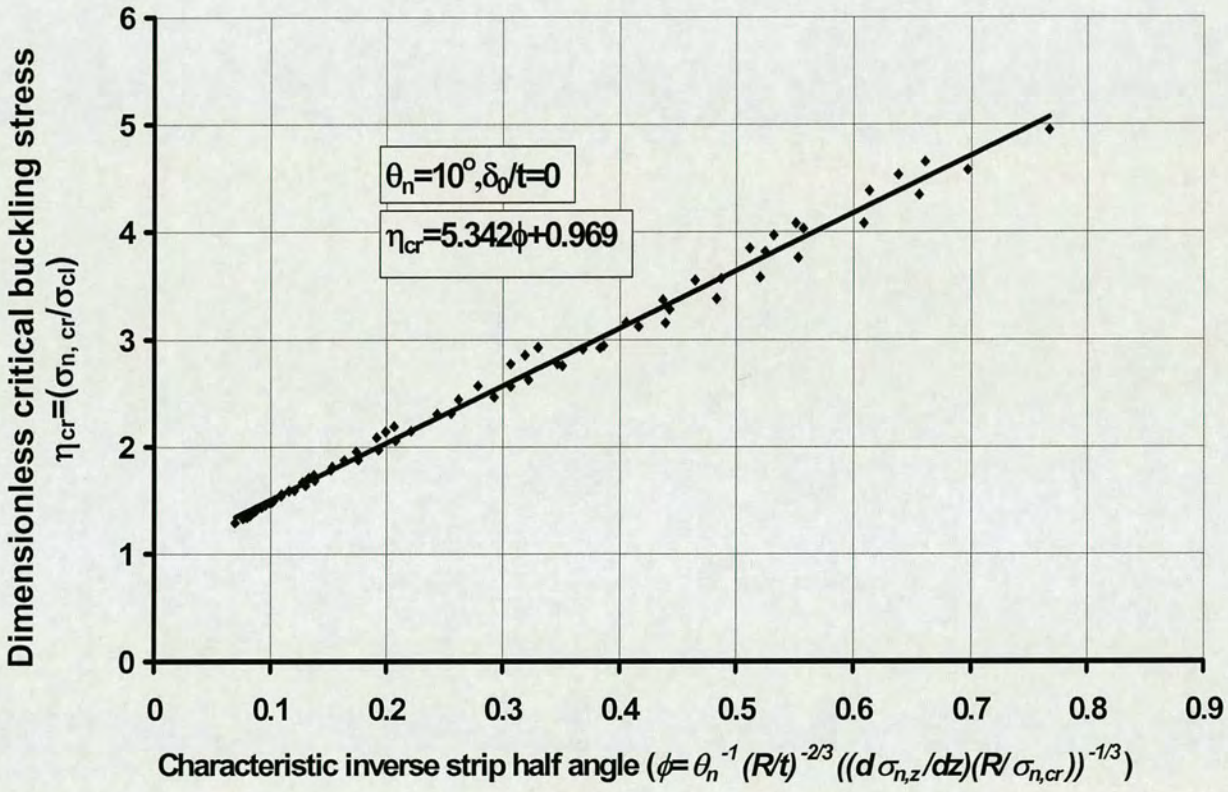

Fig. 7.6: Linear bifurcation buckling strength for all strip centre buckles (all R/t and θ_n included)

(Note: The continuous line shows the empirical fit, nodes show FE analyses results)

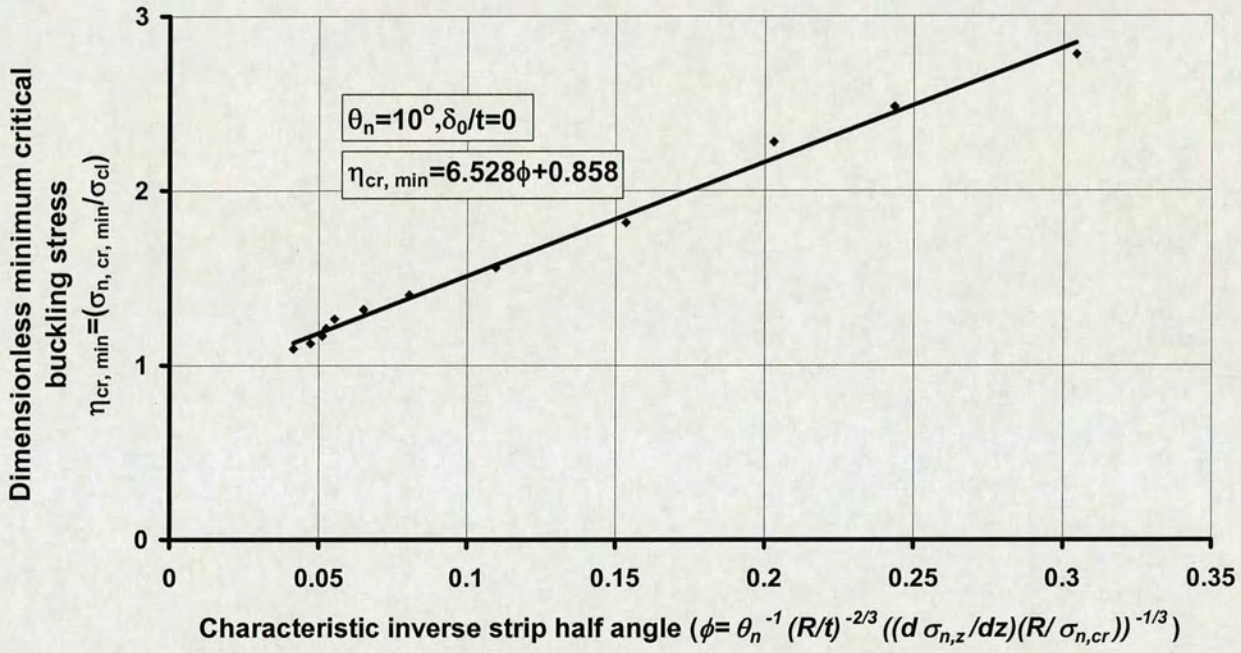

Fig. 7.7: Lowest linear buckling strength reached with strip centre buckles for each shell thickness (minimum of curves in Fig. 7.5)

(Note: The continuous line shows the empirical fit, nodes show FE analyses results)

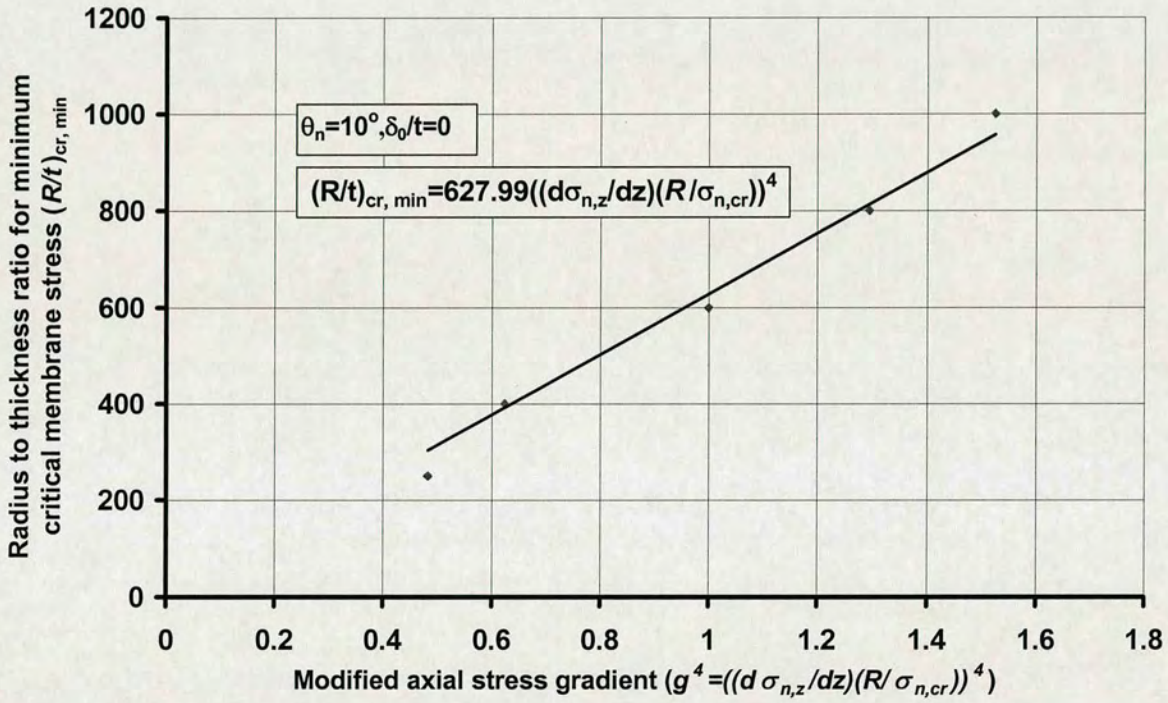

Fig. 7.8: Effect of modified axial stress gradient on the lowest buckling stress at each *R/t* (LA/LEA, Strip centre buckles)

(Note: The continuous line shows the empirical fit, nodes show FE analyses results)

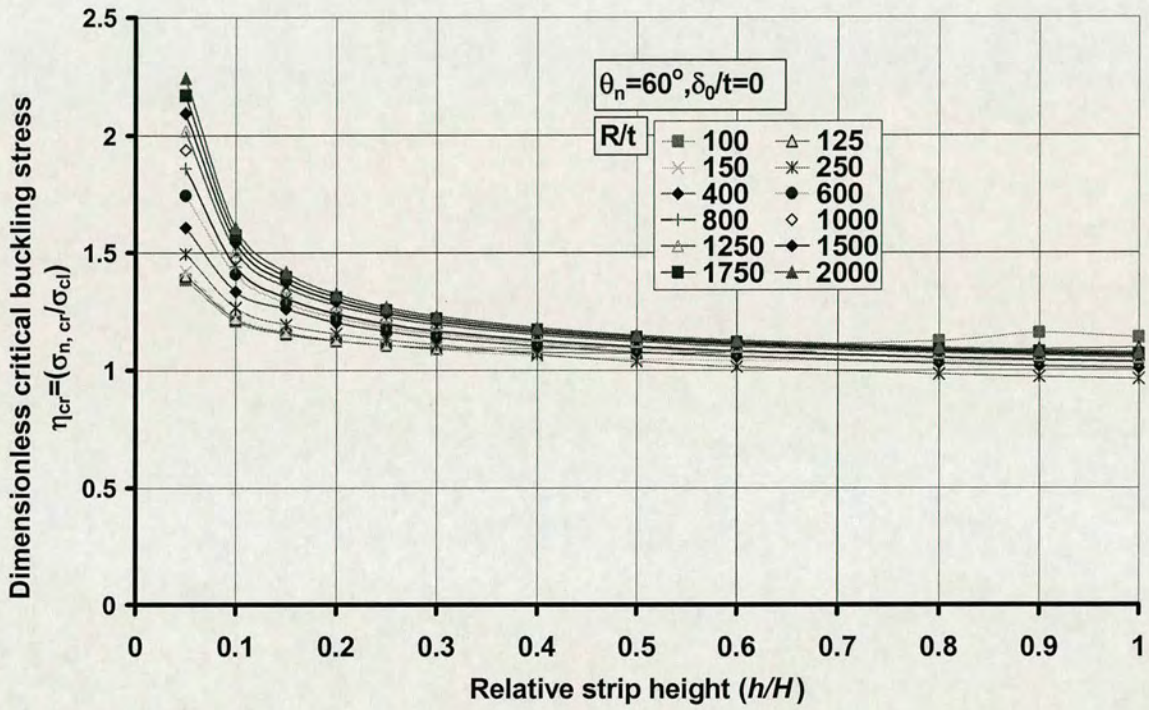

Fig. 7.9: Effect of strip load height h on the linear bifurcation buckling strength of perfect cylinders for a strip angle $\theta_n=60^o$ (LA/LEA, Strip edge buckles)

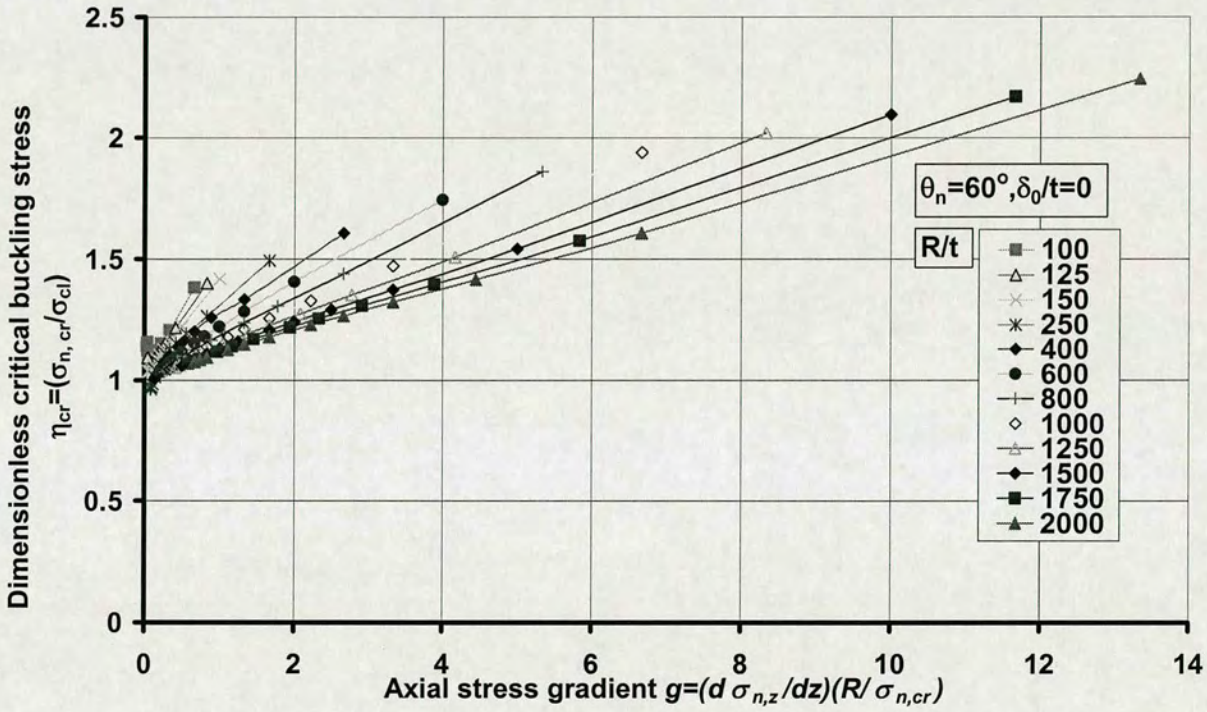

Fig. 7.10: Effect of axial stress gradient on linear buckling strength of perfect cylinders with strip edge buckles (LA/LEA)

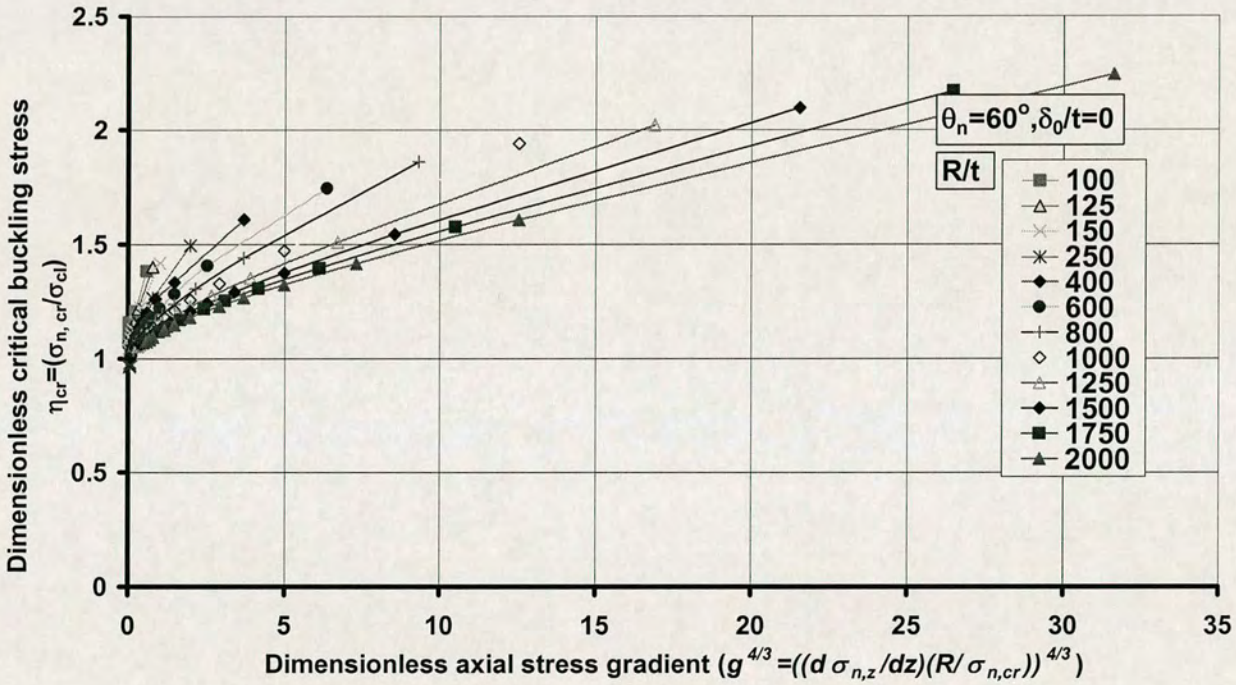

Fig. 7.11: Effect of modified axial stress gradient on linear buckling strength of perfect cylinders with strip edge buckles (LA/LEA)

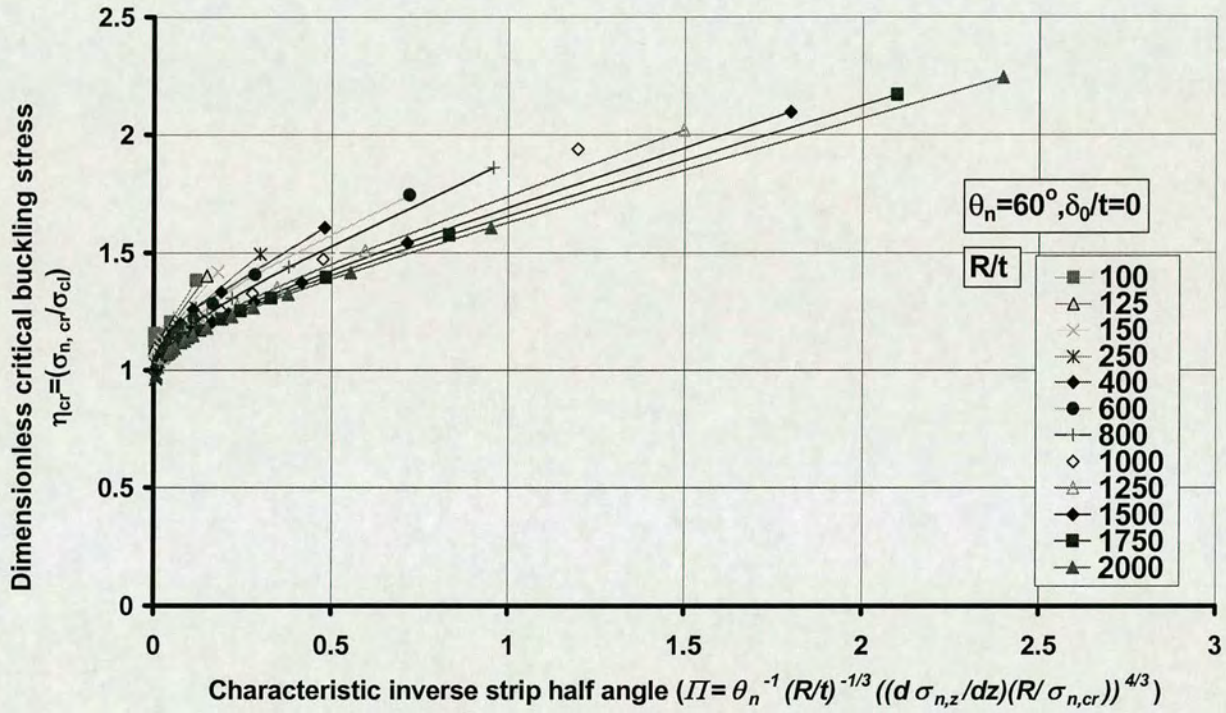

Fig. 7.12: Effect of characteristic inverse strip half angle on linear buckling strength of perfect cylinders with strip edge buckles (LA/LEA)

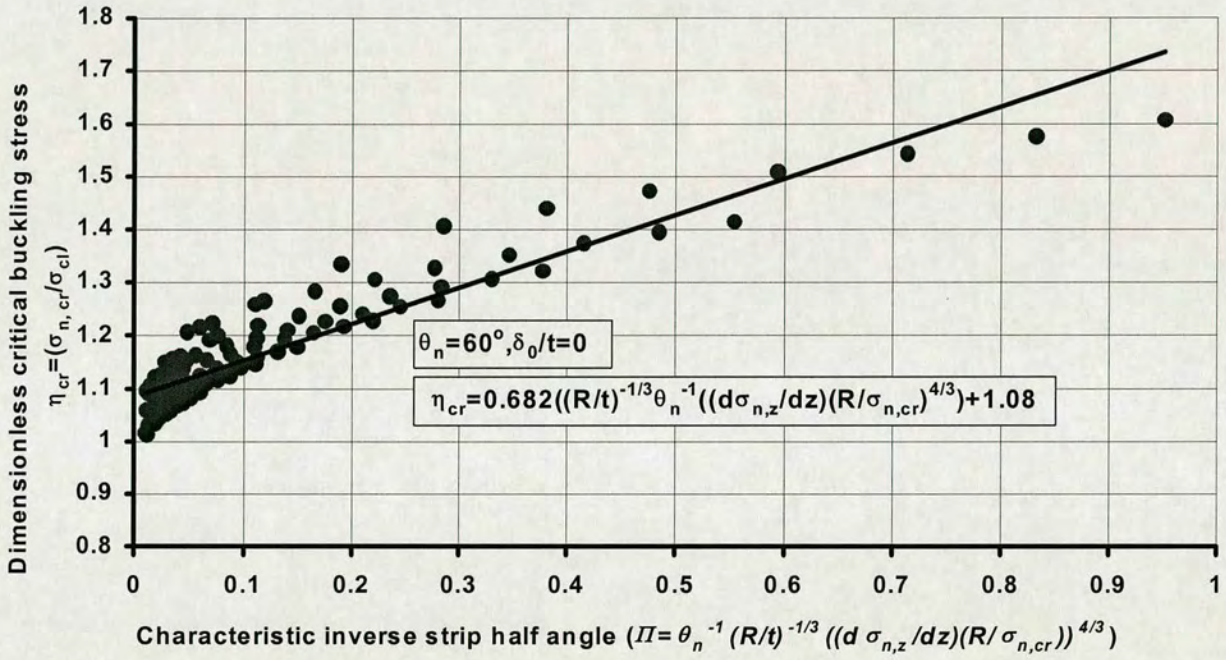

Fig. 7.13: Linear bifurcation buckling strength for all strip edge buckles (all R/t and θ_n included)

(Note: The continuous line shows the empirical fit, nodes show FE analyses results)

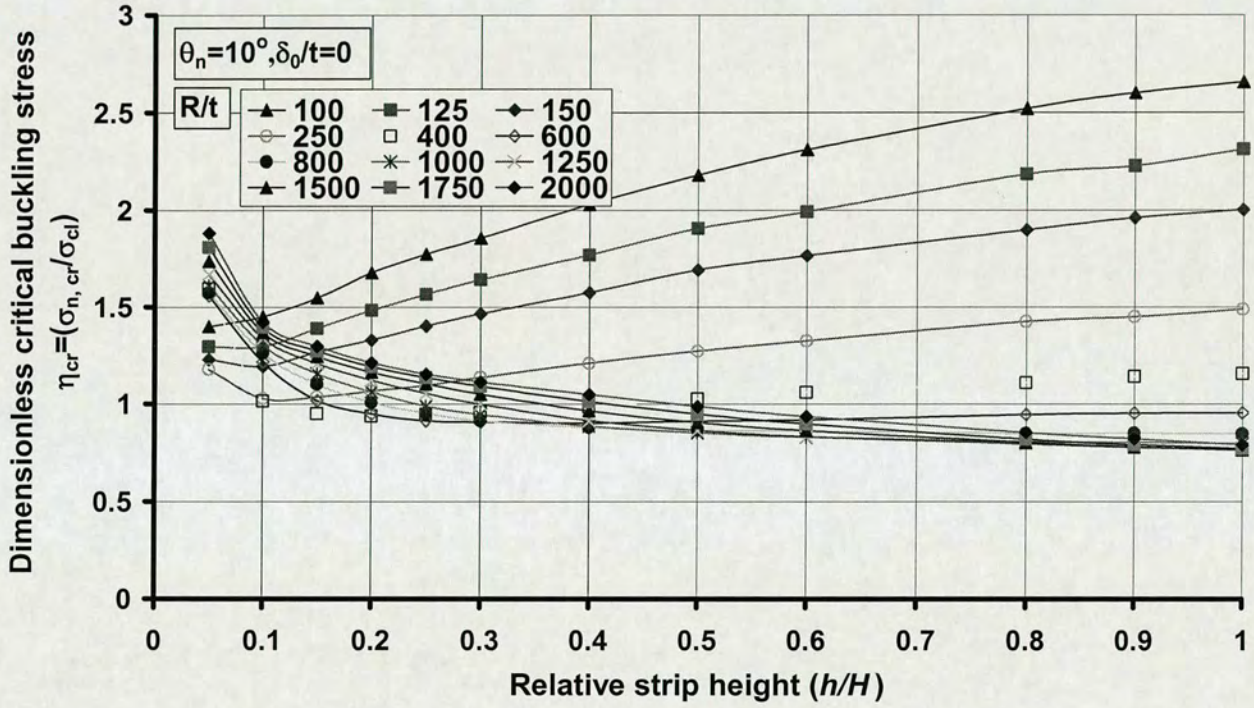

Fig. 7.14: Effect of strip load height *h* on non-linear buckling strength of perfect cylinders for a strip angle θ_n=10° (GNA, Strip centre buckles)

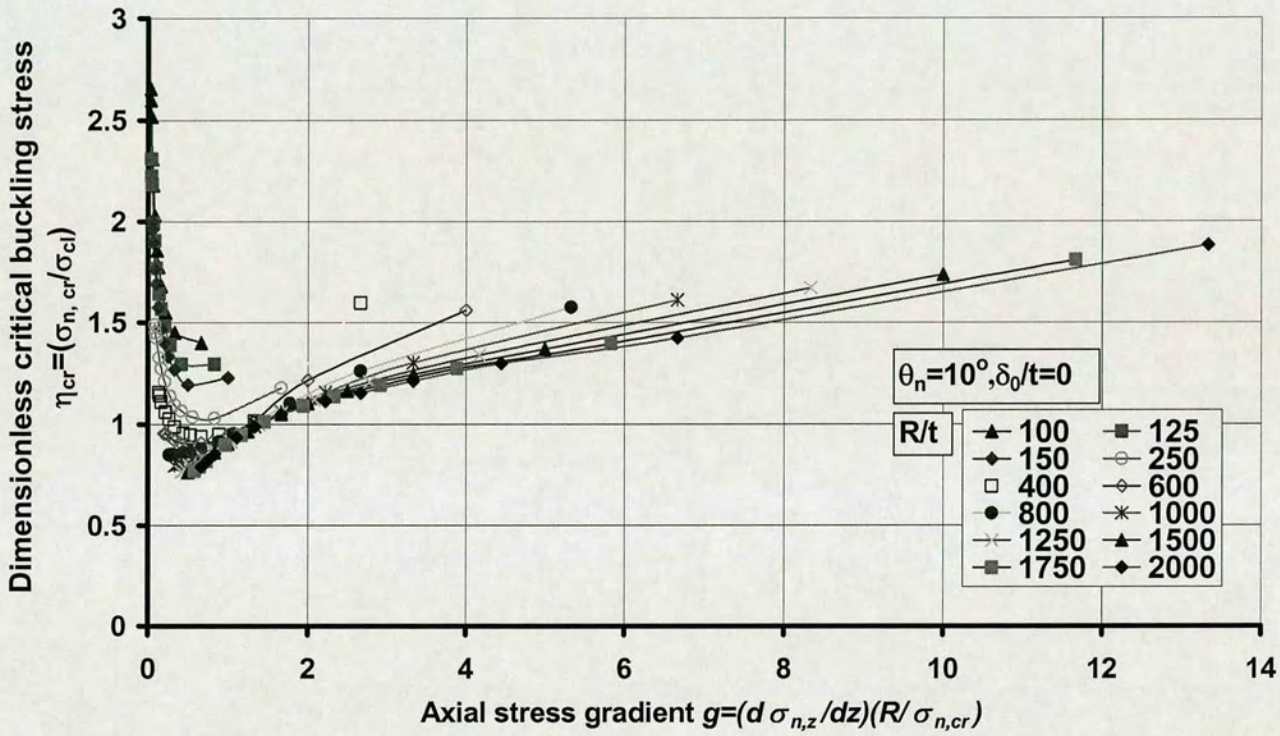

Fig. 7.15: Effect of axial stress gradient on non-linear buckling strength of perfect cylinders with strip centre buckles (GNA)

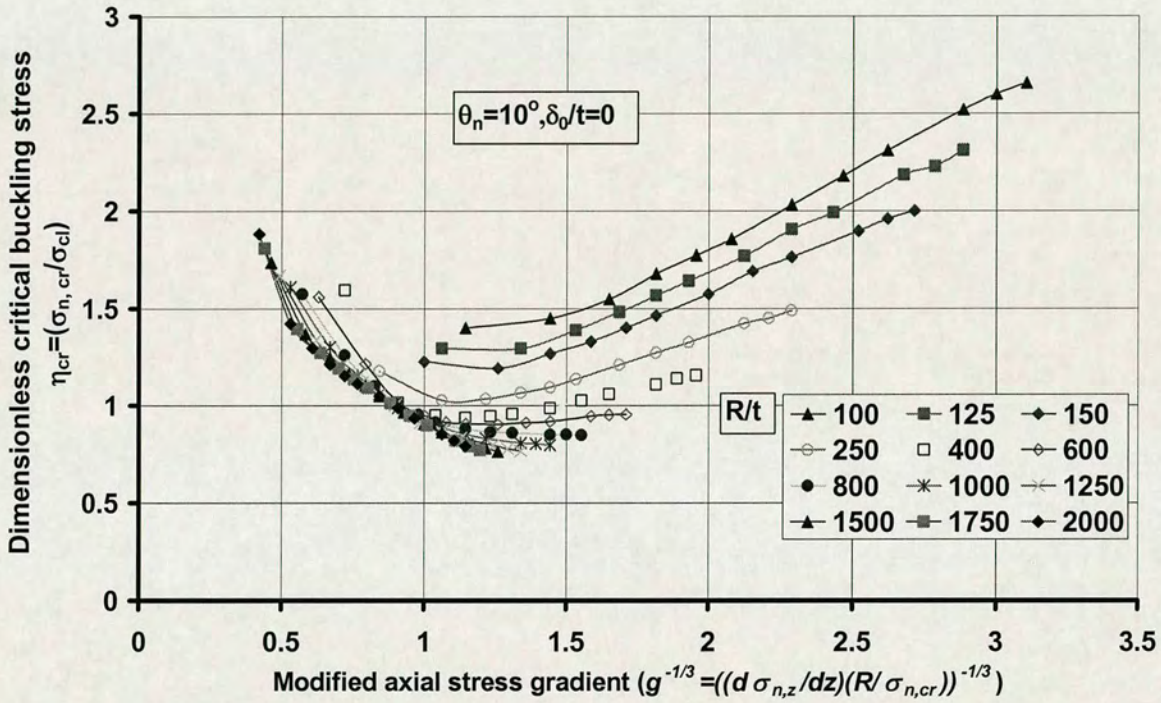

Fig. 7.16: Effect of modified inverse axial stress gradient on non-linear buckling strength of perfect cylinders with strip centre buckles (GNA)

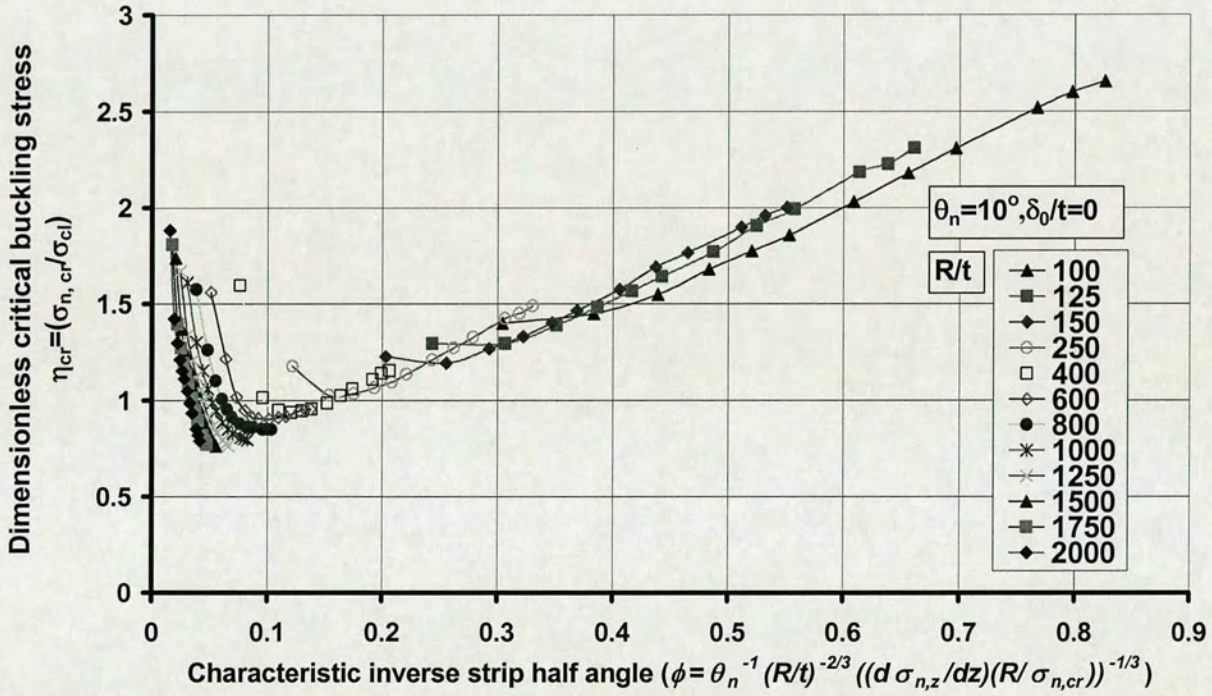

Fig. 7.17: Effect of characteristic inverse strip half angle on non-linear buckling strength of perfect cylinders with strip centre buckles (GNA)

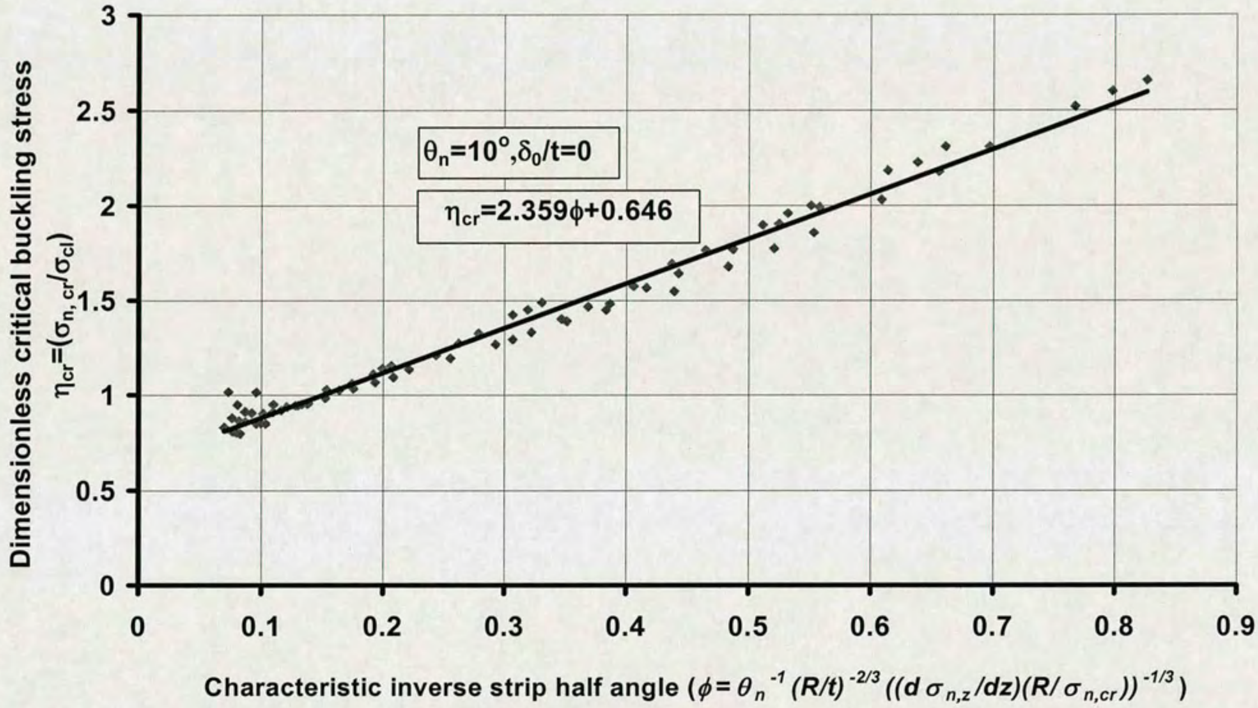

Fig. 7.18: Non-linear buckling strength for all strip centre buckles (all R/t and θ_n included)

(Note: The continuous line shows the empirical fit, nodes show FE analyses results)

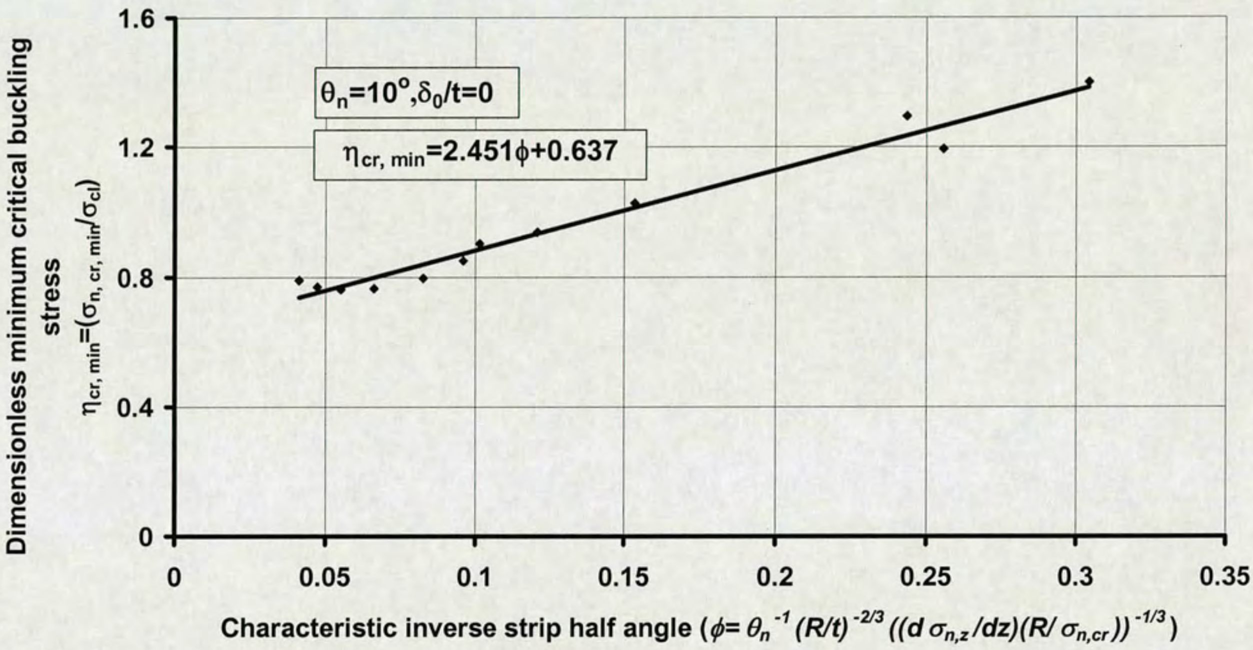

Fig. 7.19: Lowest non-linear buckling strength reached with strip centre buckles for each shell thickness (minimum of curves in Fig. 7.17)

(Note: The continuous line shows the empirical fit, nodes show FE analyses results)

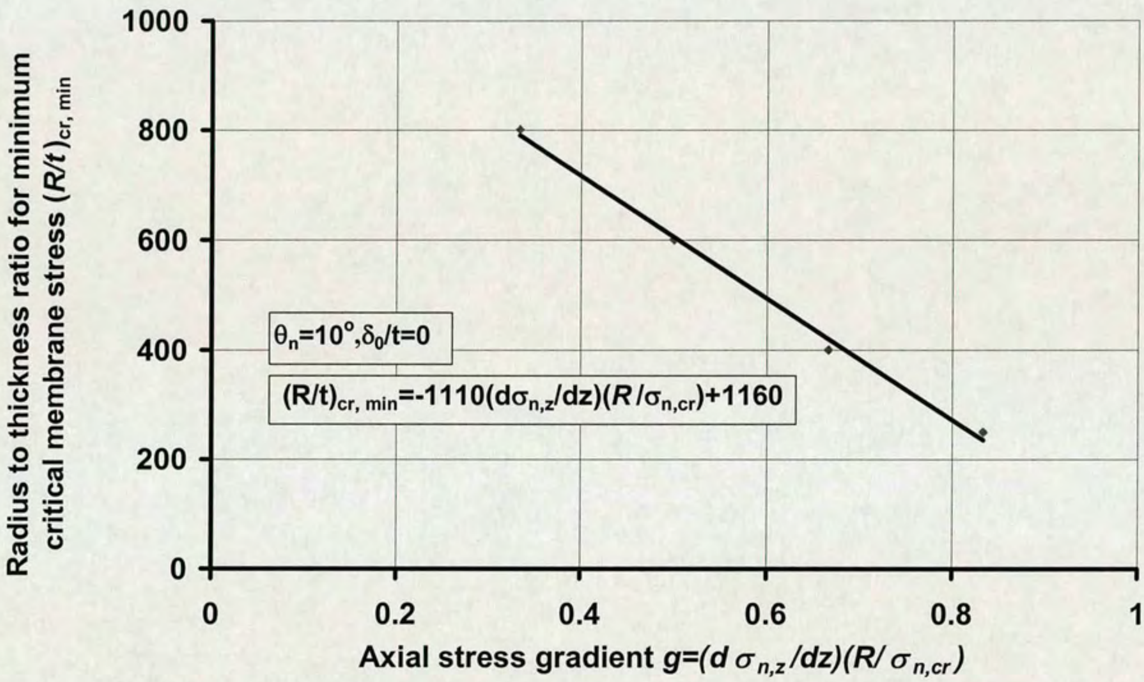

Fig. 7.20 Effect of axial stress gradient on the lowest buckling stress at each *R/t* (GNA, Strip centre buckles)

(Note: The continuous line shows the empirical fit, nodes show FE analyses results)

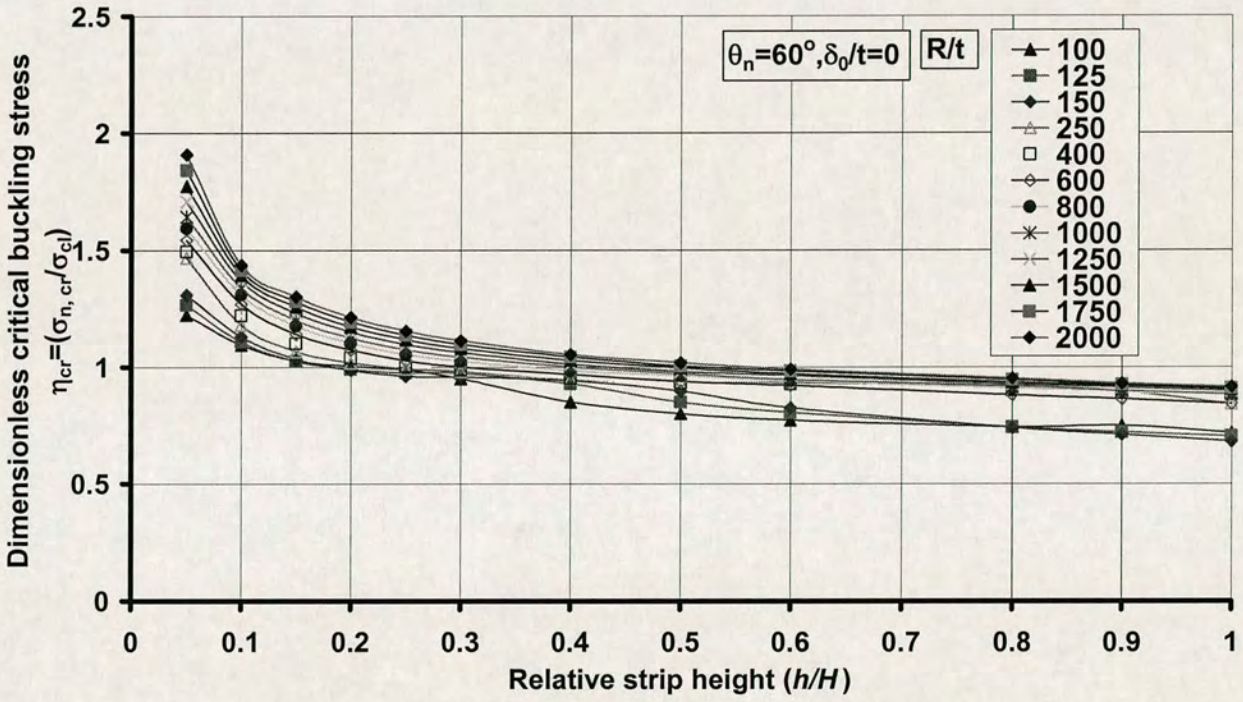

Fig. 7.21: Effect of strip load height *h* on non-linear buckling strength of perfect cylinders for a strip angle $\theta_n=60^o$ (GNA, Strip edge buckles)

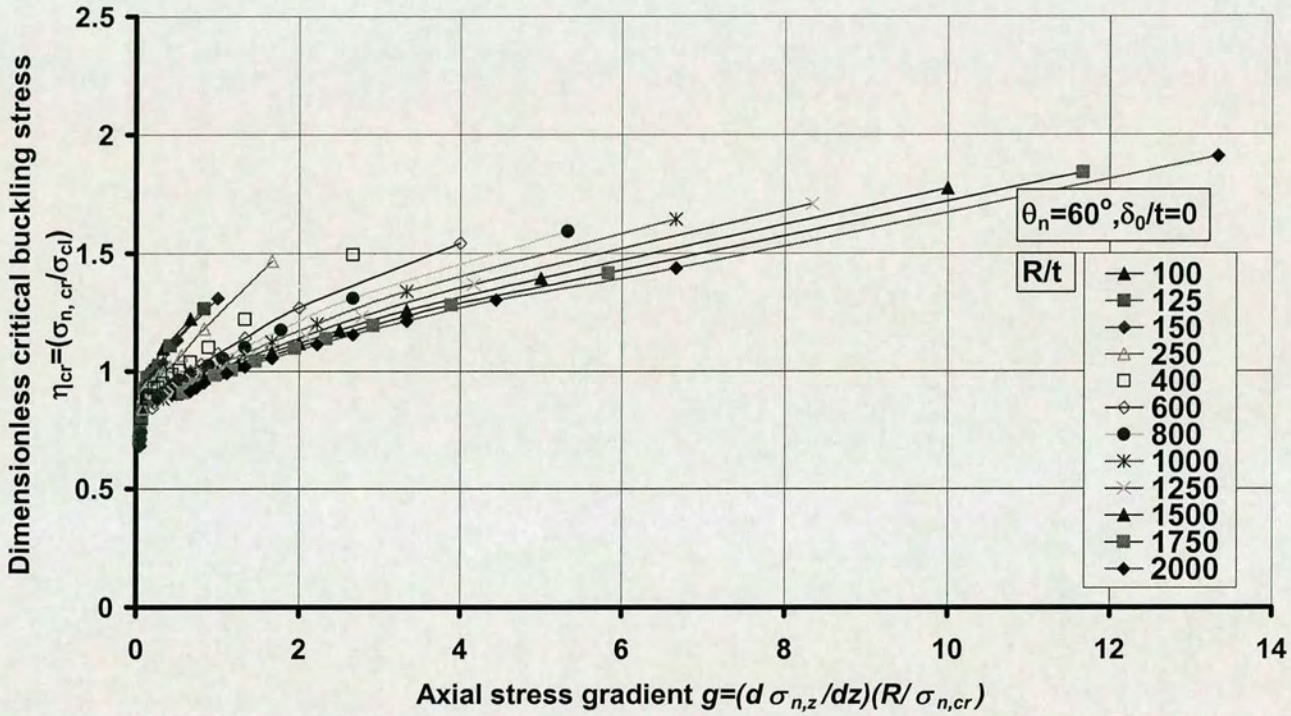

Fig. 7.22: Effect of axial stress gradient on non-linear buckling strength of perfect cylinders with strip edge buckles (GNA)

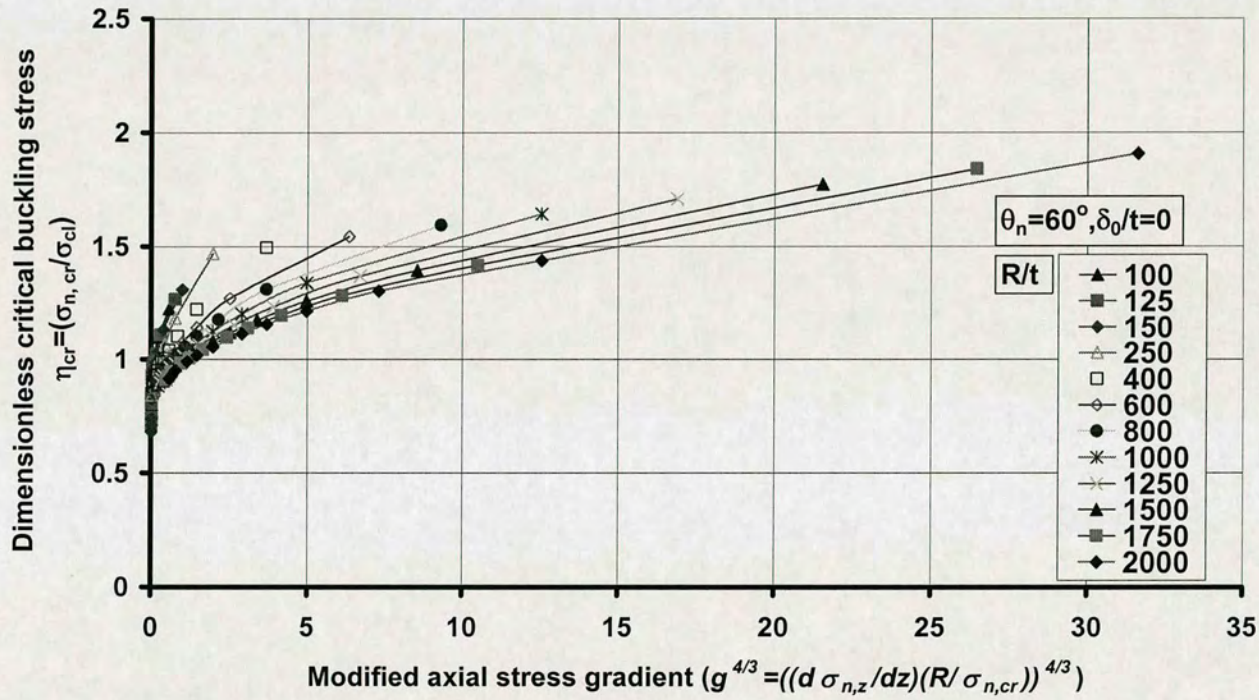

Fig. 7.23: Effect of modified axial stress gradient on non-linear buckling strength of perfect cylinders with strip edge buckles (GNA)

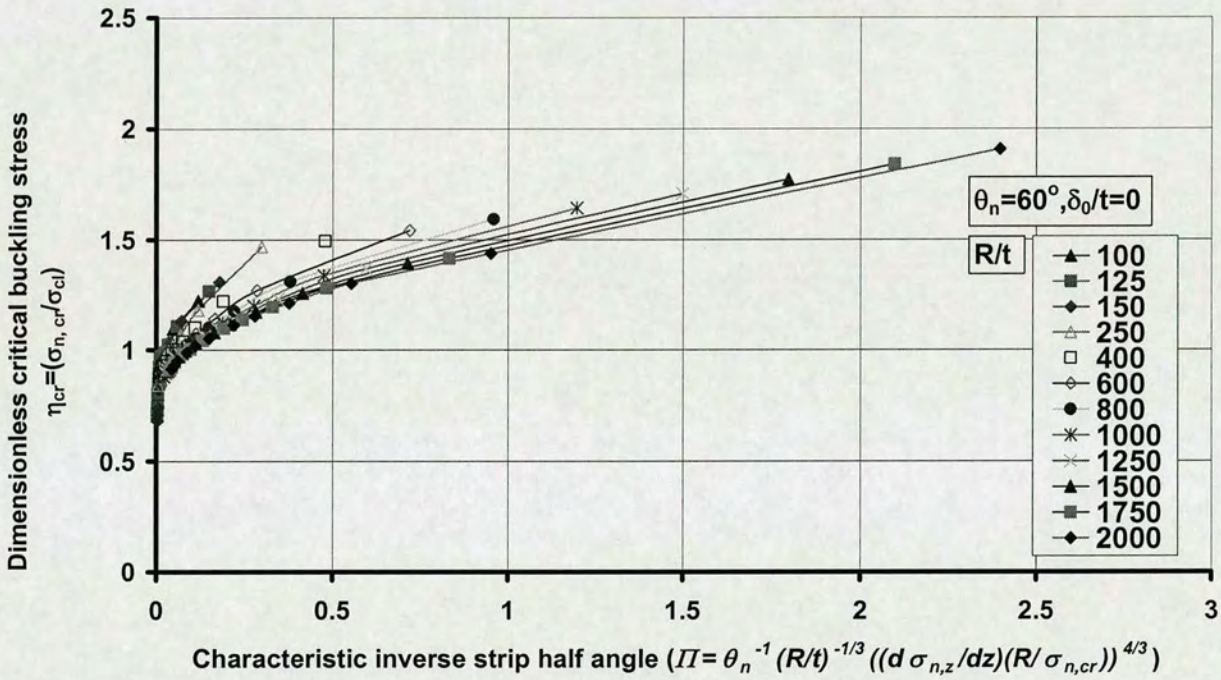

Fig. 7.24: Effect of characteristic inverse strip half angle on non-linear buckling strength of perfect cylinders with strip edge buckles (GNA)

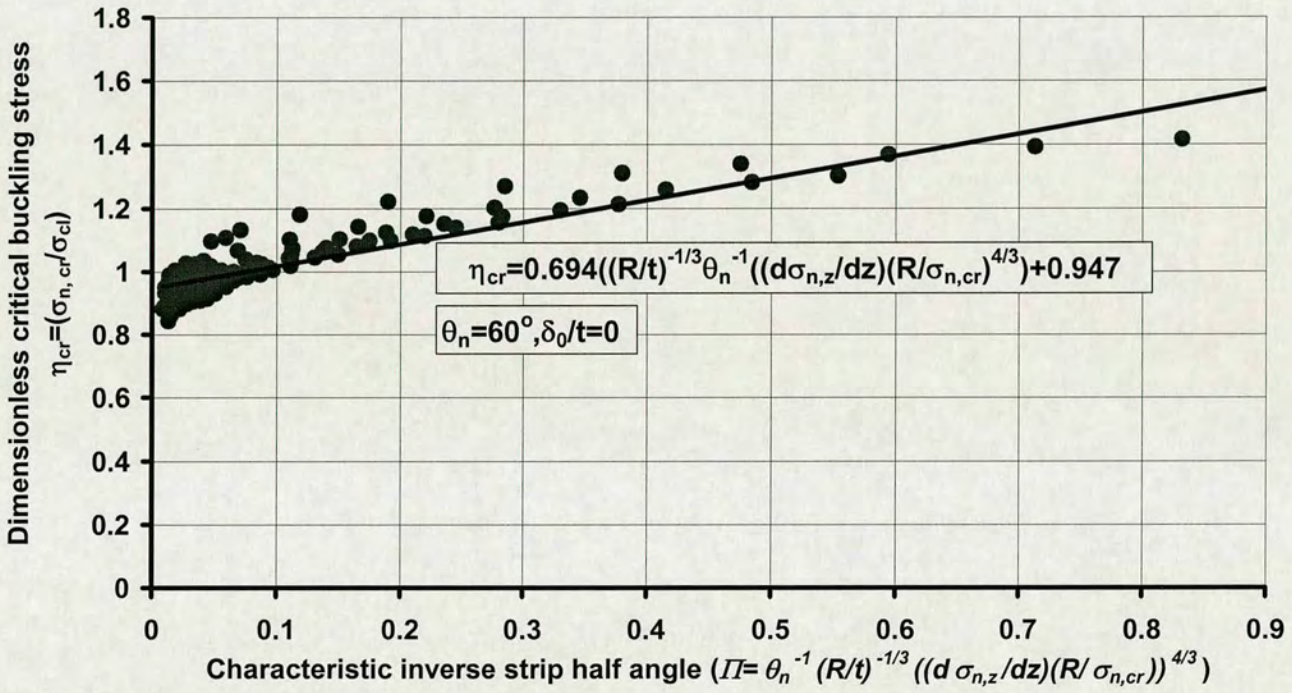

Fig. 7.25: Non-linear buckling strength for all strip edge buckles (all *R/t* and θ_n included)

(Note: The continuous line shows the empirical fit, nodes show FE analyses results)

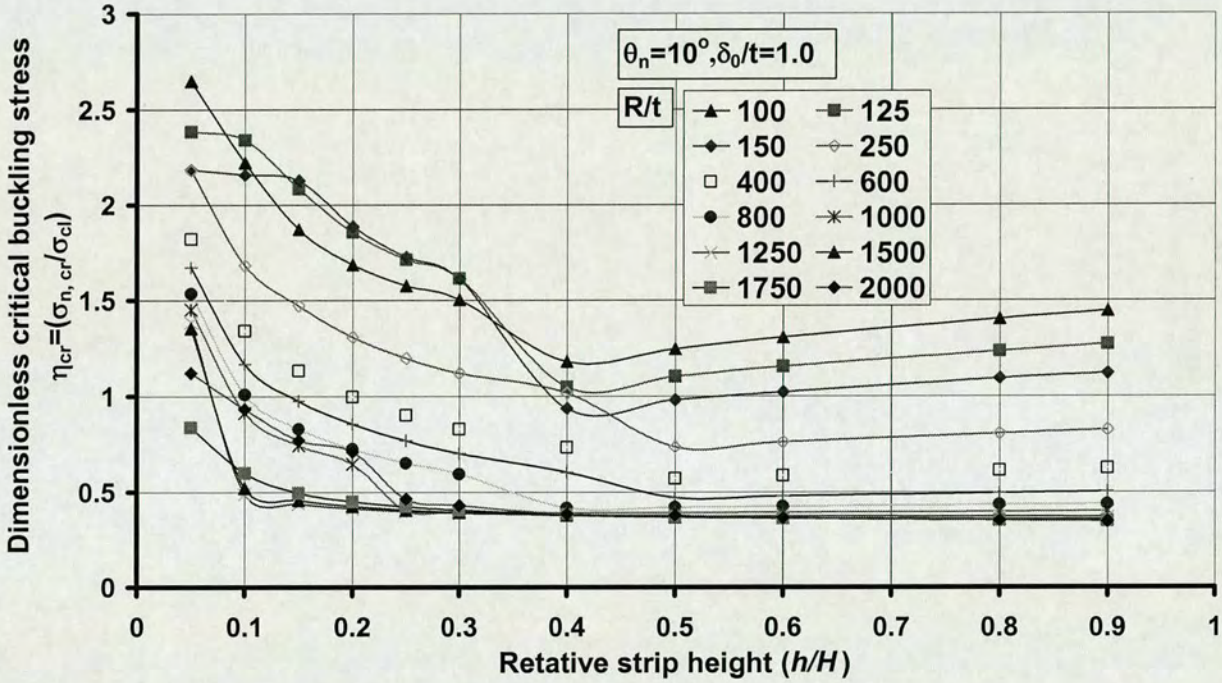

Fig. 7.26: Effect of strip load height *h* on non-linear buckling strength of imperfect cylinders for a strip angle θ_n=10° (GNIA, Strip centre buckles)

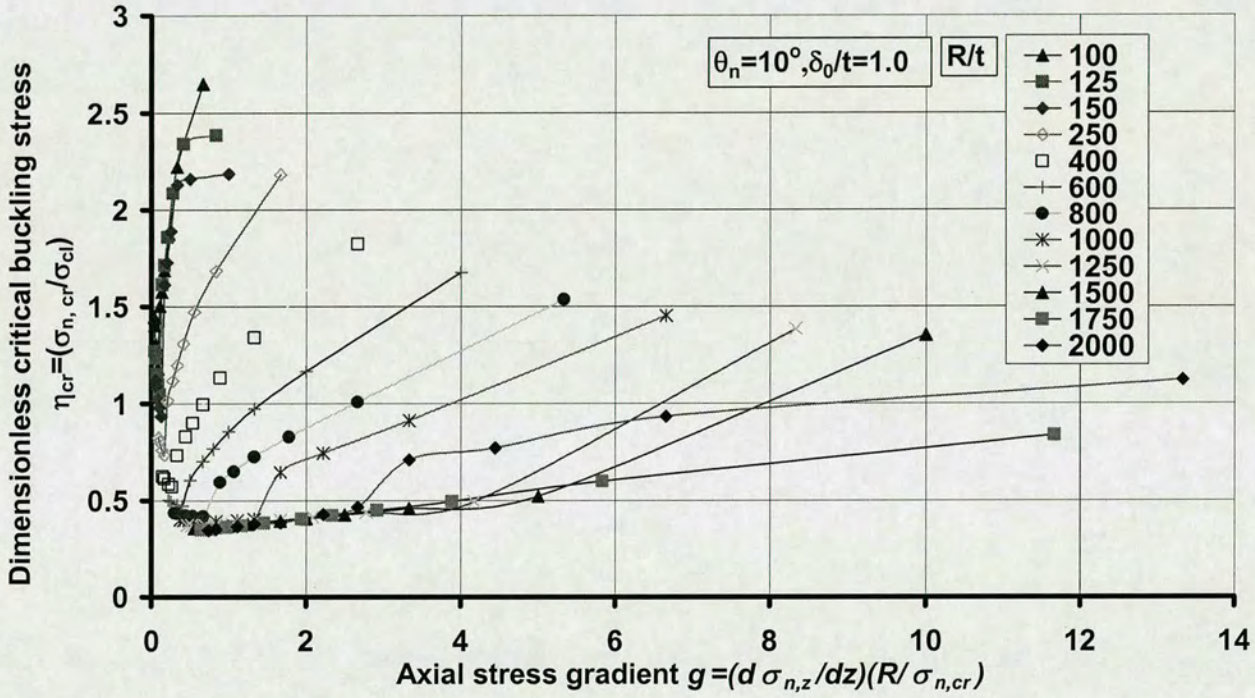

Fig. 7.27: Effect of axial stress gradient on non-linear buckling strength of imperfect cylinders with strip centre buckles (GNIA)

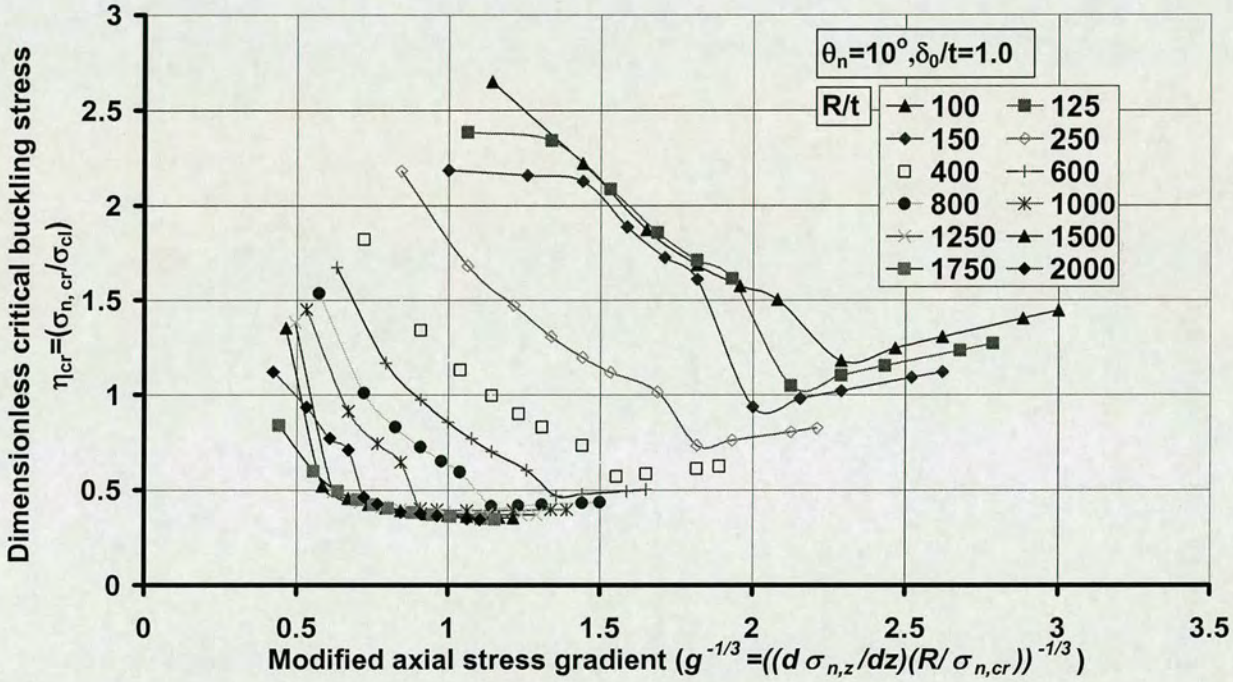

Fig. 7.28: Effect of modified inverse axial stress gradient on non-linear buckling strength of imperfect cylinders with strip centre buckles (GNIA)

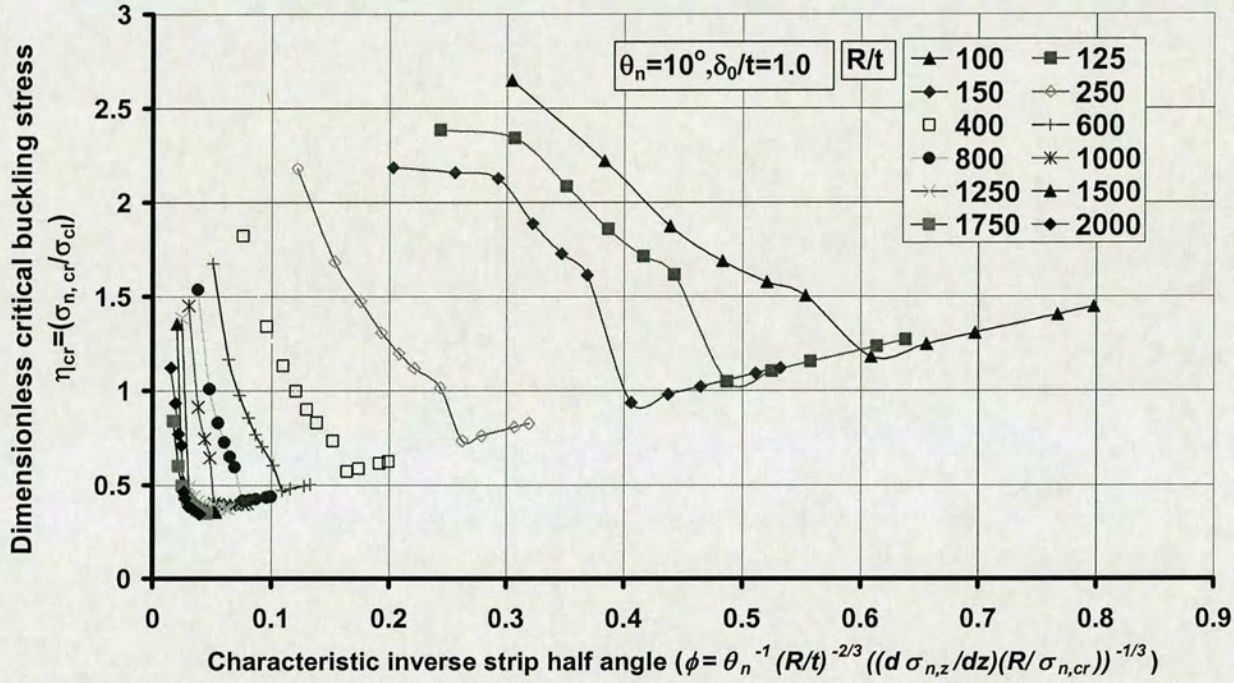

Fig. 7.29: Effect of characteristic inverse strip half angle on non-linear buckling strength of imperfect cylinders with strip centre buckles (GNIA)

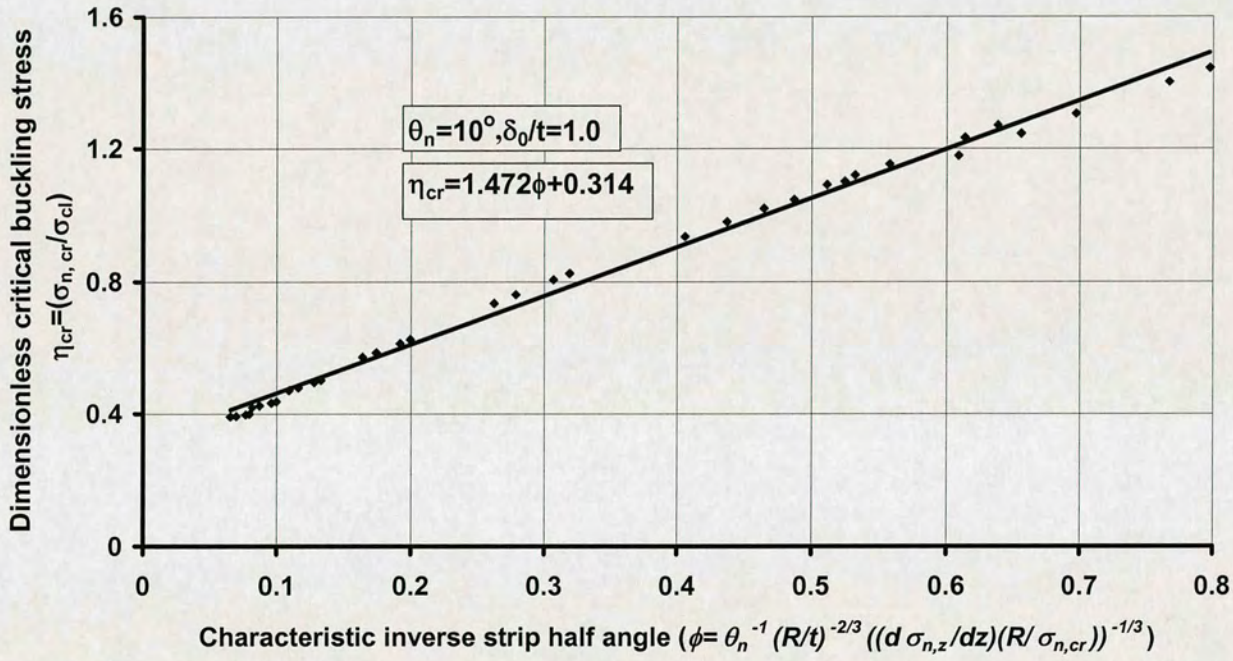

Fig. 7.30: Non-linear buckling strength of imperfect cylinders for all strip centre buckles (all *R/t* and θ_n included)

(Note: The continuous line shows the empirical fit, nodes show FE analyses results)

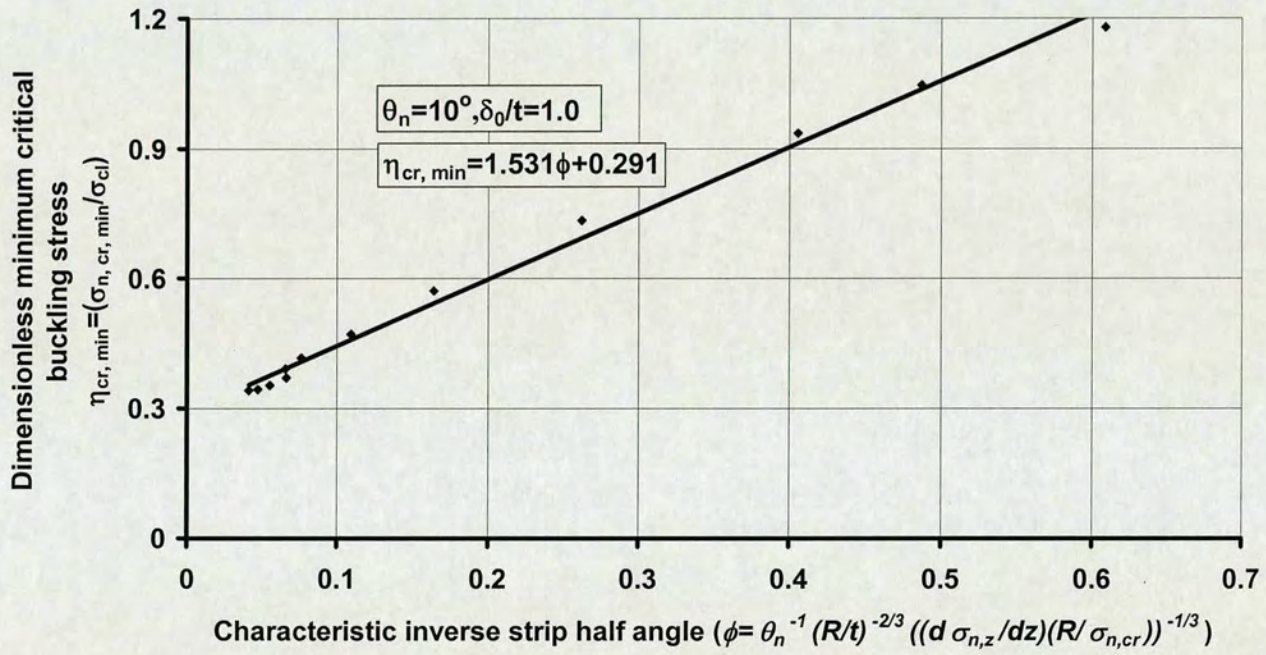

Fig. 7.31: Lowest non-linear buckling strength of imperfect cylinders reached with strip centre buckles for each shell thickness (minimum of curves in Fig. 7.29)
(Note: The continuous line shows the empirical fit, nodes show FE analyses results)

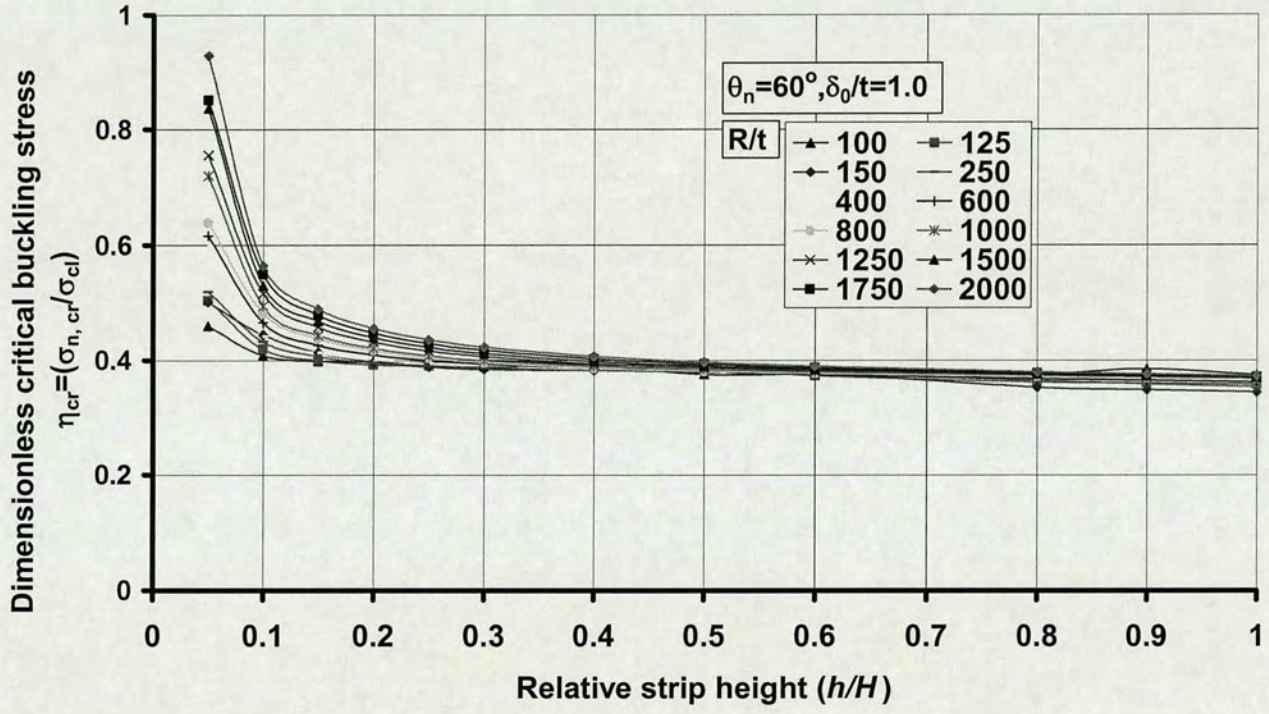

Fig. 7.32: Effect of strip load height *h* on non-linear buckling strength of imperfect cylinders for a strip angle θ_n=60° (GNIA, Strip edge buckles)

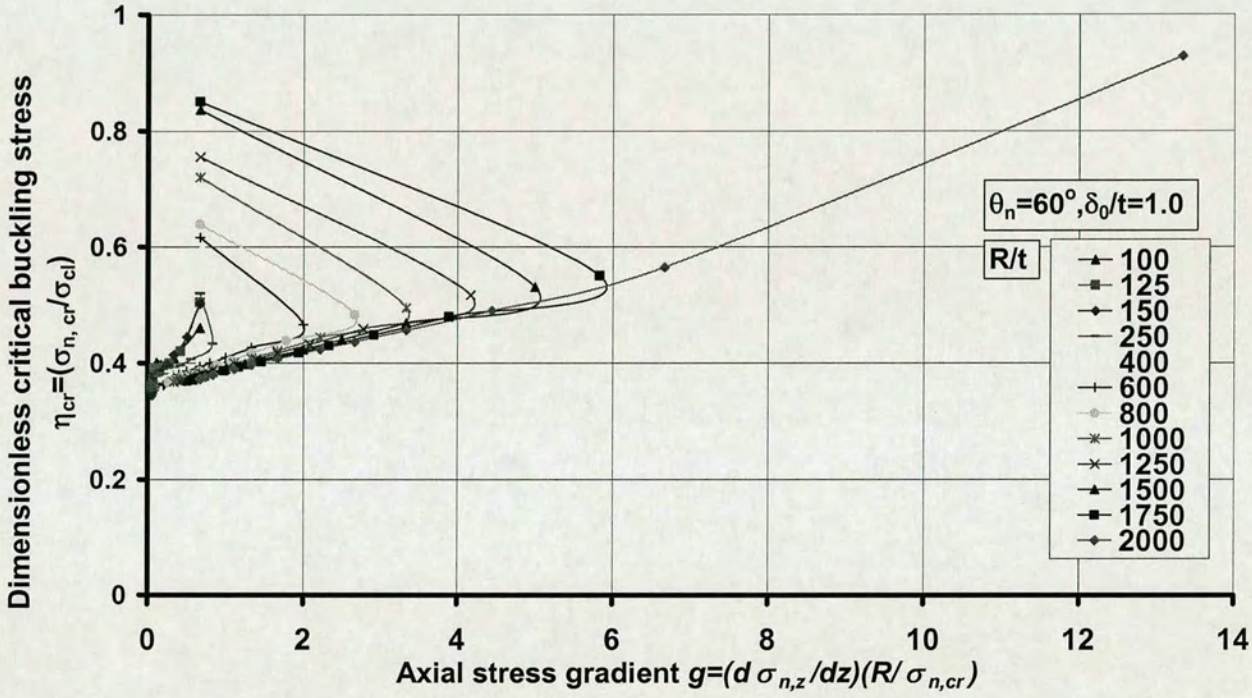

Fig. 7.33: Effect of axial stress gradient on non-linear buckling strength of imperfect cylinders with strip edge buckles (GNIA)

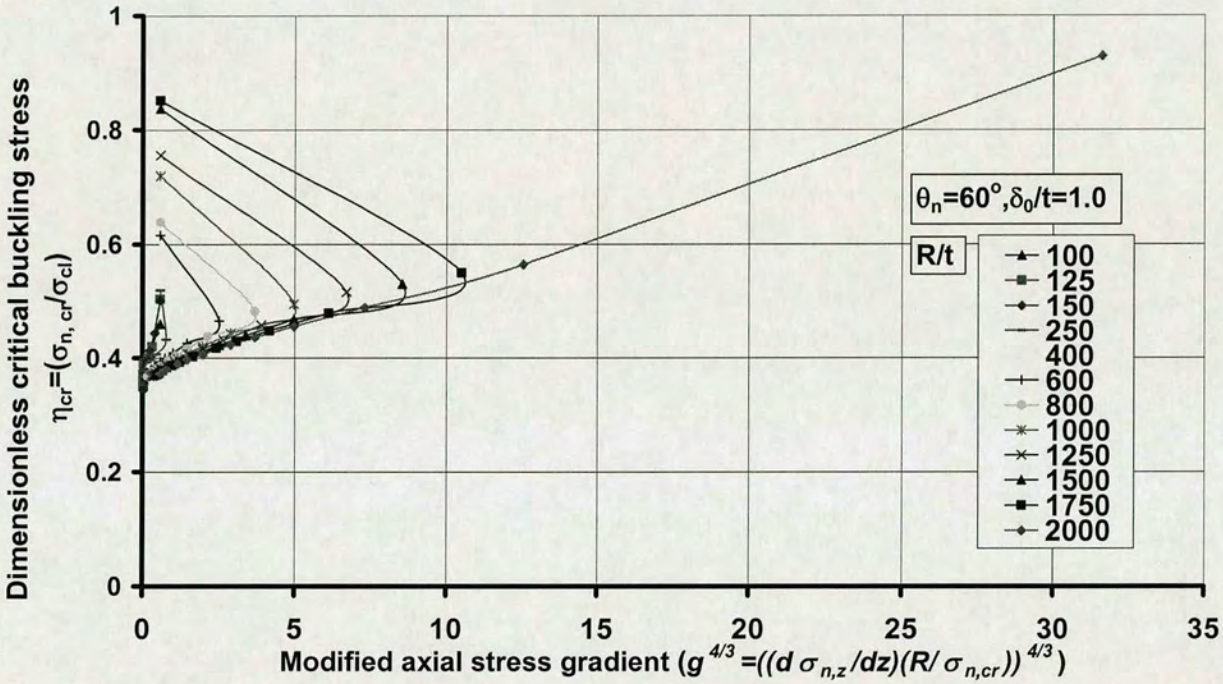

Fig. 7.34: Effect of modified axial stress gradient on non-linear buckling strength of imperfect cylinders with strip edge buckles (GNIA)

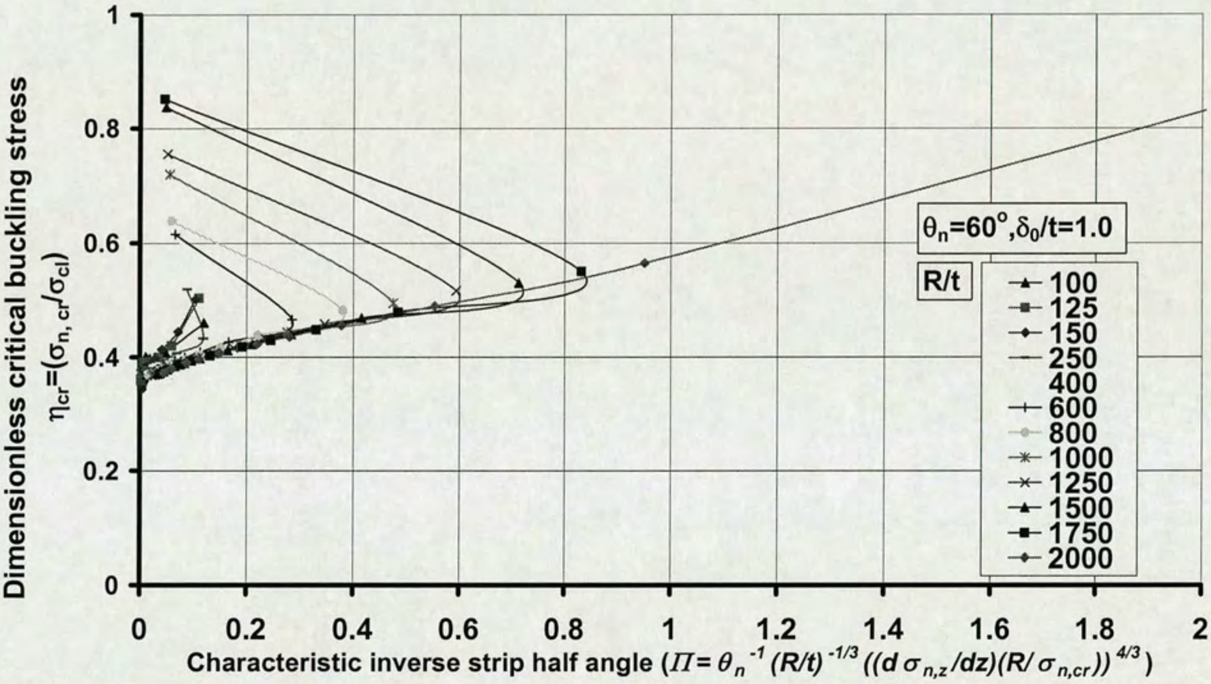

Fig. 7.35: Effect of characteristic inverse strip half angle on non-linear buckling strength of imperfect cylinders with strip edge buckles (GNIA)

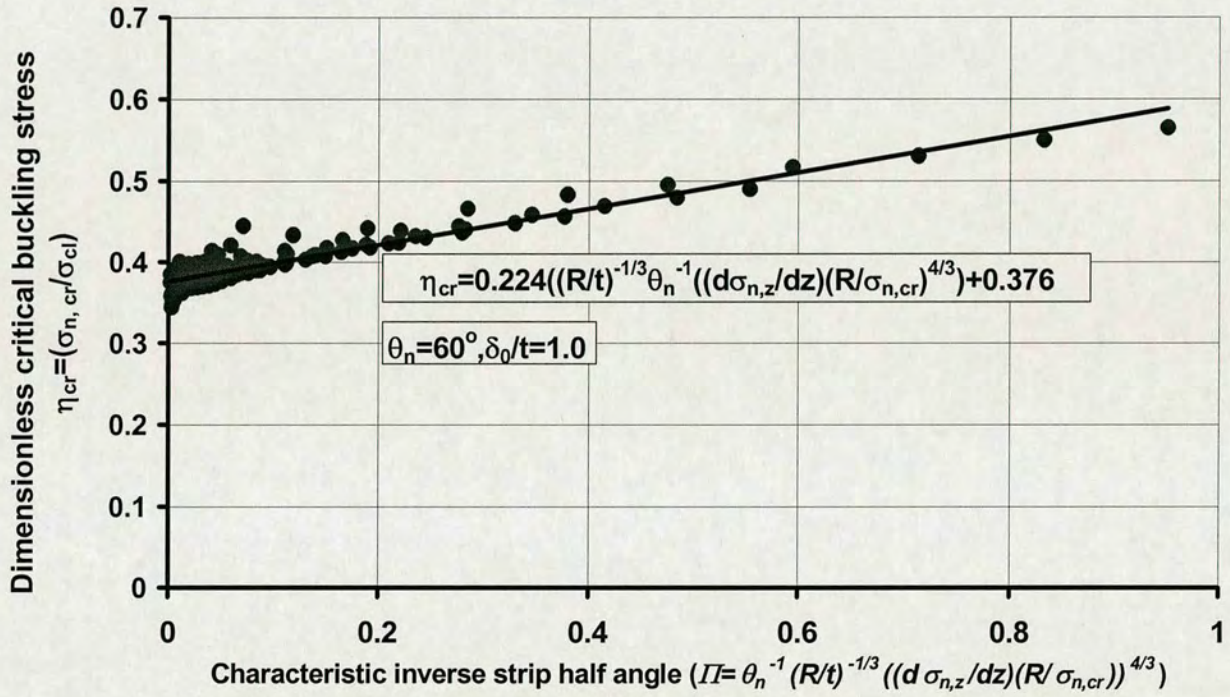

Fig. 7.36: Non-linear buckling strength of imperfect cylinders for strip edge buckles (all *R/t* and θ_n included)

(Note: The continuous line shows the empirical fit, nodes show FE analyses results)

Chapter 8

CHARACTERISATION OF THE STRESS PATTERN AROUND THE CIRCUMFERENCE

8.1 Introduction

Real loading in silos is different to the stylised loading used in all analyses of the parametric studies presented in this thesis (Chapters 5, 6 & 7) and it is important to be able to interpret the above results in terms of characterising the shape of a local axial stress peak around the circumference at a key point. The only known method of characterising local stress distributions for this propose is the stress localisation parameter proposed by Rotter (1986; 2001) and it was adopted into the European standard (ENV 1993-4-1, 1999). For the specialisation of the load cases in all above analyses, only the circumference at the mid plane of the shell was taken into account.

8.2 Model

The finite element model, load cases and co-ordinate system descriptions have all been described in the previous chapters. Again, the commercial finite-element analysis package ABAQUS (HKS, 1998) was chosen for this analysis. The aim of this chapter is to permit the buckling analyses of previous chapters, which were based on nonlinear and eigenvalue analyses, to be exploited in designs which use only linear analyses. It is therefore the linear stress distribution, which will be characterised in this chapter.

8.3 Membrane Stress Distribution around the Circumference under Local Compression

8.3.1 Introduction

Local high axial compressive stresses certainly can cause buckling failures. However, to assess the effects of general loads, it is necessary to relate the stresses they cause to the idealised stylised load from which the buckling strength has been found in order to find a possible new approach to this failure criterion (Rotter, 1986).

First, in order to know the membrane stress distribution in the shell, LA results have been used.

For the idealised loading used in this thesis, the peak axial membrane stress usually lies in the zone where the strip load is applied. This observation works in concert with the previous chapters for all conditions before post-buckling, and it is valid for the full parameter range (R/t=(100,1,000), θ_n=(1°, 90°)) that has been analysed. Two diagrams (Figs. 8.1 & 8.2) below show the axial membrane stress distribution on meridional and circumferential lines, which led to the same conclusion as above (Fig. 8.3). The definition of all the meridional and circumferential lines used here and hereafter is shown in Fig. 8.3.

From all the buckling modes shown above, it is important to assess the probable buckling strength of cylinders subject to stresses like those in Fig. 8.4. The only practical way currently known of describing this is to find a localisation parameter (Rotter, 1986) and this method is adopted in the corresponding part of the current code (ENV 1993-4-1, 1999). In the zone of high axial stress, the shape of the stress peak is characterised by the localisation parameter n, which is defined in the Eqn. (8.1).

$$n = \frac{\cos^{-1} a}{\theta_1} \tag{8.1}$$

where a and θ_1 are in radians.

The parameter that Rotter (1986) devised is generally useful, but the stress level at which a shell might buckle for a given value of n remained unknown. To address this difficulty, Rotter originally proposed this parameter n, could be introduced into a modification of Koiter's relation as (Eqn. (8.2), Koiter, 1945):

$$\sigma_0 = \sigma_{cl}\{1 - 1.239\left|\frac{\delta}{t}\right|[\sqrt{1 + \frac{2}{1.239}\left|\frac{t}{\delta}\right|} - 1]\} \tag{8.2}$$

where Rotter defined the parameters as:

$$\frac{\delta}{t}=\frac{0.06}{q}f\sqrt{\frac{R}{t}} \qquad f=\frac{1-b_1 n}{1+b_2 n}$$
$$b_1=0.5\sqrt{\frac{t}{R}} \qquad b_2=\frac{3-5b_1}{2} \tag{8.3}$$

Following the same idea, a similar conclusion can be drawn here from FE results (Stress Distribution TYPE I in Fig. 8.5a). In addition, a new stress pattern, which is different from the first, is shown as Stress Distribution TYPE II in Fig. 8.5b. This can be easily understood if the high axial membrane stress extends over a larger part of the circumference. It is similar to the division between strip centre buckles and strip edge buckles from the previous chapters but not identical.

8.3.2 Classification of Two Types

Schematic drawings of these two types of stress distribution are shown in Fig. 8.5: TYPE I shows that a stress distribution reaches its peak membrane stress around the circumference on the symmetry line of the meridian (centre of strip load). TYPE II shows that a stress distribution reaches its peak axial membrane stress around the circumference at a position that is not on the symmetry line of the applied loading (as θ_i represented). This distribution relates to the different buckling modes described before: TYPE I generally leads to strip centre buckles and TYPE II generally causes strip edge buckles. However, the location of the peak stress is not a perfect identifier of the buckling mode.

As a result, there is a need to distinguish these two types of stress distribution in order to find the appropriate methods of treating them correspondingly. With the analyses results from the parametric study, the change of two types between $100 \le R/t \le 1000$ for all strip width was investigated. The effect of R/t ratio is plotted with the changing angle between these two types in Fig. 8.6 and Eqn. (8.4) are found in the following for this purpose:

$$\theta_{cr} = 64(\frac{R}{t})^{-2/3} \quad (in \quad radians) \tag{8.4}$$

$\theta_n > \theta_{cr}$ TYPE II

$\theta_n < \theta_{cr}$ TYPE I

The definition of θ_n is the half angle of strip load as before (Figs. 6.1 & 8.5).

8.3.3 Calculations of θ_i, σ_0, and θ_0

The big difference between the two types of stress distribution is the location of the peak membrane stress. In Type II, the peak stress point lies a distance from the centre of strip load. The *R/t* ratio, the half strip angle θ_n and the peak stress angle θ_i were brought into the analyses (Eqn. (8.5)).

$$\begin{aligned} \vartheta &= \theta_i / \theta_n \\ \xi &= \theta_n^{-1}(R/t)^{-2/3} \\ \theta_n &\quad (in \quad radians) \end{aligned} \tag{8.5}$$

With the application of those parameters, Fig. 8.7 shows dimensionless angle at the peak stress ϑ plotted against dimensionless strip angle ξ. If the case belongs to TYPE II, the angle θ_i where the peak stress occurs can be calculated as the following Eqn. (8.6) obtaining from Fig. 8.7.

$$\vartheta = 0.0194\xi^{-0.75} \tag{8.6}$$

The relative error bounds are given here by (-0.27%, +13.93%).

As shown in Fig. 8.5, two parameters, the peak stress σ_0 at a level and the angle where the axial stress at this level first reaches zero θ_0, are used:

$$\begin{aligned} \varsigma &= \theta_0 / \theta_n \\ \xi &= \theta_n^{-1}(R/t)^{-2/3} \\ \theta_n &\quad (in \quad radians) \end{aligned} \tag{8.7}$$

Because of the special strip load applied in this study, the level here always refers to the mid-plane of the cylinder. The following several figures (Figs. 8.8 & 8.9) show dimensionless angle at which the axial stress first reaches zero plotted against dimensionless strip angle ξ. Equations (8.8) and (8.9) give empirical fits for this purpose.

$$\varsigma = 43.083\xi^{1.1} \tag{8.8}$$

$$\varsigma = 38.322\xi^{1.1} + 1 \tag{8.9}$$

The boundary between the zones of application of these two equations is as the following Eqn. (8.10) derivable from Fig. 8.10. As before, it is derived from a series of converged studies to get a satisfactory accuracy. In fact, the majority of the approximations are controlled by empirical equation 8.9 in practice.

$$\theta_{cr} = 1.112(R/t)^{-2/3} \quad (in \quad radians) \tag{8.10}$$

$\theta_n > \theta_{cr}$ Eqn. (8.9)

$\theta_n < \theta_{cr}$ Eqn. (8.8)

The relative error bounds are given here by (-18.48%, +14.65%).

After examining a large number of calculations for shells with different radius to thickness ratios, it was evident that the peak axial membrane stress σ_0 depended on the dimensionless strip width χ (Eqn. 8.11).

$$\begin{aligned} \eta_0 &= \sigma_0 / \sigma_n \\ \chi &= \theta_n (R/t)^{2/3} \\ \theta_n &\quad (in \quad radians) \end{aligned} \tag{8.11}$$

Using these parameters, the dimensionless peak axial stress for many different strip width and shell thickness is shown in Fig. 8.11 and the detailed form of the early part of the curve is shown in Fig. 8.12. For narrow strips (Type I stress distribution), the problem is less than the nominal stress σ_n, but as the strip width increases, the peak stress progressively rises to a maximum of 1.1 σ_n before falling back to a stable value of 1.05 σ_n. All Type II stress distributions give σ_0 very close to 1.05 σ_n. The plotted results can be closely approximated by the empirical fit:

$$\eta_0 = 5\times10^{-6}\chi^3 - 1.1\times10^{-3}\chi^2 + 0.06\chi - 1\times10^{-4} \tag{8.12}$$

$$\eta_0 = 1.05 \tag{8.13}$$

The relative error bounds are given here by (-10.31%, +5.43%).

8.3.4 Bound between the Two Types of Stress Distribution

Eqn. (8.14), which is shown in Fig. 8.13, determines the bound distinguishing the two types of stress distributions:

$$\theta_{cr} = 148.869\left(\frac{t}{R}\right)^{2/3} \quad (in \quad radians) \tag{8.14}$$

$\theta_n > \theta_{cr}$	Type II	Eqn. (8.12)
$\theta_n < \theta_{cr}$	Type I	Eqn. (8.11)

After getting all the necessary parameters σ_0, θ_0, & θ_i mentioned above from σ_n & θ_n, the equation for the stress variation around the circumference at this level can be obtained as the follows.

8.3.5 Stress Distribution Prediction

First of all, the type of stress distribution must be determined according to Eqn. (8.4). Then the stress variation around the circumference at this level can be found using the following equations. The equivalent harmonic treatment (Rotter, 1986) is adopted in the formulae:

8.3.5.1 TYPE I

$$\sigma = \sigma_0 \cos(m\theta) \tag{8.15}$$

where

$$m = \frac{\pi/2}{\theta_0}$$
$$\theta \quad (in \quad radians) \tag{8.16}$$
$$\theta_0 \quad (in \quad radians)$$

8.3.5.2 TYPE II

$$\sigma = \sigma_0 \cos[m(\theta - \theta_i)] \tag{8.17}$$

where

$$m = \frac{\pi/2}{(\theta_0 - \theta_i)}$$
$$\theta \quad (in \quad radians) \tag{8.18}$$
$$\theta_0 \quad (in \quad radians)$$
$$\theta_i \quad (in \quad radians)$$

Figures 8.14 and 8.15 show the two canonical examples for the variation of the axial membrane stress around the circumference at the mid-plane of the cylinder. Fig. 8.14 represents the Type I while Fig. 8.15 stands for the Type II stress distributions. Using the equations in this section, the following two examples have been calculated and the difference between the calculation and the real stress distribution from FE can be seen from these two figures.

In Fig. 8.14 (Type I), the membrane stress empirical equation is almost identical to that of the analysis result in the peak stress distribution content.

In Fig. 8.15 (Type II), the membrane stress empirical equation is still consonant with the analysis result in the peak stress distribution extent. Because of the long plateau of high membrane stress, the relationship is much simpler. Therefore the difference between the real distribution and the membrane theory solution seems to be less meaningful than for TYPE I, but anyway it provides a new approach to describing this phenomenon was not previously known.

8.3.6 Comparisons

8.3.6.1 Method 1

To see the difference between all the different calculation equations for the peak stress σ_0 prior to bifurcation among FE results, this thesis and the (ENV1993-4-1, 1999) (based on (Rotter, 1986)) for different parameter combination (including the variation of *R/t* ratio as well as strip load angle θ_n, the following Fig. 8.16 is listed. The curves show the peak stress versus strip load angle θ_n for different *R/t* using several distinguishing calculation equations. In such a way, the empirical equations based on this study can provide a more accurate empirical equation for the peak buckling stress if the safety factor is not taken into account.

8.3.6.2 Method 2

It is also interesting to show the same results but from a different view and take the widely used localisation parameter *n* (Rotter, 1986). As a result, the following Figs. 8.17 & 8.18 are listed.

Using this variable, the current European code (ENV1993-4-1, 1999) (based on Rotter (1986)) shows a nicer and smoother curve than the approach provided by this study. The empirical equation by this study and FE show a similarity between them and it proves the continuum in-between. Moreover, a recall can also been seen from Fig. 8.18 in detail.

8.3.6.3 Method 3

From the previous two methods, a new localisation parameter χ, as defined in Eqn. (8.13), has been used for the same comparison (Figs. 8.19 – 8.26).

These comparisons show that in the extent where $1/\chi$ is smaller than 0.1, a very local peaks can been seen here though it is not an ideal curve for the drop in some cases when approaching zero due to the dispersal of the analyses results.

8.3.6.4 Discussions

The most interesting thing here is that with the increase of χ to infinite (i.e. decrease of $1/\chi$ to infinitesimal), both FE results and the new approach in this study provide a higher peak membrane stress while the other two (Rotter, 1986; ENV1993-4-1, 1999) have a drop there.

As $1/\chi=\theta_n^{-1}(R/t)^{-2/3}$, the decrease means that strip angle increases if ratio of R/t is fixed or ratio of R/t increases with the same strip angle.

For the first case, it means an apparent more uniformly loaded and a decrease in buckling strength will be reasonable in that case. In the second case, it means more possibility of Type II occurrence. In summary, both of these two cases will be approaching to the likeness of uniform compression (Rotter, 1986) with the increase of χ to infinite.

This shows the contradiction of the notion that it will absolutely lead to lower peak membrane stress in a more uniform likely compression. Therefore, the following two diagrams have been used to explore on this. The ratio of R/t increases from 100 (Fig. 8.28) to 1,00 (Fig. 8.27) if strip angle is fixed (θ_n =5° in both cases), this will lead to decrease of $1/\chi$ approaching 0. According to the previous definition, it will show more uniformity during this procedure and thus it should decrease its peak stress. Firstly, it decreases its critical buckling strength, but what's more, the peak stress increases from σ_0/σ_n=0.1 in R/t=100 to σ_0/σ_n=0.5 in R/t=1,000 simultaneously. The final result of these contradictory influences reaches higher output than expected according to the traditional

notion of localisation and uniform compression. Actually, the R/t=100 cases shows a more uniformly distributed stress pattern though both cases belong to stress distribution Type I from previous study.

The complete effect curve has been shown in (Fig. 8.29). It is not surprising that they merge into almost one curve among different R/t ratio due to the fact that this ratio had been considered already in the variable.

8.4 Conclusions and Outlook

8.4.1 Summary

High local membrane stresses do not always affect the strength much, provided the zones over which they occur is small compared with a potential buckle (Rotter, 2001). The stress pattern around the circumference has been studied to explore the relationship between local high membrane stresses and buckling strength and a comparison of the two different approaches, current code and the finite element analyses results describing the buckling strength has been provided.

8.4.2 Conclusions

A new approach is described to deal with stress pattern around the mid-plane circumference, to interpret the criterion of buckling failure under the local high axial compression and a comparison of the other two approaches has been shown;
The classification of two types is provided due to the different stress distributions around the circumference.

8.4.3 Outlook

First of all, more data are needed to show the continuum of the curves used for empirical equations in this chapter.

Second, the direction of the strip load applied on the cylinder also needs consideration. The strip load applied here limits the wide application of the empirical equations in reality, though with the combination of the internal pressure, the buckling stress increases

and even reaches the classic value (Lorenz, 1908; Timoshenko, 1910; Southwell, 1914) if sufficiently high compression is given. But, what is more important is that some studies recently also show the increase of axial membrane stress somewhere either near the mid-height or down at the bottom due to the decrease of partial internal pressure. Thus, the systematic analysis empirical equation on shell buckling under the combination of the strip load and patch load is needed.

In such cases, more efforts are needed to obtain these different types of local load in order to make a much better understanding of the buckling behaviour under an axial compression that acts over only a small part of the wall.

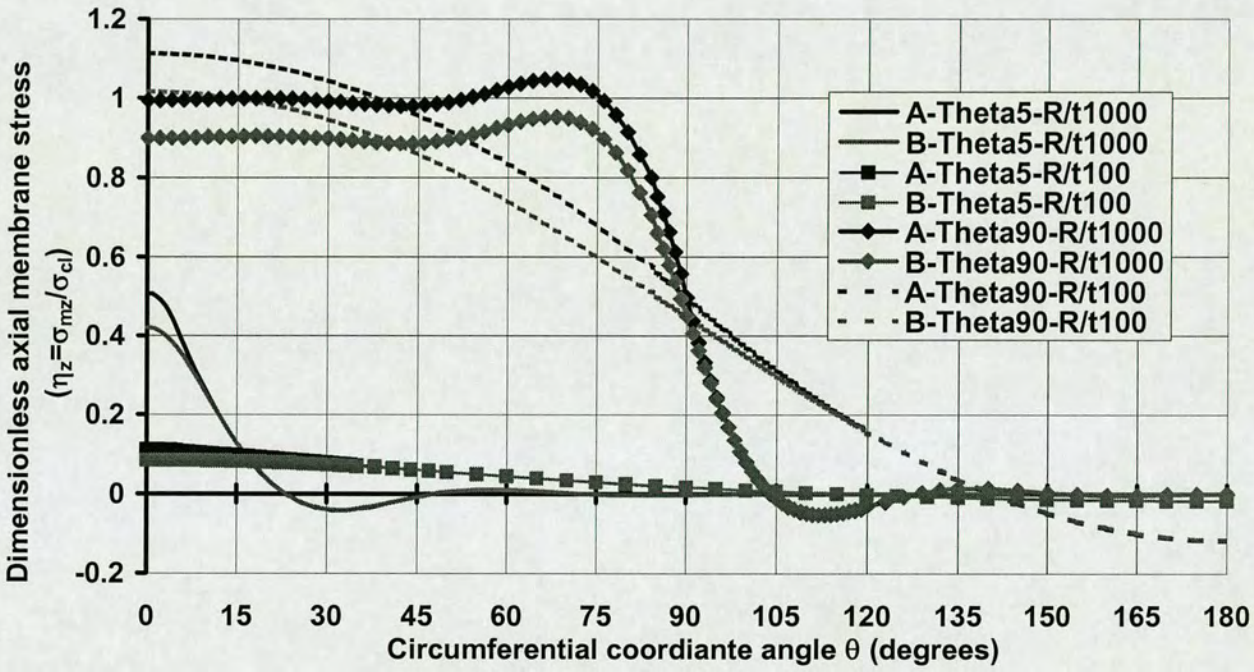

Fig. 8.1: Axial membrane stress distribution around circumference
(Note: *A, B* refer to different circumferential lines in cylinder; theta means strip angle θ_n in degrees (Fig. 8.3))

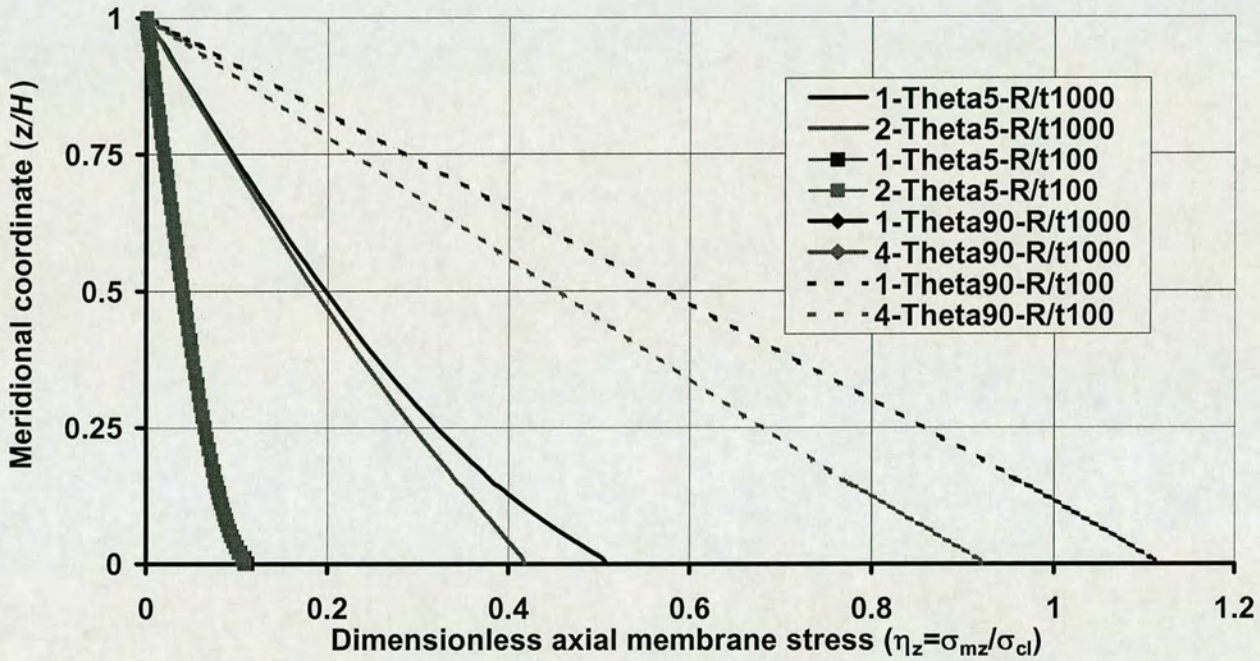

Fig. 8.2: Axial membrane stress distribution along meridian

(Note: 1, 2, 4 refer to different meridional lines in cylinder; theta means strip angle θ_n in degrees (Fig. 8.3))

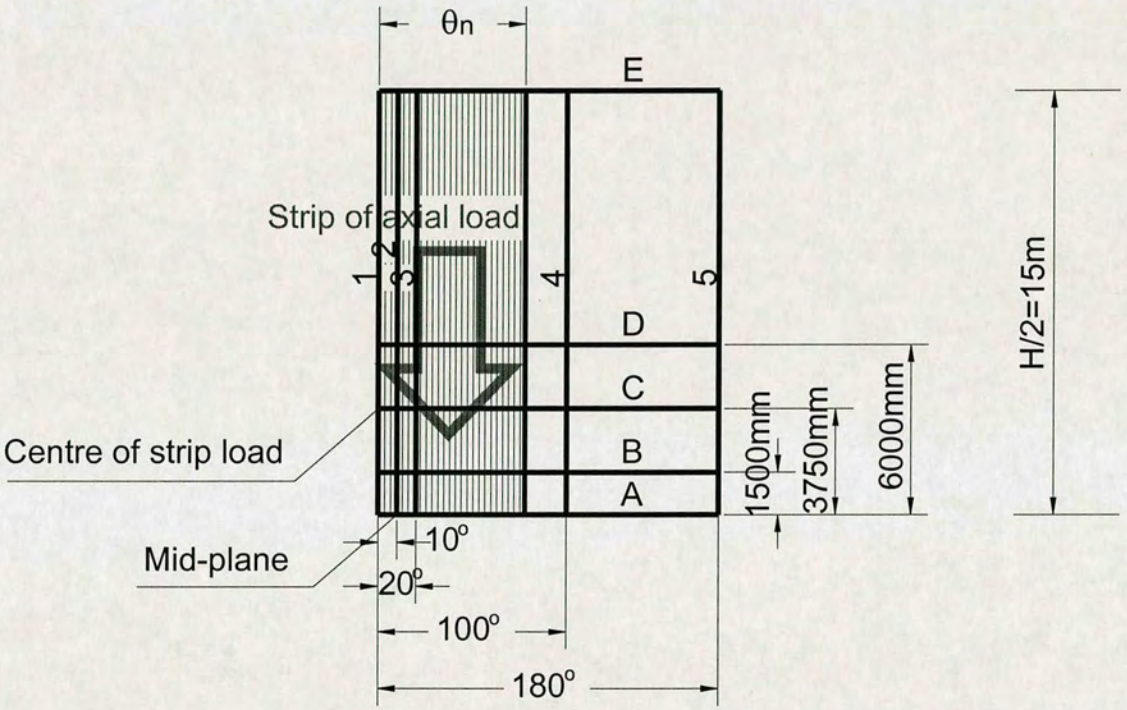

Fig. 8.3: Definition of all the special lines in the analyses

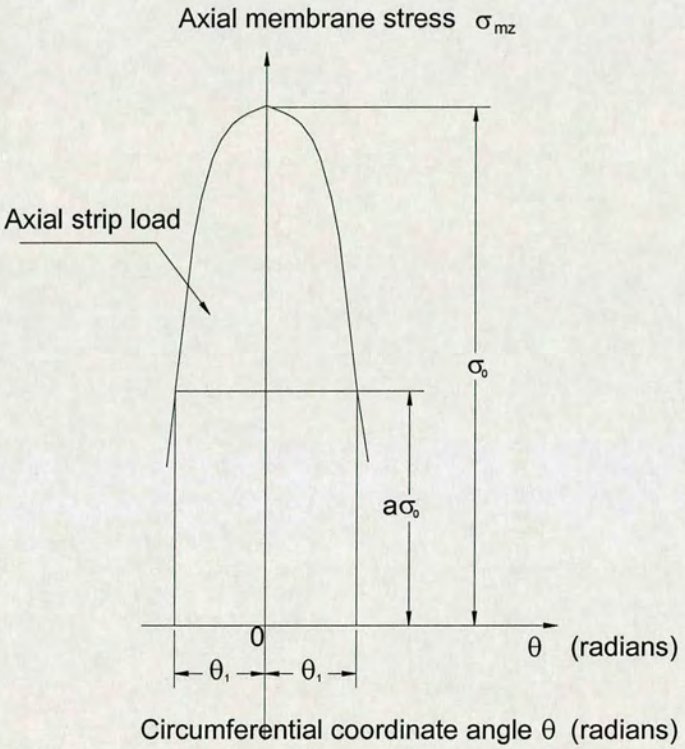

Fig. 8.4: Characteristic shape of a local axial stress peak
(Note: Abstracted from (Rotter, 1986; CEN ENV1993-4-1, 1999))

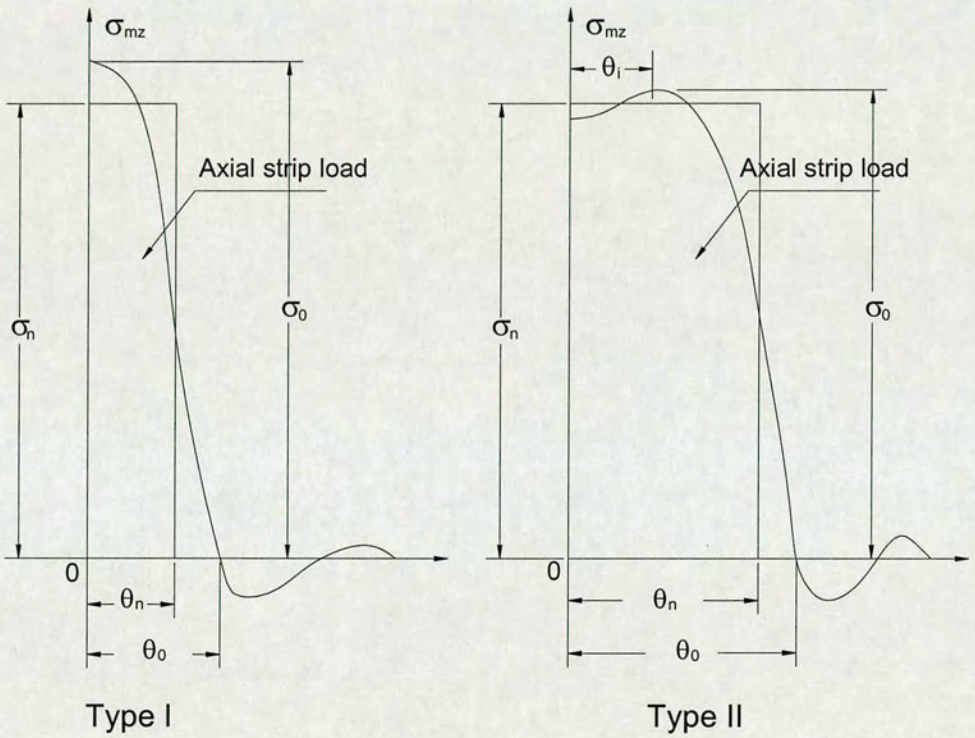

Fig. 8.5: The two types of stress distribution
(Note: The variation of stress distribution around the circumference.)

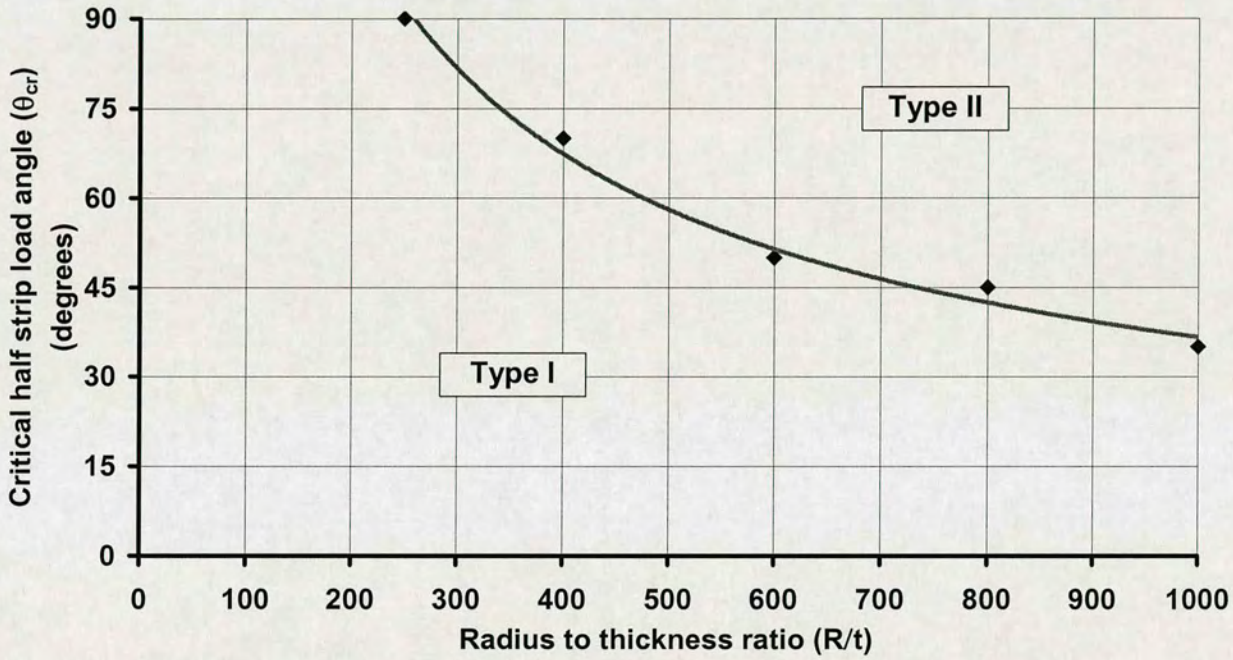

Fig. 8.6: Zones of occurrence of the two types of stress distribution

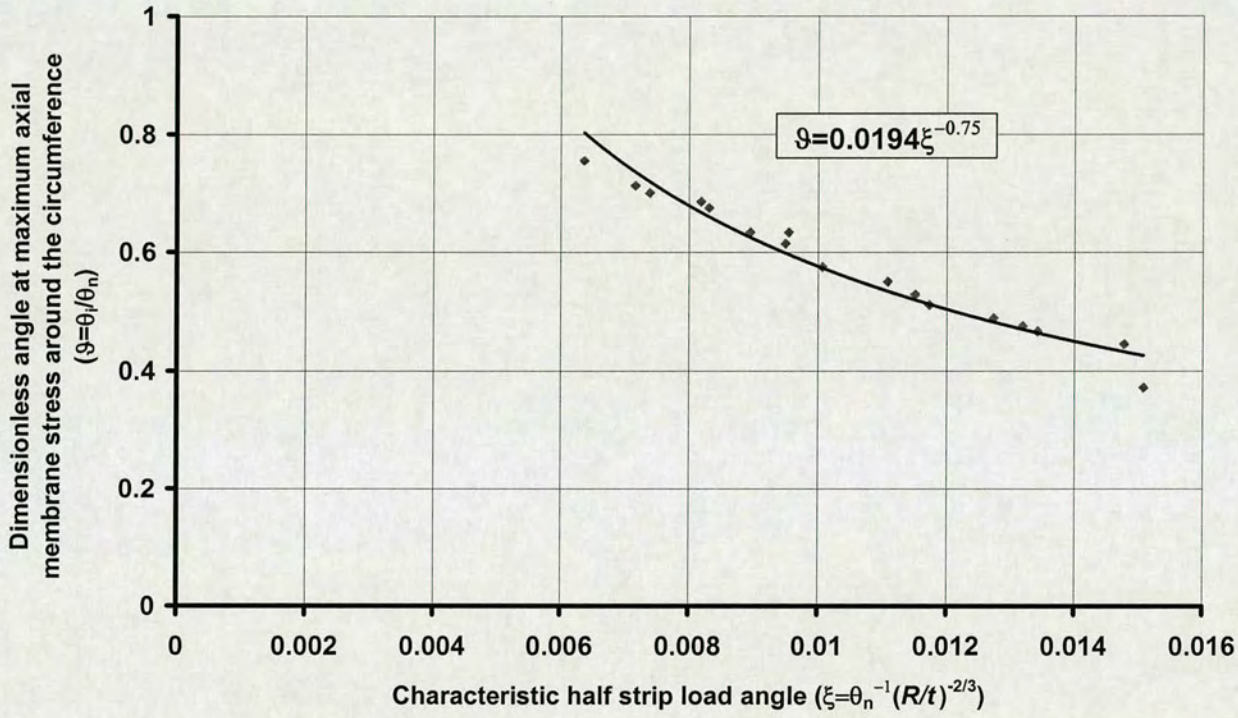

Fig. 8.7: Prediction of θ_i

(Note: The continuous line shows the empirical equation, nodes show FE analyses results.)

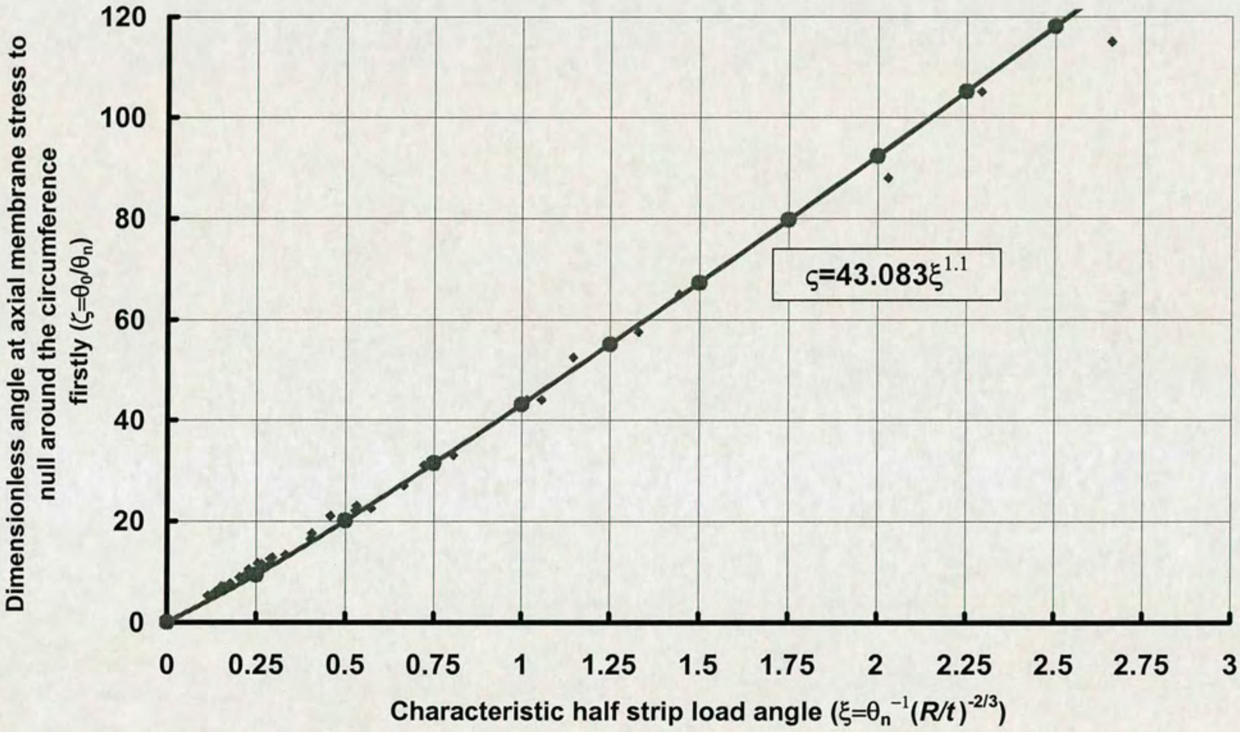

Fig. 8.8: Prediction of θ_0 (1)

(Note: The continuous line shows the empirical equation, nodes show FE analyses results.)

K:\MeshPapers\Pattern\Version8\Files-mE2-x&Formula Calc-1 (8)

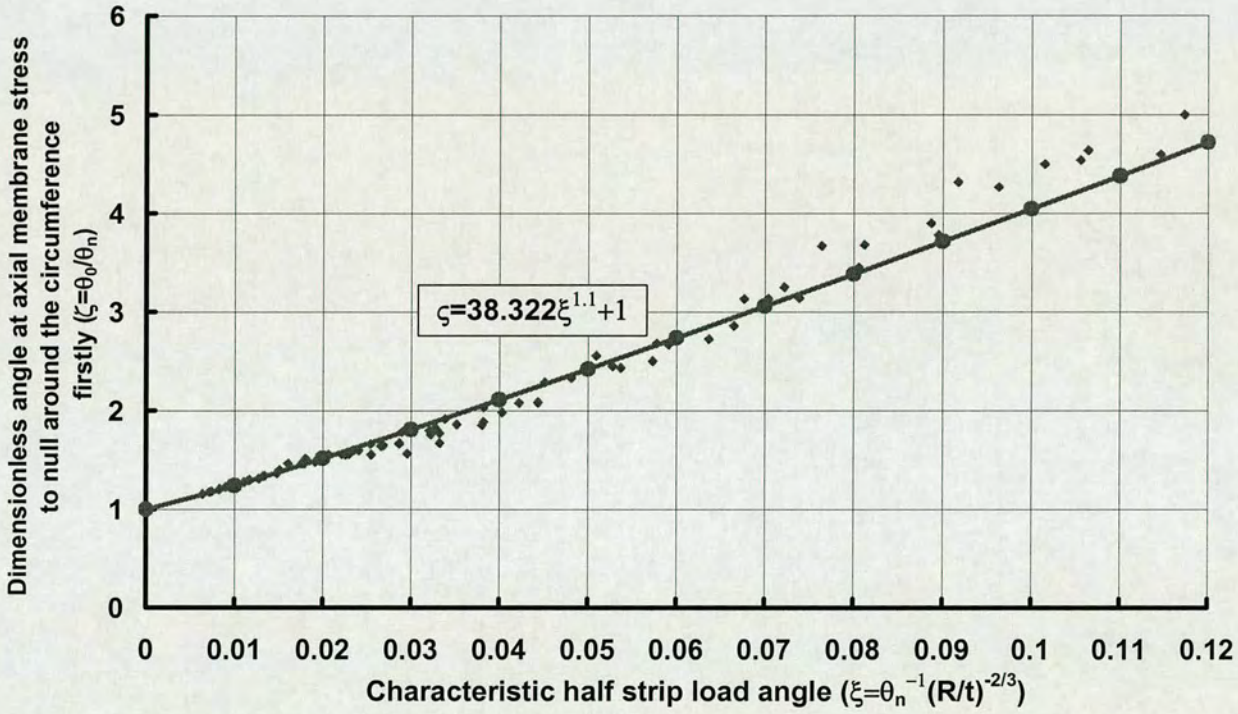

Fig. 8.9: Prediction of θ_0 (2)
(Note: The continuous line shows the empirical equation, nodes show FE analyses results.)

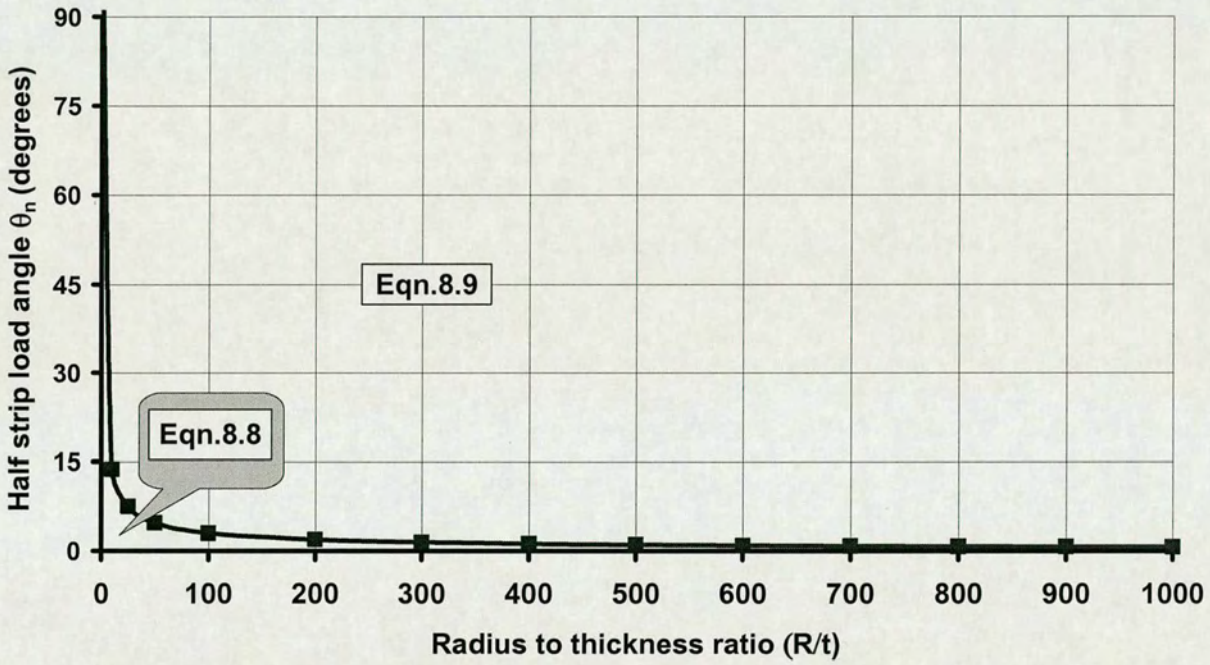

Fig. 8.10: Zones of application of Eqns. 8.7 & 8.8

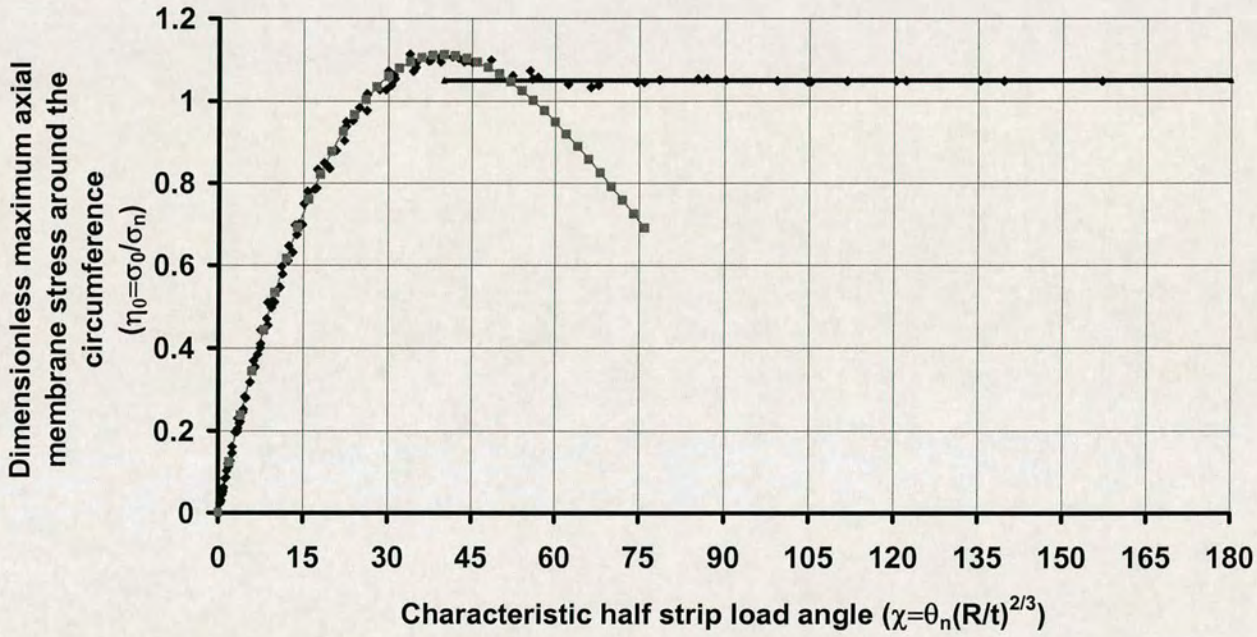

Fig. 8.11: Peak stress value
(Note: The continuous line shows the empirical equation, nodes show FE analyses results.)

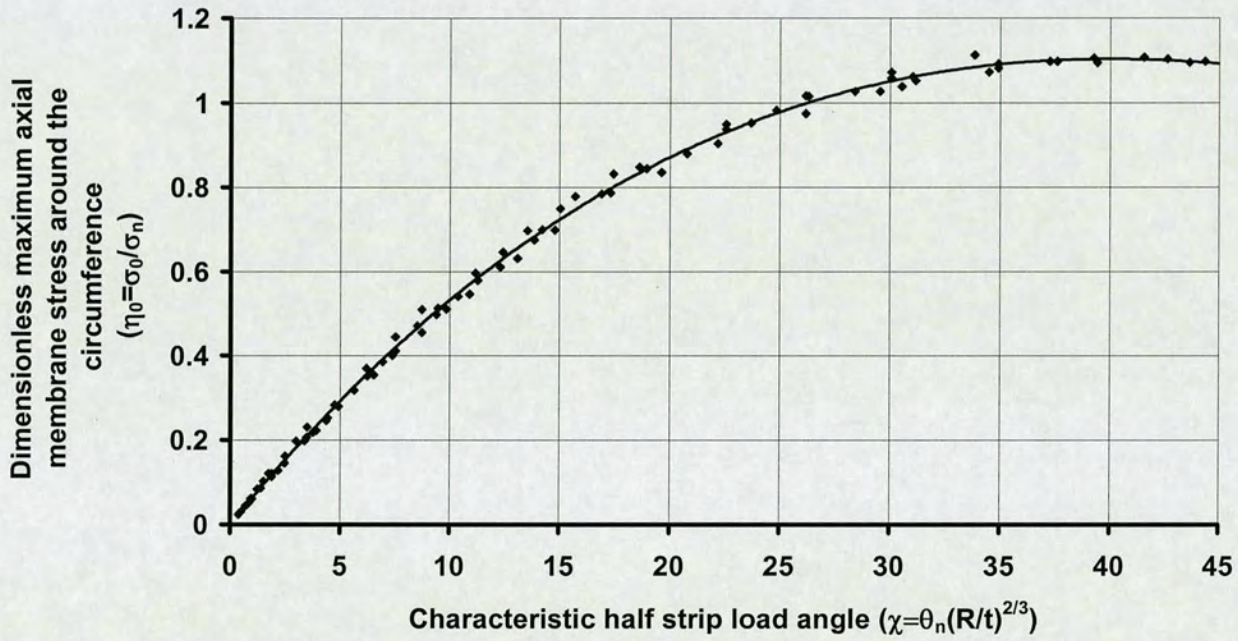

Fig. 8.12: Peak stress value (in detail)
(Note: The continuous line shows the empirical equation, nodes show FE analyses results.)

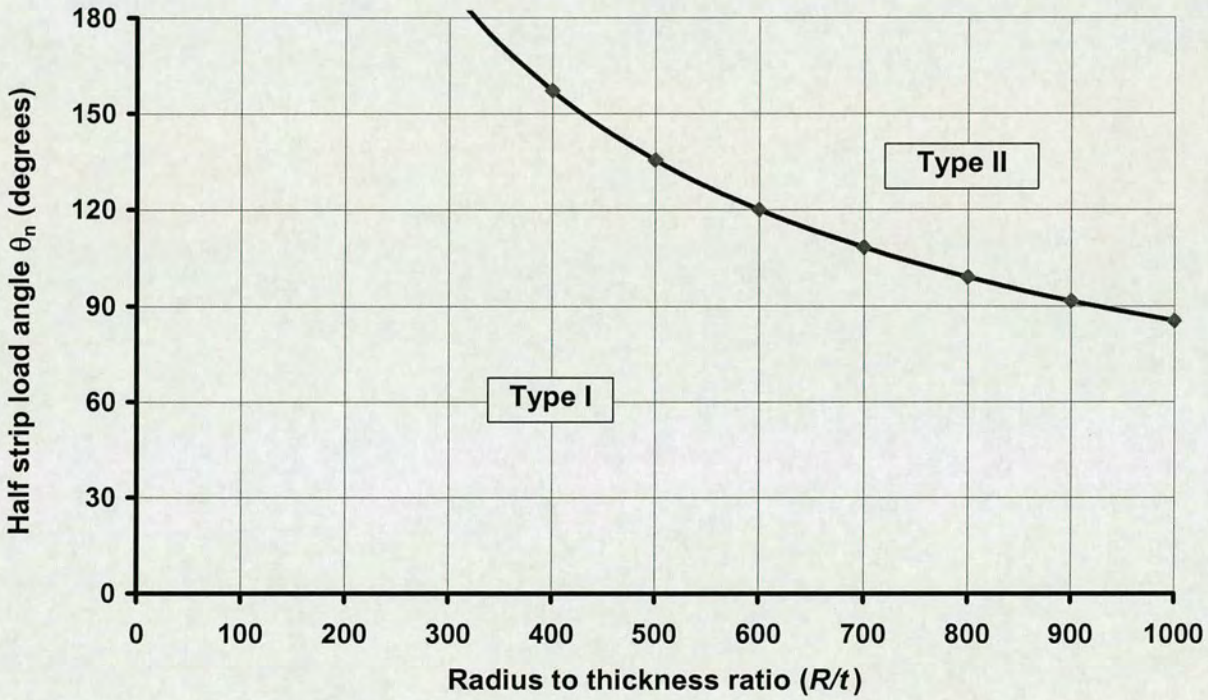

Fig. 8.13: Bound between the two types of stress distribution: peak stress value

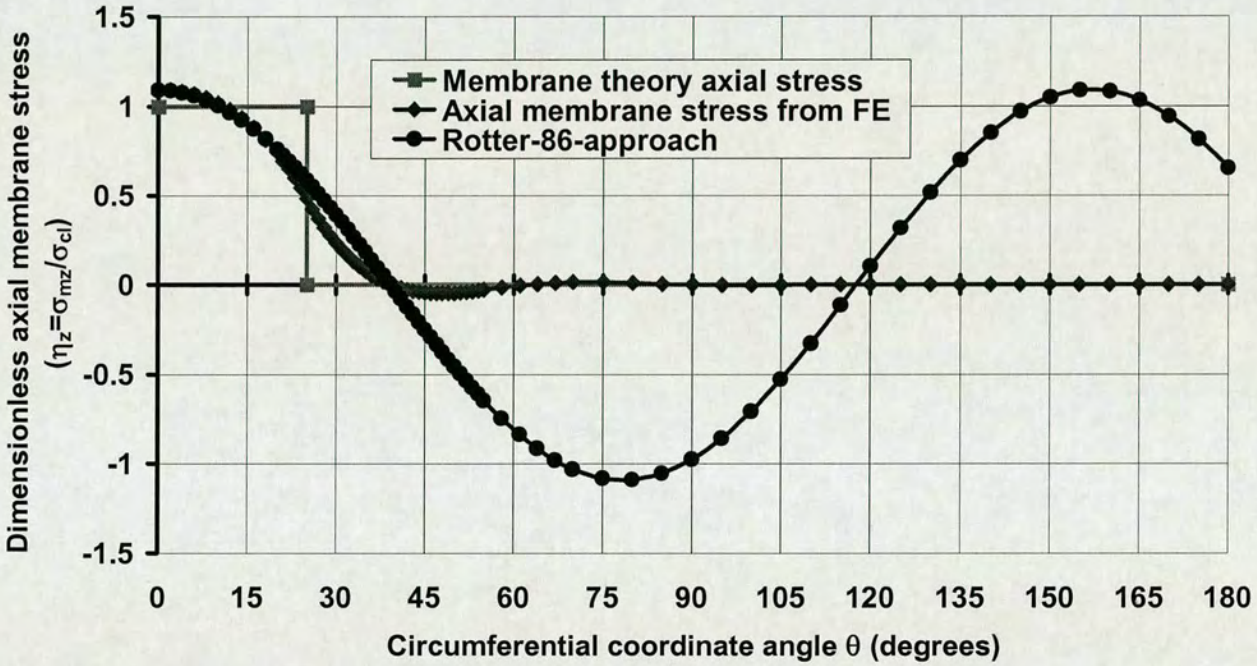

Fig. 8.14: Axial membrane stress distribution (TYPE I stress distribution)
(Note: FE for the finite element analyses results, Rotter-86-approach calculated by (Rotter, 1986))

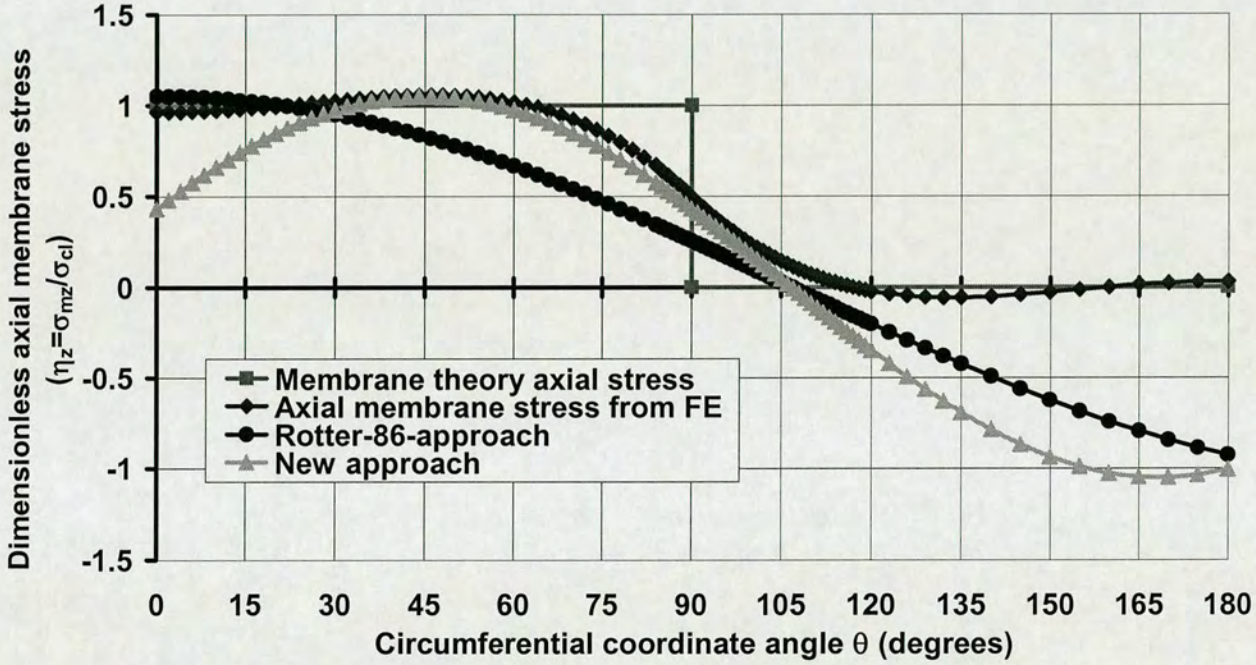

Fig. 8.15: Axial membrane stress distribution (TYPE II stress distribution)
(Note: FE for the finite element analyses results, Rotter-86-approach calculated by (Rotter, 1986), New approach is based on the method of this study)

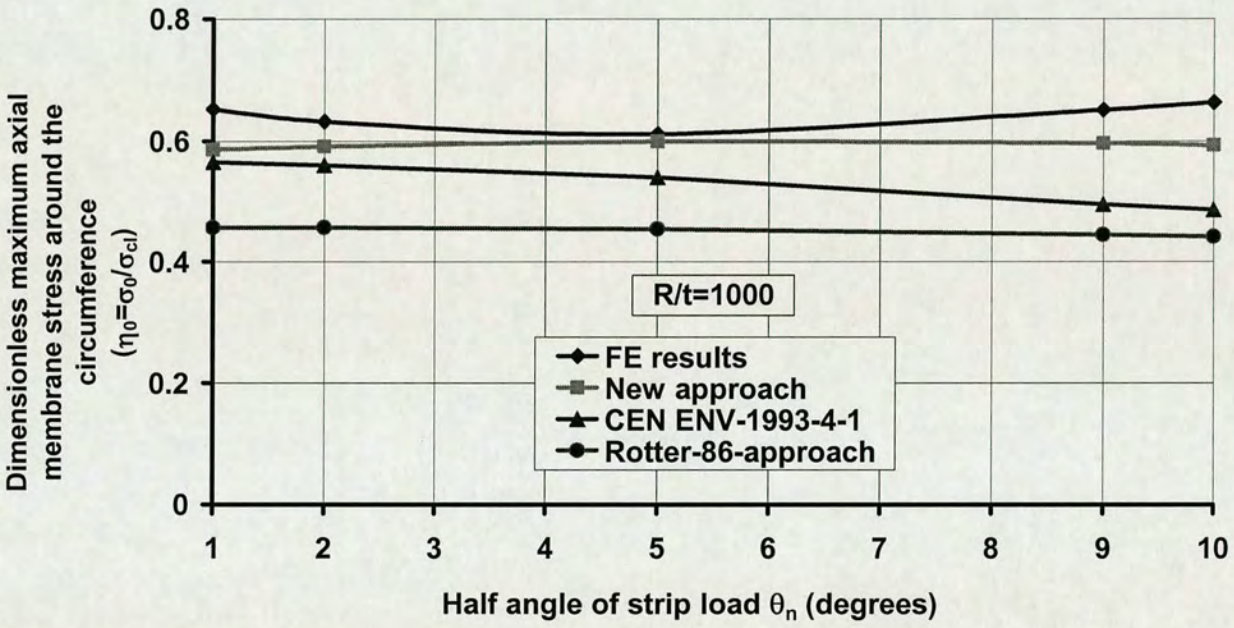

Fig. 8.16: Comparison of stress peak localisation on buckling stress (R/t=1000) – Method 1 (θ_n)

(Note: FE for the finite element analyses results, Rotter-86-approach for the localisation parameter f calculated by (Rotter, 1986), New approach is based on the method of this study, CEN ENV-1993-4-1 represents for localisation parameter ψ calculated by the current European code (ENV 1993-4-1, 1999))

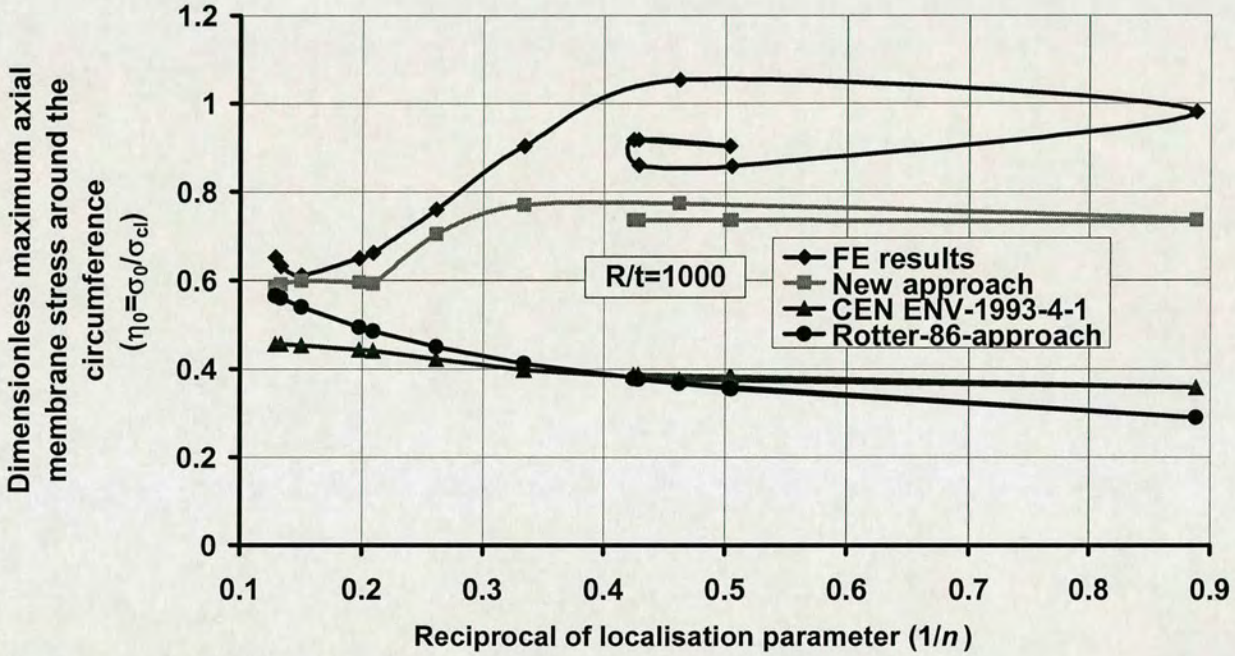

Fig. 8.17: Comparison of stress peak localisation on buckling stress (*R/t*=1000) – Method 2 (*n*)

(Note: All the parameters combination diagrams show the same trend and since only one case is listed here and notes for names of curves as before)

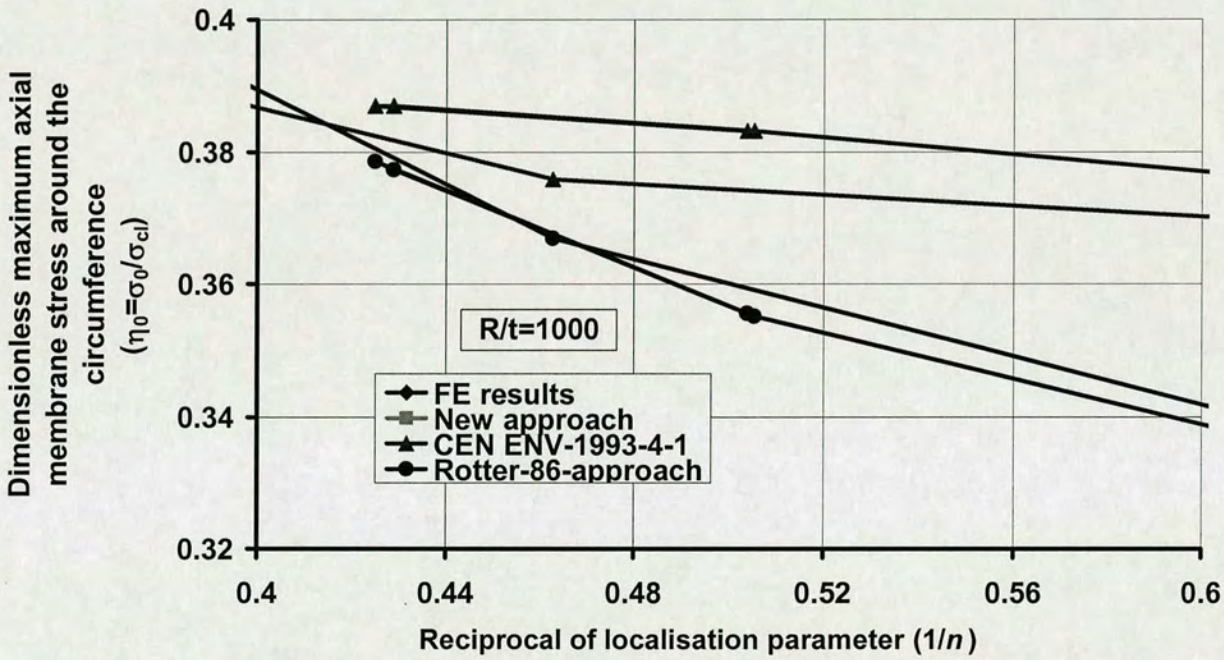

Fig. 8.18: Comparison of stress peak localisation on buckling stress (*R/t*=1000, in detail) – Method 2 (*n*)

(Note: notes for names of curves as before)

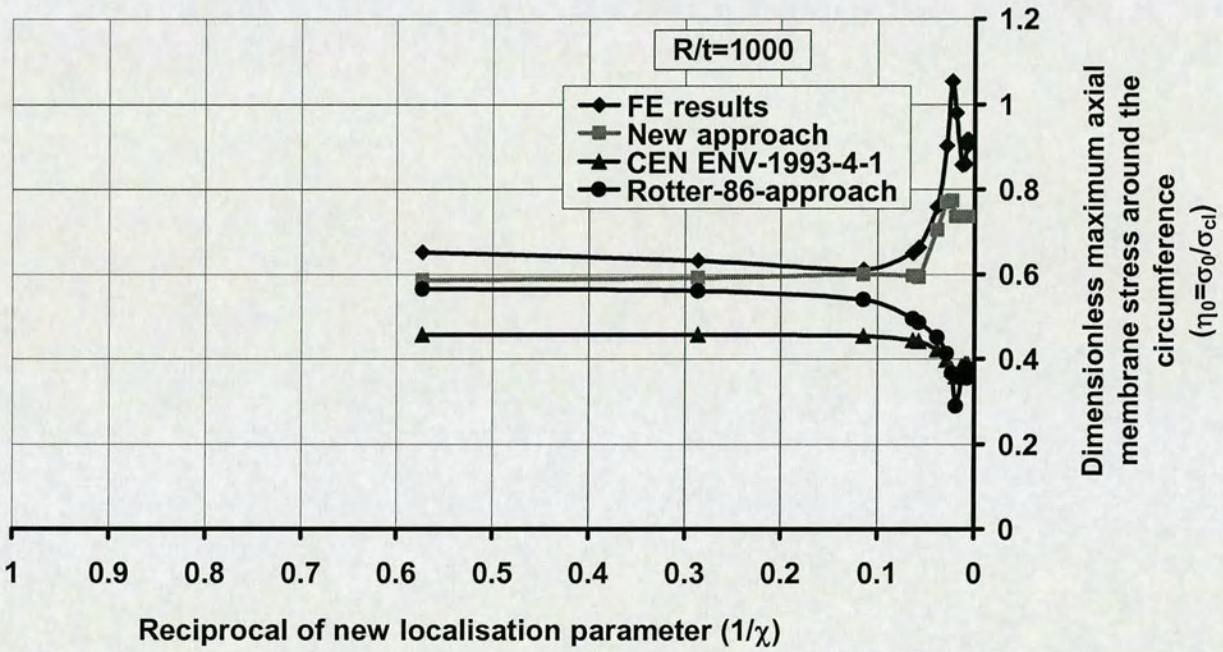

Fig. 8.19: Comparison of stress peak localisation on buckling stress (*R/t*=1,000) – Method 3 (χ)

(Note: notes for names of curves as before)

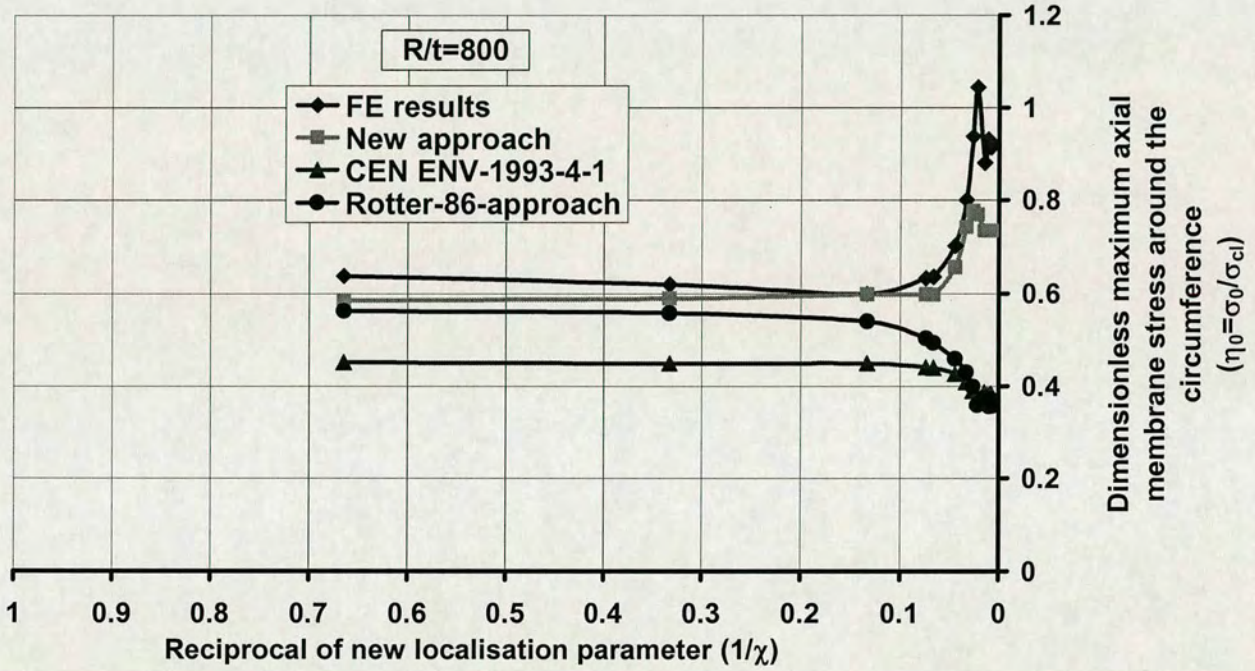

Fig. 8.20: Comparison of stress peak localisation on buckling stress (*R/t*=800) – Method 3 (χ)

(Note: notes for names of curves as before)

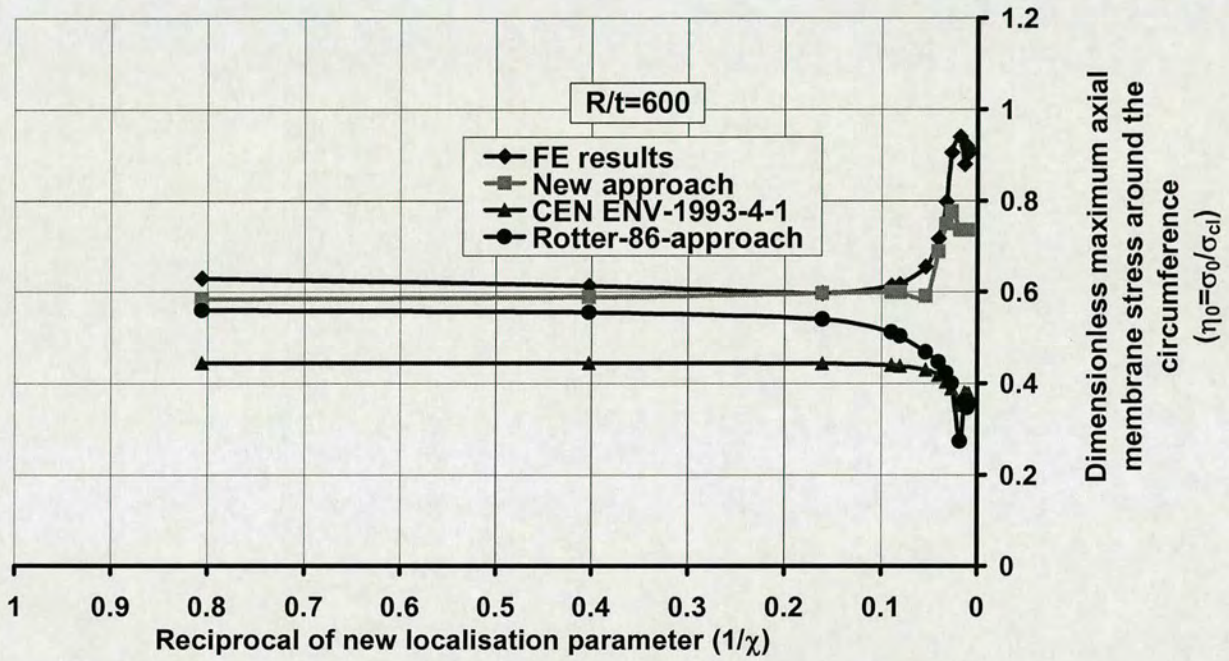

Fig. 8.21: Comparison of stress peak localisation on buckling stress (*R/t*=600) – Method 3 (χ)

(Note: notes for names of curves as before)

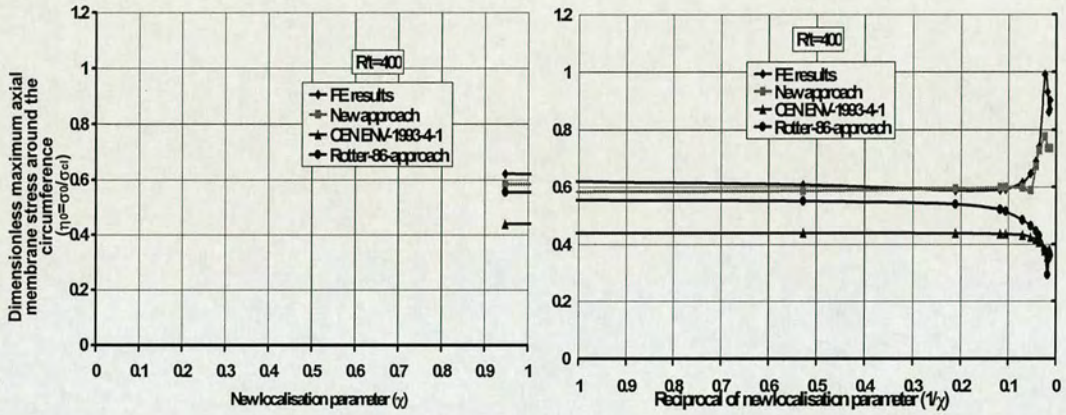

Fig. 8.22: Comparison of stress peak localisation on buckling stress (*R/t*=400) – Method 3 (χ)

(Note: notes for names of curves as before)

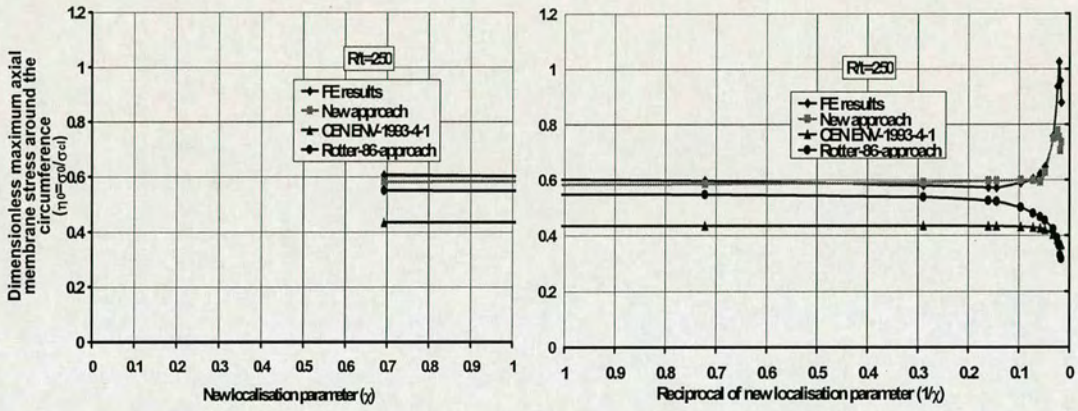

Fig. 8.23: Comparison of stress peak localisation on buckling stress (*R/t*=250) – Method 3 (χ)

(Note: notes for names of curves as before)

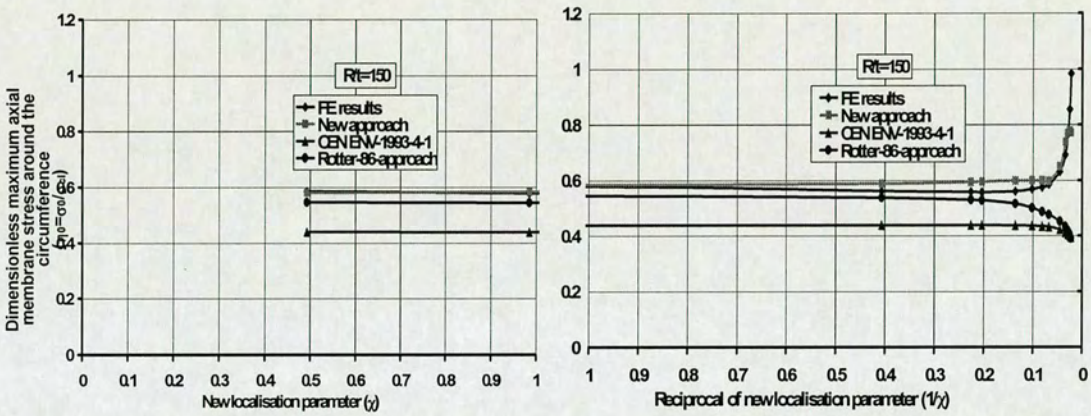

Fig. 8.24: Comparison of stress peak localisation on buckling stress (R/t=150) – Method 3 (χ)

(Note: notes for names of curves as before)

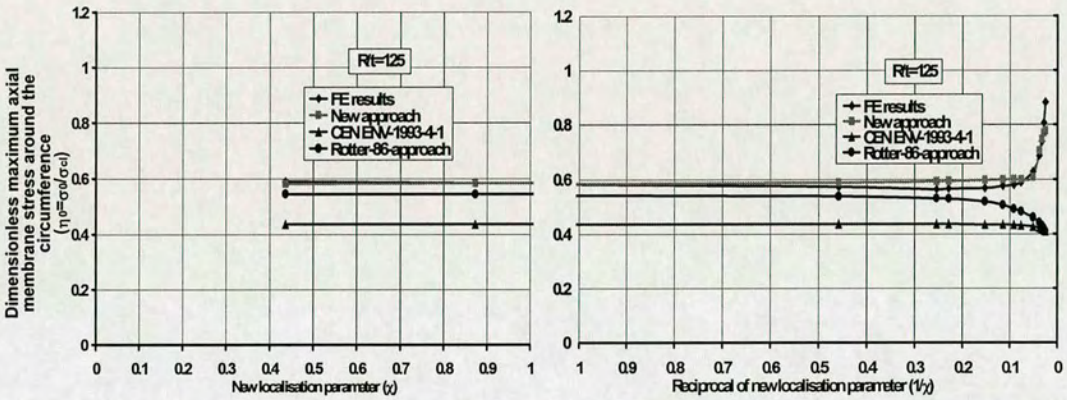

Fig. 8.25: Comparison of stress peak localisation on buckling stress (R/t=125) – Method 3 (χ)

(Note: notes for names of curves as before)

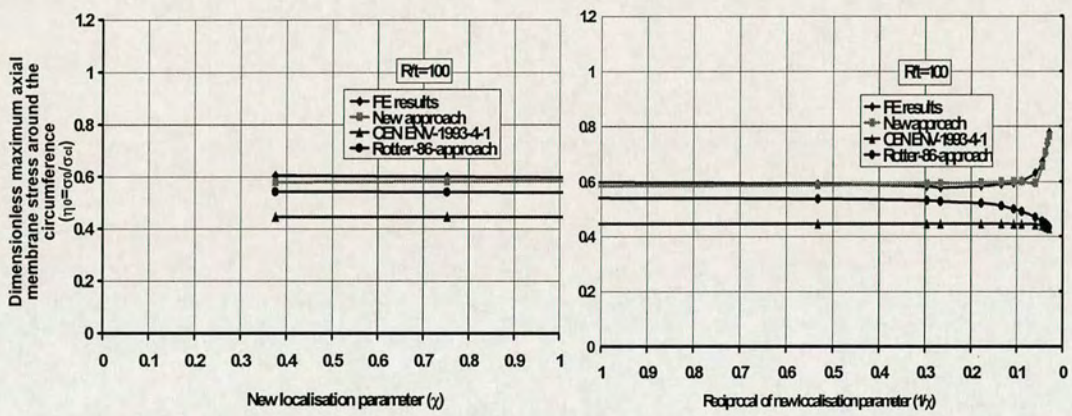

Fig. 8.26: Comparison of stress peak localisation on buckling stress (R/t=100) – Method 3 (χ)

(Note: notes for names of curves as before)

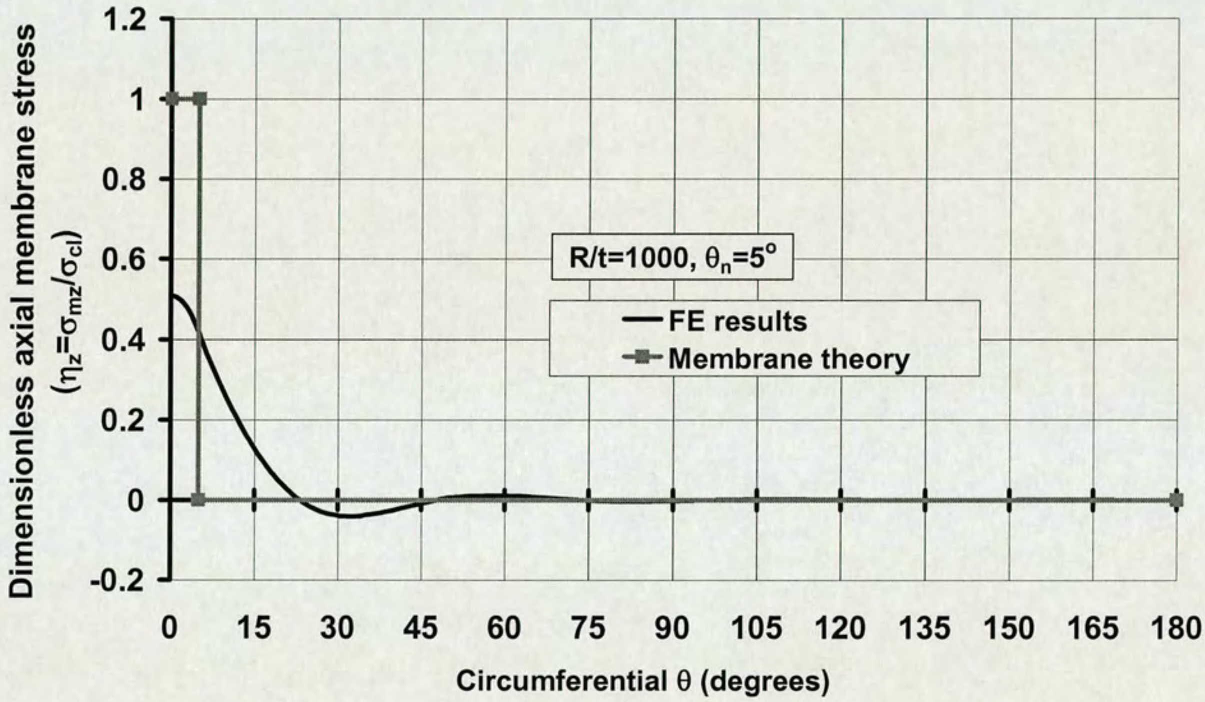

Fig. 8.27: Axial membrane stress distribution (R/t=1,000, θ_n=5°)

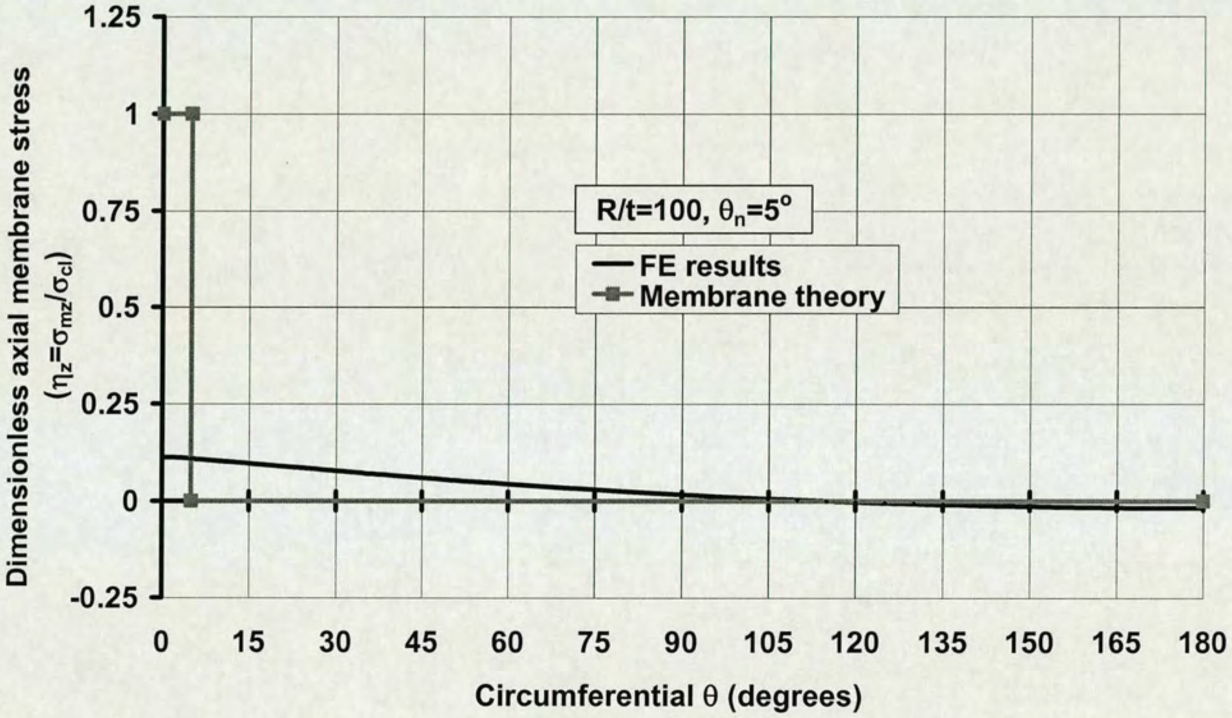

Fig. 8.28: Axial membrane stress distribution (*R/t*=100, θ_n=5°)

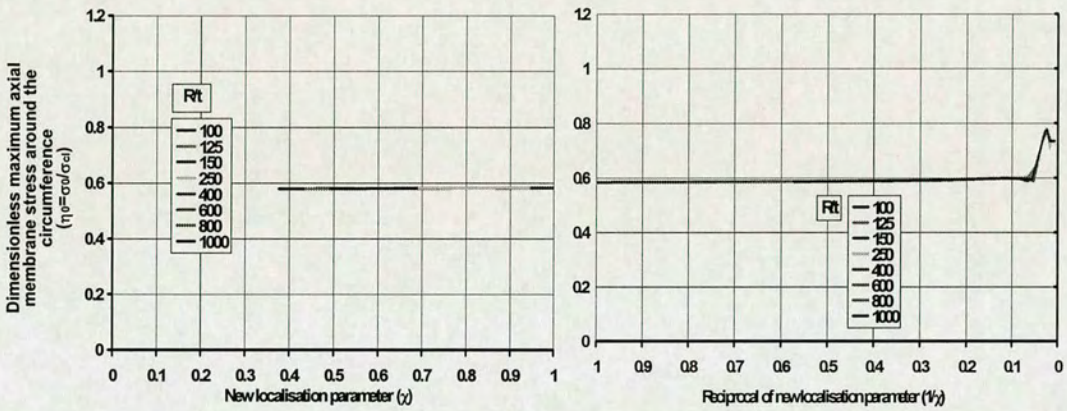

Fig. 8.29: Comparison of stress peak around the circumference of mid-plane using χ (Method 3)

Chapter 9

CONCLUSIONS AND RECOMMENDATIONS FOR FUTURE WORK

9.1 Summary

Unsymmetrical features of silo wall loads (Ooi et al., 1990) lead to local high axial compressive membrane stresses (Rotter, 1986; 1998; 2001) (Fig. 1.6), which is probably the commonest cause of buckling failures in service. Similar conditions develop in tanks under wind loading and above local supports. The local value of the stress that can be sustained without before buckling is very sensitive to the overall stress distribution, and where high stresses act on only a small zone, the peak value may reach a value (Rotter, 1986, 2001; ENV 1993-4-1, 1999) much higher than that for uniform axial compression buckling. However, the conditions that lead to buckling under non-uniform stresses have received very little attention. The few explorations of this problem have either used linear buckling (Bijlaard & Gallagher, 1959; Peter, 1974; Libai & Durban, 1977) or deal only with buckling above a support (e.g. Guggenberger et al, 2000).

Geometric imperfections in the shell play a key role in reducing the cylinder buckling strength. The buckling strength of a thin cylindrical shell under uniform axial compression is known to be very sensitive to geometric imperfections (e.g. Yamaki, 1984). One of the most detrimental and well-defined imperfections is a local depression due to the rolling process of the steel plate and shrinkage of the weld (Rotter and Teng, 1989; Rotter, 1996, 1997; Berry et al, 2000; Holst et al, 1999, 2000; Schmidt and Winterstetter, 2001). The rationally based local axisymmetric inward Type A imperfection of Rotter and Teng (1989), which has been used in many later studies, was adopted in the analysis.

This study is the first to consider buckling under local axial compression using a geometrically nonlinear analysis, considering geometric imperfections, and exploring the

buckling strength under a stress regime that is within the shell and distant from restraining boundaries.

The following summaries all work done, phenomena observed and discovered by the author as well as the most important conclusions and related topics discussed.

9.2 Contents of Study

9.2.1 Background Knowledge

The definition and application of silos in civil engineering was introduced first. The loads on silos and corresponding strength analyses from both theories and experiments, which limited in the domain of study on the shell wall, were presented and the big deviation between the theory and experiment showed the reason why this problem needed to be addressed in this study in a theoretical and numerical way examining specifically the effect of geometric imperfections under high local stresses conditions for the shell buckling study. The popularly adopted shell design codes were listed and the research philosophy of this study was also presented to support the rationale of the many analyses. The study procedures were stated according to the research philosophy.

Theories on both the classic method based on hand calculation and modern numeric method based on computing were next presented, limited in scope to thin cylindrical shell structures. The key point lies in local axial compression, which was the aim of the whole study. However, the classical shell theories, which most designers must rely on, have many limitations in application and sometimes are far away from the conditions in real structures. At the same time, modern powerful numerical methods based on computing have had little impact on silo designers. With the application of the finite element analysis package ABAQUS, it has been the aim of this study to provide a set of simple but reliable recommendations for practical design based on rigorous analyses, which can be implemented in future design codes.

Unsymmetrical loads are unavoidable in practice and their vital role in silo failure has been often noted. Several investigations were made into the effect of non-uniform

pressure (normal direction) in changing the axial stress distribution to one in which local high axial compression develops, but little appears to have been done on evaluating the buckling strength under these stresses. The shell buckling strength under an axial compression that acts over only a part of the circumference and a part of the height (typically resulting from an unsymmetrical load on the silo walls) has not previously been explored at all.

The buckling strength of a thin cylindrical shell under axial compression is known to be very sensitive to geometric imperfections in the wall and one of the most detrimental and well-defined imperfections is a local depression due to the rolling process of the steel plate and shrinkage of the weld. It is therefore sensible to suppose that geometric imperfections will also play a key role in reducing the cylinder buckling strength under local axial compression. The vein of the developing in the imperfection study of the shell buckling was described in detail. Some important features of the imperfection (forms, amplitude and spreading width) and their influence were also stated from previous studies. A representative idealised local axisymmetric inward imperfection (Type A) was introduced (Rotter and Teng, 1989b) and used throughout the whole thesis.

All above indicates the importance of elevated local axial compression and a local imperfection in shell buckling studies. However, a reliable quantification of these effects presents a considerable challenge. This study is the first known study to examine this problem systematically.

The draft European Standard for Metal Shells (ENV 1993-1-6, 1999) was used as a reference design code to be implemented and the analyses types used to predict shell buckling strength were taken from that standard. These were Linear Analysis (LA), Geometrically Non-linear Analysis (GNA), and Geometrically Non-linear Analysis with Imperfections (GNIA). The influence of the material non-linearity (GMNA & GMNIA) was also briefly explored.

Although it is well known that the internal pressure from the stored material reduces the detrimental effects of the imperfections, and that the stiffness of the solid also increases shell buckling strength further, since this is the first study of the problem, these strengthening effects were ignored in the present study. In this respect, all the analyses of this thesis provide conservative and safe strength evaluations for design.

Because little attention has previously been paid to shell buckling under elevated local axial compression, this thesis has presented a theoretical numerical study examining specifically the effect of geometric imperfections under high local stress conditions. The studies performed in this thesis were concerned with geometrically linear and non-linear, elastic and elastic-plastic shell stability (buckling and collapse) problems, with and without local axisymmetric imperfections under elevated local axial stresses conditions.

In this thesis, only numerical methods were used, due to the very complicated stability problems of shell buckling under all the factors mentioned above. Different forms and amplitudes of realistic imperfection were used to identify and explore the relationships between the empirical rules of the codes and the finite element analyses. The aim of this study was to provide an insights into silo structural behaviour under local stresses states and to produce a rigorous and rationally based set of rules to be implemented in the future shell design standards economically and safely.

9.2.2 Computer Modelling on Shell Buckling Analysis

The procedure of finite element analysis was introduced first. In general, unstable collapse and post-buckling analyses of the shell buckling require two steps:

Step 1: a linear eigenvalue analysis is performed to obtain estimates of the buckling loads and modes. This provides guidance in mesh design and the mesh convergence studies. The buckling modes achieved can be used for partial modelling in the more complicated analysis in order to save time and computer resource. This uses the *BUCKLE step for a linear static analysis in ABAQUS.

Step 2: a non-linear load-displacement analysis is performed using the mesh resulting from the former study of the buckling analysis. The true failure mode and the load at which failure occurs can be found using a fully non-linear analysis of the perfect or imperfect shell model (GNA/GNIA/MNA/GMNIA analyses). *STATIC, RIKS defines a traditional step for a non-linear static analysis in ABAQUS.

There are two kinds of the non-linearity in the analyses: either material or geometric non-linearity. Different non-linear treatments in the computer analysis have been presented accordingly with their limitations.

The mesh convergence study was undertaken for several different load cases and a general conclusion from this study is that the effect of mesh refinement in the meridional direction is much faster than that of longitudinal counterpart for this shell problem. A satisfactory mesh from the convergence study, with reasonable element numbers, for the shell buckling analysis under local axial compression with/without local geometric imperfections, was obtained.

A new computational procedure was devised that combined the non-linear (Riks method) and linear (buckling method) procedures, This process can reduce the computing time significantly, but still gives accurate buckling strength predictions.

In short, Chapter 4 described the details of the computer model and how to obtain accurate predictions efficiently. The use of each individual analysis type was noted according to its potential applications and limitations. The focus was put on the mesh study due to the sensitivity of the mesh refinement in the finite element analyses.

9.2.3 Shell Buckling Behaviour under Elevated Localised Axial Compression Stresses

A simple model was found that defines the range of non-uniform stress states. Numerical predictions using the program ABAQUS (HKS, 1998) were presented for a number of cases and compared with available theoretical and experimental results. Beginning with

the imperfection forms previously calibrated against uniform compression and considering the effect of non-uniformity in the stresses, several imperfections patterns were explored to calculate the buckling resistance under non-uniform stress states. The theoretical investigation of shell buckling under elevated local axial compression stresses examined the mechanics underlying failure in order to set up a model comparable with the results obtained previously and now provides a better understanding of the phenomena.

The influence of the assumed boundary conditions used in the analyses was examined, with the final adoption of simply supported boundaries for shell buckling calculations under elevated axial compression. The influence of geometric imperfections was also considered and different amplitudes of imperfection were taken into account. Two different buckling phenomena were identified with corresponding, and distinct, buckling mode forms by using the deflected shapes and axial membrane stress distributions, which provided a key line for the whole study in this thesis. Based on the content above, the following conclusions can be drawn:

A. Two possible and distinct buckling phenomena have been identified for a wide range of shell geometries subject to a wide range of strip loads;
B. For narrow strips, a Strip Centre buckle occurs;
C. For wider strips, a Strip Edge buckle is observed;
D. The influence of geometric imperfection amplitudes was examined and shown to have a moderate effect on the buckling strength of the shell;
E. In general, non-linearity plays a minor role in determining the stress distribution at buckling;
F. The influence of boundary conditions in the finite element analyses was explored in order to prove the validity of the results here and afterwards.

9.2.4 Shell Buckling Strength under Localised Axial Compression: Effect on Load Zone Width

A full series of parametric studies were presented which examined the effect of local elevated axial compression on the buckling strength of geometrically perfect and

imperfect cylindrical shells. Focus was placed on the influence of the width of the compression zone. Drafted design rules were obtained, based on these calculations. Empirical equations for different analyses types according to the current Eurocode (ENV 1993-1-6, 1999) were obtained numerically. The influences of geometric imperfections, geometric non-linearity and material non-linearity were all considered (LA/LEA, GNA, GNIA, GMNA, GMNIA).

The results of a full set of parametric analyses support the hypothesis from the previous Chapter 5: the empirical equation for the shell buckling strength under local axial compression with or without geometric imperfections can be divided into two distinguishing phenomena because of their corresponding buckling mechanism – Strip Centre buckles and Strip Edge buckles. A full set of simple empirical prediction equations were devised accordingly.

In sufficiently thin cylindrical shells, buckling occurs before yielding. The point is that whether buckling or yielding occurs first for the sufficiently thin cylinder is difficult to distinguish. The following conclusions can be drawn from study:

A. Parametric studies have been used to devise simple empirical design equations;
B. Empirical equations were obtained using three different analysis types conforming to the requirements of the draft European Standard for Metal Shells (ENV 1993-1-6, 1999);
C. Two different buckling phenomena were again found;
D. The boundaries between the buckling phenomena were found and expressed in the form of empirical formulae;
E. Material non-linearity has little influence on practical applications because of the high R/t ratio and the quality of real construction;
F. A comparison of the boundaries between the two buckling phenomena shows that the bounds for GNA and GNIA analyses cannot be distinguished because they are very close to each other. Hence only two empirical expressions were given for these boundaries: one for linear eigenvalues and the other for non-linear analyses.

9.2.5 Shell Buckling Strength under Localised Axial Compression: Effect on Load Zone Height

Another full parametric study, which examined the effect of non-uniform loading on the buckling strength of geometrically perfect and imperfect shells focusing on the rate of decay of compression in the axial direction from the point of maximum stress. Local axisymmetric welding imperfections were used in conjunction with several different analyses types. The chapter produced a revised set of empirical equations for different analyses types (LA/LEA, GNA, GNIA).

As another half of the full analyses in the local axial compression of the shell buckling, the effect of the meridional extent of the compression zone was explored. A similar conclusion can be drawn from the results of the parametric analyses here: irrespective of which feature is explored, the meridional extent of the compression zone or the circumferential extent of the compression zone, with or without geometric imperfections, in all cases the buckling of cylinders under non-uniform axial compression can be divided into Strip Edge buckles and Strip Centre buckles due to their separate buckling mechanisms and the conclusions are:

A. Parametric studies lead to simple empirical equations on the shell buckling prediction of the non-uniform axial compression height;
B. Empirical equations are obtained using three different analyses types conforming to the requirement of draft European Standard for Metal Shells (ENV 1993-1-6, 1999);
C. The notion of two different buckling phenomena in the local axial compression has been proved again.

9.2.6 Characterisation of the Stress Pattern around the circumferences

Very high local bending stresses do not always affect the strength much provided satisfactory boundary conditions and/or equilibrium are met. The stress pattern around the circumference has been studied to explore the relationship between local high stresses and buckling strength. A comparison of the two different approaches, current code and the finite element analyses results describing this phenomenon has been provided to

characterise the shape of a local axial stress peak in a shell at a key point. A summary of conclusions reached is:

A. A new approach is described to deal with stress pattern around the mid-plane circumference, to interpret the criterion of buckling failure under the local high axial compression and a comparison of the other two approaches has been shown;
B. The classification of two types is provided due to the different stress distribution around circumference.

9.3 Outlook

This thesis has produced a series of design charts and design formulae to identify safe working loads, failure criteria and failure mechanisms for the buckling strength of steel thin cylindrical shells under elevated local axial compression. More data needs to be collected in order to clarify the relationships between the empirical predictions equations of this thesis and their application to real stress states.

In addition, the effect of internal pressure on the buckling strength needs consideration. The strip load applied here is limited in application, though it gives a safe conservative treatment of the shell strength. All the calculations of this thesis ignored the strengthening effect of internal pressure, even though the buckling strength increases markedly with internal pressure and can even reach the classic value.

Some recent studies have also shown that a local decrease of internal pressure can cause an increase in the axial membrane stress either near the mid-height or at the bottom of the shell. Thus, a systematic exploration of shell buckling under the combination of a strip load and non-axisymmetric internal pressure is needed. In such cases, more efforts are needed to obtain these different types of local load in order to give a more complete understanding of the buckling behaviour under local stresses states.

Further, non-axisymmetric boundary conditions arising from discrete column supports must also be considered. Because of the convenience of usage in practice, column supported cylinders are more common in industry. A locally supported silo in service is

References

Allen, H. G. and Bulson, P. S. (1980) "Background to buckling", McGraw-Hill, London, England.

Almroth, B. O. (1963) "Postbuckling behavior of axially compressed circular cylinders", *Journal of the American Institute of Aeronautics and Astronautics*, March, Vol. 1, No. 3, pp. 630-633.

Almroth, B. O. (1966a) "Influence of edge conditions on the stability of axially compressed cylindrical shells", *Journal of the American Institute of Aeronautics and Astronautics*, Vol. 4, No. 1, pp 134-140.

Almroth, B. O. (1966b) "Influences of imperfections and edge restraints on the buckling of cylindrical shells under axial compression", CR-432, NASA.

Almroth, B. O., Burns, A.B. and Pittner, E.V. (1970) "Design criteria for axially loaded cylindrical shells", *Journal of Spacecraft & Rockets*, June, Vol. 7, No. 6, pp. 714-720.

Amazigo, J. C. (1969) "Buckling under axial compression of long cylindrical shells with random axisymmetric imperfections", *Quart. Appl. Math.*, Vol. 26, pp 537-566.

Amazigo, J. C. (1974) "Buckling of stochastically imperfect structures", *in Buckling of Structures*, edited by Budiansky, Springer, New York, pp 172-182.

Amazigo, J. C. and Budiansky, B. (1972) "Asymptotic formulas for the buckling stresses of axially compressed cylinders with localised or random axisymmetric imperfections", *Journal of Applied Mechanics*, Vol. 39, Series E, No. 1, pp 179-184.

Ansourian, P. (1992) "On the buckling analysis and design of silos and tanks", *J. Construct. Steel Research*, Vol. 23, pp 273-294.

Ansourian, P. and Rotter, J. M. (1981) "Buckling: Vertical load", *in Structural Aspects of Metal Silos and Tanks*, School of Civil and Mining Engineering, University of Sydney, Aug., pp 10.1-10.24.

API 620 (1978) "Recommended rules for the design and construction of large, welded, low-pressure storage tanks", *American Petroleum Institute*, 6th Edn, Washington, D.C.

Arbocz, J. (1974) "The effect of initial imperfections on shell stability", *in Thin Shell Structures*, edited by Y.C. Fung and E.E. Sechler, Prentice Hall, pp 205-246.

Arbocz, J. (1982) "The imperfection data bank: A means to obtain realistic buckling loads", *in Buckling of Shells*, edited by E. Ramm, Springer-Verlag, Berlin 1982, pp 535-567.

Arbocz, J. (1983) "Shell stability analysis: Theory and practice", *in Collapse*, edited by J. M. T. Thompson and G. W. Hunt, Cambridge University Press, Cambridge, England, pp 43-74.

Arbocz, J. (1987) "On improved design procedures for thin-walled buckling sensitive shell structures", *Proc. Int. Colloquium on the Stability of Plate and Shell Structures*, Gent, Belgium, 6-8 April, ECCS, pp 255-260.

Arbocz, J. and Babcock, C. D. Jr (1969) "The effect of general imperfections on the buckling of cylindrical shells", *Journal of Applied Mechanics*, Vol. 36, pp 28-38.

Arbocz, J. and Sechler, E. E. (1974) "On the buckling of axially compressed imperfect cylindrical shells", *Journal of Applied Mechanics*, Transactions of the American Society of Mechanical Engineers, Vol. 41, pp 737-743.

Arbocz, J. and Williams, J. G. (1977) "Imperfection surveys on a 10-ft-diameter shell structure", *Journal of the American Institute of Aeronautics and Astronautics*, July, Vol. 15, No. 7, pp. 949-956.

Babcock, J. and Sechler, E. E., (1963) "The effect of initial imperfections on the buckling stress of cylindrical shells", NASA TN D-2005.

Baker, E. H., Kovalevsky, L. and Rish, F. L., (1972) "Structural analysis of shells", McGraw Hill.

Ball, R. E. (1968) "A geometrically non-linear analysis of arbitrarily loaded shells of revolution", United States National Aeronautics and Space Administration, Contract Report 909, January.

Ball, R. E. (1972) "A program for the static and dynamic analysis of arbitrarily loaded shells of revolution", *Computers and Structures*, Vol. 2, pp 141-162.

Berry, P. A. (1997) "Buckling under axial compression of cylindrical shells with circumferential weld shrinkage depression", PhD thesis, The University of Sydney, March.

Berry, P. A. and Rotter, J. M. (1996) "Partial axisymmetric imperfections and their effect on the buckling strength of axially compressed cylinders", *Imperfections in Metal Silos Workshop*, edited by Jullien, J.F., INSA Lyon, April, pp 35-48

Berry, P. A., Bridge, R. Q. and Rotter, J. M. (1999) "Characterising asymmetry of the initial imperfections in steel silos", *Mechanics of Structures and Materials*, edited by M. A. Bradford, R. Q. Bridge and S. J. Foster, Balkema, Rotterdam, pp. 233-238.

Bijlaard, P. P. (1954) "Stresses from radial loads in cylindrical pressure vessels", *Welding Journal (Supplement)*, Vol. 33, December, pp 615s-623s.

Bijlaard, P. P. (1955) "Stresses from local loadings in cylindrical pressure vessels", *Transaction of ASME*, Vol. 77, August, pp 805-816.

Bijlaard, P. P. (1955) "Stresses from radial loads and external moments in cylindrical pressure vessels", *Welding Journal*, Vol. 34, December, pp 608-617.

Bijlaard, D.L. and Gallagher, R.H. (1959) "Elastic instability of a cylindrical shell under arbitrary circumferential variation of axial stresses", *Journal of the Aerospace Sciences*, 27(11), pp 854-858, 866.

Bodarski, Z., Hotala, E. and Pasternak, H., (1982) "Zum Einfluss der Biegedrillsteifigkeit des Fussrings auf den Storungsbereich im Mantel von Metalsilos", *Bauingenieur*, Vol. 57, pp 423-427.

Bornscheuer, F. W. (1982) "To the problem of buckling safety of shells in the plastic range", *in "Buckling of Shells: Proceedings of a State-of-the-Art Colloquium"*, edited by E. Ramm, Springer-Verlag, Berlin, pp 601-619.

Bornscheuer, F. W. and Hafner, L., (1983a) "The influence of an imperfect circumferential weld on the buckling strength of axially loaded circular cylindrical shells", *Prelim. Report, 3rd Internat. Coll. on Stability of Metal Structures*, Paris, Nov., pp 407-414.

Bornscheuer F. W., Häfner L. and Ramm E. (1983b) "Zur Stabilität eines Kreiszylinders mit einer Rundschweissnaht unter Axialbelastung", *Der Stahlbau*, Vol. 10, pp 313-318.

Bridge, R. Q. and Pircher, M. (2001) "Buckling and post-buckling of cylindrical shells with circumferential weld imperfections subjected to axial load", *Festschrift Richard Greiner, Celebration volume for the 60th birthday of Prof. Richard Greiner*, TU Graz, Austria, October pp 53-62.

Brush, D. O. and Almroth, B. O., (1976) "Buckling of bars, plates and shells", McGraw-Hill, New York.

Bucklin, R.A., Ross, I.J. and White, G.M. (1983) "The influence of grain pressure on the buckling loads of thin-walled bins", 1983 Summer Meeting, *American Society of Agricultural Engineers*, Paper No. 83-4005, Bozeman, Montana, June 1983.

Buckling of thin-walled circular cylinders, NASA SP8007, 1968.

Budiansky, B. (1959) "Buckling of Clamped Shallow Spherical Shells", *Proceedings, IUTAM Symposium on Theory of Thin Elastic Shells*, Edited by W.T. Koiter, Delft, 1959, North Holland, Amsterdam, 1960, pp 64-94.

Budiansky, B. (1969) "Post-buckling behaviour of cylinders in torsion", *Pro. Second IUTAM Symposium on the Theory of Thin Shells*, Copenhagen, edited by F. I. Niordson, Springer-Verlag, pp 212-233.

Budiansky, B. and Hutchinson, J. W. (1972) "Buckling of circular cylindrical shells under axial compression", *in Contribution to the Theory of Aircraft Structures*, presented tp A. Van der Neut, Delft University Press, pp 239-259.

Bushnell, D. (1981) "Buckling of shells - Pitfall for designers", *Journal of the American Institute of Aeronautics and Astronautics*, Vol. 19, No. 9, September, pp 1183-1226.

Bushnell, D. (1985) "Computerized buckling analysis of shells", Dordrecht.

Cai, M. J., Holst, J. M. F .G. and Rotter, J. M. (2002) "Buckling Strength of Thin Cylindrical Shells under Localized Axial Compression", *the 15th Engineering Mechanics Division Conference of ASCE*, New York, USA, June 2002, pp 87-102.

Cai, M.J., Holst, J.M.F.G. and Rotter, J.M. (2003a) "Parametric Study on the Buckling of Thin Steel Cylindrical Shells under Elevated Axial Compression Stresses", the 16th Engineering Mechanics Conference, University of Washington, Seattle, July 16-18th, 2003.

Cai, M.J., Holst, J.M.F.G. and Rotter, J.M. (2003b) "Buckling of Cylindrical Tank Shells under Local Axial Compression Stresses", Internal Conference on Design, Inspection, Maintenance and Operation of Cylindrical Steel Tanks and Pipelines, Under the auspices of ECCS, Prague-Kralupy nad Vltavou, Czech Republic, October 8-11th, 2003, pp 70-76.

Calladine, C. R. (1983) "Theory of Shell Structures", Cambridge University Press, Cambridge.

Calladine, C. R. (1995) "Understanding imperfection-Sensitivity in the buckling of thin-walled shells", *Thin-Walled Structures*, Vol. 23, pp 215-235.

Coleman, R., Ding, X. L. and Rotter, J. M. (1992) "The Measurement of Imperfections in Full-Scale Steel Silos", *Proc., 4th Int Conf Bulk Matls Storage Handling and Transptn, IEAust.*, Wollongong, June 1992, pp 467-472.

Deml, M. and Wunderlich, W. (1997) "Direct evaluation of the 'worst' imperfection shape in shell buckling", *Computer methods in applied mechanics and engineering*, Vol. 149, 1997, pp 201-222.

Ding, X. L. (1992) "Precise Engineering Surveying - Application to the Measurement of Large Scale Steel Silos", PhD Thesis, University of Sydney, Australia, July 1992, 252 pp

Donnell, L. H. and Wan, C. C. (1950) "Effect of imperfections on buckling of thin cylinders and columns under axial compression", *Journal of Applied Mechanics*, Transactions of the American Society of Mechanical Engineers, Vol. 17, pp 73-83.

ENV1993-1-6 (1999) *European Pre-standard CEN/TC 250/SC3/PT4 Euro-code 3 Part1.6: Design of steel structures general rules: Supplementary rules for shell structures.* European Committee for Standardisation, rue de Stassart 36, Brussels.

ENV1993-4-1 (1999) *European Pre-standard CEN/TC 250/SC3/PT4 Euro-code 3 Part4.1: Design of steel structures: Silos.* European Committee for Standardisation, rue de Stassart 36, Brussels.

FEA (2002) *LUSAS Modeller User Manual,* FEA Ltd, Forge House, 66 High Street, Kingston upon Thames, UK, Version 13.4-5 edition.

Fischer, G. (1963) "Über den Einfluss der gelenkigen Lagerungauf die Stabilitat dunnwandiger Kreizylinderschlen unter Axiallast und Innendruck", *Z. f. Flügwissenschaften*, Vol. 11, pp 111-119.

Fischer, G. (1965) "Influence of boundary conditions on stability of thin-walled cylindrical shells under axial load and internal pressure", *AIAA Journal*, Vol. 3, pp 736-738.

Flügge, W. (1973) "Stresses in Shells", 2nd edn, Springer-Verlag, Berlin.

Fung, Y. C. and Sechler, E. E. (1957) "Buckling of thin-walled circular cylinders under axial compression and internal pressure", *J. Aeronat. Sci.*, Vol. 24, No. 5, pp 351-356.

Gerard, G. (1957) "Plastic stability of thin shells", *J. Aeronat. Sci.*, Vol. 24, No. 4, pp 269-274.

Guggenberger, W. (1996) "Effect of geometric imperfections taking into account the fabrication process and consistent residual stress fields of cylinders under local axial loads", *Imperfections in Metal Silos Workshop*, edited by Jullien, J.F., INSA Lyon, April, pp 217-228.

Guggenberger, W., Greiner, R. and Rotter, J.M. (2000) "The Behaviour of Locally-Supported Cylindrical Shells: Unstiffened Shells", *Journal of Constructional Steel Research*, Vol. 56, 2, Nov, pp 175-197.

Harris, L. A., Suer, H. S., Skene, W. T. and Benjamin, R. J. (1957) "The stability of thin-walled unstiffened circular cylinders under axial compression including the effects of internal pressure", *J. Aeronat. Sci.*, Vol. 24, No. 8, pp 587-596.

Hayes, J. C. & Lee, L. H. N. (1970) "Inelastic buckling of axisymmetric shells", *Journal of the Engineering Mechanics Division*, Vol. 96, No. EM6, pp 1107-1122.

HKS (1998) *ABAQUS/Standard User's Manual,* Hibbitt, Karlsson & Sorensen, Inc., Pawtucket, Rhode Island, USA, Version 5.8 edition.

Hodge, P. G. Jr. (1956) "Displacements in an elastic-plastic cylindrical shell", *Journal of Applied Mechanics*, ASME, Vol. 23, pp 73-79.

Hoff, N. J. (1965) "Low buckling stresses of axially compressed circular cylindrical shells of finite length", *Journal of Applied Mechanics*, ASME, Vol. 32, pp 533-541.

Hoff, N. J. and Rehfield, W. (1965) "Buckling of axially compressed circular cylindrical shells at stresses smaller than the classical critical value", *Journal of Applied Mechanics*, ASME, Vol. 32, pp 542-546.

Hoff, N. J. and Soong, T. C. (1965) "Buckling of circular cylindrical shells in axial compression", *International Journal of Mechanics Sciences*, Vol. 7, pp. 489-520.

Holst, J. M. F. G., Rotter, J. M. and Calladine, C. R. (1999) "Imperfections in cylindrical shells resulting from fabrication misfits", *J. Eng. Mechanics*, Vol. 125, No. 4, pp 410-418.

Holst, J. M. F. G., Rotter, J. M. and Calladine, C. R. (2000) "Imperfections and buckling in cylindrical shells with consistent residual stresses", *J. Construct. Steel Research*, Vol. 54, pp 265-282.

Hutchinson, J. W. (1967) "Imperfection-sensitivity of externally pressurized spherical shells", *Journal of Applied Mechanics*, ASME, Vol. 34, pp 49-55.

Hutchinson, J. W., Tennyson, R. C. and Muggeridge, D. B. (1971) "Effect of a Local Axisymmetric Imperfection on the Buckling Behaviour of a Circular Cylindrical Shell under Axial Compression", *AIAA Jnl*, Vol. 9, No. 1, Jan., pp 48-53.

Ilyushin, A. A. (1943) "Some problems of the theory of plastic deformations", *Prikl. Mat. Meckh.*, Vol. 7, pp 245-272.

Ilyushin, A.A. (1944) "An approximate theory of elastic-plastic deformations of axially symmetric shells", *Prikl. Mat. Meckh.*, Vol. 8, pp 15-24.

Janssen, H. A. (1895) "Versuche über getreidedruck in Silozellen", *Zeitschrift des Vereines Deutscher Ingenieuer*, Vol. 39, No. 35, pp 1045-1049.

Jenike, A. W., Johanson, J. R. and Carson, J. W. (1973) "Bin loads-part 3: mass flow bins", *Jnl. Engng Industry*, ASME, Vol. 95, Series B, No. 1, pp 6-12.

Kármán, T. v., Dunn, L. G. & Tsien, H. –S. (1940) "The influence of curvature on the buckling characteristics of structures", *Journal Aeronaut. Sci.*, Vol. 7, pp 276-289.

Klement, P. (1962) "Theorie der Elastisch-Plastischen Zylinderschale", *Oester. Ing.-Archiv.*, Vol. 16, pp 199-211.

Knoedel, P. and Schulz, U. (1992) "Buckling of cylindrical bins – recent results", *Proc., International Conference: "Silos-Forschung und Praxis*, Universität Karlsruhe, October, pp 75-82.

Knoedel, P. and Ummenhofer, T. (1996) "Substitute imperfections for the prediction of buckling loads in shell design", *Proc. International Workshop on Imperfections in Metal Silos*, CA-Silos, Lyon, France, 19 April, pp 87-102.

Knoedel, P., Ummenhofer, T. and Schulz, U. (1995) "On the modelling of different types of imperfections in silo shells", *Thin-Walled Structures*, Vol. 23, pp 283-293.

Koiter, W. (1945) "The stability of elastic equilibrium", PhD Thesis, Technische Hooge School, Delft. English translation by E. Riks, 1970: Technical report AFFDL-TR-70-25, Air Force Flight Dynamics Laboratory, Air Force System Command, Wright Patterson Air Force Base, Ohio.

Koiter, W. (1963) "The effect of axisymmetric imperfection on the buckling of cylindrical shells under axial compression", edited by Koiter, W.T., *Proceedings of Koninklijke Nederlandse Akademie van Wetenschappen,* Vol. 66, Series B, pp 265-279.

Li H. Y. (1994) "Analysis of steel silo structures on discrete supports", PhD thesis, The University of Edinburgh, September.

Libai, A. and Durban, D. (1977) "Buckling of cylindrical shells subjected to nonuniform axial loads", *J. Appl. Mech.*, Vol. 44, No. 4, Trans. ASME, Dec., pp 714-720.

Lorenz, R. (1908) *Z. Ver. Deut. Ingr,* Vol. 52, pp. 1766.

Martens, P. (1988) (Ed. Martens, P.) "Silo-Handbuch", Ernst & Sohn, Berlin, Germany.

Murphy, L. M. & Lee, L. H. N. (1971) "Inelastic buckling prcess of axially compressed cylindrical shells subject to edge constraints", *International Journal of Solids and Structures*, Vol. 7, pp 1153-1170.

Nanninga, N. (1956) "Gibt die übliche Berechnungsart der Drücke auf die Wande und den Boden von Silobauten Sichere Ergebnisse", *Der Ingenieur,* Vol. 68, No. 44, Nov.

Nielsen, J. (1983) "Load distribution in silos influenced by anisotropic grain behaviour", *Proc., International Conference on Bulk Materials Storage, Handling and Transportation*, Institution of Engineers, Australia, Newcastle, August, pp 226-230.

Ohira, H. (1961) "Local buckling theory of axially compressed cylinders", *Procedings, 11th Japanese National Congress on Applied Mechanics*, pp 37-41.

Ohira, H. (1963) "Linear local buckling theory of axially compressed cylinders and various eigenvalues", *Procedings, 5th International Symposium on Space Technology and Science*, Tokyo, pp 511-526.

Ooi, J. Y. and She, K. M. (1997) "Finite element analysis of wall pressure in imperfect silos", *Int. J. Solids Structures*, Vol. 34, No. 16, pp 2061-2072.

Ooi, J. Y., Pham, L. and Rotter, J. M. (1990) "Systematic and random features of measured pressures on full-scale silo walls", *Eng. Struct.,* Vol. 12, No. 2, pp 74-87.

Peter, J. (1974) "Zur Stabilität von Kreiszylinderschalen unter Ungleich-maßig Verteilten Axialen Randbelastungen", PhD Dissertation, Technical University of Hanover, Germany.

Pieper, K. (1969) "Investigation of silo loads in measuring models", *Journal of Engineering for Industry*, pp 365-372.

Riks, E. (1979) "An incremental approach to the solution of snapping and buckling problems", *International Journal of Solids and Structures*, Vol. 5, pp 529-551.

Roth, R. S. (1961) "Plastic buckling of thin shallow spherical shells", PhD thesis, Harvard University, Aug.

Rotter, J.M. (1985a) "Stability problems in cylindrical bins under axial compression", *Proceedings, Joint US/Australian Workshop on the Loading, Analysis and Stability of Thin Shell Bins, Tanks and Silos*, University of Sydney, March, pp 106-117.

Rotter, J.M. (1985b) "Buckling of ground-supported cylindrical steel bins under vertical compressive wall loads", *Proc., Metal Structures Conference*, Institution of Engineers Australia, Melbourne, May, pp 112-127.

Rotter, J. M. (1986a) "On the specification of loads for the structural design of bins and silos", *Proc., Second International Conference on Bulk Materials Storage Handling and Transportation*, Institution of Engineers, Australia, Wollongong, pp 82-88.

Rotter, J. M. (1986b) "The analysis of steel bins subject to eccentric discharge", *Proc., Second International Conference on Bulk Materials Storage, Handling and Transportation*, Institution of Engineers, Australia, Wollongong, pp 264-271.

Rotter, J.M. (1987a) "Membrane Theory of Shells for Bins and Silos", *Transactions of Mechanical Engineering, Institution of Engineers, Australia*, Vol. ME12 No.3 September, pp 135-147.

Rotter, J.M. (1987b) "Bending Theory of Shells for Bins and Silos", *Transactions of Mechanical Engineering, Institution of Engineers*, Australia, Vol. ME12 No.3 September, pp 147-159.

Rotter, J. M. (1995) "Challenges for the future in the design of bulk solid storages", *IABSE Colloquium on reliable containment for the future*, 11/12 July, Pembroke College, Cambridge.

Rotter, J. M. (1996a) "Elastic plastic buckling and collapse in internally pressurised axially compressed silo cylinders with measured axisymmetric imperfections: interactions between imperfections, residual stresses and collapse", *Proc. International Workshop on Imperfections in Metal Silos: Measurement, Characterisation and Strength Analysis*, CA-Silos, Lyon, France, 19 April, pp 119-140.

Rotter, J. M. (1996b) "Shell structures: design standard, recent progress and unsolved problems", Invited plenary paper, *Proc. International Conference on Structural Steelwork*, Hong Kong, December 1996, pp 621-636.

Rotter, J.M. (1997) "Design standards and calculations for imperfect pressurised axially compressed cylinders", *International Conference on Carrying Capacity of Steel Shell Structures*, Czech Republic, Brno, pp 354-360.

Rotter, J.M. (1998) "Shell structures: the new European standard and current research needs", *Thin-Walled Structures*, Vol. 31, pp 3-23.

Rotter, J.M. (1999a) "Proposal for generalisation of the elastic-plastic buckling interaction rule from Eurocode 3 Part 1.6", submission to CEN TC250/SC3/PT4 and ECCS TWG8.4 Buckling of Shells, March 1999, 8 pp.

Rotter, J.M. (1999b) "Flow and pressures in silo structural integrity assessments", *Proc., International Symposium: Reliable Flow of Particulate Solids III*, Porsgrunn, Norway, Aug 1999, pp 281-292.

Rotter, J.M. (2001a) "Pressures, Stresses and Buckling in Metal Silo containing Eccentrically Discharging Solids", *Festschrift Richard Greiner, Celebration volume for the 60th birthday of Professor Richard Greiner,* TU Graz, October, pp 85-104.

Rotter, J. M. (2001b) "Guide for the economic design of circular metal silos", Spon, London, 235pp.

Rotter, J. M. (2002) "Shell buckling and collapse analysis for structural design: The new framework of the European Standard", *Proc. Festschrift for Professor Chris Calladine, Celebration volume for the 60th birthday of Prof. C.R. Calladine*, University of Cambridge, Sept, Cambridge.

Rotter, J.M. and Jumikis, P.T. (1985) "Elastic buckling of stiffened ringbeams for large elevated bins", *Proc., Metal Structures Conference*, Institution of Engineers Australia, Melbourne, May, pp 104-111.

Rotter, J. M. and Teng, J. G. (1989a) "Elastic stability of lap-jointed cylinders", *J. Struct. Engg,* ASCE, Vol. 115, No. 3, March, pp 683-697.

Rotter, J. M. and Teng, J. G. (1989b) "Elastic stability of cylindrical shells with weld depressions", *J. Struct. Engg,* ASCE, Vol. 115, No. 5, May, pp 1244-1263.

Rotter, J. M. and Zhang Q. (1990) "Elastic buckling of imperfect cylinders containing granular solids", *J. Struct. Engg*, ASCE, Vol. 116, No. 8, pp 2253-2271.

Rotter, J.M., Pham, L. and Nielsen, J. (1986) "On the specification of loads for the structural design of bins and silos", *Proc., Second International Conference on Bulk Materials Storage Handling and Transportation*, Institution of Engineers, Australia, Wollongong, pp 82-88.

Schnell, W. (1959) "Zur Stabilitat dunnwandiger Langsgedruckter Kreiszylinderschalen bei Zusatzlichem Innendruck", *Proc.,IUTAM Symposium on the Theory of Thin Elastic Shells,* Delft, Aug., pp 167-188.

Schmidt, H. (2000) "Stability of steel shell structures; General Report", *Journal of Constructional Steel Research,* Vol. 55, No. 1-3, pp 159-181.

Schmidt, H. and Winterstetter, T. A. (2001) "Substitute geometrical imperfections for the numerical buckling assessment of cylindrical shells under combined loading", *Proc. European Mechanics Conference: Euromech 424,* Rolduc-Kerkrade, Germany, September, pp 82-84.

Seide, P. (1962) "The stability under axial compression and lateral pressure of circular-cylindrical shells with a soft elastic core", *Journal of the Aerospace Sciences*, Vol. 29, No. 7, July 1962, pp 851-862.

Southwell, R. V. (1914) *Phil. Trans. Roy. Soc.,* Vol. 213, Series A, pp 187.

Stiglat, K. (1988) (Ed. Martens, P.) "Silo-Handbuch", Ernst & Sohn, Berlin, Germany.

Teng, J. G. (1990) "Buckling and collapse of shells and rings for steel silos", PhD thesis, The University of Sydney, March.

Teng, J.G. (1996) "Buckling of Thin Shells: Recent Advances and Trends", *Applied Mechanics Reviews*, ASME, Vol. 49, No. 4, April, pp 263-274.

Teng, J. G. and Rotter, J. M. (1992) "Buckling of pressurized axisymmetrically imperfect cylinders under axial loads", *J. Eng. Mechanics,* Vol. 118, No. 2, pp 229-247.

Teng, J.G. and Song, C.Y. (2001) "Numerical Models for Nonlinear Analysis of Elastic Shells with Eigenmode-Affine Imperfections", *International Journal of Solids and Structures*, Vol. 38, No. 18, May, pp. 3263-3280.

Timoshenko, S. P. (1910) *Z. Math. Physik,* Vol. 58, pp 378.

Timoshenko, S.P. (1953) "History of Strength of Materials", McGraw-Hill, New York.

Timoshenko, S.P. and Gere, J.M. (1961) "Theory of Elastic Stability", 2nd edn, McGraw-Hill, New York.

Trahair, N. S., Abel, A., Ansourian, P., Irvine, H. M. and Rotter, J. M. (1983) "Structural design of steel bins for bulk solids", *Australian Institute of Steel Construction*, November, Sydney.

Tsurkov, I. S. (1956) "On elastic-plastic equilibrium of shells of revolution for small axisymmetric deformations", *Izwestya AN SSST*, OTN, No. 11, pp 106-110.

Tsurkov, I. S. (1961) "Elastic-plastic deformations at the clamped end of a thin cylinder", *Inzh. Sborn.*, OTN, Vol. 31, pp 93-100.

Weingarten, V. I. (1962) "The buckling of cylinderical shells under longitudinally varying loads", *Journal of Applied Mechanics*, ASME, Vol. 29, Series E, pp 81-85.

Walker, D. M. (1966) "An approximate theory for pressure and arching in hoppers", *Chemical Engineering Science*, Vol. 21, pp 975-997.

Walters, J. K. (1973) "A theoretical analysis of stresses in silos with vertical walls", *Chemical Engineering Science*, Vol. 28, pp 13-21.

Yamaki, N. (1984) "Elastic stability of circular cylindrical shells", North-Holland, Amsterdam, The Netherlands.

Yamaki, N. and Kodama, S. (1972) "Buckling of circular cylindrical shells under compression", Report 3, (Solutions based on the Donnell type equations considering prebuckling edge rotations), Report of the Institute of High Speed Mechanics, No. 25, Tohoku University, pp 99-141.

Young, T. (1807) "Course of lectures on natural philosophy and the mechanical arts", Vol. 2, Section 323, London.

Zienkiewicz, O. C. (1967) "The finite element method", McGraw-Hill, London, U.K.

Appendix

NOTATION

The following notation is used in this thesis. All symbols are defined where they first appear in the text. In general, only one meaning is assigned to each symbol, but in those cases where more than one meaning is possible, the correct one will be evident from the context in which it is used.

A Latin letters

a	vector of nodal displacement
A	area/the plan cross-sectional area of the barrel section
B	strain-displacement matrix
D	matrix of elastic constants
e	element
E	Young's modulus of elasticity
g	dimensionless axial stress gradient = $(d\sigma_{n,z}/dz)(R/\sigma_{n,cr})$
h	half height of strip load/ shell thickness
H	length/ height of total modelled cylinder
K	structure stiffness matrix
L	length of the column/ height of total modelled cylinder
N	Reaction force (Yamaki, 1984)
n	localisation parameter
P	current axial compressive load
r	radial coordinate/ the circular silo radius
R	structure force vector/ middle surface radius of cylindrical shell/ resistance
t	shell thickness
T	transpose of the matrix
u	axial displacement component
U	is the plan cross-sectional perimeter of the barrel section
v	circumferential displacement component
V	volume of the structure members

w radial displacement component/amplitude of the imperfection

w_0 a measure of the geometrical imperfection of the shell in its initial, unloaded condition

z axial coordinate with origin at mid-plane of cylinder/ the distance below the equivalent surface of the solid at maximum filling height (full condition)

B Greek letters

β plastic range factor

δ size of imperfection at a given axial coordinate z

δ_0 initial amplitude of an axisymmetric imperfection

η dimensionless membrane stress

λ imperfection half wavelength/ the lateral pressure ratio (ratio between horizontal stress and mean vertical stress in the stored solid)

$\lambda/\ \bar{\lambda}$ relative slenderness ($\bar{\lambda}=\sqrt{R_{pl}/R_{cr}}$)

λ_0 linear meridional bending half wavelength $\approx 2.44(Rt)^{1/2}$/ squash limit relative slenderness

λ_{cl} classical elastic axisymmetric buckling half wavelength $\approx 1.73(Rt)^{1/2}$

$\lambda_p/\ \bar{\lambda}_p$ plastic limit relative slenderness ($\bar{\lambda}_p=\sqrt{\frac{\alpha}{1-\beta}}$)

γ is the upper characteristic value of the solid unit weight γ_u

ν Poisson's ratio

θ circumferential coordinate

ϕ dimensionless strip load extent/characteristic inverse strip half angle (expression 1) $= \theta_n^{-1}(R/t)^{-2/3}((d\sigma_{n,z}/dz)(R/\sigma_{n,cr}))^{-1/3}$

Π dimensionless strip load extent/characteristic inverse strip half angle (expression 2) $= \theta_n^{-1}(R/t)^{-1/3}((d\sigma_{n,z}/dz)(R/\sigma_{n,cr}))^{4/3}$

σ stress

ξ dimensionless inverse strip half load angle $= \theta_n^{-1}(R/t)^{-2/3}$

χ dimensionless strip half load angle, which is reciprocal of $\xi = \theta_n(R/t)^{2/3}$/ relative buckling strength ($\chi=R/R_{pl}$)

ϑ dimensionless angle at the maximum axial membrane stress $= \theta_i/\theta_n$

ς dimensionless angle while membrane stress decreases first to zero from the centre of strip load $= \theta_0/\theta_n$

μ is the wall friction coefficient for the barrel section

C Subscripts

0	maximum stress around the circumference/initial state
1	first state/ correspond to the infinitesimal increments during buckling, which are generally considered to be functions of both x and y (Yamaki, 1984)
b	bending
cl	classical
cr	critical
e	elastic
E	Euler load
ep	elastic-plastic
l	linear
m	membrane
min	minimum
n	nominal
nl	non-linear
p/pl	plastic
z	axial direction
θ	circumferential direction

PROGRAMS

The following programs were used in this thesis to construct the ABAQUS master input file, the node file, the element file and the two loading-case files. Contributions to the following Master ABAQUS input program from Guggenberger, O'fner & Holst is gratefully acknowledged by the author.

A Master ABAQUS Input Program

```
*HEADING
 RIKS ANALYSIS OF IMPERFECT CYLINDER BUCKLING UNDER PARTIAL
 AXIAL LOAD ONLY 15-10-PI-{j_}.RIKSN
**********************************************************************
 PARTIAL LOAD + IMPERFECTION=PI
*****************Parameter Output ************************************
*PARAMETER,NAME=j_, LOOP=1,INDEX=(1,8)
 1000,800,600,400,250,150,125,100
*PARAMETER,NAME=j,  LOOP=1,INDEX=(1,8),DATA CARD
 1000
 800
 600
 400
 250
 150
 125
 100
*PARAMETER,NAME=s_, LOOP=1,INDEX=(1,8)
 0.0080666666,0.010083332,0.013444443,0.020166665
 0.032266664, 0.053777773,0.064533328,0.08066666
**********************************************************************
*CREATE STANDARD INPUTFILES,NAME=15-10-PI-{j_}.RIKSN
```

```
**********************************************************************
*NODE,SYSTEM=C,NSET=ALL,INPUT={j_}IMPER100.0RI.NOD
**      INCLUDE DATA GENERATED BY PROGRAM
**      s15.180F-{j_}I100.0RI.f
*NSET,NSET=BND1,GENERATE
 2500000,4000000,15000
*NSET,NSET=BND2,GENERATE
 2500360,4000360,15000
*NSET,NSET=BND,GENERATE
 2500000,2500360,1
*NSET,NSET=LOADB,GENERATE
 4000000,4000360,1
*TRANSFORM,TYPE=C,NSET=ALL
 0.,0.,0., 0.,0.,1.
**********ELEMENT*************************************************
*ELEMENT,TYPE=S4R5,INPUT=CONVERs10L15000.ELE,ELSET=EALL
*ELEMENT,TYPE=S4R5,INPUT=STRIPs10L15000.ELE, ELSET=ESTRIP
*ELEMENT,TYPE=S4R5,INPUT=PATCHs10L15000.ELE, ELSET=EPATCH
*SHELL SECTION,MATERIAL=STEEL,ELSET=EALL
 10
*MATERIAL,NAME=STEEL
*ELASTIC
 200.E3,.3
**************BOUNDARY*****************************************
*BOUNDARY
 BND1,YSYMM
 BND2,YSYMM
 BND,ZSYMM
 LOADB,1,2
 LOADB,4
 LOADB,6
```

```
**************PROCEDURE*****************************************
*STEP,NLGEOM,INC=99
*STATIC,RIKS
 .001,1.,,0.01,,2500000,3,5
*DLOAD
 ESTRIP,BZ,-{s_}
*PREPRINT,ECHO=NO,HISTORY=NO,MODEL=NO
*NODE PRINT,FREQUENCY=0
*EL PRINT, FREQUENCY=0
*END STEP
```

B Fortran Nodes Construction Program

```
CC-----PROGRAM TO GENERATE HALF-LENGTH NODES IN CONVERGED
C       MESH FOR MODEL ANALYSIS
C
        OPEN(UNIT=15,STATUS='NEW',FILE='800IMPER0.0RI.NOD')
        ZI=10000.
        ZE=40000.
        N0=1
        ISTARTM0=0
        IENDM0=100
        DTHETA=0.5
        Z=ZE-ZI
        ZDELTA=Z*0.5/(N0*(IENDM0-ISTARTM0))
        ZDELTA0=N0*ZDELTA
        NDELTA0=INT(ZDELTA0*(IENDM0-ISTARTM0)/10)*1000
        NDST0= INT(ZI*100)
        NDST1= NDST0+NDELTA0
        ZI0=ZI
        ZE0=ZI0+(IENDM0-ISTARTM0)*ZDELTA0
        ZI1=ZE0
```

```
      ZE1=ZI1+(IENDM0-ISTARTM0)*ZDELTA0
      CALL NGENU(   0., DTHETA,NDST1,       0,     360,
     &  ISTARTM0, IENDM0, ZI1,  ZE1 ,ZDELTA0,   0.0)
      STOP
      END
C
      SUBROUTINE
     &  NGENU(THETA,DTHETA,NDST,ISTARTC,IENDC,ISTARTM,IENDM,
     &  ZI, ZE ,ZDELTA ,DELTA)
C
C     RR  = CYLINDER RADIUS
C     H    = CYLINDER THICKNESS
C     L    = CYLINDER LENGTH
C     STHETA = ANALYSIS ANGLE
C
      RR=8000.
      H=10.
      L=15000.
      STHETA=180.
      T=10.
      GAMA=0.3
      sleimta=0.707*(3.14159265*SQRT(RR*T))/((3*(1-GAMA*GAMA))**0.25)
      T=THETA
      NODE=NDST
      Z=ZI
      SNDELTA=INT(ZDELTA/10)*1000
      DO 60 I=ISTARTC,IENDC
      DO 40 J=ISTARTM,IENDM
      ZZ=3.14159265*(Z-ZI)/sleimta
      R=RR-DELTA*EXP(-1.0*ZZ)*(SIN(ZZ)+COS(ZZ))
      WRITE(15,10) NODE,R,THETA,Z
```

```
 10   FORMAT(I7,2(',',F11.5),',',F11.1)
      NODE=NODE+SNDELTA
      Z=Z+ZDELTA
 40   CONTINUE
      NDST=NDST+INT(2*DTHETA)
      NODE=NDST
      Z=ZI
      THETA=THETA+DTHETA
 60   CONTINUE
      THETA=T
      RETURN
      END
```

C Fortran Elements Construction Program

```
CC-----PROGRAM TO GENERATE HALF-LENGTH ELEMENTS IN
C      CONVERGED  MESH FOR MODEL ANALYSIS
C
C      IS   = THETA  OF STRIP LOAD
C      L    = LENGTH OF STRIP LOAD
C      n    = NUMBER OF DIVISION IN MERIDIONAL
C      m    = NUMBER OF DIVISION IN CIRCUMFERENTIAL
C      IT   = TOTAL    ELEMENTS
C
       DIMENSION NODE(4)
       DIMENSION IDM(6)
       DIMENSION IDMN(6)
       DIMENSION LM(6)
       DIMENSION LLM(7)
       DIMENSION IM(6)
       DIMENSION IIM(7)
       DIMENSION IDC(4)
```

```
      DIMENSION LC(4)
      DIMENSION LLC(5)
      DIMENSION IC(4)
      DIMENSION IIC(5)
      DIMENSION NO(4,6)
      OPEN(UNIT=15,STATUS='NEW',FILE='CONVERs15L15000.ELE')
      DATA IDM/1,2,1,2,10,1/
      DATA IDC/4,2,6,10/
      DO 5 I=1,6
      IDMN(I)=IDM(I)*15000
    5 CONTINUE
CCCCCCCCCCCCCCCCCCCCCCCCCCCCCCCCCCCCCCCCCCCCCCCCCCCCCCCCCCCCCCCCCC
      IS=15
      L=15000
CCCCCCCCCCCCCCCCCCCCCCCCCCCCCCCCCCCCCCCCCCCCCCCCCCCCCCCCCCCCCCCCCC
      n=L/150
      IF (n .GT. 95) GOTO 6
      n1=INT((n-18)/2)
      n2=INT((95-n)/2)
      n3=INT((92-n-2*n2)/10)
      n4=95-n-10*n3-2*n2
      n5=n-18-2*n1
      nt=23+n1+n2+n3+n4+n5
      IM(1)=15+n5
      IM(2)=n1
      IM(3)=3+n4
      IM(4)=n2
      IM(5)=n3
      IM(6)=5
      GOTO 7
    6 n1=INT((n-20)/2)
```

```
      n2=INT((95-n)/2)
      IF (n2 .LE. 0) n2=0
      n3=INT((95-n-2*n2)/10)
      IF (n3 .LE. 0) n3=0
      n4=95-n-10*n3-2*n2
      IF (n4 .LE. 0) n4=0
      n5=n-20-2*n1
      nt=20+n1+n2+n3+n4+n5
      IM(1)=15+n5
      IM(2)=n1
      IM(3)=n4
      IM(4)=n2
      IM(5)=n3
      IM(6)=5
7     m1=INT((IS-5)/2)
      IF (m1 .LE. 0) m1=0
      IF (m1 .LE. 0) IDC(1)=0
      IF (m1 .LE. 0) IC(1)=0
      m2=IS-m1*2
      m3=30+m2
      m4=INT((180-2*m1-m3)/3)
      IF (m4 .GE. 5) THEN
      m5=5
      m6=INT((165-2*m1-m3)/5)
      ELSE
      m5=m4
      m6=0
      END IF
      m3=180-m1*2-m5*3-m6*5
      mt=m1+m3+m5+m6
      IT=nt*mt
```

```
      IC(1)=m1
      IC(2)=m3
      IC(3)=m5
      IC(4)=m6
      LLM(1)=0
      IIM(1)=0
      LLC(1)=0
      IIC(1)=0
      DO 8 I=1,6
      LM(I)=IDMN(I)*IM(I)
      LLM(I+1)=LLM(I)+LM(I)
      IIM(I+1)=IIM(I)+IM(I)
 8    CONTINUE
      DO 10 I=1,4
      LC(I)=IDC(I)*IC(I)
      LLC(I+1)=LLC(I)+LC(I)
      IIC(I+1)=IIC(I)+IC(I)
10    CONTINUE
      IE=0
      DO 30 I=1,6
      DO 20 J=1,4
      IELE=1+IIC(J)+IE
      NODE(1)=2500000+LLM(I)+LLC(J)
      NODE(2)=NODE(1)+IDMN(I)
      NODE(3)=NODE(2)+IDC(J)
      NODE(4)=NODE(1)+IDC(J)
      IF (IM(I) .EQ. 0) GOTO 20
      IF (IC(J) .EQ. 0) GOTO 20
      CALL ELGEN(IELE, mt, NODE, IDC(J), IDMN(I), IC(J), IM(I))
20    CONTINUE
      IE=mt*IIM(I+1)
```

```
 30   CONTINUE
      STOP
      END
C
      SUBROUTINE
     & ELGEN(IELE, mt, NODE, IDC, IDMN, IC, IM)
      DIMENSION NODE(4)
      IELE0=IELE
      DO 60 I=1,IM
      DO 40 J=1,IC
      WRITE(15,10) IELE,NODE
 10   FORMAT(I4,4(',',I7))
      IELE=IELE+1
      NODE(1)=NODE(1)+IDC
      NODE(2)=NODE(2)+IDC
      NODE(3)=NODE(3)+IDC
      NODE(4)=NODE(4)+IDC
 40   CONTINUE
      NODE(1)=NODE(1)-IDC*IC+IDMN
      NODE(2)=NODE(2)-IDC*IC+IDMN
      NODE(3)=NODE(3)-IDC*IC+IDMN
      NODE(4)=NODE(4)-IDC*IC+IDMN
      IE0=IELE0+mt*I
      IELE=IE0
 60   CONTINUE
      RETURN
      END
```

D Fortran Load Case1 Construction Program (Top Load)

```
CC-----PROGRAM TO GENERATE TOP UNIFORM LOAD FOR MODEL
C      ANALYSIS
```

```
C
C       IS   = THETA  OF STRIP LOAD
C       L    = LENGTH OF STRIP LOAD
C       n    = NUMBER OF DIVISION IN MERIDIONAL
C       m    = NUMBER OF DIVISION IN CIRCUMFERENTIAL
C       IT   = TOTAL    ELEMENTS
C
        DIMENSION NODE(4)
        DIMENSION IDM(6)
        DIMENSION IDMN(6)
        DIMENSION LM(6)
        DIMENSION LLM(7)
        DIMENSION IM(6)
        DIMENSION IIM(7)
        DIMENSION IDC(4)
        DIMENSION LC(4)
        DIMENSION LLC(5)
        DIMENSION IC(4)
        DIMENSION IIC(5)
        DIMENSION NO(4,6)
        OPEN(UNIT=15,STATUS='NEW',FILE='PATCHs15L15000.ELE')
        DATA IDM/1,2,1,2,10,1/
        DATA IDC/4,2,6,10/
        DO 5 I=1,6
        IDMN(I)=IDM(I)*15000
    5   CONTINUE
CCCCCCCCCCCCCCCCCCCCCCCCCCCCCCCCCCCCCCCCCCCCCCCCCCCCCCCCCCCCCCCCCCC
        IS=15
        L=15000
CCCCCCCCCCCCCCCCCCCCCCCCCCCCCCCCCCCCCCCCCCCCCCCCCCCCCCCCCCCCCCCCCCC
        n=L/150
```

```
      IF (n .GT. 95) GOTO 6
      n1=INT((n-18)/2)
      n2=INT((95-n)/2)
      n3=INT((92-n-2*n2)/10)
      n4=95-n-10*n3-2*n2
      n5=n-18-2*n1
      nt=23+n1+n2+n3+n4+n5
      IM(1)=15+n5
      IM(2)=n1
      IM(3)=3+n4
      IM(4)=n2
      IM(5)=n3
      IM(6)=5
      GOTO 7
6     n1=INT((n-20)/2)
      n2=INT((95-n)/2)
      IF (n2 .LE. 0) n2=0
      n3=INT((95-n-2*n2)/10)
      IF (n3 .LE. 0) n3=0
      n4=95-n-10*n3-2*n2
      IF (n4 .LE. 0) n4=0
      n5=n-20-2*n1
      nt=20+n1+n2+n3+n4+n5
      IM(1)=15+n5
      IM(2)=n1
      IM(3)=n4
      IM(4)=n2
      IM(5)=n3
      IM(6)=5
7     m1=INT((IS-5)/2)
      IF (m1 .LE. 0) m1=0
```

```
      IF (m1 .EQ. 0) IDC(1)=0
      IF (m1 .EQ. 0) IC(1)=0
      m2=IS-m1*2
      m3=30+m2
      m4=INT((180-2*m1-m3)/3)
      IF (m4 .GE. 5) THEN
      m5=5
      m6=INT((165-2*m1-m3)/5)
      ELSE
      m5=m4
      m6=0
      END IF
      m3=180-m1*2-m5*3-m6*5
      mt=m1+m3+m5+m6
      IT=nt*mt
      IC(1)=m1
      IC(2)=m3
      IC(3)=m5
      IC(4)=m6
      LLM(1)=0
      IIM(1)=0
      LLC(1)=0
      IIC(1)=0
      DO 8 I=1,6
      LM(I)=IDMN(I)*IM(I)
      LLM(I+1)=LLM(I)+LM(I)
      IIM(I+1)=IIM(I)+IM(I)
8     CONTINUE
      DO 10 I=1,4
      LC(I)=IDC(I)*IC(I)
      LLC(I+1)=LLC(I)+LC(I)
```

```
      IIC(I+1)=IIC(I)+IC(I)
   10 CONTINUE
      IE=0
      DO 30 I=6,6
      DO 20 J=1,4
      IELE=1+IIC(J)+mt*(IIM(I+1)-1)
      NODE(1)=2500000+LLM(I+1)+LLC(J)-15000
      NODE(2)=NODE(1)+IDMN(I)
      NODE(3)=NODE(2)+IDC(J)
      NODE(4)=NODE(1)+IDC(J)
      IF (IM(I) .EQ. 0) GOTO 20
      IF (IC(J) .EQ. 0) GOTO 20
      CALL ELGEN(IELE, mt, NODE, IDC(J), IDMN(I), IC(J), 1)
   20 CONTINUE
   30 CONTINUE
      STOP
      END
C
      SUBROUTINE
     & ELGEN(IELE, mt, NODE, IDC, IDMN, IC, IM)
      DIMENSION NODE(4)
      IELE0=IELE
      DO 60 I=1,IM
      DO 40 J=1,IC
      WRITE(15,10) IELE,NODE
   10 FORMAT(I4,4(',',I7))
      IELE=IELE+1
      NODE(1)=NODE(1)+IDC
      NODE(2)=NODE(2)+IDC
      NODE(3)=NODE(3)+IDC
      NODE(4)=NODE(4)+IDC
```

```
 40   CONTINUE
      NODE(1)=NODE(1)-IDC*IC+IDMN
      NODE(2)=NODE(2)-IDC*IC+IDMN
      NODE(3)=NODE(3)-IDC*IC+IDMN
      NODE(4)=NODE(4)-IDC*IC+IDMN
      IE0=IELE0+mt*I
      IELE=IE0
 60   CONTINUE
      RETURN
      END
```

E Fortran Load Case2 Construction Program (Strip Load)

```
CC-----PROGRAM TO GENERATE STRIP LOAD FOR ELEVATED LOCAL AXIAL
C      COMPRESSION IN MODEL ANALYSIS
C
C      IS   = THETA  OF STRIP LOAD
C      L    = LENGTH OF STRIP LOAD
C      n    = NUMBER OF DIVISION IN MERIDIONAL
C      m    = NUMBER OF DIVISION IN CIRCUMFERENTIAL
C      IT   = TOTAL    ELEMENTS
C
       DIMENSION NODE(4)
       DIMENSION IDM(6)
       DIMENSION IDMN(6)
       DIMENSION LM(6)
       DIMENSION LLM(7)
       DIMENSION IM(6)
       DIMENSION IIM(7)
       DIMENSION IDC(4)
       DIMENSION LC(4)
       DIMENSION LLC(5)
```

```
      DIMENSION IC(4)
      DIMENSION IIC(5)
      DIMENSION NO(4,6)
      DIMENSION m(6)
      OPEN(UNIT=15,STATUS='NEW',FILE='STRIPs15L15000.ELE')
      DATA IDM/1,2,1,2,10,1/
      DATA IDC/4,2,6,10/
      DO 5 I=1,6
      IDMN(I)=IDM(I)*15000
    5 CONTINUE
CCCCCCCCCCCCCCCCCCCCCCCCCCCCCCCCCCCCCCCCCCCCCCCCCCCCCCCCCCCCCCCC
      IS=15
      L=15000
CCCCCCCCCCCCCCCCCCCCCCCCCCCCCCCCCCCCCCCCCCCCCCCCCCCCCCCCCCCCCCCC
      n=L/150
      IF (n .GT. 95) GOTO 6
      n1=INT((n-18)/2)
      n2=INT((95-n)/2)
      n3=INT((92-n-2*n2)/10)
      n4=95-n-10*n3-2*n2
      n5=n-18-2*n1
      nt=23+n1+n2+n3+n4+n5
      IM(1)=15+n5
      IM(2)=n1
      IM(3)=3+n4
      IM(4)=n2
      IM(5)=n3
      IM(6)=5
      GOTO 7
    6 n1=INT((n-20)/2)
      n2=INT((95-n)/2)
```

```
      IF (n2 .LE. 0) n2=0
      n3=INT((95-n-2*n2)/10)
      IF (n3 .LE. 0) n3=0
      n4=95-n-10*n3-2*n2
      IF (n4 .LE. 0) n4=0
      n5=n-20-2*n1
      nt=20+n1+n2+n3+n4+n5
      IM(1)=15+n5
      IM(2)=n1
      IM(3)=n4
      IM(4)=n2
      IM(5)=n3
      IM(6)=5
7     m(1)=INT((IS-5)/2)
      IF (m(1) .LE. 0) m(1)=0
      IF (m(1) .EQ. 0) IDC(1)=0
      IF (m(1) .EQ. 0) IC(1)=0
      m(2)=IS-m(1)*2
      m(3)=30+m(2)
      m(4)=INT((180-2*m(1)-m(3))/3)
      IF (m(4) .GE. 5) THEN
      m(5)=5
      m(6)=INT((165-2*m(1)-m(3))/5)
      ELSE
      m(5)=m(4)
      m(6)=0
      END IF
      m(3)=180-m(1)*2-m(5)*3-m(6)*5
      mt=m(1)+m(3)+m(5)+m(6)
      IT=nt*mt
      IC(1)=m(1)
```

```
      IC(2)=m(3)
      IC(3)=m(5)
      IC(4)=m(6)
      LLM(1)=0
      IIM(1)=0
      LLC(1)=0
      IIC(1)=0
      DO 8 I=1,6
      LM(I)=IDMN(I)*IM(I)
      LLM(I+1)=LLM(I)+LM(I)
      IIM(I+1)=IIM(I)+IM(I)
 8    CONTINUE
      DO 10 I=1,4
      LC(I)=IDC(I)*IC(I)
      LLC(I+1)=LLC(I)+LC(I)
      IIC(I+1)=IIC(I)+IC(I)
10    CONTINUE
      IE=0
      IF (n .GT. 95) THEN
      DO 30 I=1,6
      DO 20 J=1,2
      IELE=1+IIC(J)+mt*IIM(I)
      NODE(1)=2500000+LLM(I)+LLC(J)
      NODE(2)=NODE(1)+IDMN(I)
      NODE(3)=NODE(2)+IDC(J)
      NODE(4)=NODE(1)+IDC(J)
      IF (IM(I) .EQ. 0) GOTO 20
      IF (IC(J) .EQ. 0) GOTO 20
      CALL ELGEN(IELE, mt, NODE, IDC(J), IDMN(I), m(J), IM(I))
20    CONTINUE
30    CONTINUE
```

```
      GOTO 41
      ELSE
      DO 32 I=1,2
      DO 22 J=1,2
      IELE=1+IIC(J)+mt*IIM(I)
      NODE(1)=2500000+LLM(I)+LLC(J)
      NODE(2)=NODE(1)+IDMN(I)
      NODE(3)=NODE(2)+IDC(J)
      NODE(4)=NODE(1)+IDC(J)
      IF (IM(I) .EQ. 0) GOTO 22
      IF (IC(J) .EQ. 0) GOTO 22
      CALL ELGEN(IELE, mt, NODE, IDC(J), IDMN(I), m(J), IM(I))
 22   CONTINUE
 32   CONTINUE
      DO 33 I=3,3
      DO 23 J=1,2
      IELE=1+IIC(J)+mt*IIM(I)
      NODE(1)=2500000+LLM(I)+LLC(J)
      NODE(2)=NODE(1)+IDMN(I)
      NODE(3)=NODE(2)+IDC(J)
      NODE(4)=NODE(1)+IDC(J)
      IF (IM(I) .EQ. 0) GOTO 23
      IF (IC(J) .EQ. 0) GOTO 23
      CALL ELGEN(IELE, mt, NODE, IDC(J), IDMN(I), m(J), 3)
 23   CONTINUE
 33   CONTINUE
      END IF
 41   STOP
      END
C
      SUBROUTINE
```

```
     &  ELGEN(IELE, mt, NODE, IDC, IDMN, IC, IM)
        DIMENSION NODE(4)
        IELE0=IELE
        DO 60 I=1,IM
        DO 40 J=1,IC
        WRITE(15,10) IELE,NODE
  10    FORMAT(I4,4(',',I7))
        IELE=IELE+1
        NODE(1)=NODE(1)+IDC
        NODE(2)=NODE(2)+IDC
        NODE(3)=NODE(3)+IDC
        NODE(4)=NODE(4)+IDC
  40    CONTINUE
        NODE(1)=NODE(1)-IDC*IC+IDMN
        NODE(2)=NODE(2)-IDC*IC+IDMN
        NODE(3)=NODE(3)-IDC*IC+IDMN
        NODE(4)=NODE(4)-IDC*IC+IDMN
        IE0=IELE0+mt*I
        IELE=IE0
  60    CONTINUE
        RETURN
        END
```

15th ASCE Engineering Mechanics Conference
June 2-5, 2002, Columbia University, New York, NY

BUCKLING STRENGTH OF THIN CYLINDRICAL SHELLS UNDER LOCALIZED AXIAL COMPRESSION

Minjie Cai[1], J. Mark F.G. Holst[2] and J. Michael Rotter[3]

ABSTRACT

The buckling strength of a thin cylindrical shell is important in many applications in civil engineering. On the one hand, current design rules are principally based on an empirical interpretation of test data and hence very simple loading conditions are applied. On the other hand, experimental and theoretical observations show significant stress non-uniformity and hence a deviation from the buckling strength expected under uniform load. Reliable quantification of this effect is still challengingly difficult.

This paper explores a typical thin cylindrical silo shell under localized axial compression. Two different buckling phenomena are identified with corresponding, and distinct, buckling mode forms. The influence of geometric imperfections on the buckling strength of the shell is also considered.

Keywords: Buckling strength; Cylindrical shell; Non-uniform compression; Strip center buckles; Strip edge buckles; Strip load

INTRODUCTION

Cylindrical silo shells are subject to vertical stresses in their walls as a consequence of friction between the stored solid and the wall. Shell buckling under axial compression is normally the controlling design consideration especially for steel silos. The classical buckling strength (Lorenz, 1908; Timoshenko, 1910; Southwell, 1914) continues to be treated as the reference stress for problems involving axial compression.

On the one hand, Janssen theory (1895) remains the dominant method of defining silo pressures for design. On the other hand, more recent experimental (Pieper, 1969; Nielsen, 1983; Ooi *et al.*, 1990) and theoretical studies (Nanninga, 1956; Jenike *et al.*, 1973; Walker, 1966; Walters, 1973; Rotter, 1986b; Rotter, 1998; Ooi and She, 1997)) on silo loading show significant non-uniform deviations from the classical theory even under careful symmetrical filling. Unsymmetrical loads on silo walls lead to high local axial compression (Rotter, 1986a; Rotter, 1998). The buckling strength under an axial compression that acts over only a part of the circumference may be significantly changed, but the problem has been scarcely explored at all (Rotter, 1986a; Rotter, 1986b; Ansourian, 1992; Rotter, 1997). A recent investigation by Cai *et al.* (2002) is the first known study to examine this problem systematically. The present paper details some of the results

[1] Corresponding author, Mr Minjie Cai, PhD student, School of Civil & Environmental Engineering, Division of Engineering, The University of Edinburgh, Edinburgh EH9 3JN, UK. Tel: +44 131 650 5812; Fax: +44 131 650 5736; E-mail: mcai@srv0.civ.ed.ac.uk

[2] Dr J.M.F.G. Holst, Lecturer, School of Civil & Environmental Engineering, Division of Engineering, The University of Edinburgh, Edinburgh EH9 3JN, UK. Tel: +44 131 650 6768; Fax: +44 131 650 6781; E- mail: jmfgh@civ.ed.ac.uk; m.holst@ed.ac.uk

[3] Prof. J.M. Rotter, Professor of Civil Engineering, School of Civil & Environmental Engineering, Division of Engineering, The University of Edinburgh, Edinburgh EH9 3JN, UK. Tel: +44 131 650 5719; Fax: +44 131 650 7170; E-mail: michael@civ.ed.ac.uk

from their study.

In addition, the buckling strength of a thin cylindrical shell under axial compression is known to be very sensitive to geometric imperfections in the wall (Yamaki, 1984; Calladine, 1995). One of the most detrimental and well-defined imperfections is a local depression due to the rolling process of the steel plate and/or shrinkage of the weld (Bornscheuer, Häfner and Ramm, 1983; Rotter and Teng, 1989; Teng and Rotter, 1992; Rotter, 1996; Rotter, 1997; Holst *et al.*, 1999; Holst *et al.*, 2000). A local axisymmetric inward imperfection (Rotter and Teng, 1989) at the shell mid-height was therefore used in the present study.

MODEL

The cylindrical shell under investigation has a height $H = 30$ m, radius $R = 5$ m, and thickness $t = 10$ mm, which gives $R/t = 500$ and $H/R = 6$. The top and bottom boundaries of the shell are held circular (S3) (Yamaki, 1984). However, since in this case the cylinder is long, the influence of the edge boundaries is marginal. Fig.1 details the extent of the applied axial compression strip and the cylindrical coordinate system.

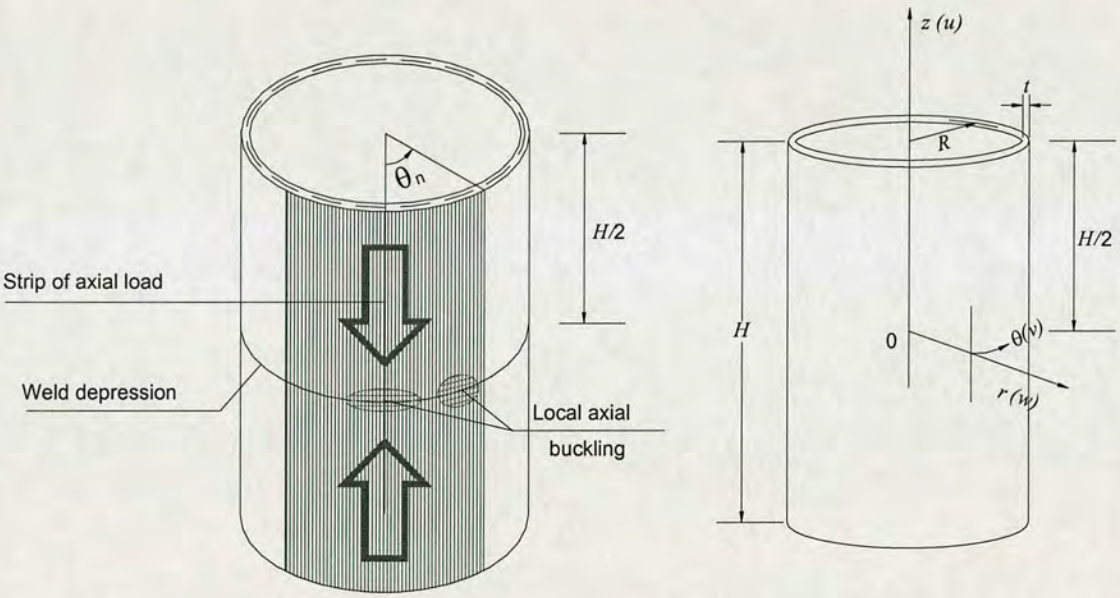

FIG. 1. Parametric study of a cylinder under localised compression

The convergent mesh (Fig.2) was obtained from a mesh convergence study (Cai *et al.*, 2002). The commercial finite-element (FE) package ABAQUS (HKS, 1998) was chosen for all analyses. A rectangular 4-node doubly curved thin shell element, with reduced integration, hourglass control and 5 degrees of freedom per node (S4R5) was adopted. In order to reduce the computational time, symmetry was exploited along the cylinder mid-plane and along the central meridian through the strip and its diametrically opposing meridian. Thus only one quarter of the complete shell is analyzed.

The linear bending half-wavelength ($\lambda_0=2.44\sqrt{Rt}$) was used as a reference for characterizing the mesh size. Thus the edge of the strip load and the areas close to the top boundary and the

imperfection were modeled using a very fine mesh, with individual elements of dimension $l \le \lambda_0 / 4$.

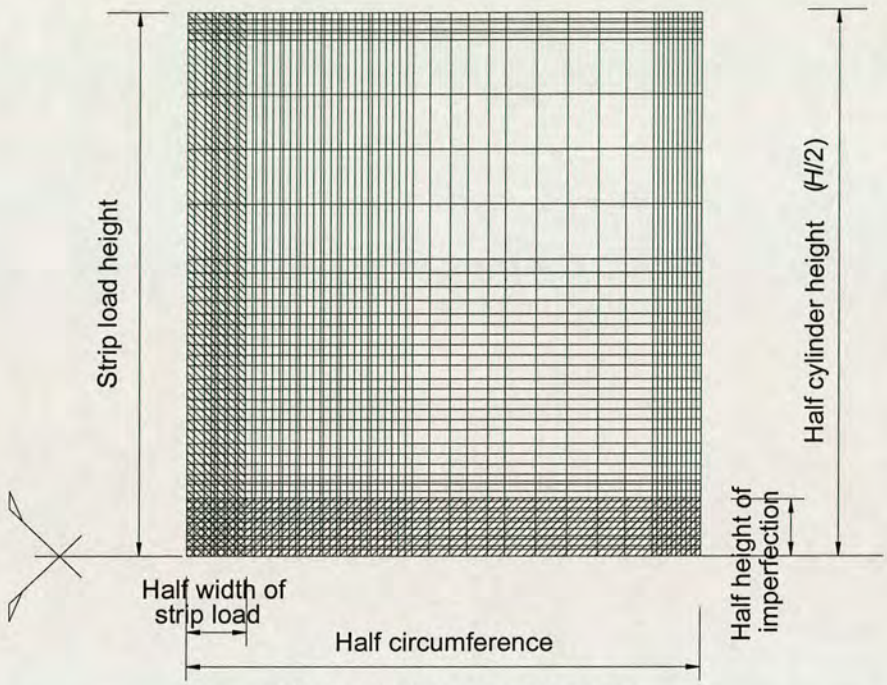

FIG. 2. Finite element mesh

The applied axial compression (equivalent to frictional traction) is uniform over the strip, which has a height equal to half the height of the cylinder (Fig. 2). Due to the symmetry boundary at the mid-plane, an equal and opposite axial compression is applied on the other half of the cylinder. The axial membrane stress according to membrane theory therefore increases linearly with the height of the shell (Fig. 3) with a maximum at the shell mid-plane. Fig. 3 shows the effect of bending on the axial membrane stress.

Geometrically nonlinear analyses with and without imperfections (GNA & GNIA) were conducted using the modified Riks method (HKS, 1998) until well into the post buckling regime. The classical buckling strength σ_{cl} (Lorenz, 1908; Timoshenko, 1910; Southwell, 1914) for a long perfect elastic cylindrical shell under uniform axial compression is used as the reference stress for all the analyses, where

$$\sigma_{cl} = E\frac{t}{\sqrt{3(1-\gamma^2)R}} \cong 0.605E\frac{t}{R} \qquad (1)$$

LOAD-DISPLACEMENT CURVES

Load-displacement curves are shown in Fig. 4 for a strip of circumferential extent $2\theta_n = 20°$. Curves for several different amplitudes of the imperfection are shown. Initially, the behavior is linear but at a larger load and for a larger imperfection the behavior becomes moderately nonlinear before the buckling load is reached. For the perfect shell the buckling load lies slightly above that predicted by the classical theory. As the imperfection amplitude is increased, the buckling loads

gradually decreases. For larger imperfections a post buckling plateau is reached at $\eta = 0.53$.

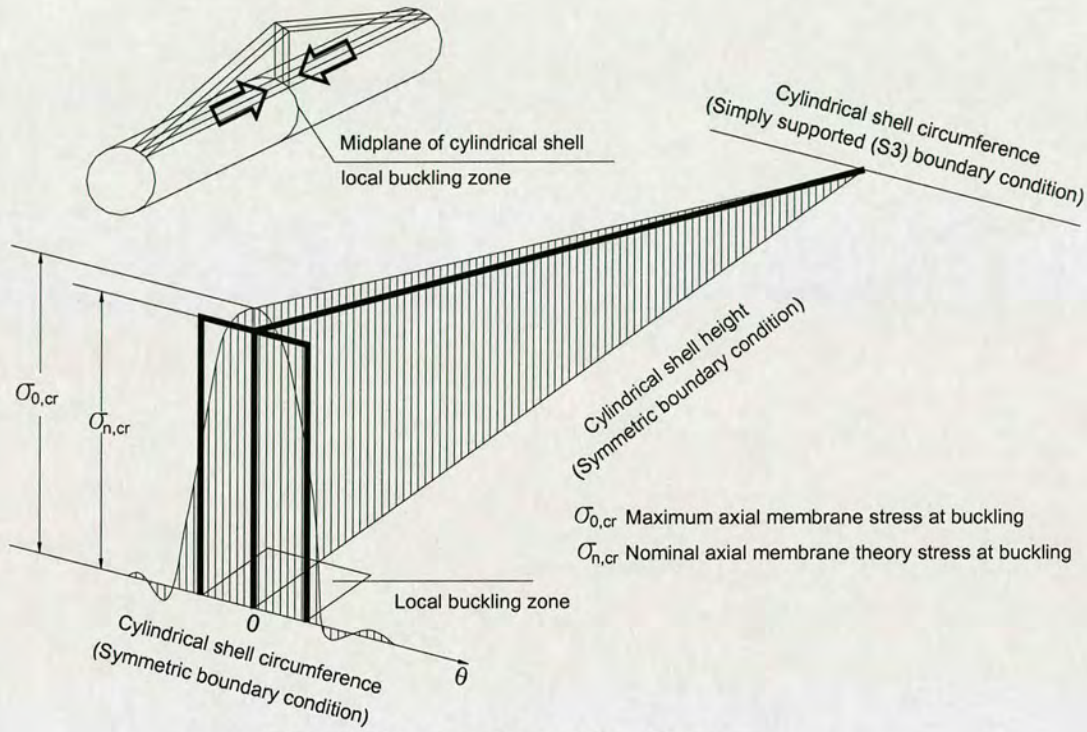

FIG. 3. Stress pattern at buckling

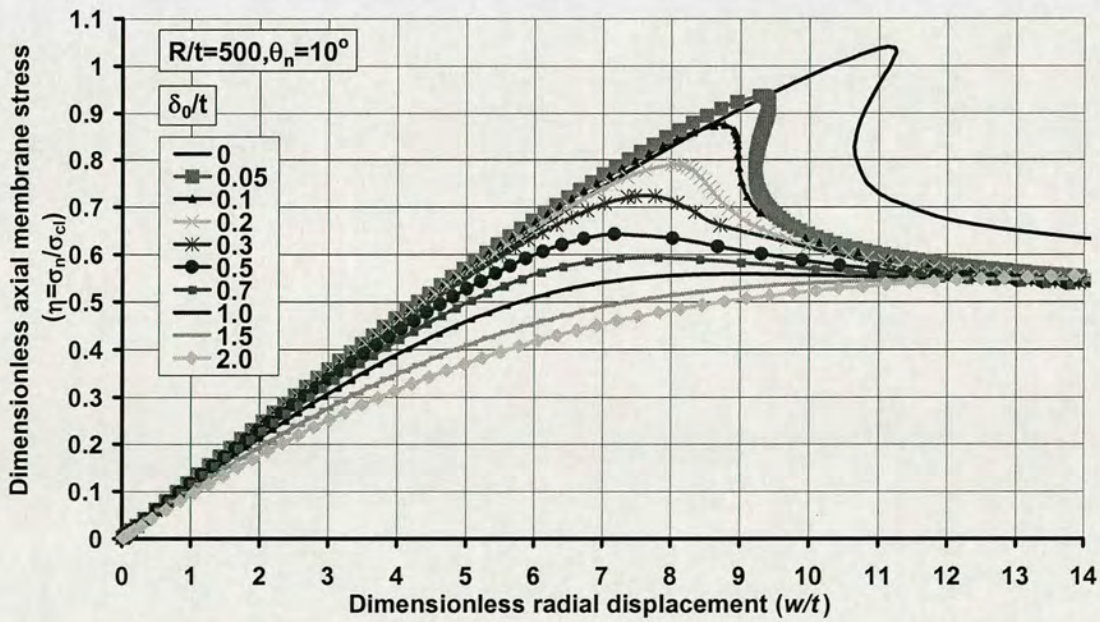

FIG. 4. Load-displacement curve of a thin-cylindrical shell under localised axial compression with the influence of different imperfection amplitudes

The axial membrane stress derived from shell membrane theory is compared in Fig. 3 with the stress pattern from a finite element analysis, which incorporates bending effects. The maximum axial membrane theory stress (at the mid-plane) is used to define the applied load and is termed the nominal stress σ_n here. At buckling, this nominal stress reaches the value $\sigma_{n,cr}$. The stresses in Fig. 3 are shown at the instant of buckling and it is clear that bending effects cause a significant smoothing of the applied stress pattern.

BUCKLING MODES

Fig. 5 shows the deformed geometry of the shell in the post-buckling regime. For the case discussed above (R/t=500, θ_n=10°) a buckle has formed at the mid-plane of the shell and at the center of the strip of load. This is defined by the term "Strip center buckle". If however a wider strip of load is applied, a completely different buckling mode is obtained. Thus for the case with R/t=500 and θ_n=45° the buckle occurs close to the strip edge and this mode is designated "Strip edge buckle".

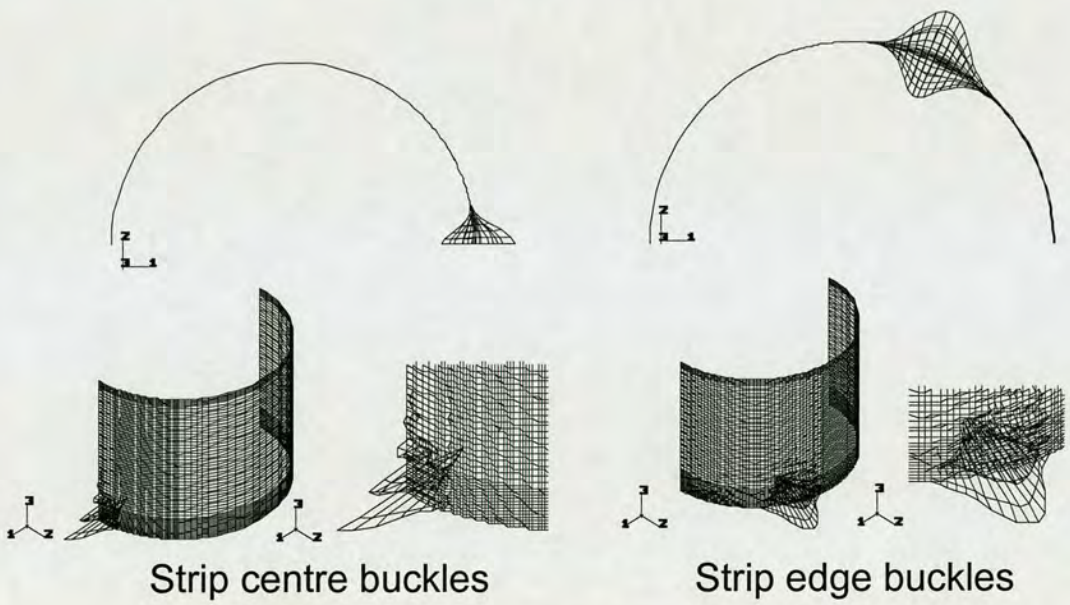

FIG. 5. Different buckling modes

A hypothesis was made that, in general, narrow strips of load lead to strip center buckles and wide strips of load to strip edge buckles. A large parametric study was conducted (Cai *et al.*, 2002) to examine this hypothesis. From a comparison of the deflected shapes for various shell geometries and sizes of strip and from the associated membrane stress distributions, it is evident that are two possible and distinct buckling phenomena for a cylindrical shell under localized axial compression, as described above.

EFFECT OF GEOMETRY NON-LINEARITY

Fig. 6 shows the axial membrane stress distribution at the mid-plane circumference at the point of buckling. It compares the results from a linear analysis (LA) with those from a nonlinear

analysis (GNA). The stress distribution according to membrane theory is shown for comparison. It is clear that the effect of geometry non-linearity is small in this case and this result is found in all other cases considered also.

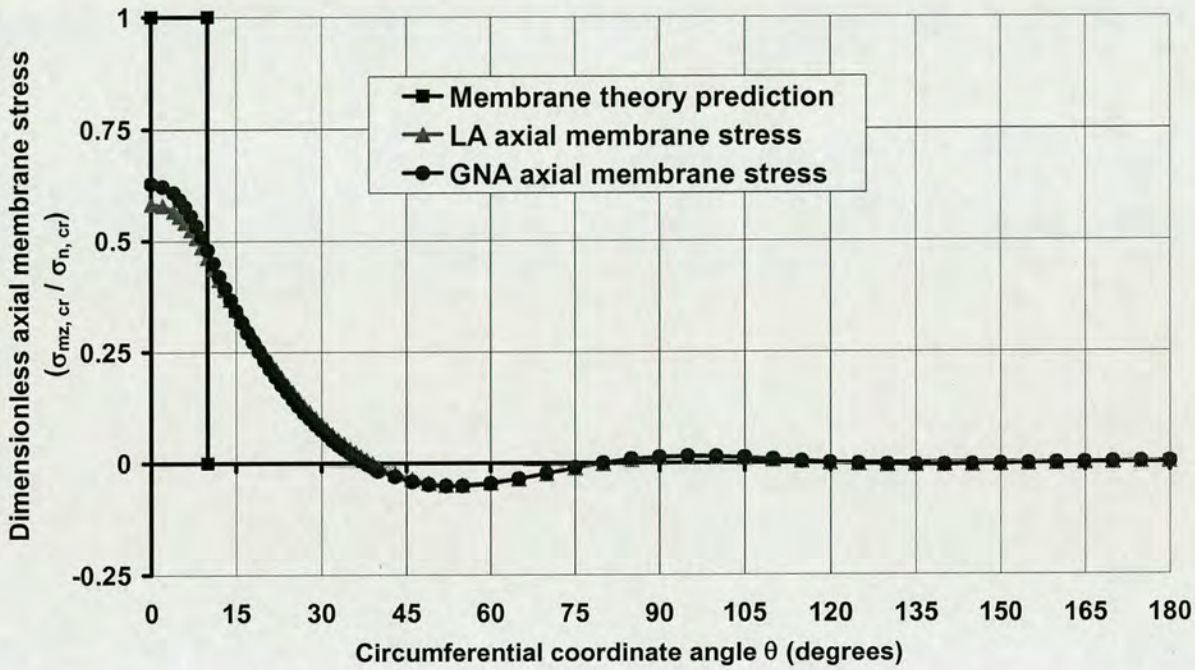

FIG. 6. Effect of geometry non-linearity on the stress distribution at buckling for LA GNA

CONCLUSIONS

- Two possible and distinct buckling phenomena have been identified for a wide range of shell geometries subject to a wide range of strip loads
- For narrow strips, a strip center buckle occurs
- For wider strips, a strip edge buckle is observed
- A parametric study is close to completion which will identify the strip angle that separates these two phenomena for various *R/t* ratios
- It is also apparent that this parametric study will lead to simple formulae for the prediction of the buckling strength of shells under localized axial compression
- The influence of imperfection amplitude has been examined and shown to have a moderate effect on the buckling strength of the shell examined
- In general, geometry non-linearity plays a minor role in determining the stress distributions at buckling

ACKNOWLEDGMENTS

Financial support through an ORS Award (ORS/C20-4, ORS/1999014046) and a Small Project Grant from the University of Edinburgh Development Trust (Ref. 77/2002) is gratefully

acknowledged by the first author.

REFERENCES

Ansourian, P. (1992) "On the buckling analysis and design of silos and tanks", J. Construct. Steel Research, Vol. 23, pp 273-294.

Bornscheuer F.W., Häfner L. and Ramm E. (1983) "Zur Stabilität eines Kreiszylinders mit einer Rundschweissnaht unter Axialbelastung", Der Stahlbau, Vol. 10, pp 313-318.

Cai, M.J., Holst, J.M.F.G. and Rotter, J.M. (2002) "Prediction of shell buckling strength under localised axial compression", Research Report R02-002, School of Civil and Environmental Engineering, Univ. of Edinburgh, January.

Calladine C.R. (1995) "Understanding imperfection-sensitivity in the buckling of thin-walled shells", *Thin-Walled Structures*, Vol. 23, pp 215-235.

HKS (1998) *ABAQUS/Standard User's Manual,* Hibbitt, Karlsson & Sorensen, Inc., Pawtucket, Rhode Island, USA, Version 5.8 edition.

Holst, J.M.F.G., Rotter, J.M. and Calladine, C.R. (1999) "Imperfections in cylindrical shells resulting from fabrication misfits", J. Eng. Mechanics, Vol. 125, No. 4, pp 410-418.

Holst, J.M.F.G., Rotter, J.M. and Calladine, C.R. (2000) "Imperfections and buckling in cylindrical shells with consistent residual stresses", J. Construct. Steel Research, Vol. 54, pp 265-282.

Janssen, H.A. (1895) "Versuche über Getreidedruck in Silozellen", *Zeitschrift des Vereines Deutscher Ingenieuere*, Vol. 39, No. 35, pp 1045-1049.

Jenike, A.W., Johanson, J.R. and Carson, J.W. (1973) "Bin loads-part 3: mass flow bins", *Jnl. Engng Industry*, ASME, Vol. 95, Series B, No. 1, pp 6-12.

Lorenz, R. (1908) *Zeitschrift des Vereines Deutscher Ingenieuere,* Vol. 52, pp. 1766.

Nanninga, N. (1956) "Gibt die übliche Berechnungsart der Drucke auf die Wände und den Boden von Silobauten sichere Ergebnisse", *Der Ingenieur,* Vol. 68, No. 44, Nov.

Nielsen, J. (1983) "Load distribution in silos influenced by anisotropic grain behaviour", *Proc., International Conference on Bulk Materials Storage, Handling and Transportation*, Institution of Engineers, Australia, Newcastle, August, pp 226-230.

Ooi, J.Y., Pham, L. and Rotter, J.M. (1990) "Systematic and random features of measured pressures on full-scale silo walls", *Eng. Struct.,* Vol. 12, No. 2, pp 74-87.

Ooi, J.Y. and She, K.M. (1997) "Finite element analysis of wall pressure in imperfect silos", *Int. J. Solids Structures*, Vol. 34, No. 16, pp 2061-2072.

Pieper, K. (1969) "Investigation of silo loads in measuring models", *Journal of Engineering for Industry*, pp 365-372.

Rotter, J.M. (1986a) "On the specification of loads for the structural design of bins and silos", *Proc., Second International Conference on Bulk Materials Storage Handling and Transportation*, Institution of Engineers, Australia, Wollongong, pp 82-88.

Rotter, J.M. (1986b) "The analysis of steel bins subject to eccentric discharge", *Proc., Second International Conference on Bulk Materials Storage, Handling and Transportation*, Institution of Engineers, Australia, Wollongong, pp 264-271.

Rotter, J.M. (1996) "Elastic plastic buckling and collapse in internally pressurised axially compressed silo cylinders with measured axisymmetric imperfections: interactions between imperfections, residual stresses and collapse", Proc. International Workshop on Imperfections in Metal Silos: Measurement, Characterisation and Strength Analysis, CA-Silos, Lyon, France, 19 April, pp 119-140.

Rotter, J.M. (1997) "Design standards and calculations for imperfect pressurised axially

compressed cylinders", *International Conference on Carrying Capacity of Steel Shell Structures*, Czech Republic, Brno, pp 354-360.

Rotter, J.M. (1998) "Shell structures: the new European standard and current research needs", *Thin-Walled Structures*, Vol. 31, pp 3-23.

Rotter, J.M. (2002) "Shell buckling and collapse analysis for structural design: The new framework of the European Standard", *Proc., Festschrift for Professor Chris Calladine*, Sept, Cambridge.

Southwell, R. V. (1914) *Phil. Trans. Roy. Soc.,* Vol. 213, Series A, pp 187.

Teng, J.G. and Rotter, J.M. (1992) "Buckling of pressurized axisymmetrically imperfect cylinders under axial loads", *J. Eng. Mechanics,* Vol. 118, No. 2, pp 229-247.

Timoshenko, S. P. (1910) *Z. Math. Physik,* Vol. 58, pp 378.

Walker, D.M. (1966) "An approximate theory for pressure and arching in hoppers", *Chemical Engineering Science*, Vol. 21, pp 975-997.

Walters, J.K. (1973) "A theoretical analysis of stresses in silos with vertical walls", *Chemical Engineering Science*, Vol. 28, pp 13-21.

Yamaki, N. (1984) Elastic stability of circular cylindrical shells, North-Holland, Amsterdam, The Netherlands.

APPENDIX I. NOTATION

A.1 Symbols

E	Young's modulus of elasticity for cylinder
H	length of total modelled cylinder
r	radial coordinate
R	middle surface radius of cylindrical shell
t	shell thickness
u	axial displacement component
v	circumferential displacement component
w	radial displacement component
z	axial coordinate with origin at mid-plane of cylinder
η_{cr}	dimensionless critical membrane stress = $(\sigma_{n,cr} / \sigma_{cl})$
θ	circumferential coordinate
θ_n	half angle of strip load
ν	Poisson's ratio
σ	stress

A.2 Subscripts

cl	classical
cr	critical
n	nominal

16th ASCE Engineering Mechanics Conference
July 16-18, 2003, University of Washington, Seattle

PARAMETRIC STUDY ON THE BUCKLING OF THIN STEEL CYLINDRICAL SHELLS UNDER ELEVATED LOCAL AXIAL COMPRESSION STRESSES

Minjie Cai[1], J. Mark F.G. Holst[2] and J. Michael Rotter[3]

ABSTRACT

It is well known that the buckling strength of a thin cylindrical shell under uniform axial compression is highly sensitive to imperfections in the shell wall. The buckling behaviour increases considerably in complexity when non-uniform stress distributions are also considered. Thus cases of local high compression have not received much attention in the literature so far even though they are of great practical relevance. Furthermore, with changing shell geometry, loading patterns and boundary conditions the buckling phenomena observed vary considerably both quantitatively and qualitatively.

This paper presents some results from a comprehensive parametric study exploring the full range of practically relevant geometries for metal cylindrical silo shells with different boundary conditions and subjected to elevated local axial compressive actions of varying magnitude and extent. In the parametric study, influences of geometric imperfections and material non-linearity on the buckling strength of the shell are also considered. Some simple rules corresponding to different types of analyses and different buckling phenomena are presented for future implementation into the appropriate design standards.

Keywords: Cylindrical shell; Axial compression; Non-uniform stresses; Strip load; Shell buckling; Strip center buckles; Strip edge buckles; Geometric non-linearity; Material non-linearity; Critical nominal membrane stress

INTRODUCTION

Thin cylindrical shell structures used for storage of bulk materials are often subjected to axial compressive stresses that can cause buckling failures. In silos, the primary sources of such axial compression are friction between the stored solid and the wall together with the more complicated effects of circumferentially non-uniform normal pressures. Similar axial compressive stresses arise in tanks under wind loading and in horizontal tanks that are partially filled with fluid. Buckling under axial compression is normally the controlling design consideration for such structures.

Localised compression may result from non-symmetric pressures on the shell wall (Rotter, 1997). Highly localised non-uniform stresses (both in-plane and out-of-plane) are unavoidable in real cylindrical shells, for example during eccentric filling and discharging of

[1] Corresponding author, Mr Minjie Cai, PhD student, Institute for Infrastructure & Environment, The School of Engineering & Electronics, The University of Edinburgh, Crew Building, The King's Buildings, Edinburgh EH9 3JN, UK. Tel: +44 131 650 5812; Fax: +44 131 650 5736; E- mail: s9907108@sms.ed.ac.uk

[2] Dr J.M.F.G. Holst, Lecturer (P.T.), Institute for Infrastructure & Environment, The School of Engineering & Electronics, The University of Edinburgh, Crew Building, The King's Buildings, Edinburgh EH9 3JN, UK. Tel: +49 40 30 69 75 00; Fax: +49 40 30 69 75 76; E-mail: m.holst@holst-ingenieure.com

[3] Prof. J.M. Rotter, Professor of Civil Engineering, Institute for Infrastructure & Environment, The School of Engineering & Electronics, The University of Edinburgh, Crew Building, The King's Buildings, Edinburgh EH9 3JN, UK. Tel: +44 131 650 5719; Fax: +44 131 650 7170; E- mail: michael@civ.ed.ac.uk

a silo. In addition, the buckling strength is very sensitive to geometric imperfections in the wall, which are common in such structures. Reliable quantification of these effects is still challengingly difficult. In a previous paper (Cai *et al.*, 2002), two different buckling modes were identified. This paper develops the conceptual ideas presented previously and identifies some key results from a comprehensive parametric study of this field. Furthermore, it is the aim of this study to produce a rigorous and rationally based set of rules that can be adopted into current design standards.

Two parametric numerical studies are introduced in this paper: the first explores the height over which elevated axial compressive stresses occur. The second explores the effect of the width of this zone. The influence of geometric imperfections is included throughout the study.

MODELLING

A parametric analysis was conducted by varying all the parameters which were found to be critical in establishing the elastic buckling strength of the shell under local high compression. The radius R was varied from 1 m to 10 m and the half angle of the strip load θ_n from 0.2° to 90° in the compression width analyses; the radius R was varied from 1 m to 20 m with two half angle of strip load θ_n 10° and 60° and a strip height between 1/100 H and the whole cylinder height H in the compression height analyses. In all analyses, the wall thickness t is 10 mm and the height of cylinder H is 30 m, giving a ratio of R/t between 100 and 2000. The variation of the model parameters is shown in Fig. 1.

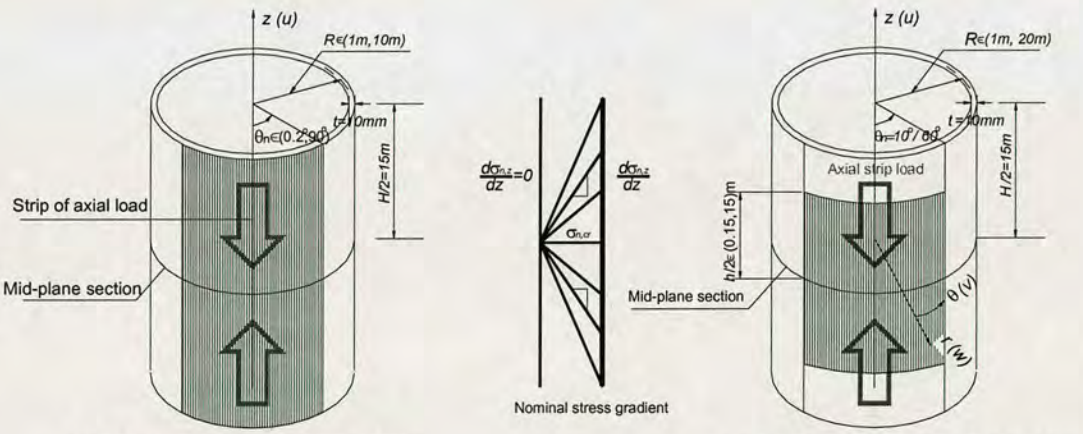

Cylinder under local compression with varying strip load width

Cylinder under local compression with varying strip load height

Fig. 1. Parametric study of a cylinder under localised compression

The converged mesh was obtained from the previous companion paper (Cai et al., 2002). The model descriptions including the properties of the material, the co-ordinate system, boundary conditions as well as its influence on the analyses results, geometric imperfection and analysis procedure were also presented there.

The full parametric study included a linear bifurcation analysis, and a geometrically non-linear analysis with and without local geometric inward imperfections. All three analysis

types were run in order to obtain a full set of elastic shell buckling strength predictions for each of the different analysis types detailed in the Eurocode (ENV 1993-1-6, 1999).
Of these, the linear analysis/linear eigenvalue analysis (LA/LEA), which predicts the behaviour of a thin-walled shell structure on the basis of small displacement and linear elastic shell bending theory, is the simplest. This analysis provides an important reference load, which may always be obtained for shells under compressive loading and which is used for interpreting results from all other analysis types in terms of the shell slenderness (ENV 1993-4-1, 1999; Rotter, 2002). Other analysis types are not easily accessible to practical design engineers. Furthermore, from the analyses presented in the companion paper (Cai et al., 2002), geometric non-linearity has only a relatively minor effect in the pre-buckling regime. Thus, the prediction of the LA/LEA is considered here first.

LINEAR EIGENVALUE ANALYSES (LA/LEA) – COMPRESSION WIDTH STUDY

Buckling strength prediction

The classical buckling stress σ_{cl} (Lorenz, 1908; Timoshenko, 1910; Southwell, 1914) and the nominal axial membrane stress at the buckling load at the mid-plane section (Cai *et al.*, 2002), $\sigma_{n,cr}$, are used here as reference values to describe the results of all the analyses simply and clearly. The results are expressed in terms of the dimensionless buckling strength parameter $\eta_{cr}=\sigma_{n,cr}/\sigma_{cl}$.

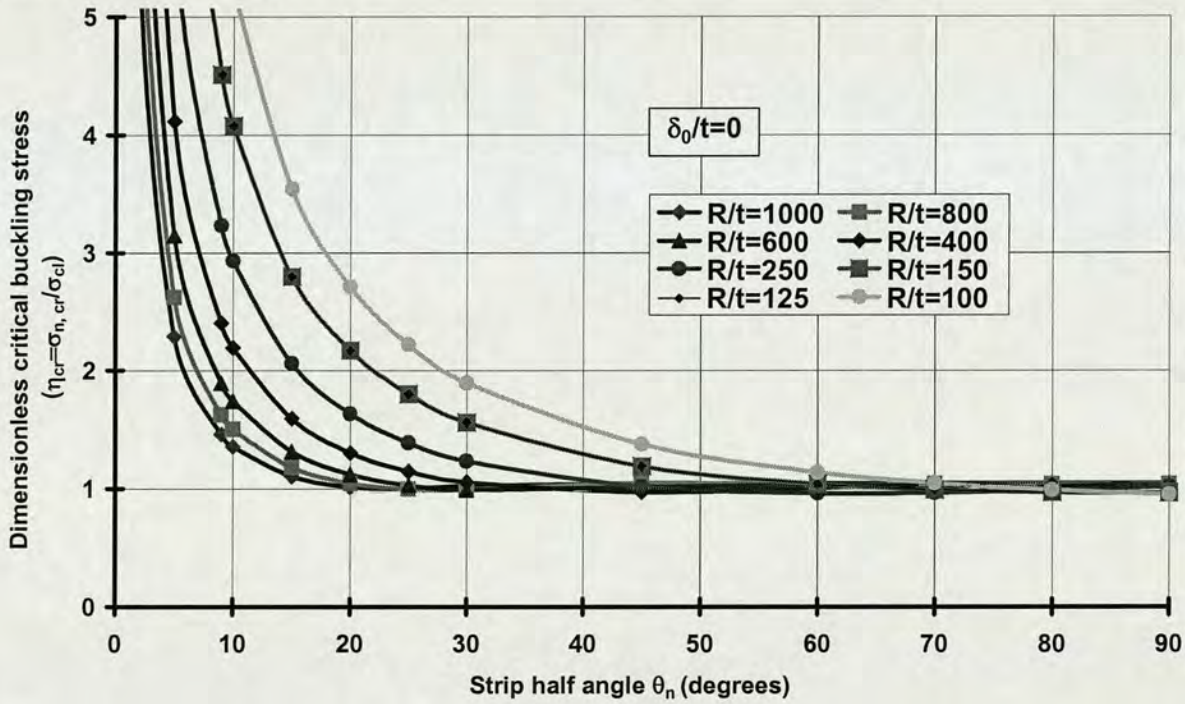

Fig. 2. Effect of strip half angle on linear bifurcation buckling strength of perfect cylinders (LA/LEA)

The analyses results display the following trends (Figs 2 & 3). First, if the *R/t* ratio is fixed, the buckling strength rises as the strip load angle decreases and it increases dramatically for small strip load angles. Second, if the angle of the strip load θ_n is fixed, the buckling strength decreases with an increase in the *R/t* ratio. The variation of smaller strip load angles is sharper than that of larger ones.

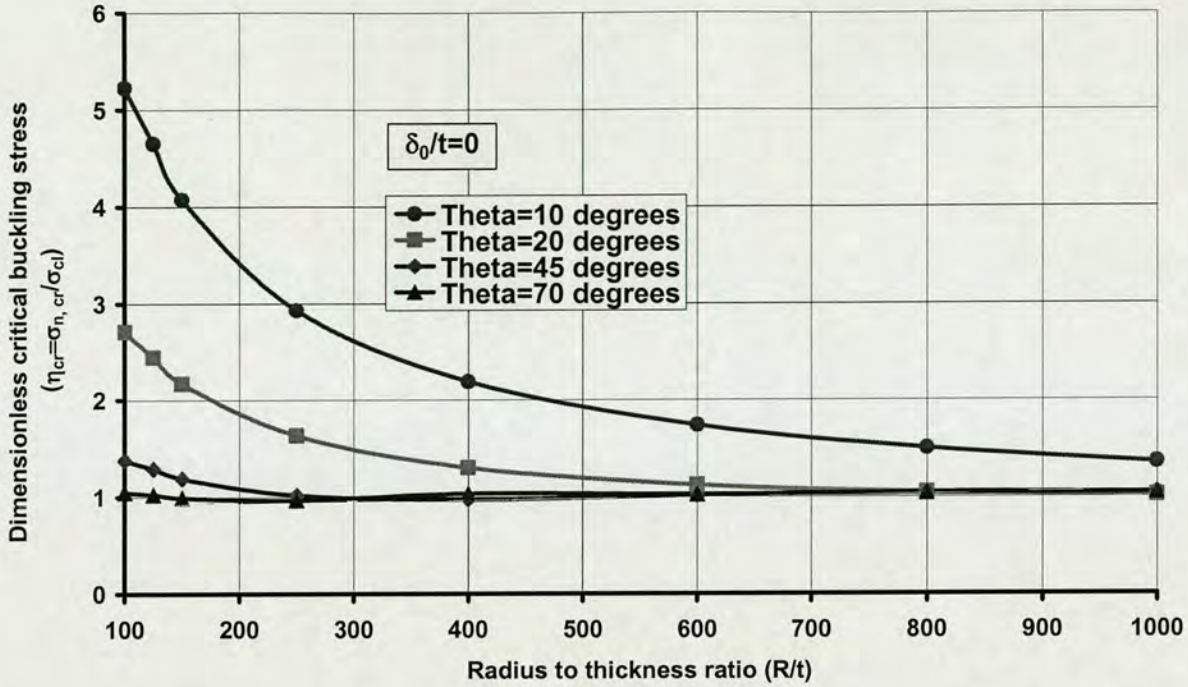

Figure 3. Effect of *R/t* ratio on linear bifurcation buckling strength of perfect cylinders (LA/LEA)

From both figures, the bucking strength of the cylinder is clearly related to the *R/t* ratio and the width of the strip load applied. But the relationships are quite complicated, and difficult to use in any design process. From observations, the calculated buckling strength for a small angle strip load applied to relatively thick cylinders is much higher than the classical solution and therefore impractical. The cases with dimensionless critical buckling strength ($\eta_{cr}=\sigma_{n,cr}/\sigma_{cl}$) higher than 5.0 have been omitted from the figures. However, the curves found for predicting the buckling strength are still relatively accurate even for this omitted range.

Variations in the ratio of *R/t* and the width of the strip load represent variations in the model and the stress applied, but it is difficult to apply these results directly. A better representation is obtained by using a further dimensionless parameter, the inverse strip half angle ξ (Eqn. 1).

$$\eta_{cr} = \sigma_{n,cr} / \sigma_{cl}$$
$$\xi = \theta_n^{-1}(R/t)^{-2/3} \qquad (1)$$
$$\theta_n \quad in \quad radians$$

This includes the effect of both the *R/t* ratio and the half strip angle θ_n and maps the analysis results onto two separate straight lines (Eqns. 2 and 3).

$$\eta_{cr} = 18.312\xi + 0.316 \qquad (2)$$

and

$$\eta_{cr} = 1 \qquad (3)$$

The relative error bounds are given by (-7.99%, +5.58%) for Eqn. 2 and (-5.20%, +5.25%) for Eqn. 3.

The prediction given by Eqn. 2 matches well with the numerical results apart from the region where the dimensionless critical buckling strength (η_{cr}) approaches 1.0. There, the numerical results diverge from Eqn. 2, but are predicted accurately by Eqn. 3 instead. Each of the two curves, Eqn. 2 and 3, can be related to a distinct buckling mode, strip centre buckles and strip

edge buckles respectively (Cai *et al.*, 2002). The following section examines how a further equation can be used to predict the bound between these two modes.

Bound between two buckling modes

The method used for obtaining a bound between the two equations is illustrated in Fig. 4. From the numerical data, curve fitting gives two separate curves, Prediction Curve 1 (Eqn. 2) and 2 (Eqn. 3). On approaching the boundary between the two curves, the buckling strength predicted by Curve 1 lies slightly below the FE results (Fig. 4) and is thus a lower bound approximation. The two curves together provide a reliable, easily applicable, and safe engineering prediction of the buckling strength.

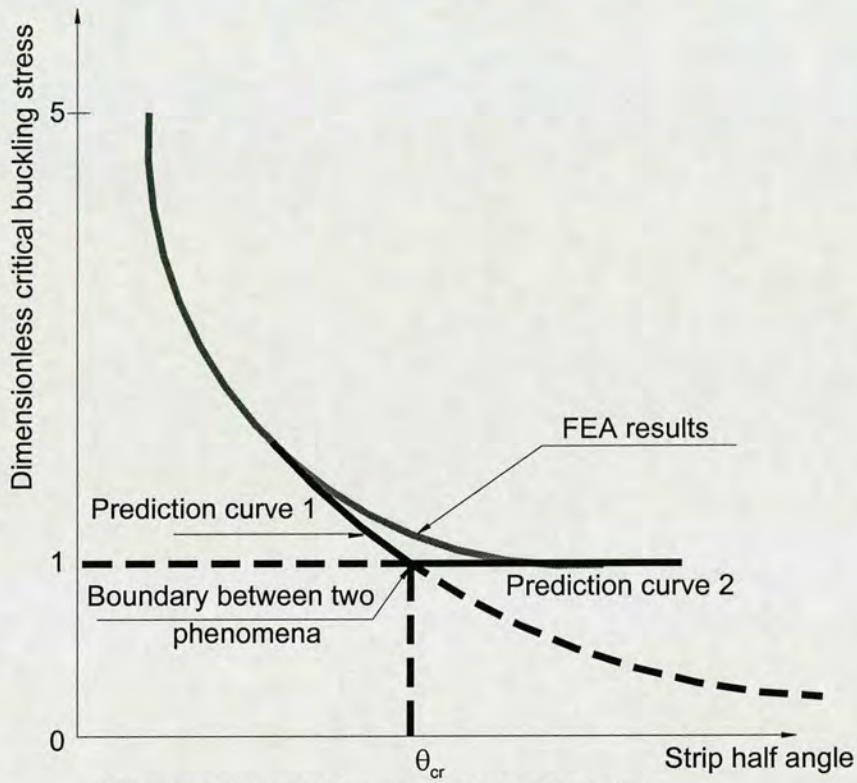

Figure 4. Prediction method explanation

The bound between the two curves and hence the bound distinguishing between the two buckling phenomena is determined by Eqn. 4.

$$\theta_{cr} = 26.76(\frac{R}{t})^{-2/3} \quad (4)$$

in radians

$\theta_n > \theta_{cr}$ Strip edge buckles

$\theta_n < \theta_{cr}$ Strip centre buckles

Summary

A prediction of the buckling strength obtained in linear elastic eigenvalue analyses can be obtained from two simple distinct equations which relate to two distinct buckling phenomena. In strip centre buckles, the local buckle forms at the centre of the strip load as a result of a highly localised peak stress. In strip edge buckles, a buckle is constructed somewhere near the strip load edge and the high stresses are found over a much greater circumferential extent. It is found that the buckling strength for strip edge buckles is almost identical to the case

where a uniform load is applied around the whole circumference. The fact that a localised buckle appears and not a partially axisymmetric one is related to the edge effects present.
For an R/t ratio between 100 and 1000 and a strip half angle θ_n between 0.2° and 90° (i.e. between 0.4° and 180° for the complete strip), linear buckling analysis results are accurately predicted by the two equations presented here. The bound between these two equations and their corresponding buckling modes is predicted by a further equation. The error margin for these equations is generally less than ± 5%, which is adequate for most engineering applications. A similar analysis was conducted to examine the effect of the compression zone height and corresponding results were obtained.
Because the LEA analyses do not take into account the influence of geometric nonlinearity and geometric imperfections, they generally predict a buckling strength much greater than the elastic critical buckling strength. Thus geometrically nonlinear analyses were also conducted, with corresponding results to those obtained for LEA.

CONCLUSIONS

The following conclusions can be drawn from the parametric study examining the effect of the compression width and height on the buckling strength of thin cylindrical shells and using three different analysis types.
1.In all cases the parametric studies led to a very clear and simple set of predictive equations.
2.The analysis types conform to the requirements of the draft European Standard for Metal Shells (ENV 1993-1-6, 1999).
3.Two different buckling modes were identified in all cases.

ACKNOWLEDGMENTS

Financial support through an ORS Award (ORS/C20-4, ORS/1999014046) is gratefully acknowledged by the first author.

REFERENCES

Cai, M. J., Holst, J. M. F .G. and Rotter, J. M. (2002) "Buckling Strength of Thin Cylindrical Shells under Localized Axial Compression", *the 15th Engineering Mechanics Division Conference of ASCE*, New York, USA, June 2002, pp 87-102.
ENV1993-1-6 (1999) *European Pre-standard CEN/TC 250/SC3/PT4 Euro-code 3 Part1.6: Design of steel structures general rules: Supplementary rules for shell structures.* European Committee for Standardisation, rue de Stassart 36, Brussels.
ENV1993-4-1 (1999) *European Pre-standard CEN/TC 250/SC3/PT4 Euro-code 3 Part4.1: Design of steel structures: Silos.* European Committee for Standardisation, rue de Stassart 36, Brussels.
HKS (1998) *ABAQUS/Standard User's Manual,* Hibbitt, Karlsson & Sorensen, Inc., Pawtucket, Rhode Island, USA, Version 5.8 edition.
Lorenz, R. (1908) *Z. Ver. Deut. Ingr,* Vol. 52, pp. 1766.
Rotter, J.M. (1997) "Design standards and calculations for imperfect pressurised axially compressed cylinders", *International Conference on Carrying Capacity of Steel Shell Structures*, Czech Republic, Brno, pp 354-360.
Rotter, J.M. (2002) "Shell buckling and collapse analysis for structural design: The new framework of the European Standard", *Proc. Festschrift for Professor Chris Calladine,* Sept, Cambridge.
Southwell, R. V. (1914) *Phil. Trans. Roy. Soc.,* Vol. 213, Series A, pp 187.
Timoshenko, S. P. (1910) *Z. Math. Physik,* Vol. 58, pp 378.
Yamaki, N. (1984) Elastic stability of circular cylindrical shells, North-Holland, Amsterdam, The Netherlands.

APPENDIX: NOTATION

E Young's modulus of cylinder
H length of total modelled cylinder
r radial coordinate
R middle surface radius of cylindrical shell
t shell thickness
u axial displacement component
v circumferential displacement component
w radial displacement component
z axial coordinate with origin at mid-plane of cylinder
γ Poisson's ratio
η dimensionless membrane stress
λ imperfection half-wavelength
λ_0 linear meridional bending half-wavelength
θ circumferential coordinate
θ_n half angle of strip load
σ stress
ξ dimensionless half strip load angle = $\theta_n^{-1}(R/t)^{-2/3}$
ϕ dimensionless strip load extent/characteristic inverse strip half angle (expression 1) = $\theta_n^{-1}(R/t)^{-2/3}((d\sigma_{n,z}/dz)(R/\sigma_{n,cr}))^{-1/3}$
Π dimensionless strip load extent/characteristic inverse strip half angle (expression 2) = $\theta_n^{-1}(R/t)^{-1/3}((d\sigma_{n,z}/dz)(R/\sigma_{n,cr}))^{4/3}$
cl classical
cr critical
m membrane/material non-linearity
n nominal
z axial direction
θ circumferential direction

BUCKLING OF CYLINDRICAL TANK SHELLS UNDER LOCAL AXIAL COMPRESSION STRESSES

Minjie Cai[1], J. Mark F.G. Holst[2] and J. Michael Rotter[3]

[1,2&3]Institute for Infrastructure & Environment, The University of Edinburgh, Edinburgh EH9 3JN, UK.
emails: s9907108@sms.ed.ac.uk, m.holst@holst-ingenieure.com, M.Rotter@ed.ac.uk

ABSTRACT

The buckling of cylindrical shells has been widely studied under uniform loads: uniform axial compression, uniform external pressure and uniform torsion. Conditions of non-uniform stresses have mostly been examined as special load cases (wind load, earthquake load, transverse shear load, horizontal cylinders partially filled with liquid etc.), and the conditions under which buckling may occur for a general stress distribution of any form has received very little attention. This is chiefly because it is difficult to characterise a general stress distribution that may cause buckling and the algebraic analysis is too difficult.

However, most realistic load cases lead to conditions of high local stress in particular parts of the structure. If the stress is high over an area far larger than a typical buckle, it may be supposed that conditions similar to uniform stress buckling will pertain, but where the stresses are more localised, higher strengths should be achieved. This paper outlines an initial study of the buckling of imperfect cylindrical shells under local axial compression, such that the maximum stress occurs within the shell and distant from restraining boundaries. A number of unexpected features of the behaviour were discovered, and the linear, nonlinear and imperfect strengths have all been described by simple empirically-derived equations, though space restrictions prevent these from being shown here.

INTRODUCTION

Unsymmetrical features of silo wall loads (Ooi et al., 1990) lead to local high axial compressive membrane stresses (Rotter, 1986; 1998; 2001) (Fig. 1), which is probably the commonest cause of buckling failures in service. Similar conditions develop in tanks under wind loading and above local supports. The local value of the stress that can be sustained without before buckling is very sensitive to the overall stress distribution, and where high stresses act on only a small zone, the peak value may reach a value (Rotter, 1986, 2001; ENV 1993-4-1, 1999) much higher than that for uniform axial compression buckling. However, the conditions that lead to buckling under non-uniform stresses have received very little attention. The few explorations of this problem have either used linear buckling (Bijlaard & Gallagher, 1959; Peter, 1974; Libai & Durban, 1977) or deal only with buckling above a support (e.g. Guggenberger et al, 2000).

Geometric imperfections in the shell play a key role in reducing the cylinder buckling strength. The buckling strength of a thin cylindrical shell under uniform axial compression is known to be very sensitive to geometric

imperfections (e.g. Yamaki, 1984). One of the most detrimental and well-defined imperfections is a local depression due to the rolling process of the steel plate and shrinkage of the weld (Rotter and Teng, 1989; Rotter, 1996, 1997; Berry et al, 2000; Holst et al, 1999, 2000; Schmidt and Winterstetter, 2001). The rationally-based local axisymmetric inward Type A imperfection of Rotter and Teng (1989), which has been used in many later studies, was adopted here.

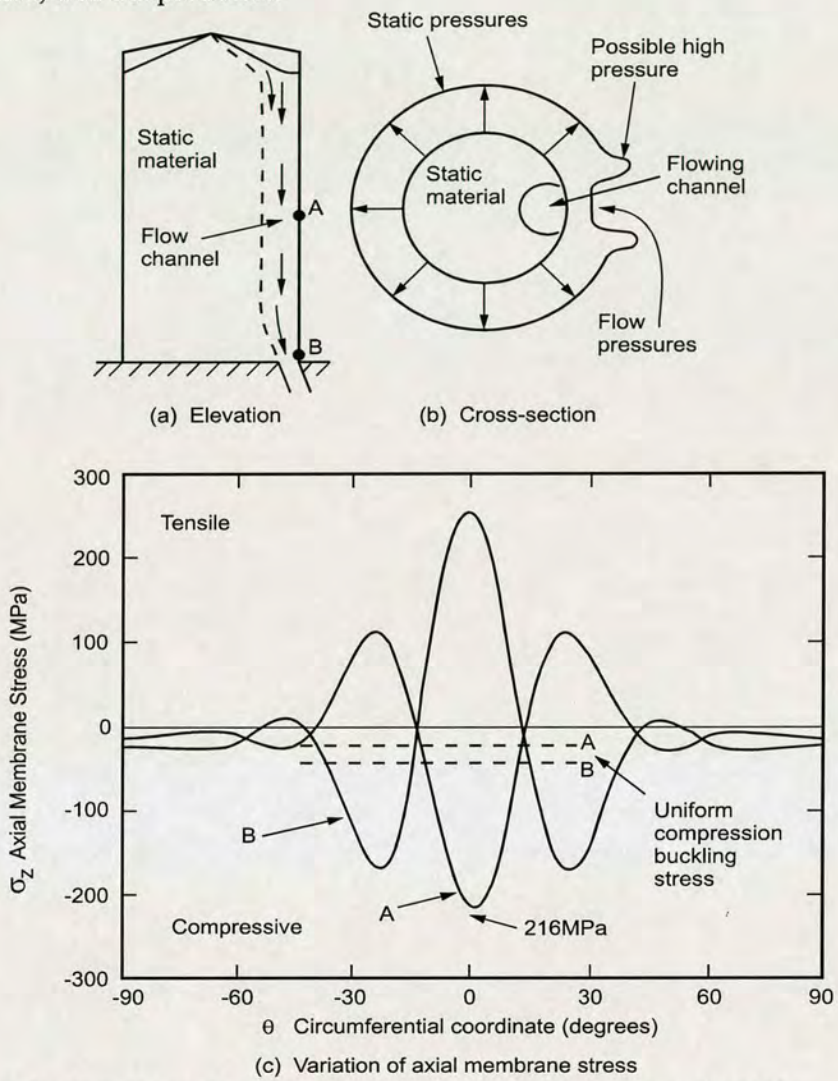

Fig. 1. Eccentrically discharged silo (after Rotter, 1986b)

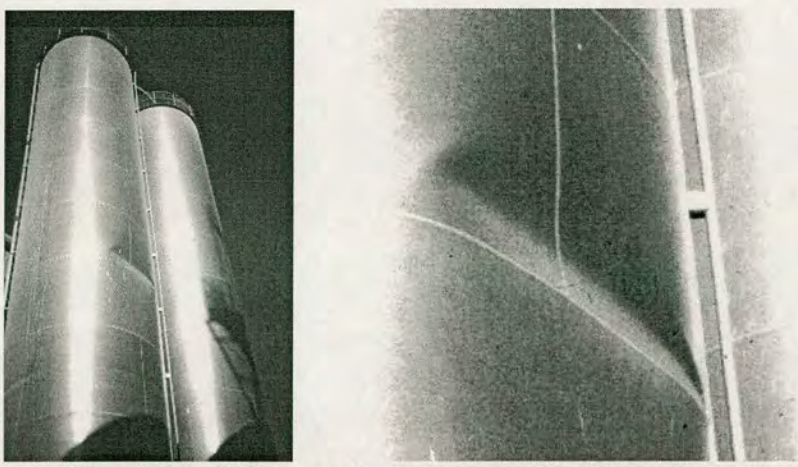

Fig. 2. Typical buckling failure under eccentric discharge (after Rotter, 2001)

This study is the first to consider buckling under local axial compression using a geometrically nonlinear

analysis, considering geometric imperfections, and exploring the buckling strength under a stress regime that is within the shell and distant from restraining boundaries. The classical buckling strength σ_{cl} for a medium length perfect elastic cylindrical shell under uniform axial compression was used as the reference stress for all the analyses.

$$\sigma_{cl} = E\frac{t}{\sqrt{3(1-\nu^2)}R} \cong 0.605E\frac{t}{R} \tag{1}$$

in which E is Young's modulus, R is the radius and t the thickness of the shell.

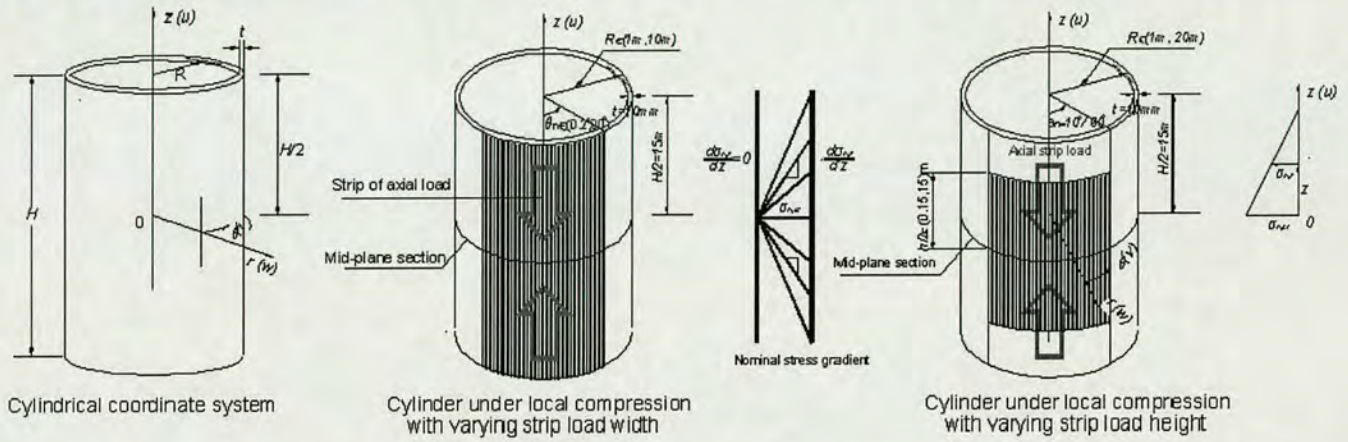

Fig. 3. Cylinder geometry and loading for parametric study under local axial compression

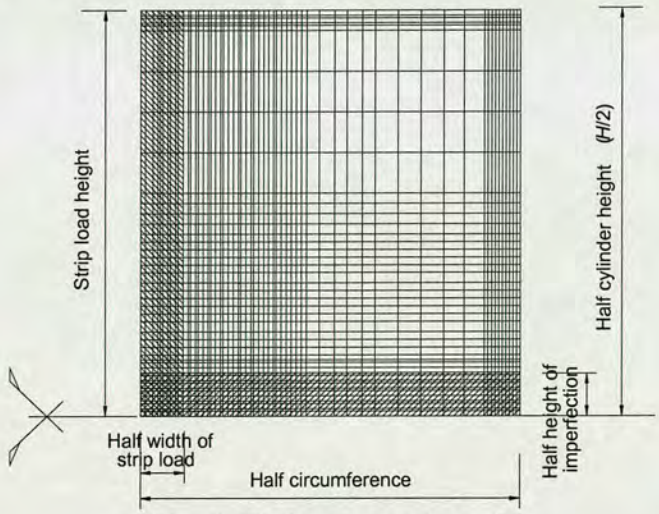

Fig. 4. Finite element mesh

MODEL TO EXPLORE LOCAL COMPRESSIVE MEMBRANE STRESSES

The cylindrical shell used to study the problem had a height $H = 30$ m, radius $R = 5$ m, and thickness $t = 10$ mm, which gives $R/t = 500$ and $H/R = 6$, making the cylinder sufficiently long for the influence of the edge boundaries to be marginal. The top and bottom boundaries of the shell were held circular (Yamaki, S3). A distributed axial compression traction was applied on a longitudinal strip (Fig. 3), to minimise the effects of bending and the development of other membrane stresses in addition to those being studied.

A validated mesh (Fig. 4) was obtained from a mesh convergence study (Cai, 2003). The commercial finite-element (FE) package ABAQUS (HKS, 1998) was chosen for all analyses. A rectangular 4-node doubly

curved thin shell element, with reduced integration, hourglass control and 5 degrees of freedom per node (*S4R5*) was adopted. To reduce the computational time, symmetry was exploited along the cylinder mid-plane and down the meridian through the centre of the loaded strip, and on the diametrically opposite meridian, reducing the calculation to one quarter of the complete shell.

The linear bending half-wavelength (λ_0=2.44$\sqrt{Rt}$) was used as a reference for characterising the mesh size. The edge of the strip load and the areas close to the top boundary and the imperfection were modelled using a very fine mesh, with individual elements of dimension $l \leq \lambda_0 / 4$ to capture all likely buckling modes.

The applied load was a uniformly distributed axial load (equivalent to frictional traction) acting throughout the strip, which extended over the half height of the cylinder (Fig. 3) in each sense, producing a simple-defined maximum stress state at the mid-plane symmetry boundary. According to membrane theory, the axial membrane stress should increase linearly with distance from the top boundary, but shell bending effects naturally lead to some changes in this pattern. The differences between membrane theory and a non-linear analysis of the perfect shell are illustrated in Fig. 5. For simplicity of presentation, the buckling strength is here described always in terms of the membrane theory stress at buckling $\sigma_{n,cr}$, even though this value is never the true maximum stress. The notation *n* indicates that it is a nominal stress. The stress pattern in Fig. 5 is an accurate plot at the instant of buckling: it is clear that bending effects cause a significant smoothing of the membrane theory stress pattern.

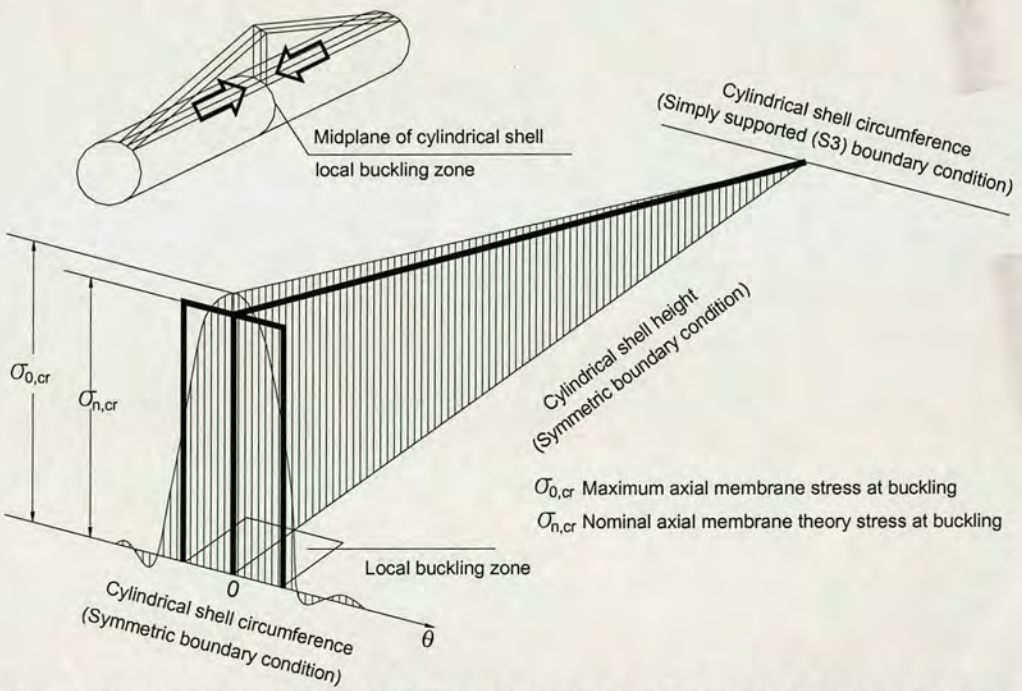

Fig. 5. Membrane stress pattern at buckling and simple characterisation

Geometrically nonlinear analyses with and without imperfections (GNA & GNIA), using the modified Riks method, were conducted far into the post buckling regime. The mesh and imperfection sensitivity calculations were verified by comparison comparing with the known buckling strength of imperfect cylinders with weld depressions under uniform axial load (Rotter and Teng, 1989).

ANALYSIS PREDICTIONS

Load-displacement curves

Load-displacement curves are shown in Fig. 6 for a strip load whose circumferential extent was $2\theta_n = 20°$, with weld depression amplitudes of zero up to twice the wall thickness t. Curves for several different amplitudes of the imperfection are shown. Initially, the behaviour is linear, but at higher loads and larger imperfections, moderate nonlinearity develops before the buckling load is reached. For the perfect shell, the maximum stress at buckling is slightly above that predicted by the classical theory. As the imperfection amplitude is increased, the buckling loads gradually decreases. For larger imperfections, a post buckling plateau is reached at $\sigma_{n,cr}/\sigma_{cl} = 0.53$ for this strip width.

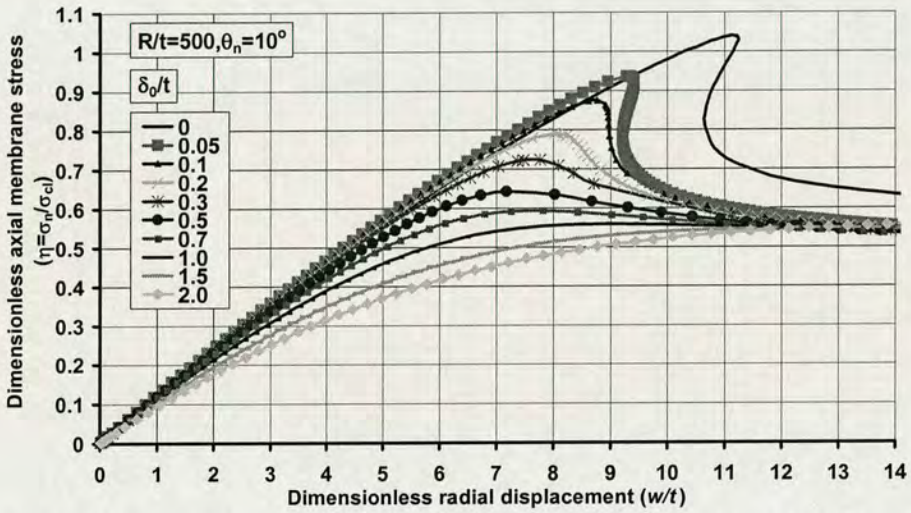

Fig. 6. Load-displacement curves for imperfect cylinders under local axial compression

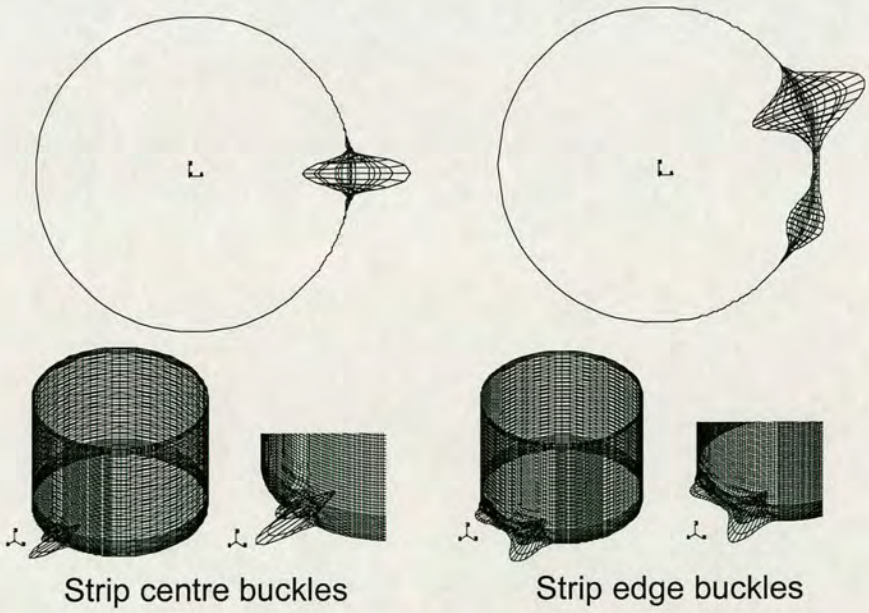

Fig. 7. The two different buckling modes

Buckling Modes

The deformed geometry of the shell in the post-buckling regime is shown in Fig. 7. For the case discussed above (R/t=500, $2\theta_n$=20°), a buckle forms at the mid-plane of the shell and at the centre of the loaded strip.

This is here termed a "strip centre buckle". When wider strips of load are applied, a completely different buckling mode is obtained: an example is shown here (R/t=500, $2\theta_n$=90°) where the buckle occurs close to the edge of the loaded strip and is here termed a "strip edge buckle". The former is dominated by the axial compression, but the latter is predominantly caused by the high membrane shear stress that develops due to the incompatibility of axial deformations at the edge of the strip.

Based on the above observations, the hypothesis was formulated that narrow loaded strips lead to strip centre buckles, but wide loaded strips cause strip edge buckles. If the axial membrane stress is high over an area far larger than a typical buckle, it may be supposed that conditions similar to uniform compression buckling will pertain and the local high shear will precipitate strip edge buckles. By contrast, where high stresses cover a zone smaller than a typical buckle, axial compression buckling with strip centre buckles will occur, at a much higher peak stress than for uniform compression. A large parametric study was conducted (Cai, 2003; Cai et al, 2002) to examine this proposition. This concluded that the hypothesis is substantially correct, and empirical equations were developed to accurately model the linear, nonlinear and imperfect shell buckling strengths, as well as the changes in stress distribution caused by bending and nonlinearity. It is evident that two possible and distinct buckling modes can occur in a cylindrical shell under local axial compression.

Effects of geometry non-linearity

The axial membrane stress distribution for a wide strip load ($2\theta_n = 90°$) is shown in Fig. 8 (on the mid-plane and at the point of buckling). The predictions of linear analysis (LA) and geometrically nonlinear analysis (GNA) are compared, with the axial membrane stress distribution according to membrane theory also shown for reference. The effect of non-linearity is comparatively small, and it was found that this observation could be made for all the other cases considered (many strip widths and heights and shell R/t ratios).

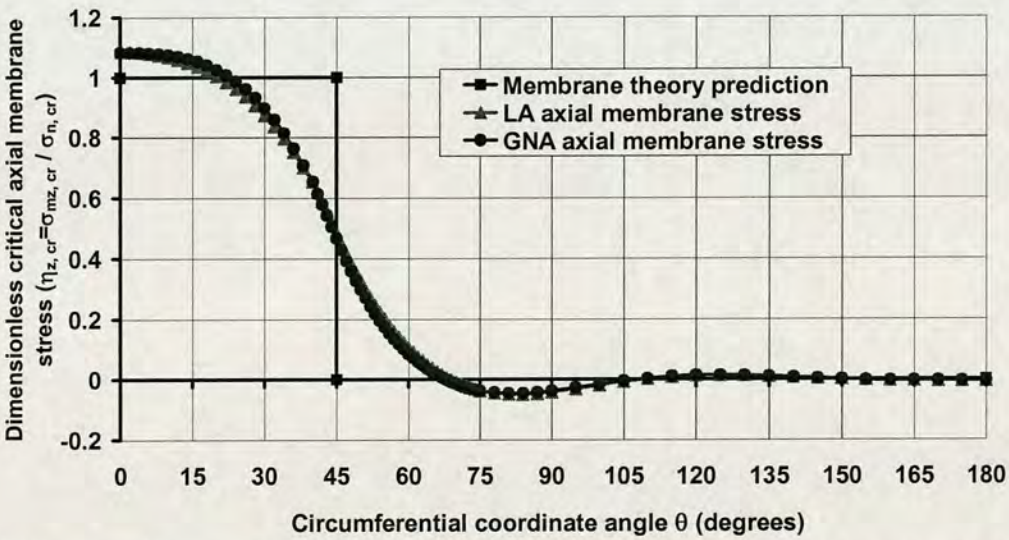

Fig. 8. Effect of geometric non-linearity on the membrane stresses at buckling (strip edge buckles)

CONCLUSIONS

- Two possible and distinct buckling phenomena have been identified for a wide range of shell geometries subject to a wide range of strip loads
- For narrow strips, a strip centre buckle occurs, but for wider strips, a strip edge buckle is caused by the

high shear induced by membrane incompatibility at the strip edge;

- A parametric study has been completed which identifies load angle that separates these two phenomena for different *R/t* ratios and different axial membrane stress gradients;
- Simple formulae have been developed to predict the buckling strength under local axial compression
- The influence of imperfection amplitude has been examined and shown to have a moderate effect;
- Geometric non-linearity seems to have a minor effect on the stress distribution at buckling.

ACKNOWLEDGMENTS

Financial support from the UK government through the ORS Award (ORS/C20-4, ORS/1999014046) is gratefully acknowledged by the first author.

REFERENCES

Bijlaard, D.L. and Gallagher, R.H. (1959) "Elastic instability of a cylindrical shell under arbitrary circumferential variation of axial stresses", Journal of the Aerospace Sciences, 27(11), 854-858, 866.

Berry, P.A., Rotter, J.M. and Bridge, R.Q. (2000) "Compression tests on cylinders with circumferential weld depressions", *Journal of Engineering Mechanics, ASCE*, **126 (4)**, 405-413.

Cai, M.J. (2003) "Buckling of cylindrical shells under non-uniform loads", PhD Thesis, Institute for Infrastructure and Environment, University of Edinburgh.

Cai, M.J., Holst, J.M.F.G. and Rotter, J.M. (2002) "Buckling Strength of Thin Cylindrical Shells under Localized Axial Compression", 15th ASCE Engrg Mechs Div Conf, Columbia Univ, New York, pp 99.

ENV 1993-4-1 (1999) *European Pre-standard Eurocode 3 Part 4.1: Design of steel structures: Silos.* European Committee for Standardisation, CEN, Brussels.

Guggenberger, W., Greiner, R. and Rotter, J.M. (2000) "The Behaviour of Locally-Supported Cylindrical Shells: Unstiffened Shells", *J. Constructional Steel Research*, **56 (2)**, 175-197.

HKS (1998) *ABAQUS/Standard User's Manual*, Hibbitt, Karlsson & Sorensen, Inc., Pawtucket, Rhode Island, USA, Version 5.8 edition, 1998.

Holst, J.M.F.G., Rotter, J.M. and Calladine, C.R. (1999) "Imperfections in cylindrical shells resulting from fabrication misfits", *J. Eng. Mechanics*, Vol. 125, No. 4, pp. 410-418.

Holst, J.M.F.G., Rotter, J.M. and Calladine, C.R. (2000) "Imperfections and buckling in cylindrical shells with consistent residual stresses", *J. Construct. Steel Research*, Vol. 54, pp. 265-282.

Libai, A. and Durban, D. (1977) "Buckling of cylindrical shells subjected to non-uniform axial loads", *Journal Applied Mechanics*, ASME, 44, pp. 714-720.

Ooi, J.Y., Pham, L. and Rotter, J.M. (1990) "Systematic and random features of measured pressures on full-scale silo walls", *Eng. Struct.*, Vol. 12, No. 2, pp. 74-87.

Rotter, J.M. (1986) "The analysis of steel bins subject to eccentric discharge", *Proc., 2nd Int Conf on Bulk Materials Storage, Handling & Transportn*, IE Aust., Wollongong, pp 264-271.

Rotter, J.M. (1997) "Design standards and calculations for imperfect pressurised axially compressed cylinders", *Int Conf on Carrying Capacity of Steel Shell Structures*, Brno, pp 354-360.

Rotter, J.M. (1998) "Shell structures: the new European standard and current research needs", *Thin-Walled Structures*, **31**, 3-23.

Rotter, J.M. (2001) *Guide for the Economic Design of Circular Metal Silos*, Spon, London.

Rotter, J.M. and Teng, J.G. (1989) "Elastic stability of cylindrical shells with weld depressions", *J. Struct. Engg*, ASCE, **115 (5)** 1244-1263.

Schmidt, H. and Winterstetter, T.A. (2001) "Substitute geometrical imperfections for the numerical buckling assessment of cylindrical shells under combined loading", *Proc, Euromech 424*, Rolduc-Kerkrade, 82-84.

Yamaki, N. (1984), *Elastic stability of circular cylindrical shells*, North-Holland, Amsterdam, The Netherlands.